Dissertation

submitted to the
Combined Faculty of Natural Sciences and
Mathematics
of Heidelberg University, Germany
for the degree of
Doctor of Natural Sciences

Put forward by
Antje Hoheisel
Born in Heidelberg, Germany
Oral examination: 22 July 2021

Evaluation of greenhouse gas time series to characterise local and regional emissions

Antje Hoheisel

Referees: Prof. Dr. Norbert Frank
Prof. Dr. André Butz

Abstract

In this thesis, high temporal resolution time series of greenhouse gases measured at three stations in Germany - Heidelberg, Zugspitze and Schauinsland - are studied regarding local and regional emissions.

The six years of CH_4 and δ^{13}C-CH_4 measurements in Heidelberg reveal a mean source signature of $-52.5 \pm 0.3‰$ and a seasonal cycle with more biogenic and less fossil CH_4 emissions in summer which is only partly explainable by residential heating. The analysis of emission inventories shows that EDGAR v5.0 overestimates the impact of isotopic enriched sources like waste incineration, while the LUBW inventory underestimates emissions but represents the composition well. At Zugspitze, we have shown that CO_2, CO and CH_4 measurements at the mountain ridge are less influenced by local anthropogenic emissions than observations at Schneefernerhaus. Strong pollution events occur at Schneefernerhaus especially during the day and in winter. The careful manual quality control removes these peaks, but the diurnal CO_2 cycles still indicate a small influence during the day. At Schauinsland measured CH_4 shows strong spikes in summer months. We demonstrate that these pollution events originate from cows which graze in the nearby pastures. The REBS peak detection method is used to filter out the influenced data and shows that hourly CH_4 averages can be shifted by them up to 50 ppb in summer and monthly values by ~ 1 ppb.

Zusammenfassung

In dieser Arbeit werden zeitlich hoch aufgelöste Zeitreihen von Treibhausgasen, welche an den drei Stationen Heidelberg, Zugspitze und Schauinsland in Deutschland gemessen wurden, auf lokale und regionale Emissionen hin untersucht.

Die Auswertung der sechsjährigen CH_4- und δ^{13}C-CH_4-Messungen in Heidelberg zeigt eine mittlere Quellensignatur von $-52.5 \pm 0.3‰$ und einen Jahresgang mit mehr biogenen und weniger fossilen CH_4-Emissionen im Sommer, der nur zum Teil durch Emissionen beim Heizen verursacht wird. Die Auswertung von Emissionskatastern zeigt zudem, dass EDGAR v5.0 den Einfluss von mit schweren Isotopen angereicherter Quellen wie Abfallverbrennung überschätzt, während das LUBW die Emissionen unterschätzt, aber die Zusammensetzung gut darstellt. Für die Zugspitze konnten wir zeigen, dass die CO_2-, CO-, und CH_4-Messungen am Zugspitzkamm weniger stark von lokalen anthropogenen Emissionen beeinflusst werden als Messungen am Schneefernerhaus. Solche starken Emissionsereignisse treten am Schneefernerhaus vor allem tagsüber und im Winter auf und können durch die sorgfältige manuelle Qualitätskontrolle entfernt werden. Allerdings deuten die CO_2-Tagesgänge darauf hin, dass tagsüber noch ein kleiner Einfluss besteht. Am Schauinsland treten in den Sommermonaten hohe und schmale Peaks in der gemessenen CH_4-Konzentrationen auf. Diese Emissionsereignisse werden durch Kühe verursacht, die auf den nahegelegenen Weiden grasen. Die REBS-Methode zum identifizieren von Peaks filtert diese beeinflussten Daten heraus und zeigt, dass stündliche CH_4-Mittelwerte im Sommer um bis zu 50 ppb und Monatswerte um etwa 1 ppb durch diese verschoben werden können.

Contents

1. Introduction **1**

2. Greenhouse gases CO_2 & CH_4 and measurement techniques **5**
2.1. Global carbon cycle and methane budget 6
2.2. Isotopic composition of CH_4 8
2.3. Carbon monoxide 8
2.4. Cavity ring-down spectroscopy 9

3. Measurement site description and first analysis of CO_2 & CH_4 time series **11**
3.1. Measurement stations 11
3.1.1. Station Heidelberg at the Institute of Environmental Physics . . . 12
3.1.2. Mountain station Schauinsland 14
3.1.3. Environmental Research Station Schneefernerhaus at Zugspitze . 14
3.2. CO_2 and CH_4 measured in Heidelberg, at Schauinsland and Zugspitze . . 16
3.2.1. Continental excess 18
3.2.2. Trends in CO_2 and CH_4 19
3.2.3. Annual variability 19
3.2.4. Diurnal variability 21

4. Six years of CH_4 and $\delta^{13}CH_4$ measurements in Heidelberg **25**
4.1. Measurement methods 26
4.1.1. Experimental set-up 26
4.1.2. Data treatment 27
4.1.3. Instrumental performance 27
4.1.4. Calibration strategy and long-term reproducibility 28
4.1.5. $\delta^{13}CH_4$ measurements of intercomparison cylinders 32
4.2. Continuous CH_4 and $\delta^{13}CH_4$ measurements 33
4.3. Comparison of $\delta^{13}CH_4$ with background and former measurements 35
4.4. Isotopic signature of CH_4 sources calculated with atmospheric measurements 38
4.4.1. Miller-Tans and Keeling plot method 38
4.4.2. Determination of isotopic source signatures 40
4.5. Radon-Tracer method to determined CH_4 fluxes 48
4.6. Comparison with emission inventories 50
4.6.1. Annual CH_4 flux 52
4.6.2. Isotopic source signature 53
4.6.3. Annual variability of monthly mean source signatures 57
4.7. Summary and Outlook 59

5. Comparison measurements at Zugspitze **63**
5.1. Measurement methods . . . 64
5.1.1. Experimental set-up . . . 64
5.1.2. Data gaps . . . 65
5.1.3. Flagging . . . 66
5.1.4. Calibration strategy . . . 66
5.1.5. Target measurement for quality control . . . 68
5.1.6. Comparison of analysers . . . 70
5.1.7. Data corrections . . . 70
5.2. Comparison between Schneefernerhaus and mountain ridge measurements 71
5.2.1. Local pollution events of CO and CO_2 . . . 73
5.2.2. Local pollution events of CH_4 . . . 75
5.2.3. Difference between measurements at Schneefernerhaus and mountain ridge . . . 78
5.2.4. Diurnal and annual cycle . . . 81
5.2.5. Weekend dependency . . . 83
5.2.6. Weekend dependency in CO_2 between 2002 and 2019 . . . 86
5.3. Summary and Outlook . . . 89

6. Ten years of high temporal resolution CH_4 measurements at Schauinsland **91**
6.1. CH_4 spikes in high temporal resolution measurements . . . 92
6.1.1. Measurement method . . . 92
6.1.2. Measured time series of CH_4 . . . 93
6.2. Identification of the origin of CH_4 spikes . . . 94
6.2.1. Characterisation of emissions from the sewage pit and cows . . . 95
6.2.2. Ambient $\delta^{13}CH_4$ measurements . . . 99
6.2.3. Emissions from cows as origin of CH_4 spikes . . . 100
6.2.4. CH_4 emission flux from the sewage pit . . . 102
6.2.5. CH_4 measurements at different heights above the sewage pit . . . 104
6.3. Influence of CH_4 spikes on the CH_4 measurements . . . 105
6.3.1. First estimation of the influence of CH_4 spikes . . . 105
6.3.2. Performance of automatic peak detection methods . . . 107
6.3.3. Peak detection methods applied to long-term measurements . . . 112
6.4. Summary and Outlook . . . 116

7. Conclusion and Outlook **117**

A. Supplementary material on measurements in Heidelberg **119**
A.1. Single-point and two-point calibration . . . 119
A.2. Mobile measurement campaigns in the catchment area of Heidelberg . . . 121
A.3. Allan standard deviation of CH_4, CO_2 and their ^{13}C isotopes . . . 122
A.4. Measurements of six intercomparison cylinders of air sampled at Neumayer station . . . 123
A.5. Night-time and daytime STILT footprints for Heidelberg . . . 124

B. Supplementary material on measurements at Zugspitze **125**
B.1. Diurnal cycles on weekend and weekday for CO and CH_4 125

C. Supplementary material on measurements at Schauinsland **127**
C.1. Mobile measurement campaigns at Schauinsland 127
C.2. Measurements at the sewage pit and near cows at Schauinsland 129
C.3. Ambient air measurement of $\delta^{13}CH_4$ and $\delta^{13}CO_2$ at Schauinsland 130
C.4. CH_4 and CO_2 soil flux 134

Bibliography **137**

List of Figures **149**

List of Tables **153**

1. Introduction

One of the most challenging problems of our time is global warming. To limit the negative effects associated with climate change like extreme weather events or sea level rise, the 2015 UN Paris Agreement on Climate Change has set the goal to limit the mean global temperature increase below 2°C, preferably to 1.5°C, compared to pre-industrial level (UNFCCC, 2015). This goal can only be achieved when the emission of greenhouse gases are strongly reduced up to carbon neutrality by mid-century, since anthropogenic emissions of greenhouse gases are the main drivers (IPCC, 2018). The European Union wants to reach this goal by reducing greenhouse gas emissions until 2030 by at least 55 % compared to levels in 1990 and realising net zero greenhouse gas emissions by 2050 (European Commission, 2021). These aims have been included in the European Climate Law.

Besides the EU, other industrialized countries of the United Nations Framework Convention on Climate Change (UNFCCC) have committed themselves to reporting regularly on their climate change policies and measures. This includes annual National Inventory Reports (NIRs) of greenhouse gas emissions which are provided by the countries for several greenhouse gases including the three most important ones: carbon dioxide (CO_2), methane (CH_4) and nitrous oxide (N_2O).

These emission inventories are based on "bottom-up" methods which involve statistical data about emitters like animal populations or the amount and type of combusted fuel and on specific emission factors that quantify the emissions from different source categories (IPCC, 2006). Both, statistical data and emission factors, can have large uncertainties due to unknown and unaccounted sources or high spatial and temporal variability for instance. In addition to national emission inventories, local emissions from different sources are also reported on a regional scale as it is done by the Landesanstalt für Umwelt Baden-Württemberg (LUBW, 2016) for each county. Other emission inventories, such as the Emissions Database for Global Atmospheric Research (EDGAR, Crippa et al., 2019), go one step further and aim to provide accurate annual emissions for different source types covering the entire globe. The different emission inventories can show, however, strong deviations in the amount and composition of emissions for the same area. Therefore, it is important to verify the reported greenhouse gas emissions given by emission inventories on a global, a national as well as a regional scale. Only then can we confirm intended reduction of greenhouse gases and if necessary adapt the mitigation strategy.

In order to verify emission inventories, so-called "top-down" approaches can be used which estimate greenhouse gas emissions out of atmospheric measurements. This is possible with different methods varying from simple box-models including trace gas measurements such as the Radon-Tracer method (e.g. Levin, 1984, Schmidt et al., 2001

and Levin et al., 2011), over box-models with representative chemical mechanisms (e.g. Prather, 1996 and Heimann et al., 2020), up to highly complex inverse models (e.g. Bergamaschi et al., 2018 and Friedlingstein et al., 2020). These inverse models simulate the mole fractions of greenhouse gases using atmospheric transport models and a priori emission inventories. To estimate greenhouse gas emissions, fluxes in the inventory are optimised so that the simulated data match the measured atmospheric mole fractions.

Top-down emission estimates are improved by a dense network of stations which measure greenhouse gases continuously with high precision. As all stations within the network operate with the same technical and scientific standards, the data are comparable and the quality improves. Furthermore, the access to the measured data sets from different stations is easier, which helps to evaluate and model greenhouse gas emissions. The Integrated Carbon Observation System (ICOS) is such a measurement network. Most ICOS stations have been built up recently, but also stations which have measured greenhouse gases for several decades such as Jungfraujoch are part of ICOS. During the last years the two stations Schauinsland and Zugspitze, which provide long-term records of greenhouse gases, have joined ICOS, too.

Historically, observation stations were often established on islands or mountains because ambient air measurements there are typically less affected by local and even regional influences than urban stations (e.g. Bousquet et al., 1996 and Schmidt et al., 2003). The long-term measurements of these remote stations are often included into models which estimate emissions at a global or continental scale and are thus important to verify emissions with the top down approach.

However, recent studies of high temporal resolution greenhouse gas measurements have shown that even at remote mountain stations the measurements are occasionally influenced by local anthropogenic activities. At Pic du Midi local CH_4 spikes (brief but high mole fractions) were noticed which are caused by a small sewage treatment facility near the air intake of the analyser (El Yazidi et al., 2018) and CO_2 measurements done at Jungfraujoch indicate an influence caused by visitors and tourism (Affolter et al., 2021). Such local pollution events near the stations cannot yet be simulated by inverse models. The influence of very local sources on the hourly averaged measurements could be seen as a large-scale peak for the whole region and thus be wrongly attributed to a larger regional source. Additionally, the occurrence of local pollution events which are not evenly distributed over the year can produce a seasonal bias. Therefore, it is important to identify and exclude the impact of local pollution on the time series of remote stations.

On a global scale several studies have analysed the atmospheric isotopic ratio of greenhouse gases such as δ^{13}C-CH_4 or δ^{13}C-CO_2 in addition to their mole fractions. In these studies the observations of greenhouse gas isotopes in the atmosphere are used to constrain emission budgets and to explain observed atmospheric trends in mole fraction and isotopic composition (e.g. Nisbet et.al, 2016, 2019 and Schaefer, 2016, 2019). This is possible, since each source type has a different isotopic signature depending on the production processes and origin. Thus the isotopic composition measured in the atmosphere contains information about the sources contributing to the measured mole fraction.

Also on a local and regional scale the measurement of the atmospheric isotopic ratio of

CH_4 provides information about the composition of CH_4 emissions. Traditionally, δ^{13}C-CH_4 in the atmosphere is measured by taking sample bags or flasks and analysing them with isotope ratio mass spectrometry coupled with gas chromatography. This method was used by Levin et al. (1999) who measured and evaluated bi-weekly atmospheric samples in Heidelberg in the 1990s. With new measurement techniques like continuous flow isotope ratio mass spectrometry, quantum cascade laser absorption spectroscopy or cavity ring-down spectroscopy the δ^{13}C-CH_4 values in the atmosphere can be measured continuously and with high temporal resolution of a few seconds up to minutes. However, there are few studies which analyse atmospheric long-term measurements of $\delta^{13}CH_4$ with high temporal resolution regarding emissions and often the studied sources have comparable isotopic signatures. Assan et al. (2018) for instance analysed $\delta^{13}CH_4$ measurements done near industrial sites and Röckmann et al. (2016) as well as Menoud et al. (2020) studied $\delta^{13}CH_4$ in rural areas in the Netherlands. CH_4 measured at urban stations however originates from heterogeneously distributed sources including waste management, natural gas distribution systems, heating, transport and agriculture. The corresponding emissions vary strongly in their isotopic ^{13}C-CH_4 composition and make the analysis and interpretation of CH_4 emissions in cities more difficult.

Careful analysis of atmospheric, high temporal resolution greenhouse gas measurements with respect to local and regional sources is therefore important for both urban and remote stations. In my thesis, I analyse CH_4, δ^{13}C-CH_4, CO_2 and CO time series measured at three observation stations in Germany – Heidelberg, Zugspitze and Schauinsland. The main part of this thesis is divided into three chapters, each chapter investigates the measured time series at one of the stations.

Before evaluating these time series, chapter 2 first provides an overview of the greenhouse gases CO_2 and CH_4 as well as the isotope ratio δ^{13}C-CH_4. Furthermore, the basics of the measurement method of the time series – absorption spectroscopy especially cavity ring-down spectroscopy – are explained. Chapter 3 characterises the three measurement stations Heidelberg, Zugspitze and Schauinsland in more detail. This also includes the comparison of CO_2 and CH_4 measurements done within the last few years at these stations.

In chapter 4, six years of atmospheric CH_4 mole fraction and δ^{13}C-CH_4 measurements at the urban station Heidelberg are analysed. These measurements were carried out continuously with a CRDS analyser since the middle of 2014. The aim of this study is to learn more about seasonal and long-term variabilities of regional and local CH_4 sources and to inspect regional emission inventories using measurement based information about the mixture and flux of CH_4 sources in the catchment area of Heidelberg. Therefore, different approaches such as the moving Miller-Tans approach and the Radon-Tracer method are used to determine the amount and composition of CH_4 emissions in the catchment area of Heidelberg. These results are then compared to a regional emission inventory provided by LUBW and the emission database EDGAR v5.0.

In the following two chapters, time series measured at the remote mountain stations Zugspitze and Schauinsland are analysed with respect to local pollution. At both stations greenhouse gas measurements have been carried out for several decades. Due to the

aforementioned high temporal resolution of CRDS, we are able to detect local pollution events in the time series of CO_2, CH_4 but also CO which were unnoticed in measurements with less temporal resolution. The aim of the evaluation of these time series is to identify the local sources, to quantify their impact on the data and to remove or if possible prevent local pollution events.

For that purpose, ambient air measured at Zugspitze-Schneefernerhaus is compared to measurements done at the mountain ridge in chapter 5. Since this new location is less influenced by local pollution, the comparison of two years of CO_2, CH_4 and CO measurements done at both locations gives us information about local pollution sources and their impact on the measurement at Schneefernerhaus.

Furthermore, 10 years of high temporal resolution CH_4 measurements at Schauinsland are analysed in chapter 6. High CH_4 spikes are visible in the time series during the summer months. We demonstrate that around 10 cows grazing in the nearby pasture are the origin of these peaks and we quantify the impact of the CH_4 spikes on the hourly and monthly averaged CH_4 mole fractions using different automatic peak detection methods.

2. Greenhouse gases CO_2 & CH_4 and measurement techniques

The CO_2 and CH_4 mole fraction in the atmosphere has increased since pre-industrial times. In figure 2.1 direct atmospheric measurements of CO_2 and CH_4 are shown as blue lines. Since those measurements were established in the second half of the 20^{th} century (e.g. Keeling et al. , 1976), they only cover a small time period. To determine atmospheric CO_2 and CH_4 mole fractions in pre-industrial times another tool has to be used. The measurement of air enclosed in ice cores make this possible (symbols in figure 2.1).

While the CO_2 mole fraction in pre-industrial times (before 1800 A.D.) varied between 275 and 284 ppm (Etheridge et al., 1996), a strong increase of about 48 % is visible in the last 300 years reaching 414.24 ± 0.12 ppm in 2020 at Mauna Loa (Tans and Keeling, 2021). The increase in the CH_4 mole fraction was even stronger than in CO_2. Between 1000 and 1800 A.D. the average of the global mean CH_4 mole fraction was only 695 ppb with variations of 40 ppb (Etheridge et al., 1998). In 2020 however, the annual mean was 1879.10 ± 0.60 ppb (Dlugokencky, 2021). Thus, the globally averaged annual mean CH_4 mole fraction in the atmosphere has increased by 170 % since pre-industrial times.

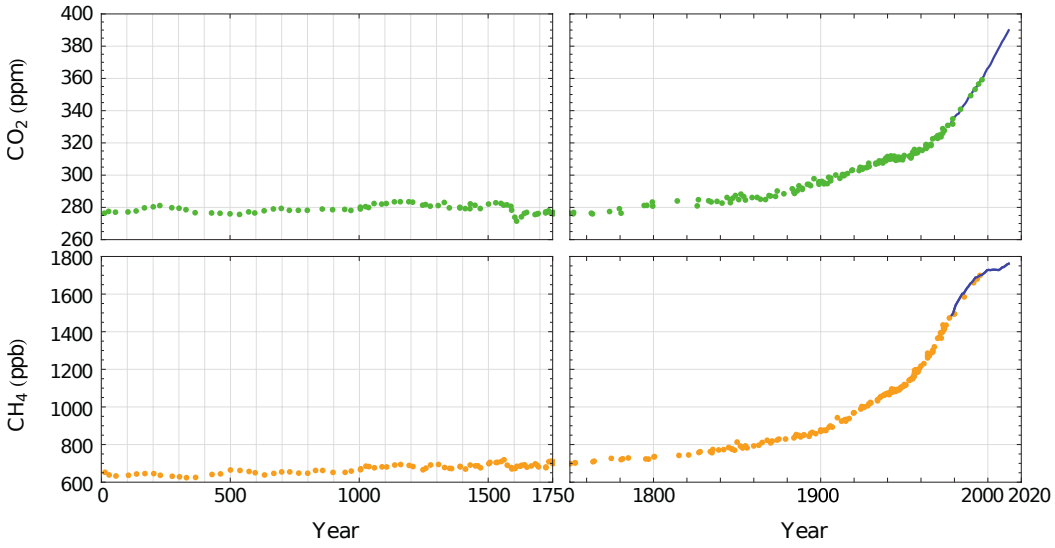

Figure 2.1.: Atmospheric CO_2 and CH_4 mole fractions determined from ice cores (symbols) and from direct atmospheric measurements at the Cape Grim observatory (blue lines). Source: IPCC (2013).

This increase of CO_2 and CH_4 mole fraction in the atmosphere has a strong impact on climate change, since CO_2 and CH_4 are the two most important anthropogenic greenhouse gases. Since pre-industrial times the increase in the globally averaged annual mean mole fraction of CO_2 and CH_4 has led to a total radiative forcing attributable to CO_2 or CH_4 of $1.68\,\mathrm{W\,m^{-2}}$ and $0.97\,\mathrm{W\,m^{-2}}$, respectively (IPCC, 2013).

The impact of greenhouse gases on global warming depends in addition on their concentration in the atmosphere on their lifetime and radiative efficiency. The global warming potential (GWP) combines the latter two effects and places them in relation to CO_2 ($\mathrm{GWP}_{CO_2} = 1$). Since CH_4 has a GWP of 84 and 28 on a 20-year or 100-year time scale (IPCC, 2013), it has a large effect on global warming although the amount of CH_4 in the atmosphere is small compared to CO_2.

2.1. Global carbon cycle and methane budget

The observed increase in the atmospheric CO_2 and CH_4 mole fraction is caused by anthropogenic emissions. In figure 2.2a the global carbon cycle is shown with globally averaged fluxes determined by Friedlingstein et al. (2020) for the decade 2010–2019. In equilibrium, the CO_2 exchange between the different CO_2 reservoirs atmosphere (860 GtC), soil (1500-2400 GtC) and ocean (38 000 GtC dissolved inorganic carbon) is balanced. CO_2 is taken up by the biosphere during photosynthesis, but the same amount is produced by biogenic respiration ($120\,\mathrm{GtC\,yr^{-1}}$). Also the exchange between atmosphere and ocean would be similar ($90\,\mathrm{GtC\,yr^{-1}}$). However, anthropogenic CO_2 emissions lead to an additional impact of CO_2 on the atmosphere. The most important are the release of fossil CO_2 during combustion of fossil fuels ($9.4\,\mathrm{GtC\,yr^{-1}}$) and CO_2 emissions due to land-use change including deforestation, degradation, and peat burning ($1.6\,\mathrm{GtC\,yr^{-1}}$). The increase of CO_2 in the atmosphere shifts the natural balance between atmosphere, land and ocean. Around $3.4\,\mathrm{GtC\,yr^{-1}}$ are additionally taken up by the biosphere and $2.5\,\mathrm{GtC\,yr^{-1}}$ by the ocean, which leads to further problems such as ocean acidification. Thus, only half ($5.1\,\mathrm{GtC\,yr^{-1}}$) of the anthropogenic CO_2 remains in the atmosphere and is noticeable as CO_2 increase (Friedlingstein et al., 2020).

The global carbon budget is described by Saunois et al. (2020) and shown in figure 2.2b. While CO_2 is not chemically decomposed in the atmosphere, the main sinks of CH_4 are chemical reactions there. The most important sink mechanism of CH_4 in the atmosphere is oxidation by hydroxyl radicals (OH) usually in the troposphere. Only a small part of atmospheric CH_4 is oxidised in soils. The strongest natural sources of CH_4 are wetlands. Inland water systems, permafrost, termites, wild animals, land geological sources and oceanic sources emit a much smaller amount of CH_4. Between 2008 and 2017, around 60 % of global CH_4 emissions are of anthropogenic origin. Emissions which are related to fossil-fuels including exploitation, transport and usage of natural gas, oil and coal, account for ∼35 % of global anthropogenic emissions. Another third is emitted by enteric fermentation and manure management of livestock and ∼12 % by waste management like landfills and waste water handling. Rice cultivation as well as biomass and biofuel burning account for around 8 % each (Saunois et al., 2020).

(a)

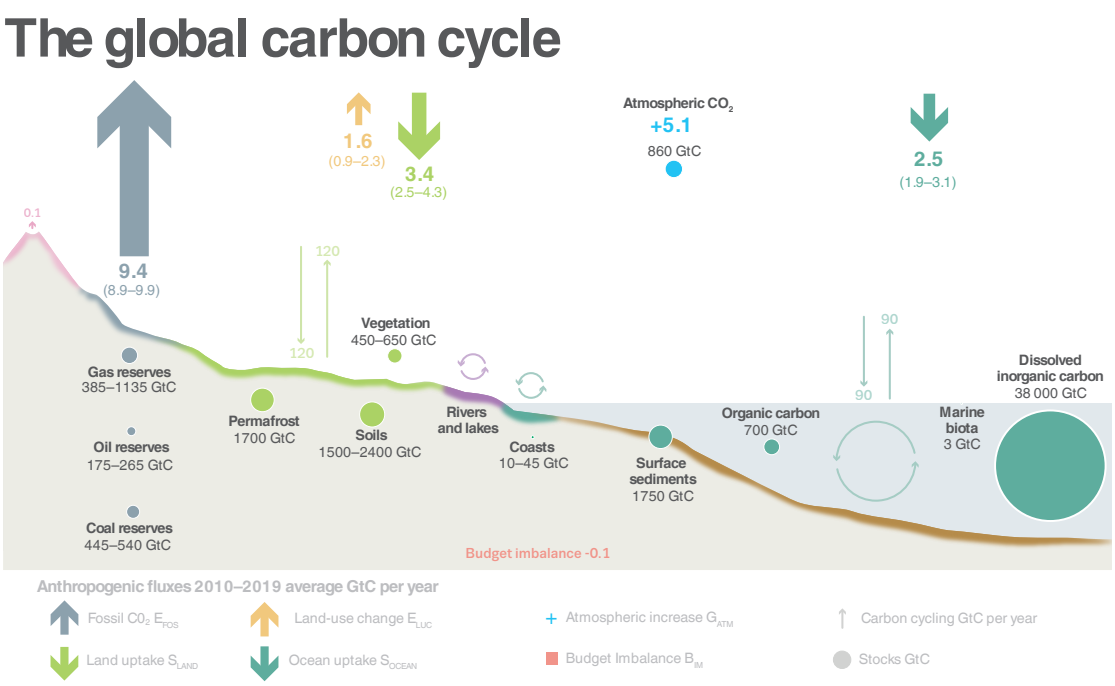

(b)

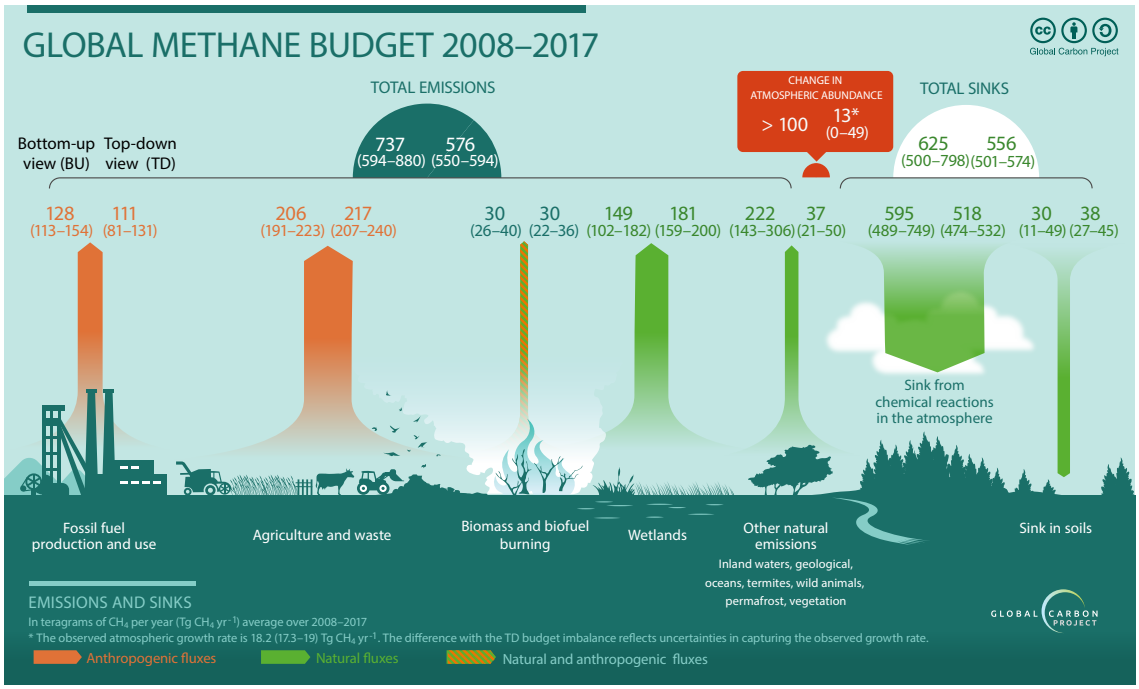

Figure 2.2.: Global carbon budget (a) and global CH_4 budget (b). Figures from Friedlingstein et al. (2020) (a) and Saunois et al. (2020) (b).

2.2. Isotopic composition of CH_4

Isotopes are atoms of the same element which only differ in their number of neutrons. Molecules which differ in their isotopic composition are called isotopoloques. Due to the different number of neutrons, isotopologues have different masses which lead to slightly different physical and also chemical properties. Therefore, the isotopic composition of a sample can change (isotopic fractionation) during physical phase transitions or chemical reactions. Thus, CH_4 emitted by different sources has a characteristic ratio between $^{13}CH_4$ and $^{12}CH_4$ depending on the production process and the initial material The isotopic composition of $^{13}CH_4$ and $^{12}CH_4$ can be described with the δ-notation (Mook, 2000):

$$\delta = \frac{\mathrm{R_{sample}}}{\mathrm{R_{standard}}} - 1 \tag{2.1}$$

The isotopic ratio R is defined as the ratio between the abundance of the rare and the abundant isotope. An international reference standard for the ratio $^{13}C/^{12}C$ is the Vienna Pee Dee Belemnite (VPDB) $R_{\mathrm{standard}} = 0.0111802$ (Werner und Brand, 2001)

The isotopic signature of CH_4 sources vary between -13 to $-70\,‰$ (IPCC, 2013). Most depleted CH_4 is specified as biogenic and is produced under anaerobic conditions due to degradation of organic matter. Typical biogenic CH_4 sources are wetlands, ruminants, landfills and wastewater treatment plants. Thermogenic CH_4 like in natural gas is formed on geological time scales out of organic matter and is more enriched with values between -25 and $-45\,‰$. Most heavy CH_4 is formed during the incomplete combustion of organic matter such as biomass burning and is characterized as pyrogenic (IPCC, 2013).

2.3. Carbon monoxide

Carbon monoxide (CO) is no greenhouse gas, but since it effects CO_2 and CH_4 in the atmosphere, it has an indirect impact on climate change.

One source of atmospheric CO is oxidation with CH_4 and other volatile organic compounds (VOCs) and its major sink is the oxidation by OH radicals. Especially through the last reaction, the CO concentration in the atmosphere affects the lifetime and abundance of CH_4 (Zheng et al., 2019), since 40% of OH in the troposphere is removed via the reaction of OH with CO (Lelieveld et al., 2016).

Furthermore, atmospheric CO originates from direct natural and anthropogenic emissions. Most direct CO emissions are caused by incomplete combustion of fossil fuels and biofuels or through biomass burning. Only a small part is emitted by plant leaves or during the marine biogeochemical cycling (Zheng et al., 2019).

Since CO is emitted in addition to CO_2 during incomplete combustion, the measurement of CO can be used as a proxy for anthropogenic CO_2.

2.4. Cavity ring-down spectroscopy

Atmospheric CO_2 and CH_4 as well as their isotopic ratio can be measured with different methods such as gas chromatography with flame ionisation detectors (GC-FID), non-dispersive infrared spectroscopy (NDIR), fourier transform infrared spectroscopy (FTIR) and cavity ring-down spectroscopy (CRDS).

Recent measurements of CH_4, δ^{13}C-CH_4, CO_2 and CO done at Heidelberg (chapter 4), Zugspitze (chapter 5) and Schauinsland (chapter 6), which are analysed in more detail in this study, are carried out with CRDS. The principles of absorption spectroscopy in general and the basics of CRDS are shortly described in the following.

Light which passes a sample gas is absorbed depending on the composition of the gas and the wavelength. This occurs since light is resonantly absorbed when a wavelength matches a rovibrational excitation energy of the molecules. These depend on the masses of the atoms of the molecules. Therefore, the absorption spectrum is characteristic of the composition of the gas from different molecules and their isotopologues.

To determine the concentration of one or several absorbers like CH_4 or CO_2, the intensity of light after it has passed the sample is usually measured by a photodetector. If a laser is used as light source, it can be tuned to several wavelengths to achieve an absorption spectrum of the sample. Different absorption features at different wavelengths are analysed depending on the gas species we are interested in.

The intensity of light with an initial intensity I_0 which travels the distance z through a medium with n absorbers decays exponentially and can be described by the general form of Lambert-Beer's law (Platt and Stutz, 2008):

$$I(\lambda, z) = I_0(\lambda) \cdot exp\left(-\int_0^z \sum_{i=1}^{n} \sigma_i(\lambda, p(s), T(s)) \cdot C_i(s)\,\mathrm{d}s\right). \tag{2.2}$$

C_i are the concentrations of each absorber and σ_i the corresponding absorption cross-sections (or extinction) which depend on wavelength λ, pressure p and temperature T. If we assume a homogeneous medium and neglect temperature and pressure dependencies, the equation is simplified to

$$I(\lambda, z) = I_0(\lambda) \cdot exp\left(-z \cdot \sum_{i=1}^{n} \alpha_i(\lambda)\right) \text{ with } \alpha_i = \sigma_i \cdot C_i. \tag{2.3}$$

The absorption coefficient α is given by the product of the cross section σ and concentration C.

When the measured absorption spectrum $I(\lambda, z)$, the spectrum of the initial intensity $I(\lambda)$ and the path length z are known, the absorption coefficient spectrum $\alpha(\lambda)$ can be calculated. The concentration is then determined by fitting experimentally derived cross-section spectra of the relevant absorbers to the measured spectra.

The exact way of how the concentration is determined out of the intensity measurements strongly depends on the method and the analyser used.

The cavity enhanced absorption method used by CRDS involves a cavity which is filled with sample gas. Light of a tunable laser which enters the cavity is reflected there multiple times between two or three highly reflecting mirrors. So the effective path length through the sample gas can reach 15 to 20 km (Rella et al., 2015) for a small cavity of around 25 ml. Therefore, the precision of the measurement is increased by increasing the effective path length and thus the intensity reduction. In addition, the pressure and temperature of the cavity are usually controlled and stabilized to reduce the influence of both on the measurement. This and the small cavity justify the assumption of a homogeneous medium and the neglect of temperature and pressure dependencies used in equation 2.3. A small fraction of light can pass each mirror and is measured behind one of them with a photodetector.

CRDS analysers measure the decay rate of intensity due to absorption but not the reduction in absolute intensity and are thus independent of laser intensity and absolute laser power. Light of a tunable laser enters a cavity with three mirrors. After the intensity has reached a threshold, the laser is turned off and the exponential decrease of intensity is detected by a photodetector. The decay constant τ, or ring-down time, of this decay depends on the reflectivity of the mirrors and the absorption due to the sample gas. An absorption spectrum is determined out of the decay constants measured at different wavelengths. Around 50 to 200 ring-down time measurements are done at 10 to 20 wavelengths distributed across an absorption feature of the relevant gas species (Rella et al., 2015). A more detailed description of CRDS analysers are given in Crosson (2008) and Rella et al. (2015).

The CRDS instruments G2201, G2301 and G2401, with which the measurements evaluated in this thesis were carried out, use lasers in the infrared range to analyse the mole fraction of several gas species every few (~ 3) seconds. The characterisation of these individual analysers used at the different stations is given in the particular chapters 4, 5 and 6.

3. Measurement site description and first analysis of CO_2 & CH_4 time series

3.1. Measurement stations

In this thesis, trace gas measurements are analysed which were done at three measurement stations in the south of Germany (figure 3.1). The first measurement station is an urban site in Heidelberg (116m a.s.l) at the Institute of Environmental Physics (IUP). The second site is the mountain station Schauinsland (1205 m a.s.l.) operated by the German Environment Agency (UBA). The third one is another but higher mountain station, the Environmental Research Station Schneefernerhaus (2670 m a.s.l.) at Zugspitze. The trace gas measurements done at Schneefernerhaus are carried out by the German Environment Agency, too. This section gives a short overview of all three stations including wind patterns, land-use and possible emission sources.

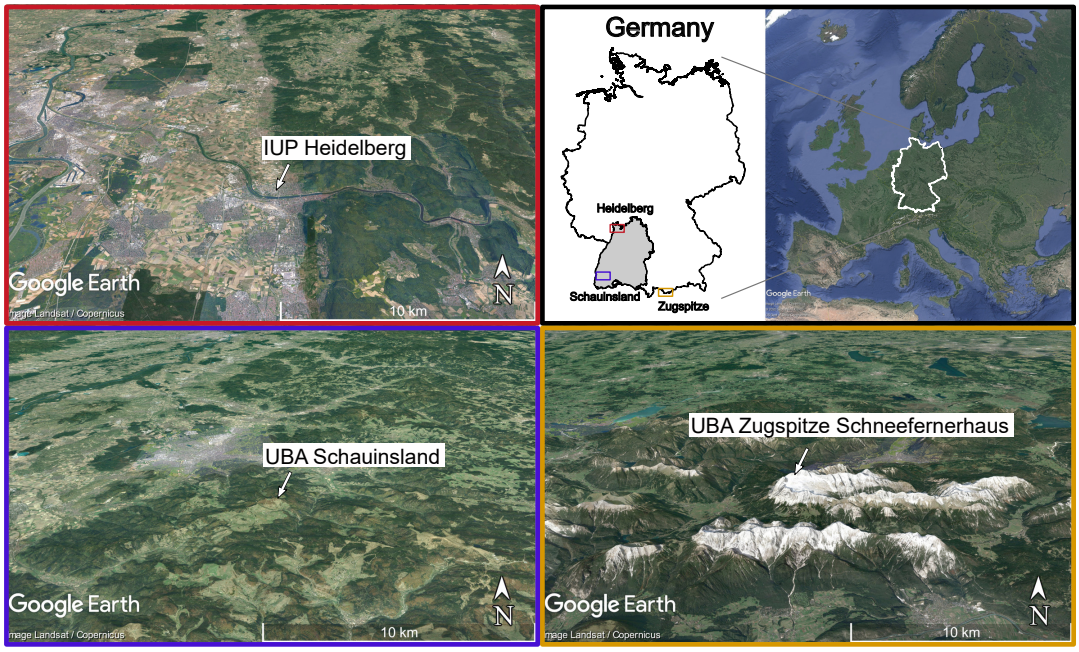

Figure 3.1.: Location of the three measurement sites Heidelberg, Schauinsland and Zugspitze.

3.1.1. Station Heidelberg at the Institute of Environmental Physics

Heidelberg ($\sim$ 160 000 inhabitants) is located in the south-west of Germany and in the north of the state of Baden-Württemberg. It is situated in the Upper Rhine Plain on the edge of the low mountain range Odenwald. Therefore, the north-east is less urban and more forested (figure 3.2a). More agricultural and urban areas are in the Upper Rhine Plain in the north-west to south-east. The industrial cities of Mannheim ($\sim$ 310 000 inhabitants) and Ludwigshafen ($\sim$ 167 000 inhabitants) are 15 to 20 km north-west of Heidelberg.

The main wind directions measured at the roof of the Institute of Environmental Physics (IUP) in Heidelberg is east to south (figure 3.2b). The measured air masses are thus mainly influenced by the city of Heidelberg itself but occasionally from the industrial cities of Mannheim and Ludwigshafen. This can also be seen in figure 3.2c. There the averaged footprints for 2018 calculated with data from the whole day are shown for the stations Heidelberg, Schauinsland and Zugspitze. The footprints are calculated with the Stochastic Time-Inverted Lagrangian Transport (STILT) model (Lin et al., 2003 and Kountouris et al., 2018) using the STILT footprint tools[1] and the provided STILT jupyter notebook service[2]. Since Heidelberg is an urban station at low altitude with multiple emission sources close-by, around half (48.5 %) of the estimated surface influence (sensitivity) for the station is within 100 km.

Due to its location within industrial, urban, agricultural and rural areas, CH_4 emissions measured in Heidelberg can originate from biogenic (e.g. dairy cows, waste water treatment plants), thermogenic (e.g. natural gas), and even pyrogenic (e.g. traffic) sources. To identify and characterise possible CH_4 sources in Heidelberg and in the surroundings, mobile measurement campaigns with a CRDS G2201-i analyser were done between 2016 and 2020. A detailed description of the mobile set-up, the measurement and analysis methods can be found in Hoheisel et al. (2019). In figure A.2 the isotopic source signatures for different CH_4 sectors measured around Heidelberg are shown.

Trace gas measurements are done at the Institute of Environmental Physics (IUP) (49°25'2"N, 8°40'28"E, 116m a.s.l). The carbon isotopic ratio ($^{13}C/^{12}C$ and $^{14}C/^{12}C$) of bi-weekly integral samples were already analysed in the years after 1977 (Levin, 1984). The CH_4 and CO_2 mole fractions have been measured since 1988, first using bi-weekly integral samples and since 1995 with an automated gas-chromatograph (GC). Between 1992 and 1996 $\delta^{13}CH_4$ was also analysed again using bi-weekly integrated air samples (Levin et al., 1999).

Since April 2014 a cavity ring-down spectroscopy (CRDS) analyser has been measuring continuously the mole fraction of CH_4 and CO_2 and its $^{13}C/^{12}C$ ratio in ambient air every few seconds. The inlet line for these ambient air measurements is on top of the roof of the institute (30 m a.g.l.). These measurements of CH_4 and $\delta^{13}CH_4$ are analysed in chapter 4 in more detail.

[1]STILT footprint tools: `https://www.icos-cp.eu/data-services/tools/stilt-footprint`
[2]STILT jupyter notebook service: `https://www.icos-cp.eu/data-services/tools/jupyter-notebook`

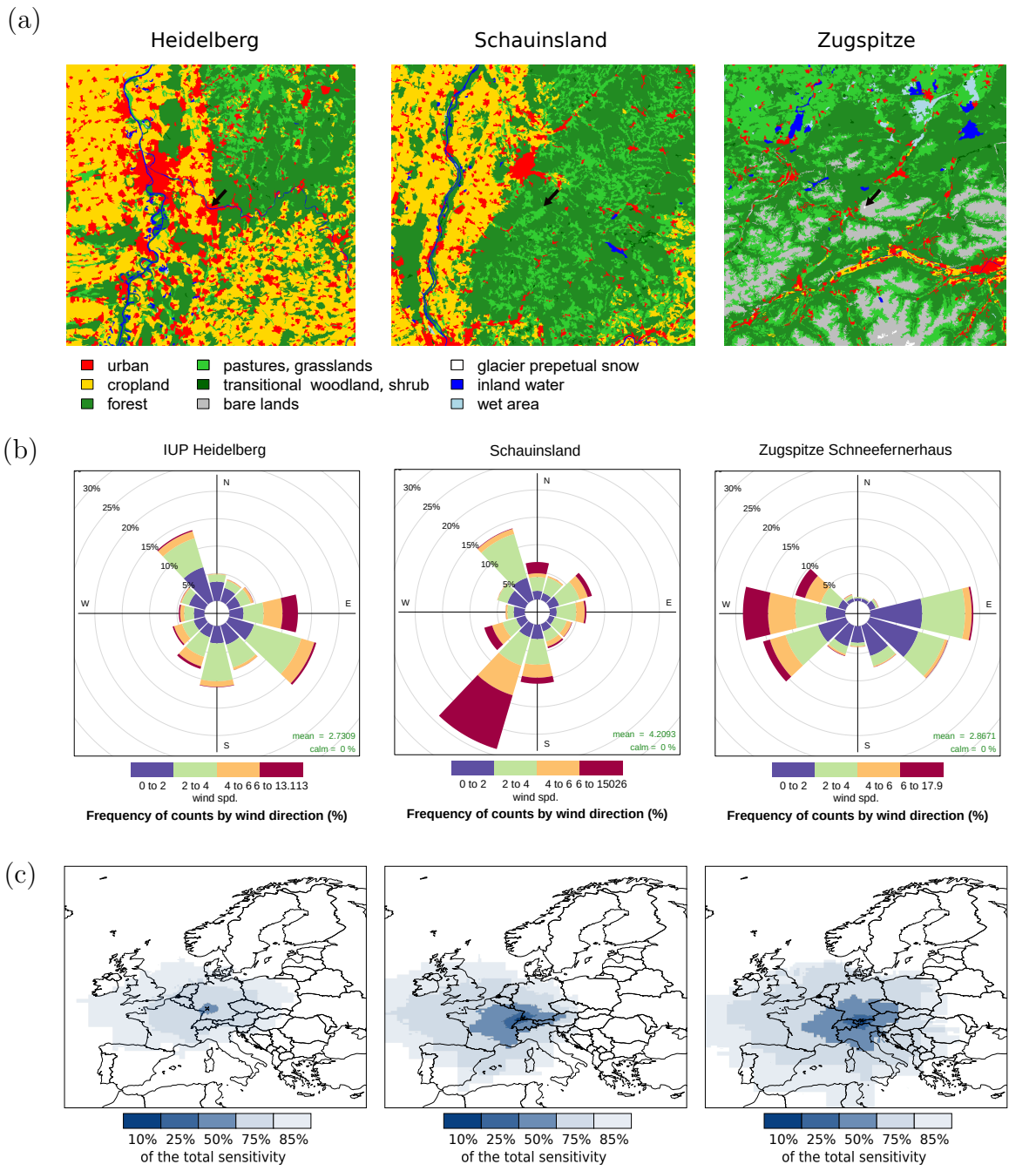

Figure 3.2.: Characterisation of the three measurement stations Heidelberg, Schauinsland and Zugspitze: land cover (a), wind roses for 2018 (b) and STILT footprints for 2018 (c). The land cover based on the Copernicus CORINE (Coordination of Information on the Environment) Land Cover (CLC) (European Union, Copernicus Land Monitoring Service 2021, European Environment Agency (EEA), `https://land.copernicus.eu/pan-european/corine-land-cover/clc2018`). The wind direction and wind speed for 2018 at Schauinsland and Zugspitze are provided by UBA. The footprints with different total sensitivity are calculated with STILT for 2018 with data from the whole day with the STILT footprint tools and STILT jupyter notebook.

3.1.2. Mountain station Schauinsland

Schauinsland (1284 m a.s.l) is a mountain in the Black Forest approximately 10 km south-east of the city of Freiburg im Breisgau ($\sim$ 230 000 inhabitants). In the north, south and east of the station Schauinsland forests, grassland and pastures predominate the land use (figure 3.2a). The meadows near the station are grazed by cows in summer and early autumn. In the west is the Upper Rhine Plain where cropland and urban areas like the city of Freiburg prevail. Since Schauinsland station with 1205 m a.s.l. is a mountain station, trace gas measurements done there are less influenced by regional and local emissions like the urban station in Heidelberg. However, there are still local influences like the biosphere for CO_2 or livestock farming for CH_4 (see chapter 6) which are visible in the measurements. In addition, during the day, especially in summer, polluted air masses from the urban Rhine valley frequently reach the station and thus increase the influence of regional anthropogenic emissions on the measurement (Levin, 1987). Due to the high elevation and thus stronger influence of the lower free troposphere, air measured at Schauinsland has a larger catchment area than Heidelberg (figure 3.2c). For Schauinsland 50.4 % of the estimated surface influence calculated with STILT is within 450 km, an area which is more than 20 times larger than the area estimated for Heidelberg. While the most common wind direction at the station is south-west (figure 3.2b), the predominant air mass influence is west with air masses coming from France (figure 3.2c).

Mobile measurement campaigns in the surroundings of Schauinsland station show us that CH_4 emissions from livestock are the main CH_4 source in the direct surroundings of the station (appendix C.1). Other sources like a landfill, a gas container or a biogas plant are placed further away in the Rhine Valley near the city of Freiburg.

The mountain station Schauinsland (47°54'50" N, 7°54'28" E, 1205m a.s.l.) is operated by the German Environment Agency (UBA). It is part of the Global-Atmosphere-Watch-Programme (GAW) of the World Meteorological Organization (WMO) and joins the Integrated Carbon Observation System (ICOS). Since 1972 the CO_2 mole fraction has been measured continuously at Schauinsland. The measurement of CO_2 was carried out with NDIR Levin (1987) and since 1991 ambient air has been analysed with GC (Schmidt et al., 1996), too. In addition to CO_2, also CH_4 was measured with the GC analyser. CH_4 and CO_2 measurements with a high temporal resolution of a few seconds have been carried out since 2011 with CRDS analysers. The CH_4 mole fraction measured with the CRDS analyser is evaluated in chapter 6 according to local pollution.

3.1.3. Environmental Research Station Schneefernerhaus at Zugspitze

Mount Zugspitze is located in the northern Alps at the border between Germany and Austria and with 2962 m a.s.l. it is Germany's highest mountain. Due to its location in the Alps, the local land cover is dominated by bare lands followed by forests and pastures (figure 3.2a). Urban areas and cropland, which are typical of the highly populated Rhine Valley next to Heidelberg and Schauinsland, only occur rarely. The nearest Ger-

man city is Garmisch-Partenkirchen which is around 11 km north-east and has around 27 000 inhabitants. The two largest cities within 100 km are Munich (∼ 1 480 000 inhabitants), which is approximately 90 km north-east of Zugspitze, and Innsbruck (∼130 000 inhabitants), which is about 35 km south-east.

In spite of the remote location at high altitude, especially in summer air masses are transported from the valley up the mountain due to thermally induced flow systems (Birmili et al., 2009, Ghasemifard et al., 2019). In addition, the summit of Zugspitze and the glacier plateau Zugspitzplatt (around 360 m below the summit), which is a ski resort in winter (mid-November to May), are tourist attractions. Each year more than 600 000 tourists (Bayerische Zugspitzbahn Bergbahn AG) visit the summit of Zugspitze and Zugspitzplatt which can be reached from the valley via cable cars or rack railway.

Trace gas measurements have been performed at mount Zugspitze since 1981; first at a pedestrian tunnel (ZPT) about 250 m below the summit, then at the terrace of the summit (ZUG) and since 2002 at the Environmental Research Station Schneefernerhaus (ZSF) (figure 3.3a).

The Environmental Research Station Schneefernerhaus (47°25'0" N, 10°58'46" E) is around 300 m below the summit of Mount Zugspitze. There, the scientific program is operated by several German research institutes aiming at monitoring the physical and chemical properties of the atmosphere and analysing various processes which influence the weather and climate (UFS, 2020). The German Environment Agency has carried out CO_2, CH_4 and CO measurements at Schneefernerhaus with GC (Yuan et al., 2019) and later off-axis integrated cavity output spectroscopy (OA-ICOS) and CRDS analysers. The greenhouse gas measurement program is part of the GAW program and it joins ICOS.

The air inlet for these measurements at Schneefernerhaus (ZSF, 2671 m a.s.l.) is

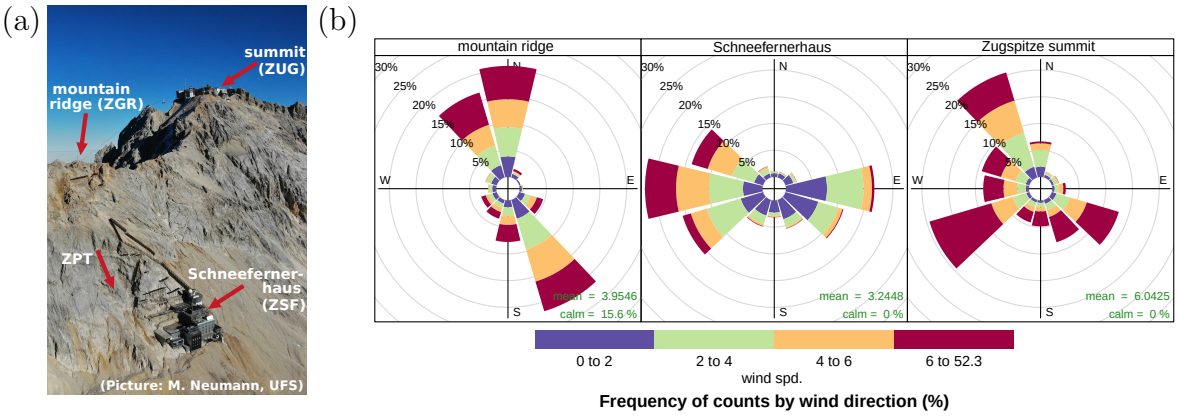

Figure 3.3.: (a): Picture of Zugspitze, including the four measurement locations: pedestrian tunnel (ZPT), summit (ZUG), Schneefernerhaus (ZSF) and mountain ridge (ZGR). (b): Wind roses for ZGR (left), ZSF (middle) and ZUG (right, Source: Deutscher Wetterdienst) determined from available wind directions and wind velocities between 2018 and 2020. The colours correspond to the frequency of different wind speed ranges.

installed on the fifth floor at the research terrace. The analysis of trace gases has shown that the measured time series are occasionally influenced by local pollution sources like snow groomers from the nearby ski resort, gasoline snow blowers, the rack railway tunnel from Schneefernerhaus to the valley or human CO_2 emissions at Schneefernerhaus. In 2013 the German Meteorological Service (Deutscher Wetterdienst - DWD) changed the inlet of their Radon (^{222}Rn) activity measurements in ambient air from ZSF to the mountain ridge around 150 m uphill of Schneefernerhaus to avoid contamination of local geogenic radon sources at Schneefernerhaus and a free inflow of air masses (Frank et al., 2017). In October 2018, a new inlet line made of stainless steel and 290 m long was installed from Schneefernerhaus to the mountain ridge (ZGR, 2825 m a.s.l.) to replace an old and broken intake line (figure 3.3a). This offers the possibility of measuring the CO, CO_2 and CH_4 mole fractions in ambient air of Schneefernerhaus and simultaneously of the mountain ridge uphill of Schneefernerhaus (see chapter 5).

The local wind patterns at Zugspitze are strongly influenced by the topography. Since Schneefernerhaus is built into the southern slope of the mountain, the prevailing wind direction is from the east or west (figure 3.3b). In contrast, the wind measurement on the mountain ridge is usually from the north or the south-south-east. At the Zugspitze summit the wind direction is less restricted and typically blows from north-west, south-west and south-east. On average, the wind velocity at Schneefernerhaus shows slightly lower values with 3.2 ms^{-1} compared to 4.0 m s^{-1} at the mountain ridge with a larger frequency of low winds between 0 an 2 m s^{-1}. At the summit the mean wind velocity is even higher (6.0 m s^{-1}).

The footprint for Zugspitze calculated with STILT indicates a stronger influence of the measured air masses from the west and east of Zugspitze (figure 3.2c). In addition, the STILT footprint points to a stronger influence of pollution sources further away. While around 50 % of the surface influence on the measurement is within 100 km for Heidelberg and 450 km for Schauinsland, it is even 550 km for Zugspitze.

3.2. CO_2 and CH_4 measured in Heidelberg, at Schauinsland and Zugspitze

The CO_2 and CH_4 mole fractions in Heidelberg and at Schauinsland and Zugspitze have been measured for several decades. In figure 3.4 the monthly averaged time series at Heidelberg (black), Schauinsland (red), Zugspitze (orange) and at the background station Mace Head (blue, Dlugokencky et al., 2020 and Dlugokencky et al., 2021) are shown for the last 20 years. The monthly averaged Schauinsland and Zugspitze data are provided by UBA and are obtained from the World Data Centre for Greenhouse Gases (WDGCC, 2021). Atmospheric CO_2 and CH_4 mole fractions in Heidelberg have been measured with a G2201-i analyser since April 2014. CH_4 data from Heidelberg until April 2014 are taken from the Integrated non-CO_2 Greenhouse gas Observing System (InGOS, 2018) and the CO_2 data from GC measurements (S. Hammer, personal communication, 15 Feb 2021).

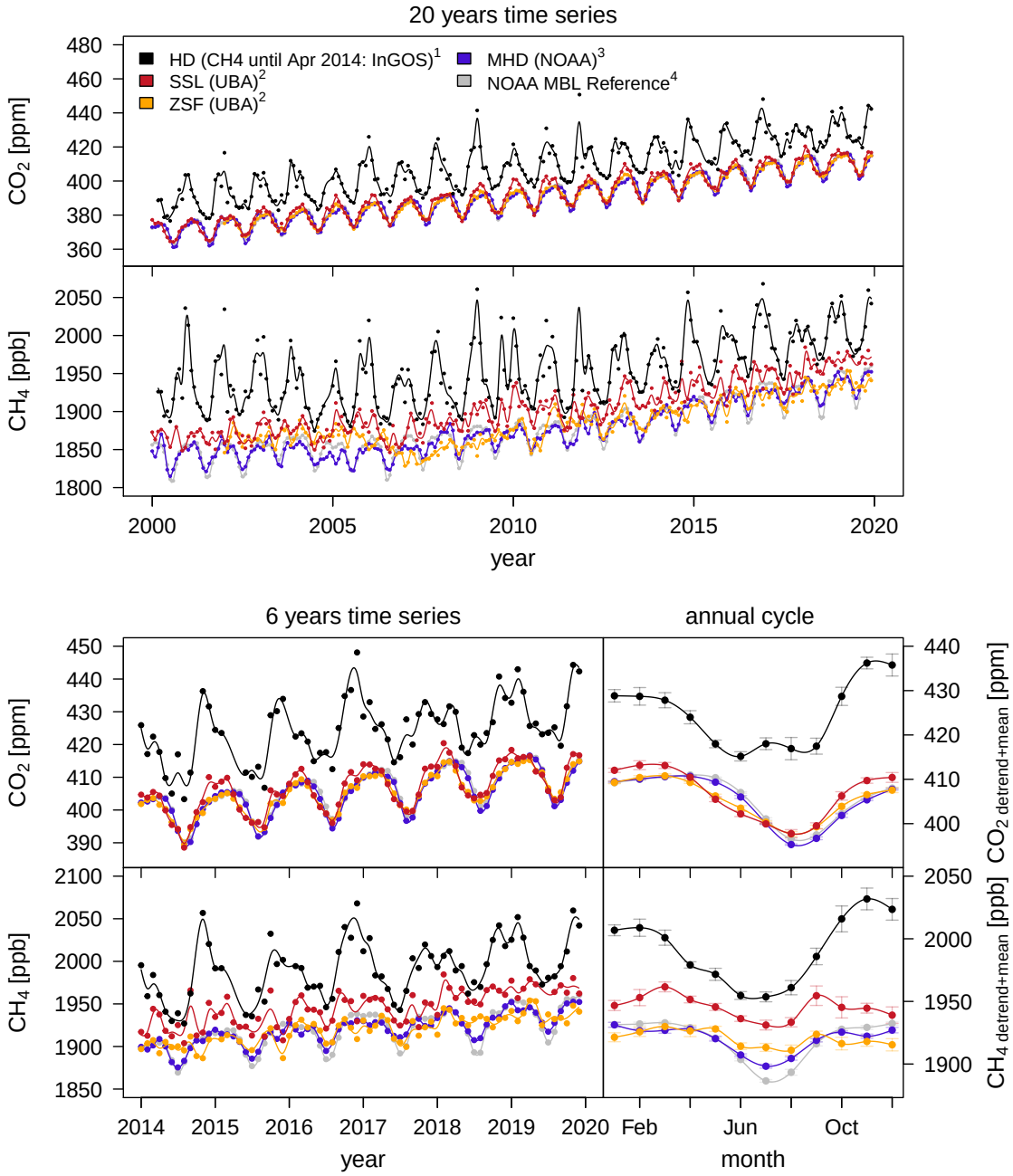

[1] Integrated non−CO_2 Greenhouse gas Observing System (InGOS): Ambient atmospheric methane observations from the ICOS/InGOS network 2000−2015, doi:10.18160/P7E9−EKEA, 2018.
[2] World Data Center for Greenhouse Gases (WDCGG): https://gaw.kishou.go.jp/, 2021.
[3] Dlugokencky et al. 2020 (https://doi.org/10.15138/VNCZ−M766) & Dlugokencky et al. 2021 (https://doi.org/10.15138/wkgj−f215)
[4] Dlugokencky et al. 2019 A & B (ftp://aftp.cmdl.noaa.gov/data/trace_gases/co2/flask/surface/) and ftp://aftp.cmdl.noaa.gov/data/trace_gases/ch4/flask/surface/)

Figure 3.4.: Long-term record of CO_2 and CH_4 mole fractions measured at Heidelberg, Schauinsland, Zugspitze and Mace Head and the corresponding annual cycles. In addition, the NOAA Greenhouse Gas (GHG) Marine Boundary Layer (MBL) Reference for the latitude range of 47 to 50 is shown.

The measured time series of CO_2 and CH_4 at each station show a trend and an annual cycle. To analyse both the digital filtering curve fitting program CCGCRV[3] which was developed by Kirk Thoning (Carbon Cycle Group, Earth System Research Laboratory (CCG/ESRL), NOAA) is applied to the monthly mean data. CCGCRV fits a polynomial equation combined with a harmonic function to the data and applies a filter to the residuals[4], thereby the time series can be separated into a trend and a detrended seasonal cycle. These mean annual cycles shown in this section are calculated by averaging the detrended seasonal cycles. To better visualise the differences between this mean annual cycles of the stations, the averaged CO_2 or CH_4 mole fraction is added. Trends in CO_2 or CH_4 for a specific time interval correspond to the slope of a linear regression fitted to the trend data given by CCGCRV for each month. Time series shown in this section contain, among measured data, the smoothed data given by CCGCRV in addition.

3.2.1. Continental excess

CH_4 and CO_2 measured at the stations Heidelberg, Schauinsland and Zugspitze show monthly mean mole fractions which deviate from each other (figure 3.4). These time series consist of a background signal and CH_4 emissions from the catchment area of the stations. The NOAA Greenhouse Gas (GHG) Marine Boundary Layer (MBL) reference for the latitude range of 47 to 50 °N (Dlugokencky et al., 2019 A; Dlugokencky et al., 2019 B) estimates the maritime background for CO_2 and CH_4 for these stations.

As Heidelberg is an urban station located in the Rhine Valley, the CO_2 mole fractions and also the CH_4 mole fractions are on average higher than the MBL reference between 2014 and 2020. The average difference is 19 ± 1 ppm in CO_2 (mean $\pm$ standard error of the mean) and 71 ± 3 ppb in CH_4.

The remote mountain stations Schauinsland (1205 m a.s.l.) and Zugspitze (2671 m a.s.l.), which are less influenced by local and regional sources, follow the observed CO_2 mole fractions of the MBL reference quite well with mean differences of 0.9 ± 0.4 ppm and -0.7 ± 0.3 ppm during the last six years. The average CH_4 mole fraction at Zugspitze is again comparable to the CH_4 MBL reference with a slight offset of -0.2 ± 2.0 ppb. However, at Schauinsland the measured CH_4 mole fraction is around 26 ± 2 ppb higher than the CH_4 MBL reference showing local influences in the surroundings of the station and of the Rhine Valley.

The station Mace Head is located on the west-coast of Ireland and measures the maritime background mole fraction when air is coming from the ocean. The CO_2 mole fractions measured at the background station Mace Head are nearly the same as the ones of the CO_2 MBL reference with an average difference of -0.5 ± 0.1 ppm. The CH_4 mole fractions at Mace Head show larger relative differences to the MBL reference than for CO_2. However, the average difference is only 0.1 ± 0.9 ppb and the deviations between

[3]CCGCRV: `https://www.esrl.noaa.gov/gmd/ccgg/mbl/crvfit/index.html` and `ftp://ftp.cmdl.noaa.gov/user/thoning/ccgcrv/`

[4]In this study we used 3 polynomial terms and 4 annual harmonic terms. The short and long term cutoff value for the low pass filter is 80 and 667 respectively.

Mace Head and MBL reference are much smaller than the difference of CH_4 between Mace Head and Heidelberg. Therefore, CH_4 measured at Mace Head can be used as background station for Heidelberg. In chapter 4 the measured $\delta^{13}CH_4$ values in Heidelberg are compared to the background station Mace Head to analyse the composition of the regional and local CH_4 sources influencing the measurements in Heidelberg.

3.2.2. Trends in CO_2 and CH_4

In the last 20 years the globally averaged annual mean CO_2 mole fraction has increased by 12 % from 369.71 ± 0.12 ppm in 2000 to 414.24 ± 0.12 ppm in 2020 (Tans and Keeling, 2021). This corresponds to an average growth rate of $2.2\,\mathrm{ppm\,yr^{-1}}$. At all measurement stations in figure 3.4 this increase in CO_2 of $2.2\,\mathrm{ppm\,yr^{-1}}$ is noticeable between 2000 and 2020. Additionally, the trend in CO_2 at the stations seems to increase slightly during the last years (2014 to 2020) to values between 2.4 and $2.6\,\mathrm{ppm\,yr^{-1}}$.

Like CO_2, the CH_4 mole fraction has increased since industrial times. However, a decrease in growth rate starting around the 1990s, a plateau in the CH_4 mole fractions from 1999 to 2006 and again an increase since 2007 is noticeable in the globally averaged annual mean CH_4 mole fractions (Dlugokencky et al., 1998 and Nisbet et.al, 2014). The latter is clearly visible in figure 3.4 for all measurement stations.

The recent increase in atmospheric CH_4 mole fraction between 2007 and 2014 is accompanied by a significant shift of δ^{13}C-CH_4 to more negative values (Nisbet et.al, 2016). This implies a change in the partitioning of CH_4 sources and sinks. Several scenarios are possible to explain these changes, like an increase in biogenic emissions from wetlands, ruminants or waste, an increase of fossil fuel emissions accompanied by a reduction of biomass burning or a reduction of CH_4 oxidation by OH radicals (Nisbet et.al, 2019 and Schaefer, 2019).

3.2.3. Annual variability

The CH_4 and CO_2 mole fractions measured at the different stations Heidelberg, Schauinsland and Zugspitze show annual (figure 3.4) and diurnal variations (figure 3.5). These are mainly determined by changes in the natural sources and sinks as well as in the behaviour of the planetary boundary layer.

The predominant natural sink of CH_4 is the oxidation with OH-radicals in the atmosphere. This reduction depends on radiation and is most effective in summer. As Mace Head is a background station, the annual cycle of CH_4 (33 ppb) is dominantly driven by the seasonal variations of this sink and inter-hemispherical airmass transport. The maximum mean CH_4 mole fraction occurs in winter (Oct to April). During spring the mole fraction decreases slightly to the minimum in late summer (Jun to August).

The seasonal variations at Heidelberg are much larger (78 ppb) and can only be explained partly by these processes. In autumn and winter high CH_4 mole fractions occur especially from October to December. These are caused by longer continental residence times of air masses due to high pressure systems and especially due to long lasting inversions as well as a much lower boundary layer height (Levin et al., 1999).

The planetary boundary layer (PBL) is the lowest part of the atmosphere where vertical mixing of air masses is strong. The height of the PBL and thus of the well-mixed layer depends on solar irradiance. Therefore, the height of the PBL is lower in winter than in summer (Glatzel-Mattheier, 1997). CH_4 emitted near the ground is thus mixed within a smaller volume leading to higher mole fractions.

In comparison to Heidelberg and Mace Head, the annual cycle of CH_4 at Schauinsland (31 ppb) and Zugspitze (16 ppb) is less prominent. Again the lowest values occur during summer (Jun-Aug), but another minimum is noticeable in winter. This second minimum occurs, because Schauinsland and especially Zugspitze are most of the time above the planetary boundary layer in winter so that more CH_4 depleted air from the lower free troposphere is measured. In summer, the stronger vertical mixing increases the influence of the more polluted lower boundary layer and higher CH_4 mole fractions are measured at Zugspitze and Schauinsland.

However, for CO_2 the annual variations visible in Heidelberg depend less on the planetary boundary layer height since the biosphere has a much stronger impact. The biosphere is the most important natural sink and source of CO_2. Especially the uptake of CO_2 due to photosynthesis determines the annual and diurnal cycle of CO_2. This uptake of CO_2 strongly depends on the seasons with a maximum in summer. At night plant and soil respiration increase the CO_2 mole fraction. At all sites the typical annual CO_2 cycle for the northern-hemisphere can be noticed which follows the growing season. The lowest CO_2 mole fractions occur during summer when the biospheric CO_2 uptake is strong and higher values are measured during winter.

The mean peak-to-peak amplitudes for Schauinsland, Zugspitze, Mace Head and the CO_2 MBL reference are similar showing values between 13 to 15 ppm. The lowest CO_2 mole fractions are measured on average in August. The strong decrease in CO_2 starts between April and May. At Schauinsland and Zugspitze this decrease is noticeable around one to two months earlier than in Mace Head. Such a phase-shift was already observed e.g. by Schmidt et al. (2003) and Yuan et al. (2019). It occurs since the continental stations Schauinsland and Zugspitze are closer to the biosphere than the maritime background station Mace Head. Thus, CO_2 at Schauinsland and Zugspitze reacts faster to the increase of photosynthetic activities leading to lower CO_2 mole fractions in May and June. As Schauinsland is less elevated than Zugspitze and surrounded by forest and meadows a faster CO_2 increase can be noticed there earlier. The recent data (2014 to 2020) also indicate that the continental biosphere still acts as net sink in early summer and as net source in autumn and winter as reported in a previous study by Levin (1987) and Schmidt et al. (2003).

At Heidelberg, the amplitude of the annual CO_2 cycle is 21 ppm and thus it is much larger than at the other stations. The strong decrease in the mole fraction due to CO_2 uptake by plants starts earlier (Mar), due to the earlier plant growth at lower altitudes. The lowest CO_2 mole fractions are again measured in summer. However, in July they slightly increase probably due to the drier conditions and therefore less CO_2 uptake by plants. In autumn, the CO_2 mole fraction increases and reaches the highest CO_2 values in winter (Oct to Feb).

3.2.4. Diurnal variability

In figure 3.5 the diurnal CH_4 and CO_2 cycles at Heidelberg, Schauinsland and Zugspitze are presented. The different colours correspond to the seasons with winter in dark-blue, spring in light-blue, summer in red and autumn in orange. To determine the diurnal cycles, the hourly mole fractions for each station are de-trended by subtracting the daily average from the corresponding hourly values in order to eliminate long term variations. Then the detrended cycles are averaged over each season. To take into account the annual cycle, the mean seasonal mole fractions are added to the seasonal diurnal cycles.

The diurnal cycle noticeable in atmospheric CH_4 mostly depends on the variations of the planetary boundary layer. During the day solar irradiance heats up the surface and thereby the ground-level air. Due to convection the air masses are vertically mixed. During the night, the surface is often cooled down, so that vertical mixing is suppressed in the lower 50 to 500 m and a so-called nocturnal inversion layer forms (Glatzel-Mattheier, 1997).

Low elevated stations such as Heidelberg are always within the PBL. For trace gases like CH_4, which are emitted usually near the surface, the mole fraction measured at

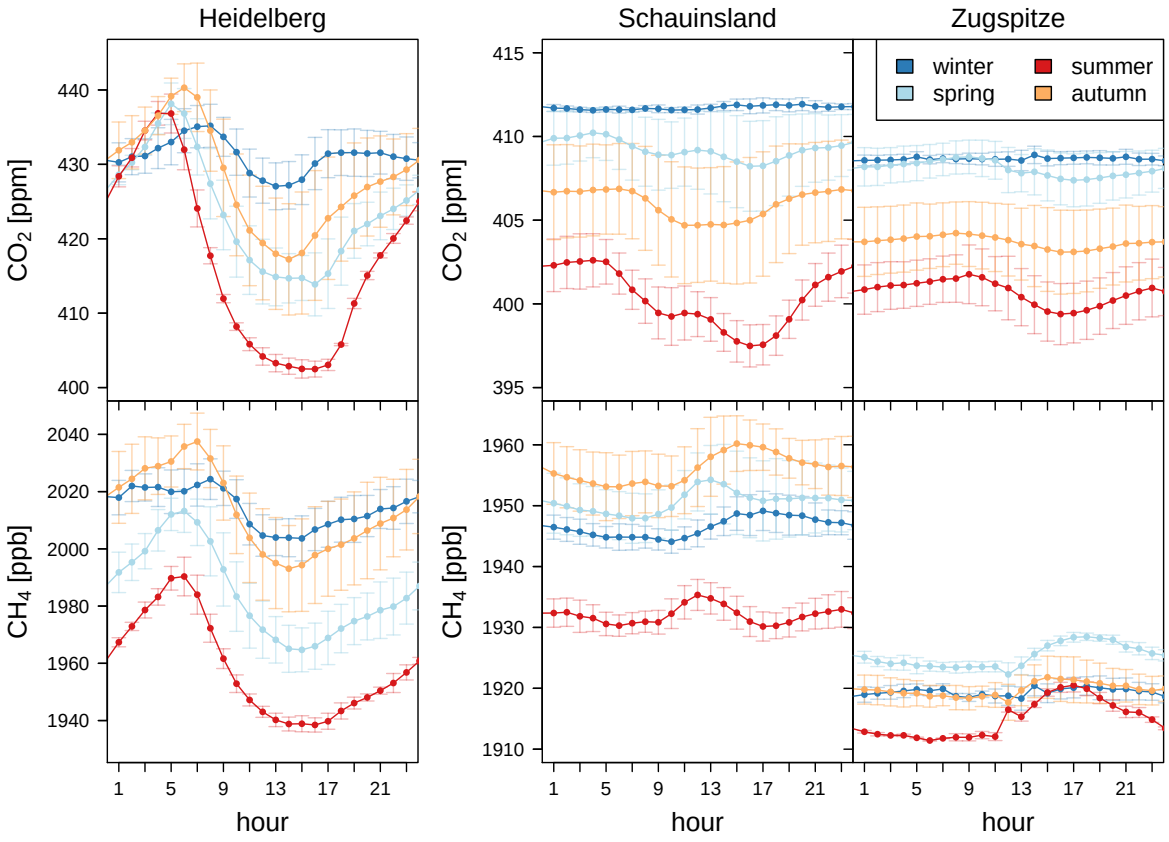

Figure 3.5.: Diurnal cycle of CH_4 mole fraction in Heidelberg, Schauinsland and Zugspitze. The colours correspond to different seasons. For each day the mean daily average is subtracted and the average value for each season is added.

low elevated stations is accumulated during the night in the inversion layer and has its maximum in the early morning (6-8 UTC). After sunrise, the nocturnal inversion layer disperses and the height of the well mixed layer increases. This transports air masses from the PBL to higher altitudes during the day. Due to vertical mixing with less polluted air masses, the mole fraction of trace gases within the PBL decreases until the afternoon (14-16 UTC). At sunset the night inversion layer forms again leading to an increase in CH_4. In winter the peak-to-peak amplitude of CH_4 in Heidelberg is 21 ppb and thus it is more than a factor of two smaller than in the other seasons (49 ppb, 52 and 44 ppb, spring to autumn). This is caused by lower vertical mixing of air masses during the day and long lasting inversions of several days in winter.

The diurnal cycles of CH_4 at Schauinsland and Zugspitze are different to the one measured at Heidelberg. These mountain stations are usually above the PBL at night measuring air masses from the lower free atmosphere. After sunrise the night inversion layer disperses and the height of the well-mixed layer increases. The normal variability of the PBL height can be increased near mountains by mountain venting, when up-slope winds increase the altitude of the PBL height locally (Kossmann et al., 1999). Therefore, the diurnal cycle of trace gases at Schauinsland and Zugspitze are determined by the alternating measurement of air masses from the PBL or the free troposphere.

A CH_4 peak around noon (10-17 UTC) is noticeable in the mean diurnal cycle at Schauinsland. This increase in CH_4 is caused by well-mixed air masses with higher CH_4 mole fractions from the valley which reach the stations. A similar peak occurs at Zugspitze, but later in the afternoon (12-19 UTC) since the station is at higher altitudes.

The CO_2 time series in Heidelberg, Schauinsland and Zugspitze show strong diurnal cycles which vary with the seasons. As the biosphere is the main driver of the diurnal CO_2 cycle, it is stronger in summer and less prominent in winter. In addition, at the station Zugspitze and Schauinsland the amplitude of the diurnal cycle is 8 to 23 times smaller than in Heidelberg, as the higher elevated stations are less influenced by the biosphere.

In Heidelberg, the decrease in CO_2 starts after sunrise, when the night-time inversion layer disperses and, more importantly, photosynthesis starts. Depending on the vegetation activity and thus on the season, the decrease differs from 8 ppm in winter to 34 ppm in summer. In the afternoon when solar irradiation and photosynthesis decrease and the impact of plant respiration increases, the CO_2 mole fraction rises again. The seasonal variations of sunrise and sunset are displayed in the position of maximum and minimum values.

In Schauinsland and Zugspitze the average diurnal cycles have very small amplitudes of 0.4 ppm in winter, because most of the time air from the lower free troposphere is measured. At Zugspitze there are nearly no plants in the surroundings of the measurement station. When air masses from the valley reach Zugspitze during the day around 12 to 19 UTC in summer, spring and autumn, a decrease in the CO_2 mole fraction is visible. These low CO_2 values occur since air from the valley is depleted in CO_2 by the CO_2 uptake of the biosphere. At Schauinsland the arrival of air masses from the Rhine-Valley can be noticed as a small peak in CO_2 especially visible in summer and spring around 10 to 17 UTC. This is different to observations done at Zugspitze. Since

Schauinsland station is surrounded by forests, grassland and pastures an additional CO_2 uptake from the biosphere during the day decreases the CO_2 mole fraction measured at Schauinsland even before air from the valley arrives. The CO_2 mole fraction of the uplifted air at Schauinsland is thus enriched in CO_2 compared to the measurements done at the stations a few hours earlier.

At Schauinsland and Zugspitze these CO_2 maxima and minima correspond well with CH_4 peaks in the mean diurnal cycle, as both changes are caused by the uplift of air from the planetary boundary layer.

4. Six years of CH_4 and $\delta^{13}CH_4$ measurements in Heidelberg

At the urban station Heidelberg the atmospheric CH_4 mole fraction and isotopic composition δ^{13}C-CH_4, hereafter referred to as $\delta^{13}CH_4$, have been measured continuously with a CRDS analyser G2201-i since mid June 2014. This new measurement device enables us to analyse CH_4 and $\delta^{13}CH_4$ at high temporal resolution of a few seconds.

So far, there are only few studies on atmospheric long-term measurements of $\delta^{13}CH_4$ that have been performed in-situ with high temporal resolution. Röckmann et al. (2016) and Menoud et al. (2020) for instance analysed $\delta^{13}CH_4$ in rural areas in the Netherlands during campaigns of five months or Assan et al. (2018) measured $\delta^{13}CH_4$ for two-weeks near an industrial site.

As an urban station CH_4 emissions around Heidelberg originate from quite different sources. In 2016 CH_4 was emitted mainly by the sectors agriculture (28 %), waste management (28 %) and natural gas distribution systems (26 %) (LUBW, 2016). Since each CH_4 source has a unique isotopic ^{13}C signature depending on the production processes and origin, the isotopic composition $\delta^{13}CH_4$ measured in the atmosphere contains information about the CH_4 sources contributing to the measured CH_4 mole fraction.

In this study a continuous six-year time series of the atmospheric CH_4 mole fraction and $\delta^{13}CH_4$ at the urban station Heidelberg is analysed to recognise and understand seasonal and long-term variabilities of regional and local CH_4 sources. These information about CH_4 emissions based on the atmospheric measurement can be used to verify the amount and composition of CH_4 emissions estimated in emission inventories. The knowledge of spatial and temporal variation of CH_4 emissions around the world and their composition from different types of sources is important to reduce CH_4 emissions effectively and to understand the influence of different CH_4 sources on climate change.

Thus, the mixture and flux of CH_4 sources in the catchment area of Heidelberg determined from atmospheric measurements are compared to the local emission inventories provided by the Landesanstalt für Umwelt Baden-Württemberg (LUBW, 2016) and the Emissions Database for Global Atmospheric Research (EDGAR v5.0, Crippa et al., 2019).

4.1. Measurement methods

4.1.1. Experimental set-up

The cavity ring-down spectroscopy (CRDS) G2201-i analyser (Picarro, Inc., Santa Clara, CA) continuously measures the mole fraction of $^{12}CH_4$ and $^{13}CH_4$ of ambient air. Additionally the carbon isotopic ratio $\delta^{13}CH_4$ is determined.

The scheme of the laboratory set-up is shown in figure 4.1 . Ambient air taken at the roof of the institute of Environmental Physics is dried with a cold trap cooled by a cryostat before entering the CRDS analyser through a 16-port rotary-valve (model: EMT2CSD16UWE, Valco Vici, Switzerland).

Especially for $\delta^{13}CH_4$ the internal water correction is insufficient for our analyser when measuring undried air (Hoheisel et al., 2019). For accurate results Rella et al. (2015) recommend to reduce the mole fraction of water vapour below 0.1 %. In our set-up, the cold trap normally reduces water vapour to mole fractions below 0.025 %. An exception occurred in 2018 when the mole fraction was only below 0.06 % when the cryogenic cooler did not work as expected.

During three periods (21 Dec 2018 to 7 Jan 2019, 18 Dec 2019 to 10 Jan 2020 and 18 Mar 2020 to 01 Jun 2020) the cold trap was replaced by a Nafion dryer set-up, when the regular and necessary exchange of the cold trap could not be provided. During these periods of time the mole fraction of water vapour was reduced to values below 0.08%. Tests have verified that the Nafion set-up has neither an effect on the measured CH_4 mole fraction nor on their isotopic composition.

The gas flow through the analyser is typically around 80 ml min^{-1} and is monitored by an electronic flowmeter (model: 5067-0223, Agilent Technologies, Inc., Santa Clara, CA). Every five hours the measurement of ambient air is interrupted to measure calibration and quality control gases for 20 minutes each. The flow used for calibration and quality control measurements is between 25 to 35 ml min^{-1}. A higher flow for ambient air measurements is chosen, to resolve shorter temporal variabilities. Tests have shown that no flow or pressure dependency occur in the used range. The measurement routine is temporarily interrupted, when the analyser is used in mobile campaigns or for the measurement of sample bags and cylinders.

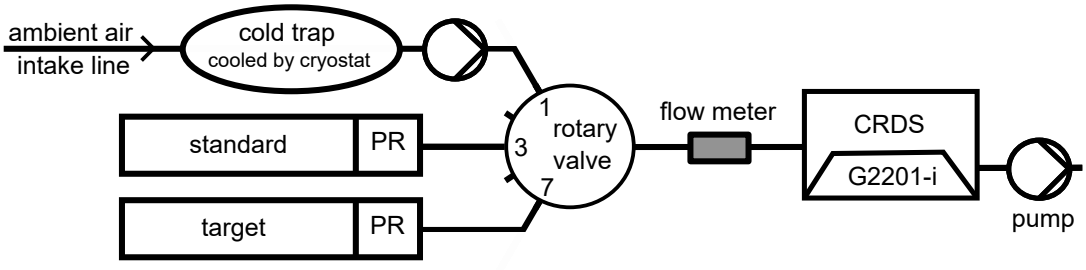

Figure 4.1.: Experimental set-up for ambient air measurements in Heidelberg.

4.1.2. Data treatment

The G2201-i analyser records CH_4 and $\delta^{13}CH_4$ data every 3.7 s, which we average to one minute values. Before analysing the minutely CH_4 and $\delta^{13}CH_4$ values of ambient air, we have to identify and exclude all invalid data. Invalid data points occur after a change of the measuring gas (ambient air, calibration or target gas). Therefore, the first five minutes after each change of the measuring gas are discarded to take into account the flushing of the cavity and stabilisation time. Thus, we can use, for example, only the last 15 minutes of the 20 minutes calibration gas measurement.

In addition, work at the experimental set-up can cause invalid data. Especially when work is done at the drying system – like changing the cold trap – room air can enter the set-up. This is visible as an increase in the water vapour mole fractions above 0.1 % and hence we exclude the corresponding data taken between four minutes before and after detection of the increased water vapour mole fraction. Furthermore, artefacts and outliers in the ambient air time series due to technical problems are excluded, too.

After we discarded all invalid data points, we characterise the performance of our analyser G2201-i and calibrate the measurements to assure accurate and precise results.

4.1.3. Instrumental performance

The precision of a measurement can be improved by measuring the same air over a longer time scale and then averaging over this time interval. This is limited, however, by the drift of the analyser which can be caused for instance by variations in the regulated temperature or pressure. The Allan variance (Allan, 1966; Werle et al., 1993) describes the regime where noise dominates the system and averaging over larger time intervals increases the precision. It also describes the regime to larger averaging periods where instrumental drift has the dominant influence. Thus, the Allan variance can be used as measure of the repeatability of a measurement over a certain time period.

The Allan variance for CH_4 and $\delta^{13}CH_4$ of the G2201-i analyser is calculated with equation 4.1 out of uncalibrated data from measurements of four different gas cylinders. These gas cylinders were analysed for at least 12 hours each in 2013 or 2019.

$$\sigma^2(\tau) = \frac{1}{2N} \sum_{i=1}^{N} [y(\tau)_{i+1} - y(\tau)_i]^2 \tag{4.1}$$

The sequential block averages $y(\tau)_i$ are calculated by dividing the data-set into N time intervals of equal length τ and averaging each. σ is called Allan standard deviation and is shown in figure 4.2 for different averaging periods.

Even for the high resolution data of one minute the Allan standard deviation of atmospheric CH_4 is below 0.11 ppb and thus more precise than the WMO compatibility goal of 2 ppb (WMO, 2020). The Allan standard deviation of $\delta^{13}CH_4$ for atmospheric CH_4 is however 0.94 ‰ for an averaging period of one minute and thus higher than our goal of 0.2 ‰ (WMO, 2020). The lowest σ for $\delta^{13}CH_4$ is determined for an averaging period around 60 min showing values of approximately 0.13 ‰.

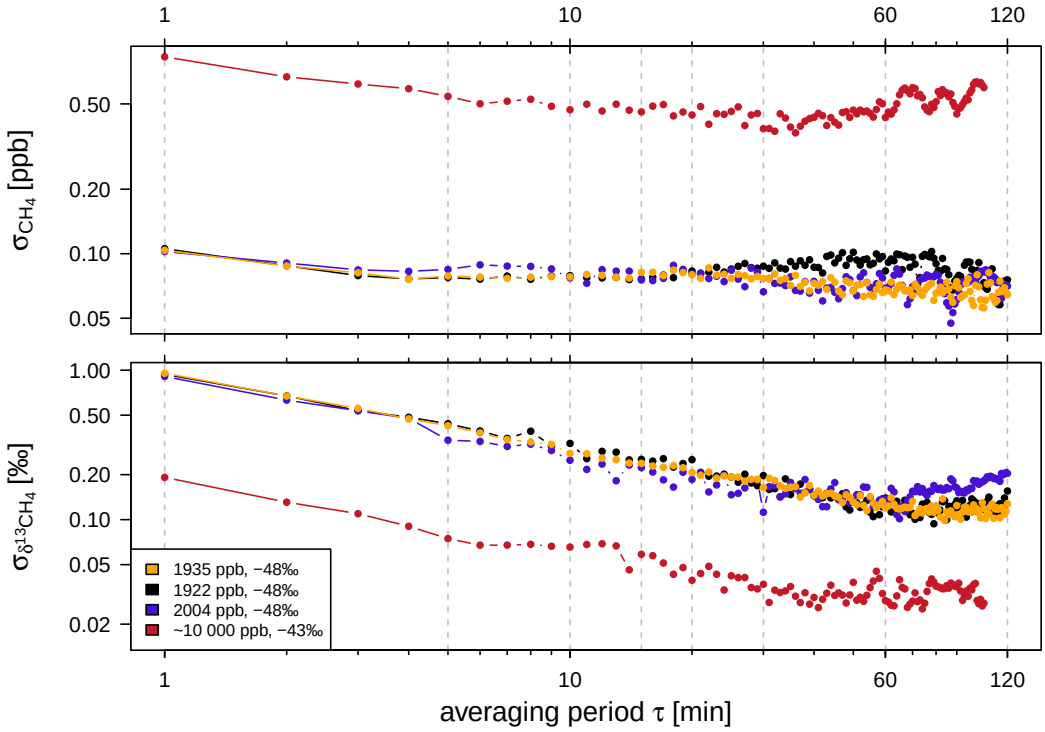

Figure 4.2.: Allan standard deviation of CRDS G2201 determined from four cylinders. One cylinder was measured in 2013 (orange) and the others in 2019 (black, blue, red).

For an averaging interval of 15 min, which is the time period of calibration and target gas measurements, the Allan standard deviation of CH_4 and $\delta^{13}CH_4$ is 0.08 ppb and 0.24 ‰ respectively for CH_4 mole fractions between 1922 and 2004 ppb. With higher mole fractions (10 000 ppb CH_4) the 15 min Allan standard deviation decreases for $\delta^{13}CH_4$ to 0.06 ‰ and increases slightly for CH_4 to 0.46 ppb.

Finally we can evaluate if the analyser changed its performance over the six years by comparing the Allan standard deviations between the former measurement in 2013 (orange) and the more recent ones in 2019 (blue and black data in figure 4.2). For CH_4 and $\delta^{13}CH_4$ no significant difference was found between the Allan standard deviations calculated with former and current cylinder measurements. Thus, the performance of the analyser did not degrade over the years.

4.1.4. Calibration strategy and long-term reproducibility

Every five hours the same calibration and target gases are measured. Ideally, the average of each 15 minute measurement would be the same within statistical fluctuations. However, the analyser shows long-term drifts which are corrected by calibration.

The calibration and the target gases (table 4.1) used in this study are compressed air with atmospheric mole fractions. In January 2019 the target gas cylinder was changed and in August 2019 the calibration gas cylinder.

Figure 4.3a shows the calibration cylinder measurements between 2014 and 2020. The

period of use	CH_4 [ppb]	$\delta^{13}CH_4$ [‰]
up to August 2019	1934.5 ± 0.1	−47.83 ± 0.05
from August 2019	2003.6 ± 0.4	−48.10 ± 0.07

Table 4.1.: CH_4 mole fraction and isotopic ratio of the two calibration gases used in Heidelberg.

two colours correspond to the two cylinders used. Each data point is the average over a 15 minute measurement of the cylinders. In addition, the grey and light-blue data-points display the monthly averaged values. Especially in the measurements of the first calibration cylinder an instrumental drift is noticeable over the five years. Furthermore, an offset between the measured and expected values occurs.

To compensate for the instrumental drift and offset, the minutely CH_4 mole fractions and the isotopic composition of CH_4 are calibrated using a single-point calibration (section A.1) and one of the calibration cylinders. To connect the CH_4 mole fractions to the WMO scale (Dlugokencky et al., 2005) and the measurements of the isotopic compositions of CH_4 to the Vienna Pee Dee Belemnite (VPDB) isotope scale (Sperlich et al., 2016), the calibration cylinders are analysed with a GC system (Levin et al., 1999) and the $\delta^{13}CH_4$ values are measured at the Stable Isotope Laboratory at Max Planck Institute for Biogeochemistry (MPI-BGC) in Jena. Therefore, two flasks were taken in 2014 and 2019 from the first calibration cylinder and in 2019 also from the second one and are then sent to MPI-BGC for analysis.

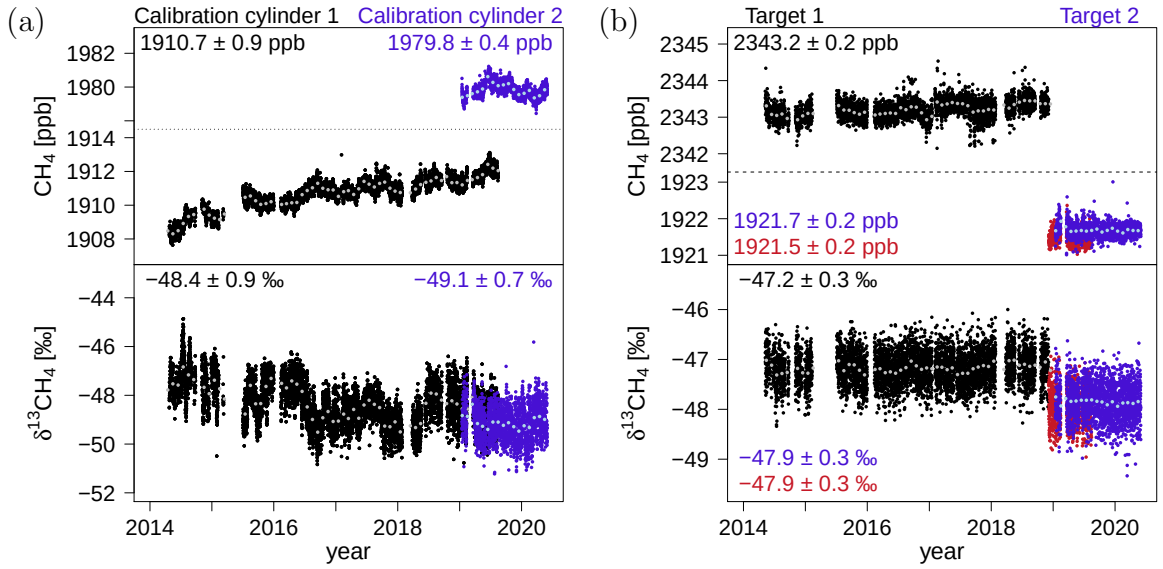

Figure 4.3.: CH_4 mole fraction and $\delta^{13}CH_4$ measurements of the calibration cylinders (a) and the calibrated target cylinder measurements (b). Calibration cylinder 1 and target 1 are shown in black and calibration cylinder 2 and target 2 in blue. The grey and light-blue data-points correspond to monthly averaged values. In addition, target 2 calibrated with calibration cylinder 1 is shown in red.

Long-term reproducibility

To verify that the applied calibration strategy successfully corrects instrumental drift, the long-term reproducibility of the CRDS G2201-i instrument is analysed. Therefore, the averages of each 15 minute target cylinder measurement period done every five hours between 2014 and 2020 is calculated (figure 4.3b). The mean values of the target 1 measurements calibrated by using calibration cylinder 1 are coloured black and the averages of target 2 calibrated with calibration cylinder 2 blue. Both target gases have a standard deviation of 0.2 ppb for CH_4 and 0.3 ‰ for $\delta^{13}CH_4$. Furthermore, no significant trend is noticeable in the mean CH_4 and $\delta^{13}CH_4$ values of the target between 2014 and 2020. Thus, the instrumental drift is corrected by the calibration.

For quality control the new calibration cylinder was measured parallel to the old one for nearly eight months. Therefore, measurements of target 2 are calibrated with calibration cylinder 1, too, and the mean values are displayed in red in figure 4.3b. The average difference between calibration with the first calibration cylinder and the second calibration cylinder of the target 2 measurements is 0.2 ppb. Since this deviation is one magnitude smaller than our goal of 2 ppb (WMO, 2020), it is negligible. $\delta^{13}CH_4$ shows no difference.

The evaluation of the target gas measurements have shown us, that the instrumental drift and offset is successfully corrected by the calibration strategy and no further trend is noticeable in the calibrated target measurements. Additionally, we have shown, that the change of the calibration cylinder did not bias our results. Therefore, we can conclude that all changes observed in the ambient air measurement are not induced by the instrumental drift or the calibration.

Recommended changes in the calibration strategy

The efficiency of the single-point calibration strategy especially depends on the duration and the frequency of calibration measurements. The measuring duration has a direct effect on the precision of the calibration data – since we use the average over each calibration measurement – and thus also on the calibrated data. The interval between calibration measurements determines how well the instrumental drift can be corrected.

The duration of the calibration and target gas measurements was chosen in 2013 when the CRDS G2201-i analyser was first characterised by Dinger (2014). Then, the Allan standard deviation of an atmospheric gas cylinder measurement was used to determine the optimum averaging period (black data in figure 4.2 and A.3). The averaging interval of 15 minutes was chosen taking into account all species (CH_4, $\delta^{13}CH_4$, CO_2 and $\delta^{13}CO_2$) measured with the G2201-i analyser. Thus, the duration of one calibration measurement has to be 20 minutes, since the the first five minutes of each cylinder measurement are discarded due to flushing and stabilisation time.

To test if the duration of the calibration and target gas measurements was chosen appropriately for our purpose, the Allan standard deviations are calculated for different gas cylinder measurements done in 2013 and 2019 (figure 4.2). The Allan standard deviation of CH_4 is below 0.11 ppm for at least all averaging intervals between 1 to 120 minutes and all atmospheric measurements. Thus even averaging intervals smaller than

15 minutes, and corresponding measurement intervals smaller than 20 min, result in CH_4 mole fractions which are precise enough for our purpose.

However, the precision of $\delta^{13}CH_4$ strongly benefits from an increase in the averaging and corresponding measurement time. To fulfil the extended WMO recommendation for $\delta^{13}CH_4$ of 0.2 ‰ (WMO, 2020) the averaging interval has to be at least 20 min. Therefore, to improve the $\delta^{13}CH_4$ measurements in future I recommend to increase the duration time of calibration and target gas measurements to at least 25 minutes.

In 2013 the length of the interval between calibration measurements was chosen to be five hours, in order to still be able to correct for medium-term variations such as a changing barometric pressure (Dinger, 2014).

The analysis of the target gas measurements has shown, that the long-term reproducibility of 15 min-mean CH_4 and $\delta^{13}CH_4$ values is 0.2 ppb for CH_4 and 0.3 ‰ for $\delta^{13}CH_4$. Thus, the CH_4 mole fractions show a sufficient reproducibility when a calibration measurement is done every five hours. For $\delta^{13}CH_4$ the value is, however, higher than our goal of 0.2 ‰. To test if shorter intervals between calibration measurements would give us noticeable better results for $\delta^{13}CH_4$, a 72 hour calibration gas measurement done in 2013 is analysed. Therefore, the cylinder measurement is divided into regular 15 min 'calibration' data and 'target' data in between varying from one to five hours. The calibrated 'target' data are averaged over 15 min to simulate cylinder measurements and the standard deviation of these simulated cylinder measurements are calculated. No significant improvement of the standard deviation of $\delta^{13}CH_4$ could be noticed. Thus, shorter intervals between calibration measurements are not necessary.

As a next step, we would like to test whether longer intervals between calibration measurements still successfully correct the instrumental drift. Therefore, the calibration and target gas measurements between 2014 and 2020 are used by calibrating the target measurements with only a part of the calibration measurements. The time interval between the chosen calibration measurements is at least x hours whereas x is varied from 5 hours to 90 days. The standard deviation of the averaged and calibrated target measurements increase for CH_4 and $\delta^{13}CH_4$ with longer time periods between the calibration measurements. However, the reproducibility of the CH_4 mole fraction is always below 0.5 ppb even for the simulations of one calibration measurement every two months. A much longer calibration cycle could therefore be chosen regarding CH_4. But the standard deviation of the averaged $\delta^{13}CH_4$ target measurements increases from 0.32 to 0.45 ‰ for time intervals of 5 to 80 hours between the calibration measurements. Therefore, we have to choose between a reproducibility which deviate less from our goal of 0.2 ‰ or fewer calibration measurements and thus less data and calibration gas loss. If we increase the calibration cycle lengths from 5 to 10 hours, the standard deviation of the mean target measurements only increases by 0.01 ‰. This small degrade in the reproducibility can be accepted, with the benefit of only half the usage of calibration gas and fewer data gaps in the ambient air time series due to calibration measurements.

In this study, the whole analysed time series is calibrated with calibration measurements done every five hours for 20 min including five minutes of stabilisation and flushing time. Although, the increase of the measurement duration to 25 minutes and the increase of the calibration cycle to 10 hours would improve our calibration strategy, we chose not

to change both within our study, to treat the whole time series equally.

However, I would recommend to change the calibration strategy in the future, when the main focus of the measurement should still be the analysis of $\delta^{13}CH_4$.

4.1.5. $\delta^{13}CH_4$ measurements of intercomparison cylinders

The $\delta^{13}CH_4$ values of the used calibration gases (table 4.1) were analysed at the Stable Isotope Laboratory at MPI-BGC in Jena to connect our measurements to the VPDB isotope scale (Sperlich et al., 2016). To compare the recent $\delta^{13}CH_4$ measurements done in Heidelberg with values measured at other laboratories, six intercomparison cylinders of air sampled at Neumayer station, Antarctica, are remeasured with the Picarro CRDS G2201 analyser. These six cylinders have already been analysed by the MPI-BGC with a GC-IRMS during an interlaboratory comparison (Umezawa et al., 2018).

Each cylinder is measured with the Picarro G2201-i for two hours at least twice and the first 30 minutes are excluded to take into account the stabilisation time. The average and standard error of the mean are then calculated for the last 90 minutes (table A.1). In table 4.2 the average $\delta^{13}CH_4$ values for the six comparison tanks are shown. In addition, the results of the MPI-BGC measurements (Umezawa et al., 2018) are displayed. The average difference between our results and the MPI-BGC measurements is 0.02 ± 0.05 ‰.

The $\delta^{13}CH_4$ measurements done in Heidelberg do not show a significant difference to the measurements done at MPI-BGC. Intercomparison between INSTAAR and MPI-

sample ID (collection date)	analysis date MPI-BGC	analysis date UHEI-Pic	$\delta^{13}CH_4$ MPI-BGC [‰]	$\delta^{13}CH_4$ UHEI-Pic [‰]	difference UHEI−MPI [‰]
GvN 88/20 (Jul 1988)	Jul 2013	May 2018 & May 2019	-47.66 (0.07, N=2)	-47.60 (0.29, N=3)	+0.06
GvN 92/12 (May 1992)	Jun 2013	May 2018 & May 2019	-47.40 (0.04, N=2)	-47.61 (0.19, N=4)	-0.21
GvN 96/03 (Feb 1996)	Jun 2013	May 2018 & Apr 2019	-47.18 (0.26, N=2)	-47.07 (0.23, N=3)	+0.11
GvN 99/14 (Dec 1999)	Jul 2013	Jun 2018 & Apr 2019	-47.23 (0.16, N=2)	-47.13 (0.02, N=2)	+0.10
GvN 06/14 (Sep 2006)	Jul 2013	May 2019 & Feb 2020	-47.19 (0.09, N=2)	-47.26 (0.23, N=3)	-0.07
GvN 08/03 (Mar 2008)	Jun 2013	Feb 2020	-47.35 (0.05, N=2)	-47.24 (0.37, N=2)	+0.11
average					+0.02 ± 0.05‰

Table 4.2.: $\delta^{13}CH_4$ measurements of six intercomparison cylinders. The $\delta^{13}CH_4$ values determined by MPI-BGC are taken from Umezawa et al. (2018) and are compared to our results. The difference in duplicate measurements is shown in parenthesis and the uncertainty of the average difference is given as standard errors of the mean.

BGC reveals a difference of 0.28 ± 0.01 ‰ (Umezawa et al., 2018). Therefore, when comparing the Heidelberg time series with measurements done by INSTAAR at Mace Head, the $\delta^{13}CH_4$ data from Mace Head are reduced by 0.28 ‰.

4.2. Continuous CH_4 and $\delta^{13}CH_4$ measurements

CH_4 and $\delta^{13}CH_4$ are measured continuously with a CRDS analyser in Heidelberg between April 2014 and May 2020. In figure 4.4 the daily mean CH_4 mole fractions are shown which varies between 1890 ppb and 2310 ppb with higher values in winter than in summer. The corresponding isotopic composition $\delta^{13}CH_4$ is between -49 and -47 ‰.

For further analysis the curve fitting program CCGCRV (see section 3.2) is applied to the monthly mean values to determine trends and seasonal variabilities. The CH_4 mole fractions show an increasing trend of 6.8 ± 0.3 ppb yr^{-1} and $\delta^{13}CH_4$ a decreasing trend of -0.028 ± 0.002 ‰ yr^{-1}.

In addition, a strong annual cycle with an amplitude (peak-to-peak height) of 78 ppb can be noticed in CH_4 (right panel of figure 4.4). The maximum mean CH_4 mole fraction occurs in late autumn (November). During winter and spring the mole fraction decreases slightly until it reaches a minimum in late summer (June to July). The seasonal variation of 78 ppb is only partly driven by oxidation with OH-radicals and inter-hemispherical airmass transport. The high CH_4 mole fractions in winter occur especially due to climatological conditions like long lasting inversions, a much lower boundary height and longer continental residence times of air masses due to high pressure systems as noted

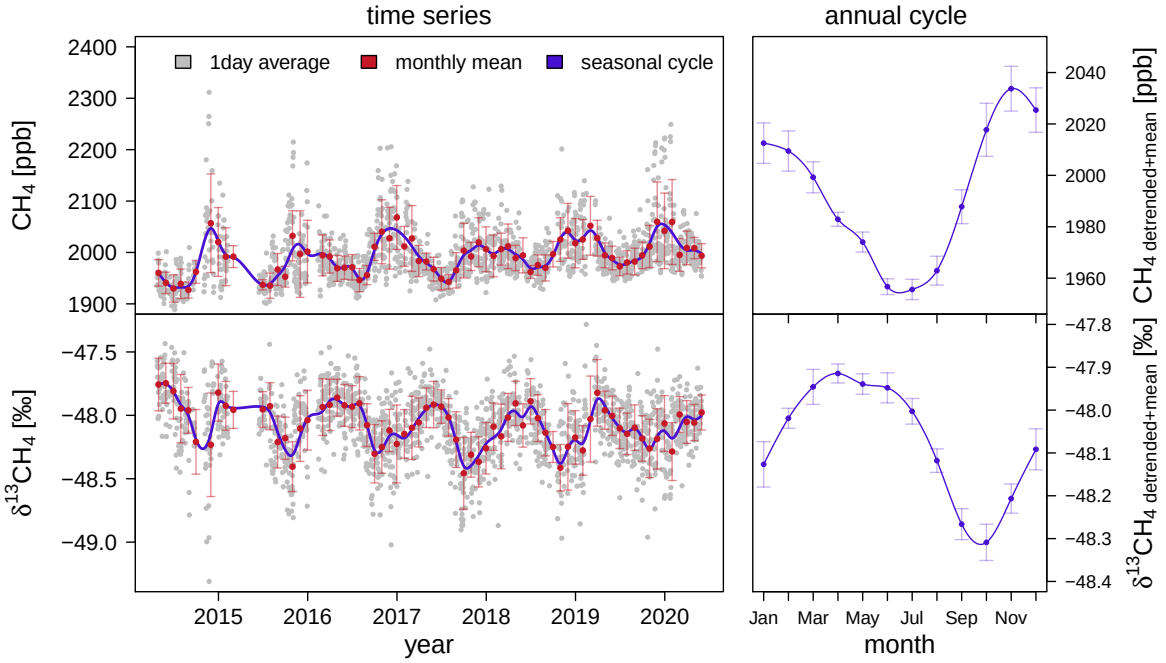

Figure 4.4.: Atmospheric CH_4 mole fraction and $\delta^{13}CH_4$ measured in Heidelberg and corresponding annual cycles.

before by Levin et al. (1999) for CH_4 measurements in Heidelberg during the 1990s.

Atmospheric $\delta^{13}CH_4$ in Heidelberg shows seasonal variations, too, with a mean amplitude of 0.4 ‰. Less enriched $\delta^{13}CH_4$ values of −48.3 ‰ occur in early autumn (September to October) and most enriched ones of −47.9 ‰ in spring (April to May). Since CH_4 sources contributing to the atmospheric CH_4 mole fraction have isotopic source signatures which can vary from more depleted values than atmospheric $\delta^{13}CH_4$ to more enriched source signatures, the annual cycle depends on the CH_4 source mixture of the background and of regional and local sources.

The CH_4 mole fraction as well as $\delta^{13}CH_4$ also show diurnal variations. The mean diurnal cycles for different seasons are presented in figure 4.5.

In the afternoon (15-16 UTC) the CH_4 mole fraction starts to increase over night, due to the lower mixing height. After sunrise the mole fraction decreases strongly due to radiation-related mixing and thus an increase of the mixing height. The mean diurnal cycles show strong seasonal differences with stronger variations in summer (52 ppb) and weaker ones in winter (21 ppb). In winter Heidelberg can be within the inversion layer for several days, so daily variations are less prominent. Since the diurnal cycle is strongly driven by the sun, the earlier sunrise and later sunset in summer compared to winter can be additionally noticed by the earlier decrease of CH_4 in the morning and later increase in the afternoon.

The diurnal variations of $\delta^{13}CH_4$ show slightly larger amplitudes in summer (0.18 ‰) and autumn (0.16 ‰) compared to winter (0.09 ‰) and spring (0.12 ‰). The lowest $\delta^{13}CH_4$ values occur around 7 to 10 UTC. $\delta^{13}CH_4$ increases during day to maximum values between 18 and 21 UTC and decreases at night. It seems that in summer, the isotopic composition is slightly more depleted in the morning compared to the other seasons.

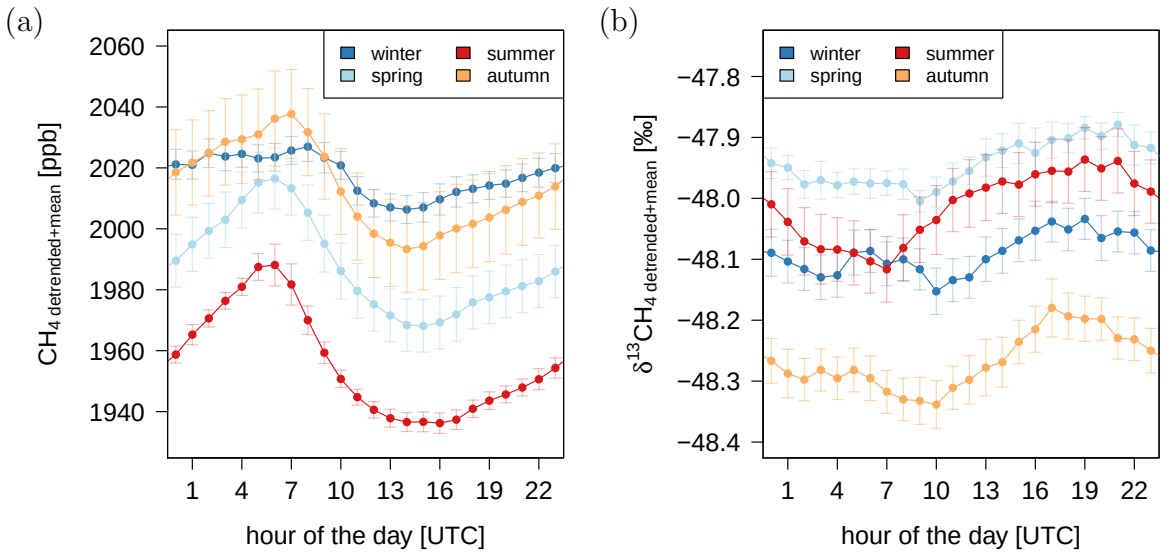

Figure 4.5.: Diurnal cycle of CH_4 and $\delta^{13}CH_4$ in Heidelberg. For each season the diurnal cycles of each month, which are detrended by subtracting the diurnal mean, are averaged and the mean CH_4 mole fraction or $\delta^{13}CH_4$ value for each season is added.

4.3. Comparison of $\delta^{13}CH_4$ with background and former measurements

To describe the influences of local and regional CH_4 emissions on our time series measured between 2014 and 2020, we compare our measurements to the clean air observation station Mace Head and to previous CH_4 and $\delta^{13}CH_4$ measurements carried out in Heidelberg between 1988 and 1997 (Levin et al., 1999).

In figure 4.6a the monthly mean CH_4 and $\delta^{13}CH_4$ measurements from Heidelberg and Mace Head are shown. Between 1988 and 1997 the CH_4 mole fraction was measured in Heidelberg with a GC system. Since the previous CH_4 mole fractions were reported on the CMDL83 scale, we take into account that the CH_4 mole fractions measured on the new WMO 2004 scale are a factor of 1.0124 ± 0.0007 larger (Dlugokencky et al., 2005). The isotopic composition of ambient air $\delta^{13}CH_4$ was analysed between 1992 and 1997 from bi-weekly integral sampling (Levin et al., 1999). To link the time series measured in the 1990s with the ones in this study (2014-2020), the CH_4 mole fraction between 2000 and 2014 from the InGOS project data base (InGOS, 2018) are displayed, too. The CH_4 mole fractions reported for Mace Head are provided by Dlugokencky et al. (2020) and the isotopic composition by White et al. (2018). The isotopic composition measured at Mace Head has to be subtracted by an offset of 0.28 ‰ to take into account the inter-comparison offset among the laboratories INSTAAR and MPI-BGC (Umezawa et al., 2018).

The two time periods from 1992 to 1998 and from 2014 to 2020, coloured in beige in figure 4.6a, are displayed in more detail in figure 4.6b. The corresponding annual cycles calculated out of the de-trended data and shifted by the average CH_4 or $\delta^{13}CH_4$ values are shown in the right panels. Again the curve fitting program CCGCRV (see section 3.2) is applied to the monthly mean values to determine trends and seasonal variabilities.

The CH_4 mole fraction measured in the 1990s did not follow the increasing trend observed at the background station Izaña (Levin et al., 1999) or Mace Head. In addition, the continental CH_4 excess at Heidelberg (Heidelberg minus Mace Head) strongly decreased between the 1990s and nowadays (2014-2020) to 71 ± 3 ppb which is only half of the value from the 1990s. These two observations can be explained by a change in the emission rate in the catchment area of Heidelberg. Such a strong decrease of the annual mean CH_4 emission rate between 1996 and 2001 was shown by Levin et al. (2011) who calculated the CH_4 fluxes with the Radon-Tracer method. This method is described in more detail in section 4.5

The recent measurements between 2014 and 2020 show that the increase of CH_4 mole fraction in Heidelberg with $6.8 \pm 0.3\,\mathrm{ppb\,yr^{-1}}$ is only slightly smaller than in Mace Head ($8.0 \pm 0.1\,\mathrm{ppb\,yr^{-1}}$). This seems to support the assumption that the CH_4 emissions in the catchment area of Heidelberg did not decrease strongly during the last years, which would continue the trend found by Levin et al. (2011) between 2001 and 2008.

The analysis of the isotopic signature of CH_4 can give us information about the composition of CH_4 emissions. In the 1990s the $\delta^{13}CH_4$ values in Heidelberg decreased strongly

(a)

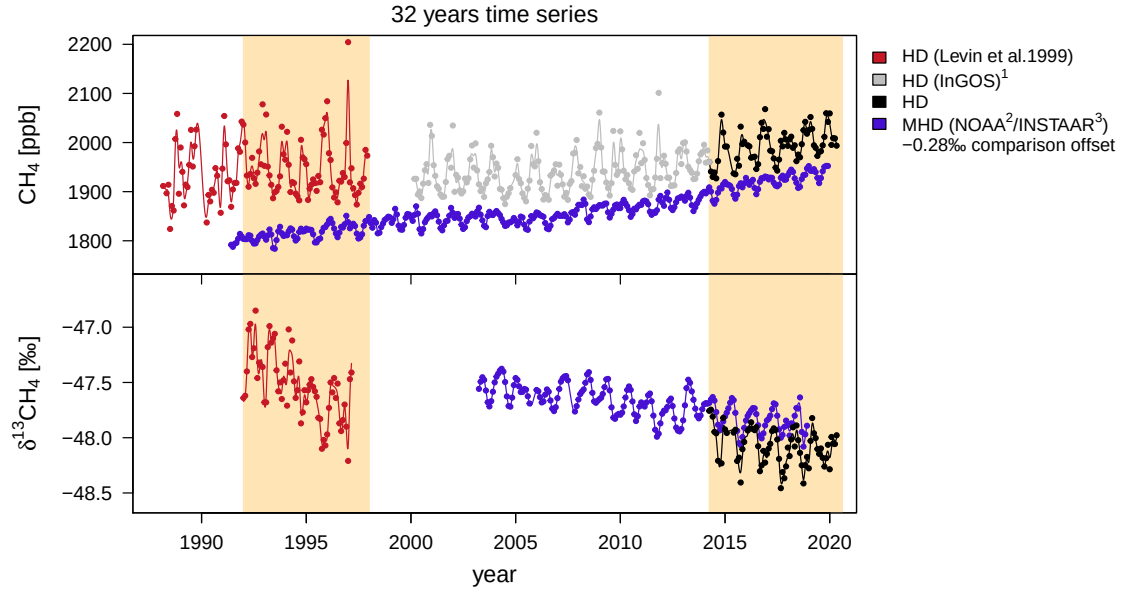

(b)

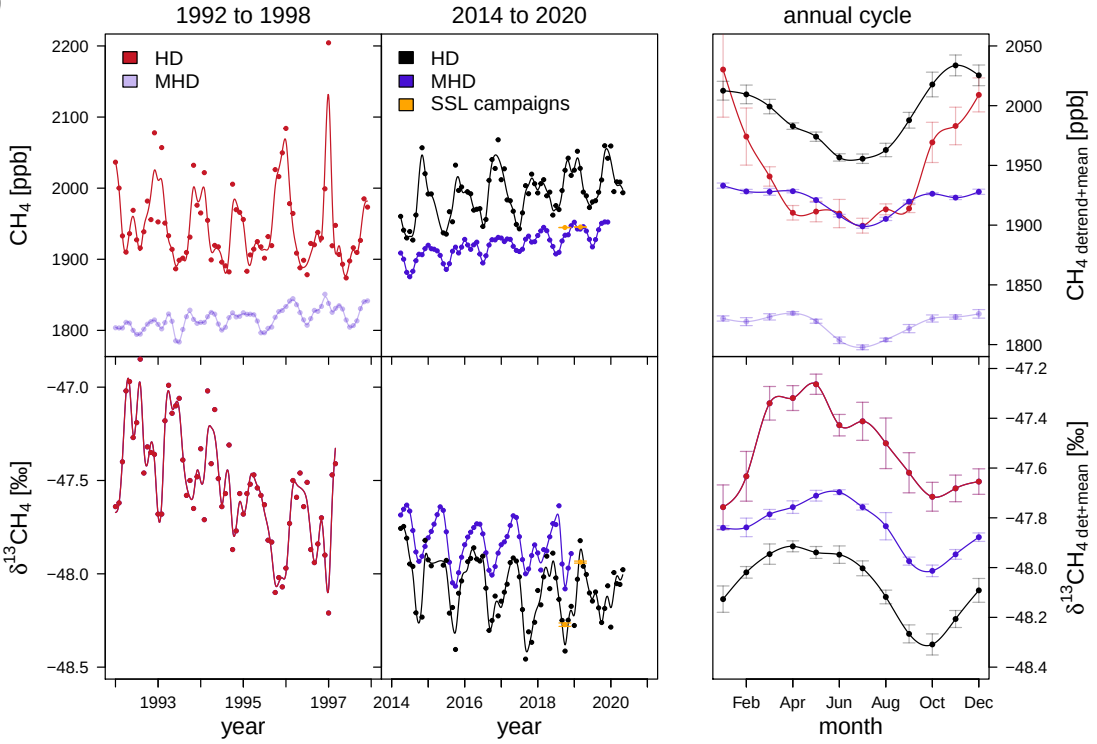

[1] InGOS (2018) (https://doi.org/10.18160/P7E9−EKEA)
[2] Dlugokencky et al. 2020 (https://doi.org/10.15138/VNCZ−M766) & Dlugokencky et al. 2021 (https://doi.org/10.15138/wkgj−f215)
[3] White et al. 2018 (ftp://aftp.cmdl.noaa.gov/data/trace_gases/ch4c13/flask/)

Figure 4.6.: Comparison of CH_4 mole fraction and $\delta^{13}CH_4$ measurements done in Heidelberg between 2014 and 2021 with former measurements in the 1990s and with measurements done at the marine background station Mace Head and the mountain station Schauinsland. In panel (a) the monthly mean CH_4 mole fraction and $\delta^{13}CH_4$ values of the last 32 years are shown. Panel (b) presents the former and current measurements from the time periods coloured beige in panel (a). In addition, the annual cycles are displayed on the right panels.

with $-0.14\,‰\ \mathrm{yr}^{-1}$, while samples from Izaña only show trends which are more than a factor of three smaller (Levin et al., 1999). This difference in the $\delta^{13}CH_4$ trends points to a change in the composition of CH_4 emissions in the catchment area of Heidelberg. Levin et al. (1999) attribute this change to a reduction of CH_4 emissions from fossil sources (mainly coal mining) and from cattle breeding. The situation is different for recent measurements (2014 to 2020). The current Heidelberg data only show a small trend in $\delta^{13}CH_4$ of $-0.028 \pm 0.002\,‰\,\mathrm{yr}^{-1}$ which is similar to the one observed at Mace Head. Therefore, the CH_4 source mixture in Heidelberg seems to be relatively constant during the last years.

The isotopic composition of CH_4 measured in Heidelberg (2014 to 2020) is on average $0.24 \pm 0.02\,‰$ more depleted than in Mace Head. Higher CH_4 mole fractions in combination with a more depleted isotopic composition $\delta^{13}CH_4$ indicate that the continent is a net CH_4 source of more biogenic origin. This agrees with the report of CH_4 emissions in Germany. In 2018 62 % of CH_4 emissions in Germany result from agriculture, especially cows, and 17 % from the waste management (UBA, 2021). Both emission sectors have more depleted isotopic source signatures than the mean atmospheric $\delta^{13}CH_4$ values at Mace Head.

The annual cycles of CH_4 and $\delta^{13}CH_4$ are displayed on the right panels in figure 4.6b. Both CH_4 and $\delta^{13}CH_4$ measured in Heidelberg show larger annual amplitudes (peak-to-peak height) in the 1990s than in the 2010s, whereas in Mace Head the amplitude of the annual CH_4 cycle does not change much. Especially in winter the CH_4 mole fractions measured in Heidelberg in the 1990s are high and $\delta^{13}CH_4$ seems to be especially enriched in spring.

In Heidelberg and in Mace Head the most depleted $\delta^{13}CH_4$ values occur from September to October and the most enriched ones from April to June. Therefore, the general annual variations of $\delta^{13}CH_4$ are similar to Mace Head and are thus reflecting the background CH_4. However, some differences occur which can give us information about regional and local CH_4 sources. In Mace Head the amplitude of $\delta^{13}CH_4$ is slightly lower ($0.08 \pm 0.05\,‰$) than in Heidelberg. In spring (Feb to Mar) the differences of $\delta^{13}CH_4$ values between Mace Head and Heidelberg are smaller than the annual average and in Sep to Oct larger. This indicates that in Heidelberg the regional and local CH_4 emissions in spring are more thermogenic and in autumn more biogenic. To analyse the seasonal variability of CH_4 sources in the catchment area in more detail, we study mean isotopic source signatures and emission inventories in the following sections.

Figure 4.6b shows $\delta^{13}CH_4$ measured during two campaigns at Schauinsland. The first was carried out for one month in Nov/Oct 2018 and the second for one month in Feb/Mar 2019. A clear difference ($0.4 \pm 0.1‰$) between the mean isotopic composition $\delta^{13}CH_4$ for summer and winter is measured at Schauinsland (yellow points). Both values match the isotopic composition $\delta^{13}CH_4$ measured in Heidelberg quite well, even though the corresponding CH_4 mole fractions are similar to the ones measured at Mace Head. The two measurement campaigns at Schauinsland are described in more detail in appendix C.3.

4.4. Isotopic signature of CH_4 sources calculated with atmospheric measurements

The measurement of the isotopic composition of CH_4 in ambient air, gives us the possibility to analyse the CH_4 sources contributing to the CH_4 mole fractions measured in Heidelberg. CH_4 enhancements measured in Heidelberg can originate from different sources with isotopic source signatures ranging between -13 to -70 ‰, depending on the origin and the production processes. CH_4 emitted by biogenic sources like dairy cows and waste water treatment plants is more depleted than the average atmospheric $\delta^{13}CH_4$ value at Heidelberg (-48 ‰). The isotopic source signature of thermogenic sources from the natural gas distribution system or even pyrogenic sources like traffic are, however, less depleted.

Figure 4.7 shows three typical dependencies of CH_4 and $\delta^{13}CH_4$ in the Heidelberg time series. During a time period with increasing CH_4, the corresponding $\delta^{13}CH_4$ measured in ambient air can decrease (black) when less enriched CH_4 e.g. from dairy cows is present, or it can increase (blue) when more enriched CH_4 e.g. from natural gas facilities is involved. The third possibility is a constant isotopic signature during an increase in CH_4 mole fraction (red) which means that CH_4 with nearly the same isotopic composition as the background is emitted, most likely due to a gas mixture of different sources.

4.4.1. Miller-Tans and Keeling plot method

The isotopic source signature is typically determined by the Keeling plot method (Keeling, 1958, 1961) or Miller-Tans method (Miller and Tans, 2003).

For both, we assume that the measured mole fraction (C_{obs}) consists of an atmospheric background (C_{bg}) and additional CH_4 (C_s) emitted by a single source.

Following Miller and Tans (2003) the balance equations can be written as:

$$C_{obs} = C_{bg} + C_s \qquad \text{and} \tag{4.2}$$

$$\delta^{13}C_{obs} \cdot C_{obs} = \delta^{13}C_{bg} \cdot C_{bg} + \delta^{13}C_s \cdot C_s \tag{4.3}$$

Rearranging these equations in two different ways yields either the Keeling plot method

$$\delta^{13}C_{obs} = \frac{C_{bg}}{C_{obs} \cdot (\delta^{13}C_{bg} - \delta^{13}C_s)} + \delta^{13}C_s \tag{4.4}$$

or the Miller-Tans method

$$\delta^{13}C_{obs} \cdot C_{obs} = C_{bg} \cdot \left(\delta^{13}C_{bg} - \delta^{13}C_s\right) + \delta^{13}C_s \cdot C_{obs}. \tag{4.5}$$

In the Keeling plot method the observed $\delta^{13}CH_{4_{obs}}$ values are plotted against $CH_{4_{obs}}^{-1}$. The isotopic source signature is then the intercept of a linear regression line. The Miller-Tans method is similar. Here, $\delta^{13}CH_{4_{obs}} \cdot CH_{4_{obs}}$ are plotted against $CH_{4_{obs}}$ and the slope of a regression line corresponds to the source signature.

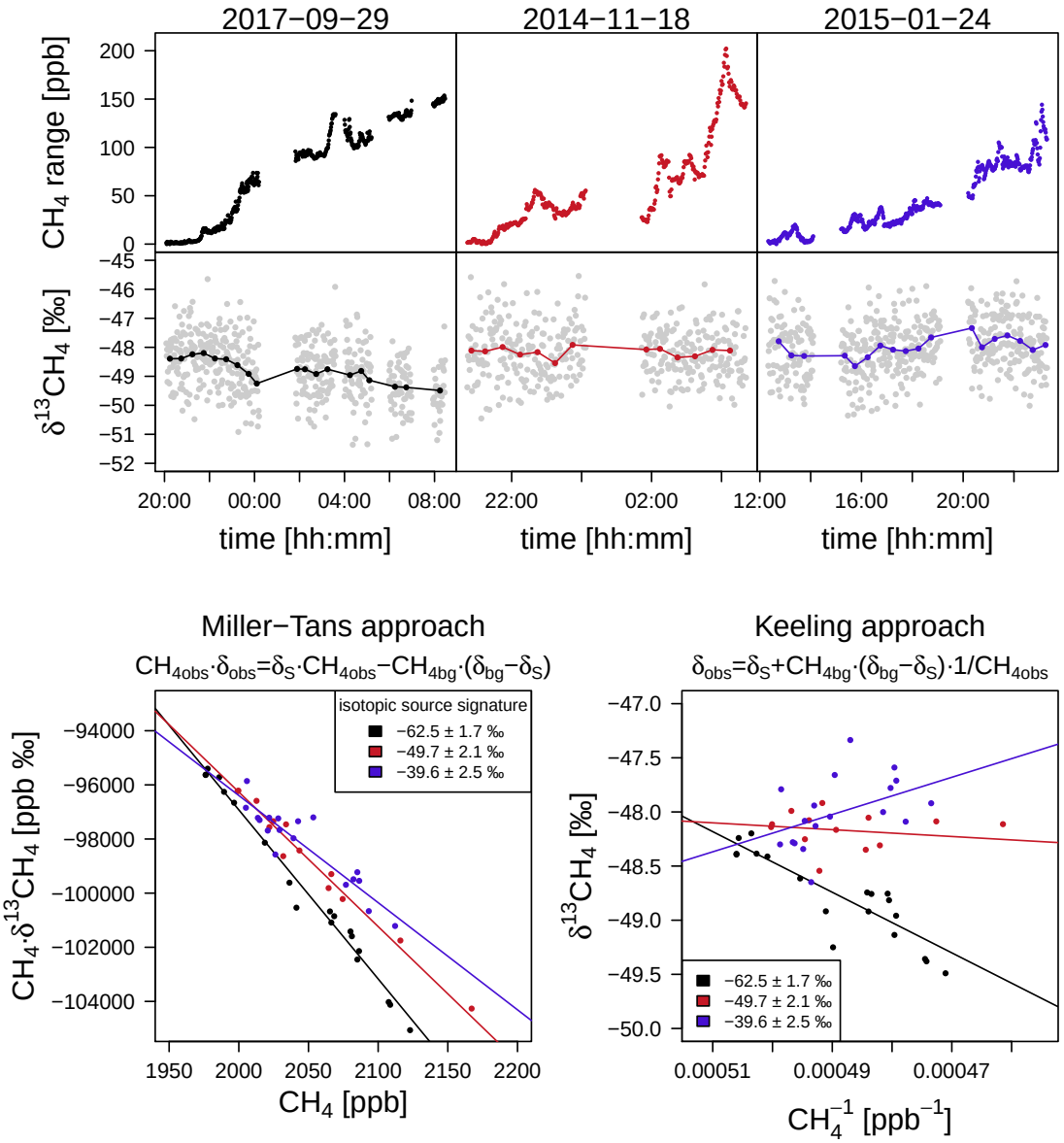

Figure 4.7.: Three typical dependencies of CH_4 and $\delta^{13}CH_4$ in the Heidelberg time series.

In most cases an increase in the atmospheric CH_4 mole fraction will be a mixture of CH_4 emitted by different sources. The determined isotopic source signature thus describes a mean isotopic signature from several sources depending on their respective emission rate.

In different studies both methods are used successfully for isotopic identification of CH_4 sources. The Keeling plot method by Röckmann et al. (2016) and Menoud et al. (2020) and the Miller-Tans method by Assan et al. (2018) for instance.

In the bottom of figure 4.7 the Miller-Tans and Keeling methods are shown for the three typical events measurable in Heidelberg. For the linear regression the York fit (York et al., 2004) is used. York's method minimises the weighted distance between

data points and fitted line, thereby taking into account uncertainties in both x and y-coordinates. Tests have shown that for our application there is no difference between the Miller-Tans or the Keeling plot method when using the York fit. The compatibility of these methods was also shown by Zobitz et al. (2006).

Therefore, in the following this study uses the Miller-Tans method in combination with the York fit. This method is applied to the minutely CH_4 and $\delta^{13}CH_4$ values for which the Allan standard deviation is used as measure of the uncertainty. The uncertainty of the source signature determined by the Miller-Tans method and the York fit strongly depends on the precision of the analyser and the peak height of CH_4 above background (Hoheisel et al., 2019). To get accurate results we apply two criteria to our data: the CH_4 range has to be larger than 100 ppb and the fit error on the slope of the regression line has to be smaller than 2.5 ‰.

4.4.2. Determination of isotopic source signatures

To get a first impression of the mean isotopic source signature of CH_4 sources in the catchment area of Heidelberg, the Miller-Tans method is applied to the whole minutely time series of six years. The resulting average isotopic source signature is -53.44 ± 0.02 ‰ (figure 4.8). The given uncertainty is the fit error on the slope which is small due to the large amount of data points. Uncertainties caused by the fact that the background is not stable during the whole time period are not included. The determined mean source signature is more depleted than the mean isotopic composition $\delta^{13}CH_4$ of ambient air measured at Heidelberg of around -48 ‰. More depleted biogenic CH_4 sources like waste management systems and agriculture contribute most to CH_4 emitted in the catchment area of Heidelberg. Calculating the mean isotopic source signatures with hourly, daily or monthly averaged data instead of the minutely ones, do not substantially change the result and the values range from -53.4 to -53.7 ‰.

The comparison of atmospheric CH_4 and $\delta^{13}CH_4$ measured in Heidelberg and at the background station Mace Head indicates that the composition of CH_4 emissions in the catchment area of Heidelberg shows seasonal variations and no strong trend over the last years. Therefore, the mean isotopic source signature for each month, night and event is determined for the six years record measured in Heidelberg to verify these assumptions. Depending on the time scale for which the mean source signature should be calculated, the Miller-Tans method is applied to different data-sets. Larger time intervals of one month have the advantage, that the CH_4 mole fractions cover a large range which increase the precision of the results of the regression line. On the other hand, uncertainties occur since the background is probably not constant for the whole time, which can be assumed for shorter time intervals of some hours. Thus, different approaches for the choice of the data-sets are tested. The most promising ones are explained in more detail in the following.

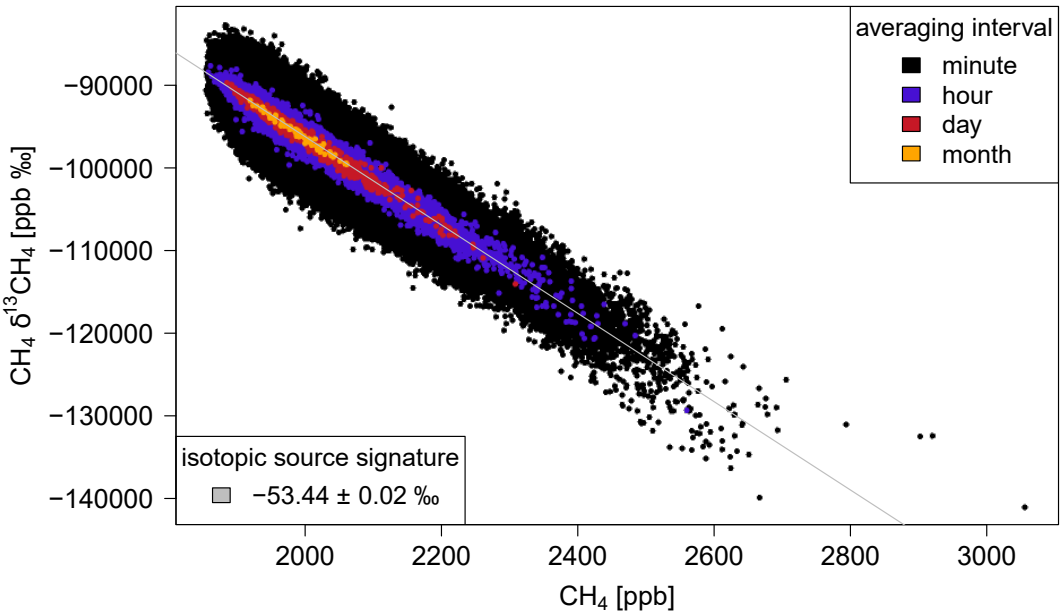

Figure 4.8.: Miller-Tans plot to determine the isotopic source signature out of all Heidelberg measurements. In addition to the minutely values, the hourly, diurnal and monthly averages are shown.

Monthly approach

To learn more about possible seasonal variations in the mean isotopic source signature and thus the CH_4 source mixture the Miller-Tans method is applied to each month of each year. Again, the minutely averaged data are used. The isotopic source signatures determined in this way are shown in black in figure 4.9a. They vary between -47 and $-61\,‰$ with an average of $-53.9 \pm 0.3\,‰$ (mean $\pm$ standard error of the mean). Furthermore, the data show an annual cycle which is displayed in figure 4.9b in black, too, with more depleted isotopic source signatures in summer and less depleted ones in winter. When analysing each year separately, we find that the annual cycle can be noticed in most of them and is thus no artefact of the average over all years. However, since the Miller-Tans approach assumes a constant background which is probably not given for the monthly values, we use another approach where the Miller-Tans method is applied to smaller time intervals.

Night-time approach

The CH_4 mole fractions show an increase at night, when the CH_4 emissions accumulate in the inversion layer. As we can assume, that the background stays constant during the night-time hours, we determine the mean source signature of the contributing CH_4 sources for each night by applying the Miller-Tans method to all data between 17 and 7 CET. To achieve good results, only night-time data-sets are used which fulfil our two

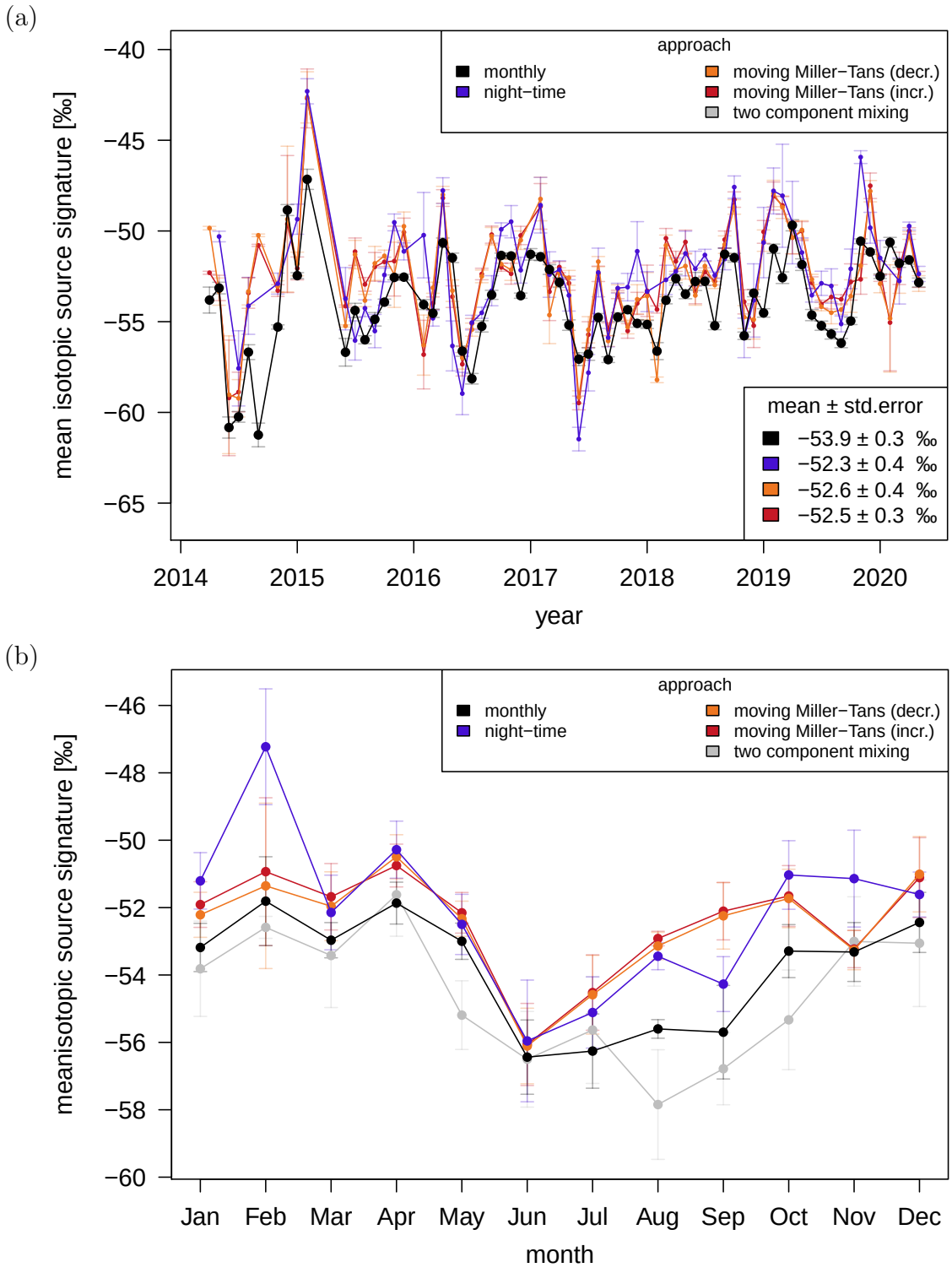

Figure 4.9.: The monthly averages (a) and the annual cycle (b) of the mean isotopic source signatures determined from the monthly data-sets (black), the night-time increase data-sets (blue) and the moving Miller-Tans approach. For the latter we start with 12 hour time windows and decrease them if the criteria are not fulfilled (orange) or we start with a one hour time window and increase it (red).

criteria of a CH_4 range of more than 100 ppb and a fit error of the regression for the slope smaller than 2.5 ‰. These criteria were only fulfilled by 21 % (460) of the night-time data-sets. The determined mean isotopic source signatures for each day vary between −75 ‰ and −32 ‰. Annual and seasonal variations in the source signature are evaluated by averaging the mean night-time source signatures for each month and by calculating the annual cycle (figure 4.9, blue lines).

The night-time approach shows similar monthly values than the monthly approach and again an annual cycle with more depleted CH_4 in summer. The average mean source signature of -52.3 ± 0.4 ‰ is however slightly more enriched than the one determined with the monthly approach.

By the interpretation of monthly mean source signatures calculated with the night-time approach we need to keep two aspects in mind. First, we used the same fixed time interval for the night-time increase of CH_4 for each day and secondly CH_4 emitted during the day is not taken into account. To test the influence of the first point, we determined the time window in which CH_4 increases for each night individually instead of using a fixed night-time window. Therefore, several automatic approaches to identify these night-time increases in the time series were carried out. For most nights these approaches recognised the CH_4 increase correctly, but unfortunately in several cases they did not. Since the determined monthly averaged isotopic source signatures did not vary strongly between the automatic approaches and the one using the fixed time window, we chose the latter one.

Moving Miller-Tans approach

Due to the high temporal resolution of our CH_4 and $\delta^{13}CH_4$ measurements, we can go one step further and determine the isotopic source signatures with a moving Miller-Tans approach similar to the ones used by Röckmann et al. (2016), Menoud et al. (2020) or Assan et al. (2018).

As we are interested in short term events, a time window with a fixed lengths of one hours is shifted over the 1 min data-set with time steps of one minute. Thus, for each minute t_i the mean isotopic source signature is calculated out of a one hour time period centred on t_i with the Miller-Tans method and the York fit. In addition, the moving Miller-Tans approach is applied 11 more times with different time intervals ranging from 2 to 12 hours. To select appropriate mean isotopic source signatures, again only those results are used which fulfil our two criteria of a CH_4 range larger than 100 ppb during the time window of one hour and a fit error of the slope smaller than 2.5 ‰. If these criteria are not fulfilled for t_i, we use results for t_i calculated with a time window which is one hour larger. This is continued until both criteria are fulfilled or the length of the time window reaches 12 hour. If the criteria are still not fulfilled for the 12 hour time interval, the result is excluded.

Thus, with this approach of a moving time window daytime and night-time CH_4 emissions are taken into account and due to small time windows between 1 and 12 hours we can assume that the background is constant.

With the moving Miller-Tans approach, we achieve results for 18 % of the minutely

values. Taking into account that several mean isotopic source signatures can describe the same event, we average over all minutely values until a gap of more than one minute occurs where the determined source signature does not fulfil our criteria.

For the six years between April 2011 and May 2020 the mean isotopic source signatures of 769 events are ranging between −77 and −30 ‰ with an average of −52.5 ± 0.3 ‰. Again, an annual cycle with more depleted values in summer is visible (figure 4.9, red lines).

Furthermore, we use the more common method in the moving Miller-Tans approach and thus start with a 12 hours time window. Then the time interval is reduced in hourly steps when our two criteria are not fulfilled The monthly averaged source signature and the annual cycle calculated out of these results are shown in orange in figure 4.9. There is no significant difference between the values of the two moving Miller-Tans scenarios (red and orange).

Simple two component mixing model

Instead of the Miller-Tans method, a two component mixing model similar to the one used by Levin et al. (1999) can be used to determine the mean isotopic source signature of CH_4 in the catchment area of Heidelberg. Therefore, a background reference is needed. In this study, we use the CH_4 mole fraction and $\delta^{13}CH_4$ values measured at Mace Head as background. The mean isotopic source signature can then be calculated as

$$\delta^{13}\mathrm{C}_{\mathrm{source}} = \frac{\delta^{13}\mathrm{C}_{\mathrm{HD}} \cdot \mathrm{C}_{\mathrm{HD}} - \delta^{13}\mathrm{C}_{\mathrm{MHD}} \cdot \mathrm{C}_{\mathrm{MHD}}}{\mathrm{C}_{\mathrm{HD}} - \mathrm{C}_{\mathrm{MHD}}} \tag{4.6}$$

The determined monthly mean isotopic source signatures vary between −47 and −64 ‰ with more depleted values in summer and an average of −54.7 ± 0.5 ‰ (figure 4.9b, grey line).

Results of the different approaches to determine the source signature

The average mean isotopic source signature of CH_4 for the whole time period of six years is −52.5 ± 0.3‰ calculated with the moving Miller-Tans approach. Only a small variation between −52.3 ‰ and −53.9 ‰ occurs depending on the used approach (figure 4.9a). Thus, biogenic CH_4 sources like waste management systems and agriculture account for the large part of CH_4 emissions in the catchment area of Heidelberg. However, we can also notice the strong influence of more enriched sources like natural gas, heating and even traffic from the urban area of Heidelberg. In comparison, the mean isotopic source signatures determined for two measurement campaigns of five months in more rural areas in the Netherlands, where ruminants are a main CH_4 source, are −60.8 ± 0.2 ‰ (Röckmann et al., 2016) and −59.55 ± 0.13 ‰ (Menoud et al., 2020).

Figure 4.9a shows in addition, that the four approaches which use the Miller-Tans method determine similar monthly mean source signatures which vary between −62 and −42 ‰. No significant trend is visible over the last six years in the monthly mean source signatures obtained from all four approaches. Therefore, we can assume that

the general composition of CH_4 emissions in the catchment area of Heidelberg has not changed or only slightly during this time period. This is different to former results in the 1990s of Levin et al. (1999). They found a change from -47.4 ± 1.2 ‰ in 1992/1993 to -52.9 ± 0.4 ‰ in 1995/1996 in the CH_4 source signature and attribute this change to a reduction of CH_4 emissions from fossil sources (mainly coal mining) and from cattle breeding.

Furthermore, the mean source signatures calculated with the different approaches have in common that a strong annual cycle with more depleted values in the summer months is visible (figure 4.9). This clearly indicates that in summer the CH_4 emissions have a larger biogenic share compared to the rest of the year. The annual cycle calculated with the two moving Miller-Tans approaches and the night-time approach shows most depleted source signatures in June. From June to October the source signatures shift to more enriched values and stay relatively constant until April. Between April and June a strong decrease to more depleted values is noticeable. The fact that the annual cycle of the moving Miller-Tans approach and the night-time approach show no significant difference indicates that the composition of CH_4 sources is the same during day and night or that the emissions during the night-time increase contribute most in the moving Miller-Tans approach, too.

The monthly approach results in similar monthly mean source signatures and a similar annual cycle. The average mean source signature is, however, around 1.4 ‰ less enriched than results from the moving Miller-Tans and the night-time approach (figure 4.9). The reason for this difference cannot be conclusively clarified. One possibility is, that this difference can be caused by the assumption of a constant background or the fact that all minutely data points of the month contribute to the determined source signature. In the night-time approach and the Miller-Tans approach nights and time periods which does not fulfil our criteria are discarded which can exclude small pollution events. As all data points are used in the monthly approach, also the small events contribute to the mean source signature.

Another explanation can be, that the considered CH_4 emissions in the monthly and night-time or moving Miller-Tans approach represent different catchment areas. CH_4 emissions from more distant sources show lower and more temporally extended CH_4 peaks than emissions from local and regional sources in the time series measurements at Heidelberg. Thus, the night-time and moving Miller-Tans approach which use small time windows of several hours probably consider more distant emissions less often than local and regional ones, since more distant emissions are included into the background or they are excluded by the selection criteria. Furthermore, at night the footprint of Heidelberg is smaller than during the day (see figure A.4). In 2018, around 47 % of the surface influence calculated with STILT for Heidelberg is within 50 km at night (time of the day: 18 to 3), but within 100 km during the day (time of the day: 6 to 15). Therefore, the monthly approach, which includes daytime data, represents a larger catchment area than the night-time approach. For measurements in the city of Heidelberg, the closer CH_4 sources are located in the urban areas of Heidelberg and are thus more enriched, while the more distant sources are located in more rural areas where more depleted CH_4 sources are dominant (see section 4.6).

This agrees with the more depleted mean source signature of CH_4 calculated with the monthly approach compared to the night-time approach.

The mean source signatures calculated with the two component mixing model and Mace Head as background represents CH_4 sources which can be even further away. The average mean source signature is around 2.2 ‰ less enriched than the ones determined by the moving-Miller-Tans or night-time approach. Furthermore, the annual cycle shows a stronger influence of biogenic CH_4 sources in late summer and autumn (figure 4.9b). However, the assumption that the Mace Head data represents the background of Heidelberg is not valid for all wind directions.

To conclude, all approaches have their advantages depending on the temporal and spatial range we are interested in. We have shown that the monthly approach is a good and easy solution to determine the monthly mean source signature and deviates only slightly from the more specific night-time and moving Miller-Tans approach. Especially for remote stations which only observe small diurnal variations in CH_4 this method is a good option, when night-time and moving Miller-Tans approach struggle with the low variations. In section C.3 we tested the monthly approach at Schauinsland to determine the mean source signature for two measurement campaigns of one month. In the summer campaign the mean source signature is -60.3 ± 0.7‰ and in the winter campaign -56.9 ± 0.4‰. We can notice again the larger impact of biogenic emissions in summer.

The advantage of the night-time and moving Miller-Tans approach is, however, that the mean source signature of individual nights or events can be studied. In figure 4.10a the histogram of the mean isotopic source signatures calculated for each night-time increase is shown in grey and in figure 4.10b a similar histogram displays the mean isotopic source signatures for the 769 events determined by the moving Miller-Tans approach.

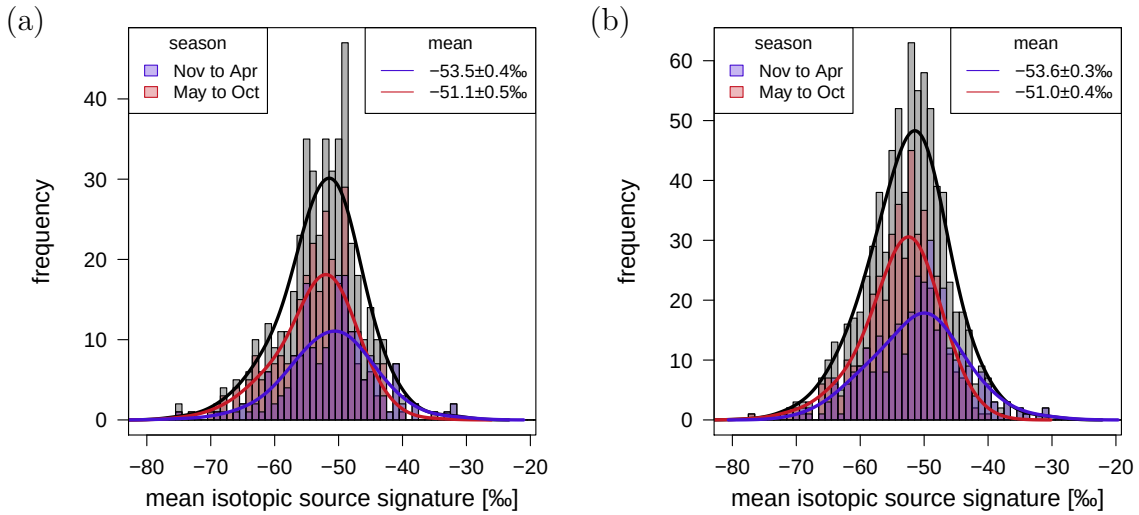

Figure 4.10.: Frequency distribution of the determined mean isotopic source signatures calculated with the night-time approach (a) or the moving Miller-Tans approach (b).

Most of the CH_4 emissions during one night or event is a mixture from several sources and cannot be attributed to one particular source. When separating the night-time and event source signatures into winter/spring (Nov to Apr) and summer/autumn (May to Oct), the shift of the mean isotopic source signature is noticeable, too. Again, more depleted mean isotopic source signatures occur from May to Oct and approximately 2.5 ‰ more enriched source signatures from Nov to Apr (figure 4.10). Both approaches have also in common, that the isotopic source signatures for less nights or events fulfil our criteria in winter. Only 41 to 43 % of the determined isotopic source signatures occur between Nov and Apr. Since the diurnal variations are usually lower in winter than in summer more night-time increases or events have ranges below the chosen threshold of 100 ppb and are therefore excluded.

Furthermore, we determined the diurnal cycle for the mean isotopic source signature calculated with the moving Miller-Tans approach. However, the year to year variations are too strong compared to the possible mean diurnal cycle to get reliable results and to exclude the possibility that the noticeable diurnal variations are only an artefact of the averaging.

Although, we can analyse the source signature at time scales below individual months, the precision of our analyser is still too low to interpret diurnal variations. However, the developments of new instrumentation with a better precision of isotopic measurements will make this possible soon.

Moreover, we tested the robustness of the above mentioned approaches which use the Miller-Tans method by varying the selection criteria. The CH_4 range was set to be at least 100, 150 or 200 ppb and the threshold for the fit error of the slope was changed from 2.5 over 5 to 10 ‰. All determined monthly mean source signatures show similar results and an annual cycle with more biogenic values in summer. The monthly values vary on average between 0.1 to 0.8 ‰ with standard deviations between 1 to 3 ‰. Therefore, we choose the CH_4 range of 100 ppb as threshold to include more data sets and 2.5 ‰ as threshold for the fit error of the slope, and thus the uncertainty of the source signature, to still assure precise results.

Wind direction

The main wind direction at the Institute of Environmental Physics in Heidelberg is south-east with some wind events from north-west between April 2014 and May 2020 (figure 4.11a). When analysing the measured atmospheric CH_4 mole fractions depending on wind direction and wind speed, we notice higher CH_4 mole fractions at lower wind speeds and slightly higher ones from east to south, which is the direction of the city centre (figure 4.11b). While at high wind speeds CH_4 emitted within and near Heidelberg is transported away, at low wind speeds this transport is only small leading to higher CH_4 mole fractions within Heidelberg and thus at the measurement station. For the measured $\delta^{13}CH_4$ values no dependence on the wind speed or direction occurs.

Furthermore, we study the determined mean isotopic source signatures with respect to the wind direction. No strong dependence on the wind direction can be detected for the mean source signature either (figure 4.11c). However, for the mean source signatures

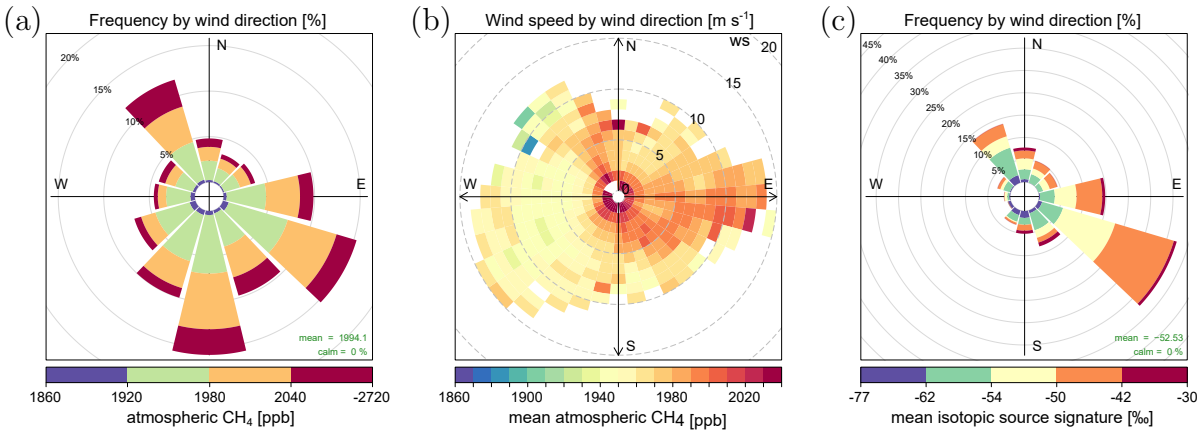

Figure 4.11.: Frequency of atmospheric CH_4 mole fractions measured in Heidelberg (a) and the CH_4 mole fraction by wind speed and wind direction (b). In addition, the frequency of the mean isotopic source signatures calculated with the night-time approach are shown depending on the mean night-time wind direction.

calculated with the night-time approach a small trend of more biogenic CH_4 emissions from south-west seems to occur.

4.5. Radon-Tracer method to determined CH_4 fluxes

Levin et al. (2011) determined CH_4 fluxes in the catchment area of Heidelberg between 1996 and 2008. The average value for this time period was $0.72 \pm 0.43\,\mathrm{mg\,m^{-1}\,h^{-1}}$. However, a strong decrease was visible until 2001 and since then annual mean CH_4 fluxes have been stable. To determine if the mean CH_4 flux has stayed constant since 2008, or has decreased again, the net CH_4 flux in the catchment area of Heidelberg for 2016 is calculated with the Radon-Tracer method (Levin, 1984, Schmidt et al., 2001 and Levin et al., 2011).

Radon is a noble gas whose only sink in the atmosphere is radioactive decay to ^{214}Po ($\lambda_{Rn} = 0.182d^{-1}$). Since it is emitted by soil it can be used as a tracer for greenhouse gases such as CH_4 whose main sources are near the ground, too. With the assumption that the sources of ^{222}Rn and CH_4 are spatially homogeneous, the trace gases emitted near the surface with an emission rate q_{Rn} and q_{CH4} accumulate overnight within the night-time inversion layer and the CH_4 flux q_{CH4} can be calculated with the following equation:

$$q_{\mathrm{CH4}} = q_{\mathrm{Rn}} \frac{\Delta c_{\mathrm{CH4}}}{\Delta c_{\mathrm{Rn}}}. \tag{4.7}$$

Δc_{CH4} and Δc_{Rn} are the CH_4 and ^{222}Rn increase over night. Since this increase is only observed during a few hours, the decay of ^{222}Rn is neglected in equation 4.7. The radioactive decay of ^{222}Rn during 8 to 12 hours has an effect of 3 to 4 % on the radon activity (Schmidt et al., 2001).

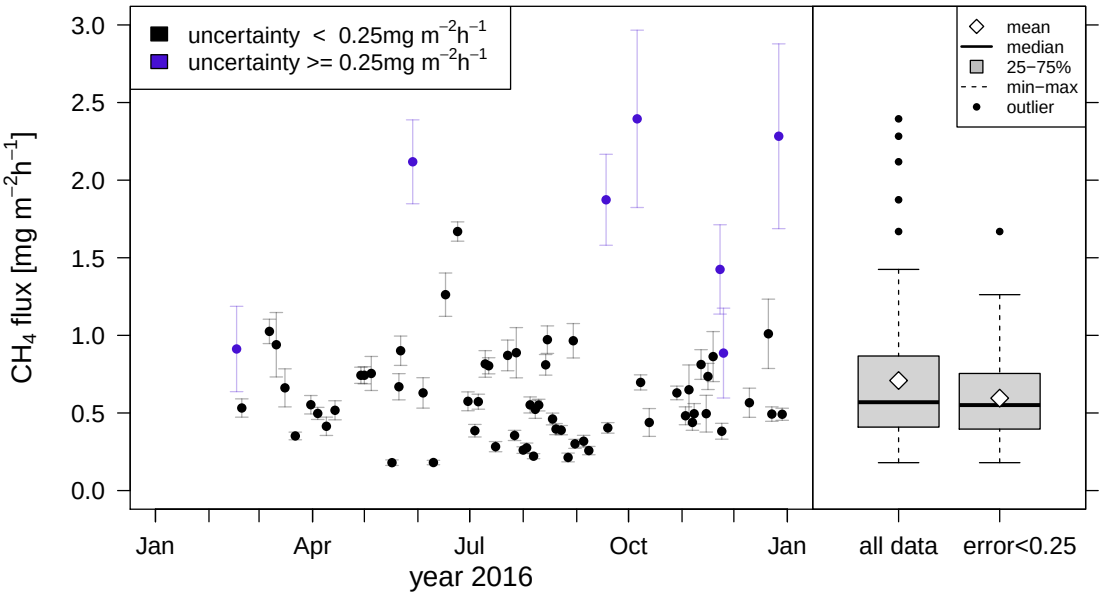

Figure 4.12.: Radon-based CH_4 fluxes calculated for individual nights in 2016.

The atmospheric ^{222}Rn activity concentration is not measured directly, but it can be determined out of the measured activity of the decay product ^{214}Po with the constant disequilibrium factor of 0.704 for Heidelberg (Levin et al., 2011). The uncertainty of the measurement is on average 8.5 % for the ^{222}Rn activity concentration (Schmidt, 1999).

The emission rate of ^{222}Rn q_{Rn} has been measured by Schüßler (1996) for the catchment area of Heidelberg and is on average 56.7 Bqm^{-2} h^{-1} with seasonal variations:

$$q_{\mathrm{Rn}}(d) = 56.7\,(1 - 0.25 \cdot \sin(2\pi\frac{d+50}{365}))\frac{Bq}{m^2 h}. \tag{4.8}$$

The net CH_4 flux for 2016 is determined out of ^{214}Po measurements in Heidelberg from 2016 (I. Levin, personal communication, 15 Feb 2021). The ratio between Δc_{CH4} and Δc_{Rn} is calculated by fitting a linear regression to the half hourly values of CH_4 and ^{222}Rn during each night-time increase between 22 and 6 local time. Only night-time increases with more than 80 % of the possible half-hourly data are used and the correlation coefficient R^2 of the regression between CH_4 and ^{222}Rn has to be larger than 0.7. These criteria were described and used by Levin et al. (2011) to calculate the net CH_4 flux for the years 1996 up to 2008. We adopted them to compare our results with the formerly determined CH_4 fluxes.

The CH_4 fluxes calculated for 2016 are shown in figure 4.12. The errors corresponds to the uncertainty of the slope of the $CH_4/^{222}$Rn regression. We can notice, that some high CH_4 fluxes occur, which have large uncertainties. These results leads to an average CH_4 flux of 0.7 mg m^{-1} h^{-1} in 2016 while the median is only 0.57 mg m^{-1} h^{-1}. The large uncertainty of the high CH_4 fluxes indicate that the correlation between CH_4 and ^{222}Rn is not sufficient to get accurate results with the Radon-Tracer method. Therefore, we

include an additional selection criterion and exclude all data with uncertainties larger than $0.25\,\mathrm{mg\,m^{-1}\,h^{-1}}$ (the excluded data are coloured in blue in figure 4.12).

Due to the uncertainty of the ^{222}Rn emission rate of 25 % (Schmidt et al., 2001), of the ^{222}Rn activity concentration and of the $CH_4/^{222}$Rn regression, the total uncertainty of the CH_4 flux is estimated to be 25-30 %.

The average CH_4 flux for 2016 is then $0.6 \pm 0.2\,\mathrm{mg\,m^{-1}\,h^{-1}}$. From 2001 to 2008, the annual CH_4 fluxes determined by Levin et al. (2011) varied between 0.57 and $0.7\,\mathrm{mg\,m^{-1}\,h^{-1}}$. This agrees with our calculations. Therefore, it is likely that no strong decrease or increase in the CH_4 flux occurred after 2008.

4.6. Comparison with emission inventories

The measurements of the atmospheric CH_4 mole fraction and the isotopic composition $\delta^{13}CH_4$ were used to calculate a mean isotopic source signature and the mean CH_4 flux for the catchment area of Heidelberg. In the following section, these results are compared to two different emission inventories to constrain their estimated emissions and to explain the noticed annual cycle in the mean source signature determined for the catchment area of Heidelberg. The first emission inventory used in this study is provided by the Landesanstalt für Umwelt Baden-Württemberg (LUBW, 2016) and the second is the Emissions Database for Global Atmospheric Research (EDGAR v5.0, Crippa et al., 2019).

Since the measurements in Heidelberg were carried out at low elevation about 30 m above ground and within the city, the atmospheric CH_4 measurements are most strongly influenced by local and regional sources. The LUBW provides detailed information about CH_4 emissions depending on different CH_4 categories for the cities of Heidelberg (HD) and Mannheim (MA), for the Rhein-Neckar-Kreis (RNK) and for complete Baden-Württemberg (BW) for the reference year 2016.

EDGAR v5.0 estimates CH_4 emissions from different categories for 0.1 degree x 0.1 degree grid cells covering the whole world. Instead of the year 2016 we have to take data from 2015 for EDGAR v5.0, since no data for 2016 are available yet. To compare the CH_4 emissions given by EDGAR v5.0 and the LUBW for different categories, we determine the emissions for the areas Heidelberg, Mannheim, Rhein-Neckar-Kreis and Baden-Württemberg from the grid cells. Therefore, the emissions for each county e.g. for Heidelberg are calculated out of the EDGAR v5.0 inventory only using grid cells which are at least partly within the borders of that county. For each of these grid cells the CH_4 emission rate and the percentage of the grid cell area which overlaps with the county are calculated. The sum of the products of CH_4 emission rate and the percentage of overlap gives us the emission for the county for one year.

To identify the largest differences between LUBW (2016) and EDGAR v5.0 (2015) inventory, we first analyse the CH_4 emissions from different sector for Heidelberg and surroundings (including HD, MA and RNK) and for Baden-Württemberg. The sectors with the largest CH_4 emissions are natural gas, waste treatment and livestock farming.

The annual emissions from these sources as well as their relative share are shown in figure 4.13. For Heidelberg and surroundings (HD,MA,RNK), we notice that the CH_4 emission rate given by EDGAR v5.0 (2015) with approximately 14800 t km^{-2} is around 3.5 times larger than the emission rate given by LUBW (2016) for Heidelberg and surroundings (figure 4.13a). For Baden-Württemberg this factor is only 1.7. Both inventories report comparable CH_4 emissions from livestock farming, but strong differences occur for emissions from the waste treatment sector. The LUBW estimates much lower emissions from landfills and waste water treatment plants than EDGAR v5.0. Furthermore, EDGAR v5.0 reports CH_4 emissions from waste incineration which are comparable to the emissions from waste water treatment plants. These emissions are not reported separately by the LUBW and can reach at most 10 % of the emissions given by EDGAR v5.0 for Heidelberg and surroundings. Moreover, the emissions from the natural gas distribution systems in Heidelberg and surroundings are five times larger in EDGAR v5.0 than in the LUBW inventory.

These strong differences between the reported CH_4 emissions by EDGAR v5.0 and LUBW are probably caused by differences in the statistical data and especially different assumptions for the emission factors used to estimate the CH_4 emissions from different sectors. This is supported by the fact that the amount of emissions from CH_4 sources like ruminants, whose emission factor is well studied and statistical data are accurate, is comparable for both inventories. CH_4 emissions estimated by EDGAR v5.0 for Germany have an uncertainty of only 16 % for the agriculture sector, while the uncertainty for the waste sector is 43 % (Solazzo et al., 2021). These values are estimated for the CH_4

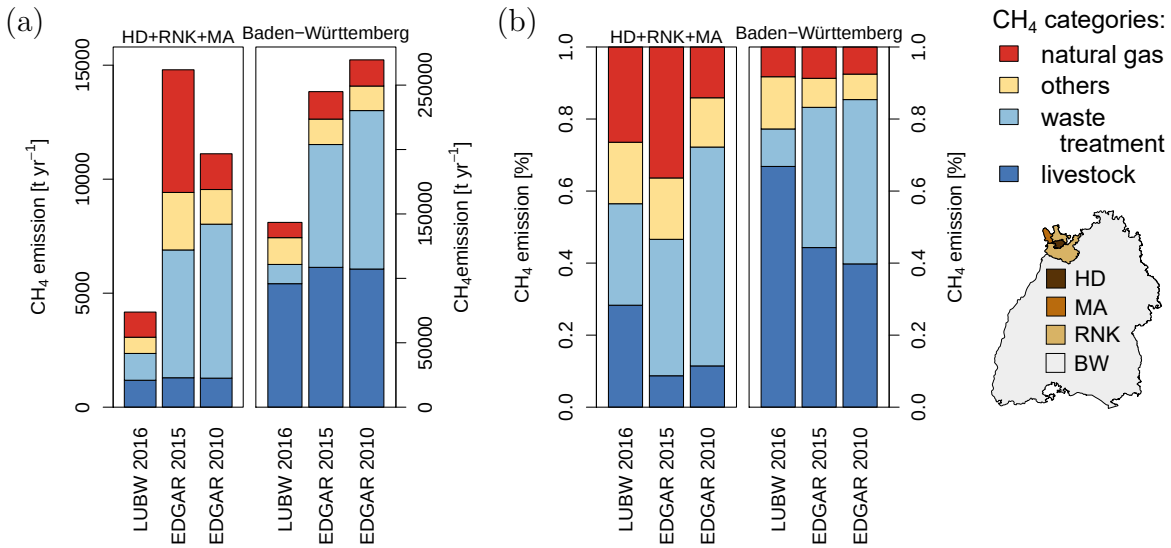

Figure 4.13.: CH_4 emissions (a) and relative proportion (b) of different source categories reported by LUBW and calculated out of EDGAR v5.0 data for Baden-Württemberg and for Heidelberg and surroundings. The latter includes the cities of Heidelberg (HD) and Mannheim (MA) as well as the county Rhein-Neckar-Kreis (RNK).

emissions of Germany. The uncertainty of individual or several grid cells can be even larger. The LUBW does not report uncertainties of the CH_4 emissions.

For Heidelberg and surroundings, deviations between LUBW and EDGAR v5.0 can also be caused by the conversion of CH_4 emissions from grid cells to counties. Especially CH_4 emissions estimated for Mannheim are calculated with grid cells which overlap with the nearby industrial town Ludwigshafen. Thus a part of the emissions may originate in Ludwidgshafen instead of Mannheim. Since Ludwigshafen is not located in Baden-Württemberg these CH_4 emissions are not reported by the LUBW. Due to the large area of Baden-Württemberg the difference caused by the change from grid cells to counties is probably very small. Thus, the strong deviations in the waste sector is caused by different assumptions for emission factors and statistical data in both inventories. Therefore, we can also assume that the difference of emissions in the waste sector visible for Heidelberg and surroundings is no effect of the change from grid cells to counties, too.

A more detailed analysis of CH_4 emissions from Mannheim, Rhein-Neckar-Kreis and Heidelberg reveal, that the CH_4 emissions attributed to natural gas for the area Mannheim calculated from EDGAR v5.0 strongly increased from 2010 to 2011 by a factor of 33. Thus, natural gas emissions correspond to only 4 % of the total emissions in 2010 and of 52 % in 2011. Such a strong increase is not noticeable for the other counties or sectors, except for the oil sector. There, the emissions from Mannheim increased between 2010 and 2011 from 0.2 % to 7.7 % of total emissions. In 2015 the natural gas emissions for Mannheim are still 19 times higher than they were in 2010, while the ratios for other sectors vary between 0.8 and 3. So far we can neither explain the origin of this strong increase in CH_4 emissions in Mannheim nor confirm those large emissions. Mobile measurements of CH_4 around Mannheim could provide more inside. In the following, we analyse the emissions from EDGAR v5.0 for the year 2015 and additionally for 2010. Data from 2010 are chosen, too, in case CH_4 emissions in the natural gas sector in Mannheim have been assumed to be too large after 2010 in the EDGAR v5.0 database.

4.6.1. Annual CH_4 flux

The annual CH_4 flux calculated for different areas around Heidelberg and for Baden-Württemberg is higher for the EDGAR v5.0 than for the LUBW inventory (table 4.3). For both inventories the CH_4 fluxes from cities (HD, MA) are larger than for the more rural area of the Rhein-Neckar-Kreis. The CH_4 flux from Heidelberg and surroundings (HD, RNK and MA) given by LUBW is only $0.4\,\mathrm{mg\,m^{-1}\,h^{-1}}$ and by EDGAR v5.0 between 1.3 (2015) and $1.0\,\mathrm{mg\,m^{-1}\,h^{-1}}$ (2010). Compared to the annual CH_4 flux of around $0.6 \pm 0.2\,\mathrm{mg\,m^{-1}\,h^{-1}}$ determined out of night-time data by the Radon-Tracer method, the LUBW inventory seems to be at the lower limit and EDGAR v5.0 seems to overestimate it.

While the CH_4 flux for the city of Heidelberg is relatively similar for EDGAR v5.0 and the LUBW inventory, EDGAR v5.0 estimates much higher CH_4 emission rates for the city of Mannheim (table 4.3). If we assume, that CH_4 emissions in Mannheim influence the CH_4 measurements in Heidelberg only occasionally, since the main wind direction in Heidelberg is east to south (section 3.1.1), then only Heidelberg and Rhein-

Area	LUBW (2016) [mg m^{-1} h^{-1}]	EDGAR v5.0 (2015) [mg m^{-1} h^{-1}]	EDGAR v5.0 (2010) [mg m^{-1} h^{-1}]
HD	0.5	0.6	0.6
MA	0.9	7.6	4.6
RNK	0.3	0.5	0.5
HD+RNK	0.3	0.5	0.5
HD+RNK+MA	0.4	1.3	1.0
BW	0.5	0.8	0.9

Table 4.3.: CH_4 fluxes reported by LUBW and EDGAR inventory for different areas around Heidelberg.

Neckar-Kreis would be a more representative catchment area. The CH_4 flux given by EDGAR v5.0 for this area is 0.5 mg m^{-1} h^{-1} and agrees with the median flux determined by the Radon-Tracer method. The LUBW inventory however reports CH_4 emission rates of only 0.3 mg m^{-1} h^{-1}. Thus, it is likely, that the LUBW inventory underestimates the CH_4 emissions from the Rhein-Neckar-Kreis.

4.6.2. Isotopic source signature

The two emission inventories of LUBW and EDGAR v5.0 report CH_4 emissions depending on source sectors. By attributing a source specific isotopic signature to the emissions of each sector, we calculate the mean isotopic source signature. These mean isotopic source signatures calculated for the LUBW and EDGAR v5.0 inventories are then compared to the mean isotopic source signature determined out of atmospheric measurements. The comparison between the mean isotopic source signature calculated out of the emission inventory and the atmospheric measurements will show us if the emission inventory estimates the composition of CH_4 emissions correctly.

The isotopic signatures for each source sector are chosen, if possible, from results of measurement campaigns in the catchment area of Heidelberg (Hoheisel et al., 2019, Levin et al., 1993). Table 4.4 summarises these isotopic source signatures used for the different sectors.

The CH_4 emission sector called energy for buildings in EDGAR v5.0 and the sector small and medium-sized combustion plants (KuMF) in the LUBW inventory are comparable and combine CH_4 emissions from combustion of wood, coal, fuel gases and liquid fuels. The amount of CH_4 emitted during the incineration and the isotopic composition differs depending on the combustible (Chanton et al., 2000). In the Agency National Inventory Report for the German Greenhouse Gas Inventory (UNFCCC-Submission UBA, 2020) the German Environment Agency estimated CH_4 emissions from the combustion systems in the residential and commercial/institutional sectors for Germany. Depending on the used emission factors, 73 to 79% of these emissions originate from wood, 8 to 19 %

Sector	Source	Isotopic signature [‰]
livestock farming	ruminants[1]	-63.9 ± 1.3
exploitation of oil and coal	coal from Europe and Russia[3]	-46.6 ± 6.4
gas distribution	natural gas[1]	-43.3 ± 0.8
solid waste landfills	landfill[1]	-58.7 ± 3.3
waste water treatment	waste water treatment plant[1]	-52.5 ± 1.4
waste incineration	waste incineration[4]	-33.2 ± 4.6
energy for buildings	combustion of wood[2], coal[4], fuel gases[1] and liquid fuel[4]	-27 ± 3
industrial emissions	combustion (industrial)[5]	-25
road transport	cars[2]	-22.8

Table 4.4.: Isotopic signatures of different CH_4 sources based on measured values in the catchment area of Heidelberg and literature: (1) Hoheisel et al., 2019, (2) Levin et al., 1993, (3) Sherwood et al., 2017, (4) Widory et al., 2006 and (5) Zazzeri et al., 2017.

from coal fuels, 6 to 8 % from fuel gases and 0.03 to 7 % from heating oil. Therefore, we calculate the isotopic source signature for the sector energy for buildings by weighting the isotopic composition of the combustion gases (Levin et al., 1993, Hoheisel et al., 2019 and Widory et al., 2006) by their relative amount.

Despite intensive literature research I have not been able to find any publications describing $\delta^{13}C$ for CH_4 emitted by the incineration of combustibles like coal fuel, heating oil and waste in the way I needed them to calculate the mean isotopic source signature. Therefore, I adopted the ^{13}C composition of different combustibles and of CO_2 produced during the incineration reported by Widory et al. (2006). This is feasible, since no strong isotopic fractionation is noticeable during the combustion for CO_2 and we assume that no strong fractionation of ^{13}C occurs for CH_4, either.

The mean isotopic source signature depends on the composition of CH_4 emissions. The fraction of CH_4 emissions provided by LUBW from natural gas distribution and waste treatment is larger in cities than in more rural areas like Rhein-Neckar-Kreis or in Baden-Württemberg (figure 4.14a). There emissions from agriculture especially from ruminants are dominant. Due to the higher contribution of thermogenic emissions like natural gas in cities and more biogenic emissions from ruminants in more rural areas, the determined annual mean isotopic source signature is more enriched in cities (HD: -49 ‰, MA: -48 ‰) than in the surroundings (RNK: -54 ‰, BW: -58 ‰). The uncertainties of the determined source signatures are 2 to 3 ‰ and are calculated from the variations in the isotopic signatures of the emission sectors. Since no uncertainties are reported for the CH_4 emissions in the LUBW inventory, their impact on the determined mean source signature could not be taken into account. To describe the near catchment area of Heidelberg, we combine again the emissions from Heidelberg, Rhein-Neckar-Kreis and Mannheim. The CH_4 sectors with the largest contribution there are waste treatment

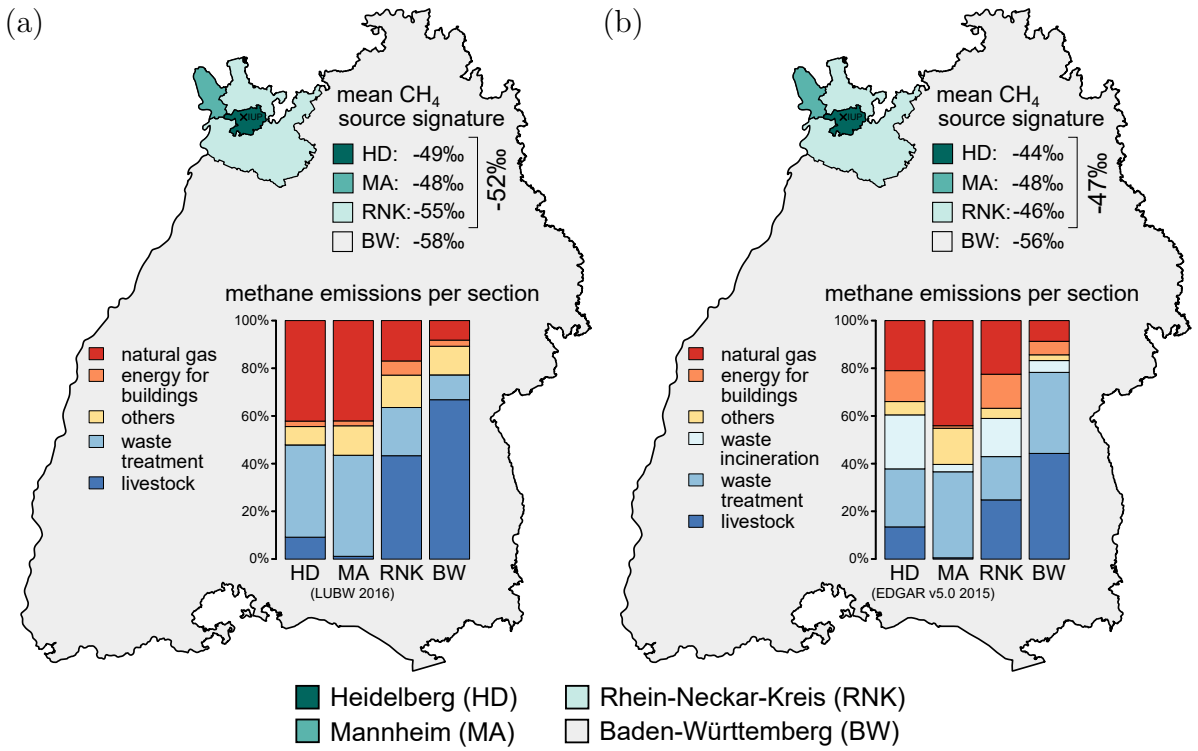

Figure 4.14.: Mean isotopic source signatures for different counties around Heidelberg and the fraction of CH_4 emissions for different sections for these counties. In panel (a) the emissions provided by LUBW for 2016 are used and in panel (b) the EDGAR v5.0 inventory for 2015.

and livestock farming with 28 % each as well as natural gas with 26 %. Thus, as expected no single source sector is dominant. This agrees with our observations, that the nighttime CH_4 increase is often a combination of several sources with a mean isotopic source signature varying around -52 ‰. The annual averaged isotopic signature of Heidelberg and surroundings (HD, RNK and MA) is -52 ± 2 ‰. If we exclude Mannheim in the LUBW inventory, following the assumption that the CH_4 measurement in Heidelberg is only occasionally influenced by emissions from this city, the mean isotopic source signature (HD and RNK) is -53 ± 2 ‰ and thus only slightly more depleted. In table 4.5 the mean source signatures calculated out of the CH_4 emissions reported by LUBW are summarised.

The mean isotopic source signatures are calculated out of data from the EDGAR v5.0 inventory, too, by using the same isotopic signatures for the different CH_4 source sectors (table 4.5). The mean source signatures from cities and rural areas do not show such strong difference as noticed for the LUBW inventory. For the cities of Heidelberg and Mannheim as well as the Rhein-Neckar-Kreis the mean isotopic source signatures are between -44 and -48 ‰. Only the mean isotopic source signature of Baden-Württemberg with -56 ± 3 ‰ is more depleted. Using EDGAR v5.0 data for 2010 instead of the one for 2015 only changes the mean source signature of Mannheim to more depleted values

Area	LUBW (2016) [‰]	EDGAR v5.0 (2015) [‰]	EDGAR v5.0 (2010) [‰]
HD	-49 ± 2	-44 ± 3	-44 ± 3
MA	-48 ± 3	-48 ± 3	-53 ± 3
RNK	-54 ± 2	-46 ± 2	-46 ± 2
HD+RNK	-53 ± 2	-46 ± 3	-46 ± 3
HD+RNK+MA	-52 ± 2	-47 ± 3	-50 ± 3
BW	-58 ± 2	-56 ± 3	-56 ± 2

Table 4.5.: Mean isotopic source signatures determined from LUBW and EDGAR v5.0 inventory for different areas. The uncertainties of the determined source signatures are based on the uncertainties of the applied isotopic signatures of the different CH_4 sectors. The uncertainties of the emission inventories are not included in them.

(-53 ± 3 ‰). The main differences between 2010 and 2015 are, that 70 % instead of 29 % of the emissions originate from landfills and only 4 % instead of 44 % from natural gas.

Thus, CH_4 emissions in Heidelberg and Rhein-Neckar-Kreis have a more enriched mean source signature when EDGAR v5.0 data are used in the calculation instead of values from LUBW. The LUBW inventory estimates a higher fraction of emissions from landfills and old waste deposit for Heidelberg and the Rhein-Neckar-Kreis compared to EDGAR v5.0 and for RNK even a higher percentage of emissions from livestock farming. Although the LUBW inventory also estimated a higher relative amount of CH_4 emissions from natural gas distribution than EDGAR v5.0, EDGAR v5.0 attributes 23 % of emissions to be emitted by waste incineration and 13 % from the sector energy for buildings. In the LUBW inventory these pyrogenic CH_4 categories have a much smaller impact. Emissions from waste incinerations are not reported by LUBW as an individual category and thus they are responsible for no more than 1 to 3 % of total emissions in Heidelberg and Rhein-Neckar-Kreis. The sector small and medium-sized combustion plants which is comparable to the sector energy for buildings is only responsible for 2 to 6 % of the total emissions.

The mean isotopic source signature determined out of the EDGAR v5.0 2015 inventory for the surroundings of Heidelberg (HD, RNK) with and without Mannheim is -47 ± 3 ‰ and -46 ± 3 ‰. Thus, the values are around 5 and 7 ‰ more enriched than the mean isotopic source signatures calculated with the LUBW inventory. For 2010 the mean isotopic source signature calculated with EDGAR v5.0 only shows a difference for the area Heidelberg, Rhein-Neckar-Kreis and Mannheim with a more depleted value of -50 ± 3 ‰.

The mean isotopic source signature for the catchment area of Heidelberg determined with atmospheric measurements is -52.5 ± 0.3‰ and agrees with the values calculated out of the LUBW inventory (HD+RNK+MA: -52 ± 2 ‰ and HD+RNK+MA:

-53 ± 2 ‰). The mean source signatures calculated with EDGAR v5.0 data show larger deviations and can only be explained partly by the high amount of emissions from waste incineration and the strong increase in CH_4 emissions from the natural gas sector in Mannheim.

4.6.3. Annual variability of monthly mean source signatures

The mean source signature calculated out of atmospheric measurements show an annual cycle with more depleted values in summer.Thus, seasonal variations in the emission composition and the emission rate of individual sources occur. The EDGAR v5.0 inventory reports, in addition to annual CH_4 emissions, the CH_4 flux for different CH_4 categories for each month of the year 2015. The monthly mean source signatures determined by these EDGAR v5.0 data will show us, if the emission inventory can model the observed annual cycle and probably which CH_4 sectors contribute to it.

The most prominent annual cycle in the CH_4 emissions estimated by EDGAR v5.0 is noticeable in the sector energy for buildings for the counties Heidelberg and Rhein-Neckar-Kreis. While in summer (Jul to Aug) only 3 % of the total monthly CH_4 emissions are attributed to the sector energy for building in winter (Jan to Feb) it is around 24 %. Since the LUBW inventory only reports CH_4 emissions per sector for one whole year, we include a modelled annual cycle for the sector small and medium-sized combustion plants (KuMF). This annual cycle is modelled similar to the one reported in EDGAR v5.0 for the sector energy for building with 18-19 % of the annual emissions from this sector in winter months and 0-1 % in summer months.

In figure 4.15 the mean isotopic source signatures for each month are shown, which are calculated out of the EDGAR v5.0 inventory (blue) or the LUBW inventory with modelled annual cycle (red). In addition, the annual cycle of the mean source signatures determined out of atmospheric measurements are displayed in black. CH_4 emissions which are used to determine the monthly mean source signatures correspond to the area of Heidelberg, Rhein-Neckar-Kreis and Mannheim in panel (a). In panel (b) the emissions from Mannheim are excluded.

Again, the monthly mean isotopic signatures for EDGAR v5.0 are more enriched and results for the LUBW inventory show similar values than the mean source signatures determined out of atmospheric measurements.

Moreover, an annual cycle with more depleted CH_4 in summer is noticeable in all calculations. The mean source signature calculated from atmospheric measurements has an annual cycle with a peak-to-peak amplitude of 5.8 ‰. The annual cycle determined with EDGAR v5.0 data shows a similar amplitude of 4.6 ‰ for HD and RNK but too enriched values. The amplitude for the annual cycle of the area HD, RNK and MA is only 2.2 ‰.

The annual cycle of the isotopic source signature calculated with the LUBW inventory follows the cycle calculated with atmospheric measurements quite well, but it has a lower amplitude of 3.3 ‰ (figure 4.15). Especially for the combined emissions from Heidelberg, Rhein-Neckar-Kreis and Mannheim, the observed annual cycle from atmospheric measurements can only be partly explained by the modelled annual cycle and

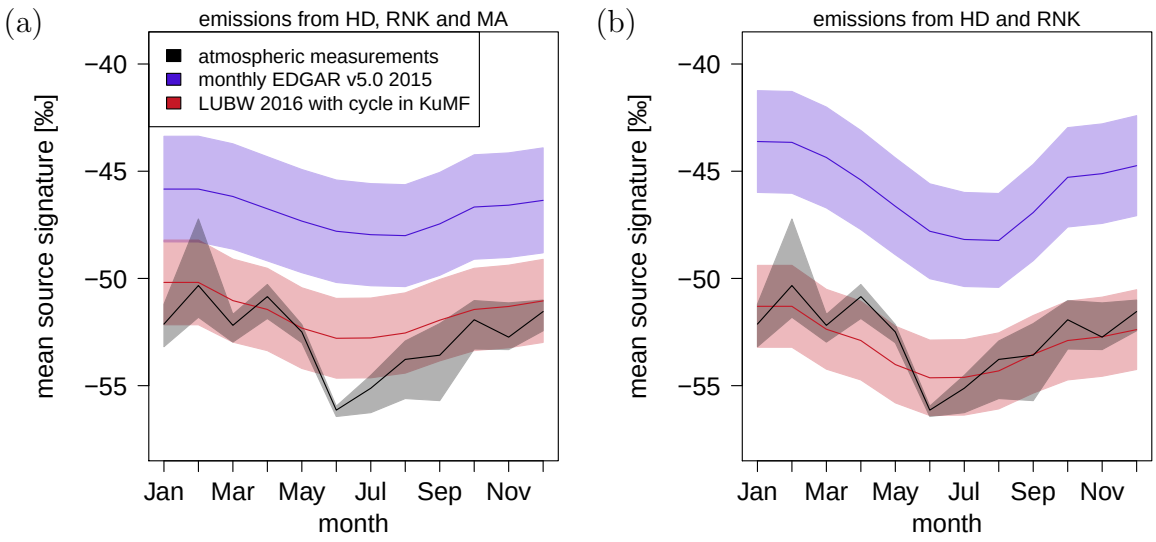

Figure 4.15.: Annual variability in the monthly mean isotopic source signatures calculated with emission inventories and atmospheric measurements. In panel (a) the combined emissions of Heidelberg (HD), Rhein-Neckar-Kreis (RNK) and Mannheim (MA) are used and in panel (b) the combined emissions of Heidelberg (HD) and Rhein-Neckar-Kreis (RNK).

thus by seasonal variations of CH_4 emissions from heating. This indicates, that emissions from another sector, which probably release biogenic CH_4, has seasonal variations too, which are not yet included into EDGAR inventory.

By using inverse models Bergamaschi et al. (2018) found an annual cycle in CH_4 emissions in Germany with the maximum in summer. Due to the limited number of studies they could not quantitatively estimates potential seasonal variations of anthropogenic sources (Bergamaschi et al., 2018). However, some studies e.g. Ulyatt et al. (2010), Spokas et al. (2011) and VanderZaag et al. (2014) reported an annual cylcle in CH_4 emissions from biogenic sources such as dairy cows, landfills or waste water with more emissions in summer. Such seasonal variations in biogenic emissions, in addition to the variations of emissions from heating, can explain the annual cycle in the catchment area of Heidelberg determined by atmospheric measurements.

4.7. Summary and Outlook

In this thesis, the continuous time series of atmospheric CH_4 and $\delta^{13}CH_4$ measured over six years in Heidelberg are used to study seasonal variations and trends of CH_4 emissions in the catchment area of Heidelberg.

To get a first impression of the regional and local sources around Heidelberg, we compare the annual cycles and trends in the measured CH_4 and $\delta^{13}CH_4$ time series with the background station Mace Head. In Heidelberg the CH_4 mole fractions are on average higher than in Mace Head since the continent is a net CH_4 source. $\delta^{13}CH_4$ measured in Heidelberg is, however, more depleted than in Mace Head. This shows that CH_4 emissions of the continent are on average more depleted than the background $\delta^{13}CH_4$ in Mace Head and thus biogenic sources contribute most to the CH_4 emissions. In addition, the trend in CH_4 at Heidelberg being similar to the one at Mace Head indicates that the CH_4 emission flux in the catchment area of Heidelberg has not changed strongly between 2014 and 2020. Furthermore, we can assume that the distribution of CH_4 emissions among the different source categories has not changed much as the trend in $\delta^{13}CH_4$ for Heidelberg and Mace Head is comparable, too. However, the comparison of the annual cycles of $\delta^{13}CH_4$ in Heidelberg and Mace Head suggest, that the CH_4 emissions in the catchment area of Heidelberg are more depleted in summer and more enriched in spring.

These observations, that the amount and composition of CH_4 emissions stayed relatively constant during the last years and that these emissions follow a seasonal cycle with more depleted CH_4 emitted in summer, are verified with the Radon-Tracer method and by determining the mean isotopic source signatures out of atmospheric measurements.

For the year 2016 we calculated the CH_4 flux for the catchment area of Heidelberg with the Radon-Tracer method. The emission rate of $0.6 \pm 0.2\,\mathrm{mg\,m^{-1}\,h^{-1}}$ agrees with the CH_4 fluxes determined by Levin et al. (2011) for 2001 to 2008. Thus we can assume that no decrease in CH_4 emissions occurred in the catchment area of Heidelberg after 2008.

The partitioning of local and regional CH_4 emissions among different source categories was analysed by determining the mean isotopic source signature of the catchment area of Heidelberg. Therefore, the six-year time series of atmospheric CH_4 and $\delta^{13}CH_4$ are used. Different approaches were tested to calculate the mean source signatures which corresponds to different time intervals. In the monthly approach, the Miller-Tans method is applied to the monthly data sets. Since the background in the Miller-Tans approach is assumed to be constant, which is probably not the case for one month, we apply the Miller-Tans method to the CH_4 night-time increases, too. Due to the high temporal resolution of our measurements, we can go one step further and use the moving Miller-Tans approach to determine the mean source signatures. In this approach the background can be assumed to be constant and also daytime data are used.

In all these methods no significant trend in the monthly mean source signature occurs during the last six years. This confirms that the source composition in the catchment area of Heidelberg did not change between 2014 and 2020.

The average mean source signatures calculated with the above mentioned approaches

vary between −52.3 and −53.9 ‰. Due to the urban area of the city and the more rural surroundings, CH_4 emissions measured in Heidelberg originate from quite different sources. They range from biogenic sources like livestock over waste treatment to thermogenic sources like natural gas and even to pyrogenic ones like traffic and wood-firing installations. Furthermore, the determined monthly mean isotopic source signatures of all approaches show an annual cycle (−56 ‰ to −50 ‰) with a stronger biogenic CH_4 contribution in summer. The comparison with emission inventories have shown, that this cycle can only be partly explained by seasonal variations in the CH_4 emissions from heating in winter.

Furthermore, we used the mean source signatures and the CH_4 flux determined for the catchment area of Heidelberg out of atmospheric measurements to verify the CH_4 emissions reported by two emission inventories.

EDGAR v5.0 seems to overestimate CH_4 emissions from more enriched sources. The mean source signature determined out of EDGAR v5.0 data is around 6 ‰ more enriched than the one determined from atmospheric measurements. This large difference can be partly explained by the large amount of CH_4 emissions estimated by EDGAR v5.0 for waste incineration and the sector energy for buildings. In addition, emissions from the natural gas and oil sector strongly increased in Mannheim, which is within the catchment area of Heidelberg, between 2010 and 2011. Mobile measurements in Mannheim can help us to understand if the large CH_4 emissions estimated for Mannheim are reasonable and where they originate from. EDGAR v5.0 also reports monthly CH_4 emissions. The most prominent annual variations occur in the sector energy for buildings. We can notice an annual cycle in the monthly mean isotopic source signatures calculated with EDGAR v5.0 data with an amplitude smaller than the one noticed in the monthly mean source signatures calculated out of atmospheric data. However, the interpretation is difficult as the mean source signature determined by EDGAR v5.0 is much more enriched.

The LUBW inventory estimates much lower CH_4 emissions than EDGAR v5.0 especially for the waste sector. It seems to underestimate the total amount of emissions in the catchment area of Heidelberg. However, the mean source signature calculated using the emissions reported by LUBW agrees with the result from atmospheric measurements. Since the LUBW only reports CH_4 emissions for the whole year, we include a modelled annual cycle to the sector of small and medium-sized combustion plants which is comparable to the energy for building sector in EDGAR v5.0. The monthly mean source signatures follow the results calculated from atmospheric measurements quite well. However, the amplitude is not as large as the one determined for the atmospheric measurements. Therefore, the noticed annual cycle in the mean source signature from atmospheric measurements can only be partly explained by an annual cycle in the CH_4 emissions from small and medium-sized combustion plants. Thus, additional seasonal variations probably occur in biogenic CH_4 emissions from waste water, landfills or dairy cows. However, there is still a great need for research in order to understand and describe potential annual cycles of CH_4 sources precisely.

The study done in this thesis gives only a first impression about how well the emission inventories represent the CH_4 emissions in the catchment area of Heidelberg. A more detailed analysis could be done by simulating atmospheric CH_4 and $\delta^{13}CH_4$ with atmo-

spheric models like the Stochastic Time-Inverted Lagrangian Transport model (STILT) or the chemistry-transport model CHIMERE.

A first test to simulate the atmospheric CH_4 mole fractions and $\delta^{13}CH_4$ for Heidelberg was done by Szénási (2020) with the CHIMERE model for the time period between November 2016 and March 2017. While a similar analysis done by Szénási (2020) for the more rural area in Lutjewad, in the Netherlands, shows a good agreement between observed and modelled $\delta^{13}CH_4$ values, in Heidelberg strong deviations occurred probably due to the more complex measurement location in the city. The higher contribution of CH_4 emissions which have larger uncertainties in the inventories such as emissions from the waste and natural gas sectors could bias the system. Furthermore, the high CH_4 emissions in EDGAR v5 reported for Mannheim have to be investigated properly to confirm them and to reduce a possible false influence on the modelled data. A further, more detailed analysis of the whole time series would be important to specify the catchment area of Heidelberg and to verify the CH_4 emissions given by the inventories.

5. Comparison of atmospheric CO, CO_2 and CH_4 measurements at Schneefernerhaus and the mountain ridge at Zugspitze

At Mount Zugspitze (see section 3.1.3) trace gas measurements have been carried out for several decades (e.g. Yuan et al., 2019, Ghasemifard et al., 2019 or Giemsa et al., 2019). Such long-term records from remote stations can help to get a better understanding of the global carbon cycle and the impact of greenhouse gases on global warming.

At a high mountain station, the measurements are typically less affected by regional and local influences than urban stations. El Yazidi et al. (2018) and Affolter et al. (2021) have however noticed that the CH_4 measurements at Pic du Midi or the CO_2 measurements at Jungfraujoch respectively are occasionally influenced by local anthropogenic activities.

Due to new measurement techniques with a temporal resolution of nearly 1 Hz spikes can also be detected in the high resolution CO, CO_2 and CH_4 measurements carried out at Schneefernerhaus. To prevent an influence of these local pollution events on the long-term record, the measured spikes have to be excluded manually.

Another possibility of reducing the influence of local pollution on the measured time series is to change the location of the intake line. A promising location is an ambient air inlet at the mountain ridge (ZGR, 2825 m a.s.l.) around 150 m uphill Schneefernerhaus. Since 2014 the German Meteorological Service (DWD) has used this intake line at the mountain ridge for their Radon (^{222}Rn) activity measurements to avoid contamination of local geogenic radon sources and to have a free inflow of air masses (Frank et al., 2017). In 2018, a new inlet line made of stainless steel and 290 m long was installed from Schneefernerhaus to the mountain ridge to replace an old and broken intake line.

This allows additional CO, CO_2 and CH_4 mole fraction measurements in ambient air of the mountain ridge since October 2018. The two-year long comparison measurement is analysed in this study to characterise local pollution events and to compare their influence on the Schneefernerhaus and mountain ridge measurements.

5.1. Measurement methods

5.1.1. Experimental set-up

At the Research Station Schneefernerhaus the mole fractions of CO_2, CH_4 and CO in ambient air of Schneefernerhaus and the mountain ridge are measured with three analysers(figure 5.1). These measurements are carried out by the German Environment Agency (UBA). All three analysers share the same multi-position rotary valve (model: EMT2SF6MWE, Valco Vici, Switzerland) and the same calibration and target gases, which are measured simultaneously. However, two different intake lines are used to measure all three trace gases in parallel at two locations. One inlet is at the research terrace of Schneefernerhaus and the other one at the mountain ridge above Schneefernerhaus (see figure 3.3a).

At Schnefernerhaus the intake line is located at the research terrace on the fifth floor 2.5 m above the terrace floor (ZSF, 2671 m a.s.l.). The top of the glass inlet is heated to avoid freezing. Ambient air is flushed with a flow rate of $50\,\mathrm{l\,min^{-1}}$ through the glass inlet and is then distributed in the laboratory to several analysers. A part of the flow is used to measure the mole fraction of CO_2 and CH_4 with the CRDS G2301 (Picarro, Inc., Santa Clara, CA) and the CO mole fraction with the OA-ICOS (LGR EP30, Los Gatos Research) analysers. The air is dried before the measurement by passing through a ∼350 ml cold trap (Gaßner Glastechnik GmbH, Germany). This cold trap is cooled in a fluid bath filled with silicon oil (model: M90.055/03, Huber Kältemaschinenbau AG, Germany) to −80°C with an cryogenic cooler (model: TC100E,

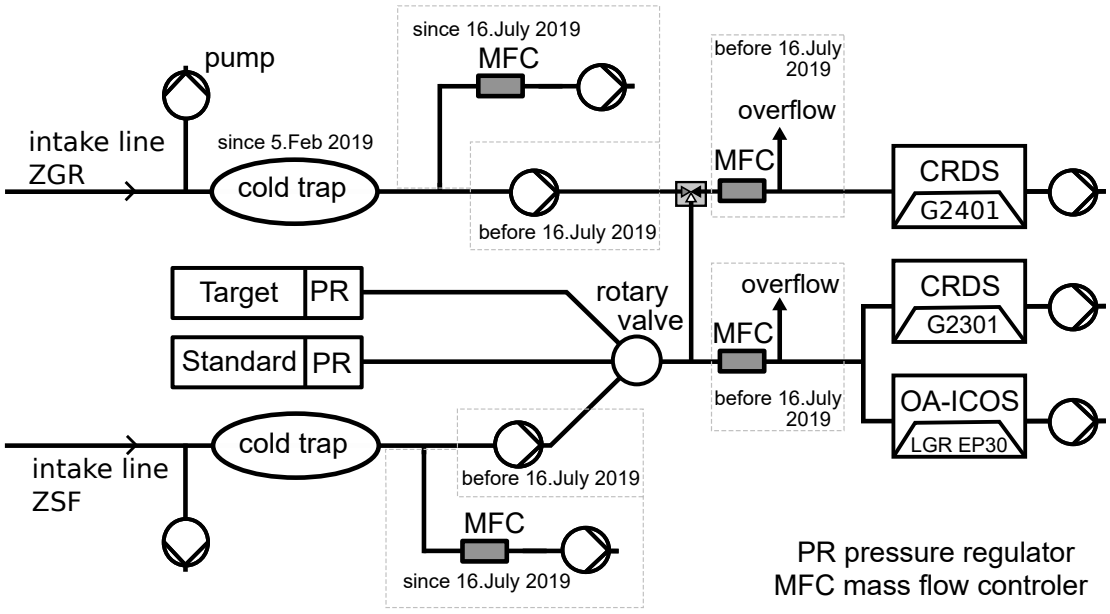

Figure 5.1.: Experimental set-up to measure the CO, CO_2 and CH_4 mole fractions in ambient air of Schneefernerhaus and of the mountain ridge in parallel.

Huber Kältemaschinenbau AG, Germany). The flow through the CRDS G2301 and the OA-ICOS LGR EP30 analyser is regulated between 0.2 to 0.4 l min^{-1} and leads to a residence time of air from the inlet at the research terrace to the analyser of 35 s.

Ambient air of the mountain ridge (ZGR, 2825 m a.s.l.) is pumped with a flow of 16 l min^{-1} through a 290 m stainless steel tube to Schneefernerhaus. It is not possible to heat the top of the inlet at the mountain ridge to avoid freezing, but fortunately this did not occur. The CO, CO_2 and CH_4 mole fractions in ambient air of the mountain ridge are measured with the CRDS G2401 (Picarro, Inc., Santa Clara, CA) analyser. A test to measure the residence time of air from mountain ridge to Schneefernerhaus results in 6 min 40 s. The first measurements of ambient air of the mountain ridge were performed without drying system, but on 5 February 2019, a drying system analogous to the one used for the Schneefernerhaus measurements was installed.

A further modification of the set-up was conducted for both sampling lines on 16 July 2019. Two pumps (one for each sampling line) were relocated out of the direct flow-path to the analysers in order to exclude any influence of the pumps on the sampled air. The modifications of the experimental set-up are summarised in table 5.1.

5.1.2. Data gaps

The CO, CO_2 and CH_4 time series at Schneefernerhaus are usually measured with the OA-ICOS LGR EP30 and the CRDS G2301 analyser. Ambient air of the mountain ridge is analysed with the CRDS G2401 instrument. The CRDS G2301 and the OA-ICOS LGR EP30 analyser were sent to the ICOS Atmosphere Thematic Centre (ATC) Metrology Laboratory for validation in the course of the ICOS labelling process. Thus two large data gaps occur in the time series. From 9 May 2019 to 8 Aug 2019 the CRDS G2301 analyser was sent to ATC. It was replaced by the CRDS G2401 analyser, which usually measure air of the mountain ridge, to reduce the data gap at Schneefernerhaus. Therefore, we ensure a continuous time series at Schneefernerhaus. However, no CO,

time interval			CO, CO_2 and CH_4 analysers at ZSF	at ZGR	additional set-up changes
01 Oct 2018	to	08 May 2019	G2301 & EP30	G2401	since 05 Feb 2019 ZGR measurement is dried
08 May 2019	to	08 Aug 2019	G2401 & EP30	-	since 16 Jul 2019 pump set-up outside flowpath
08 Aug 2019	to	01 Jan 2020	G2301 & EP30	G2401	
01 Jan 2020	to	08 Jul 2020	G2301	G2401	
08 Jul 2020	to	21 Jul 2020	G2301 & EP30	G2401	
21 Jul 2020	to	05 Aug 2020	G2301 & EP30	-	
05 Aug 2020	to	31 Sep 2020	G2301 & EP30	G2401	

Table 5.1.: Modifications of the experimental set-up to measure CO, CO_2 and CH_4 at Schneefernerhaus and the mountain ridge.

CO_2 and CH_4 mole fractions are available for the mountain ridge in this time period. The OA-ICOS LGR EP30 was at ATC between 1 Jan 2020 and 8 Jul 2020. Thus, during this time no CO mole fractions were measured in ambient air of Schneefernerhaus.

5.1.3. Flagging

The mole fractions of CO, CO_2 and CH_4 measured with high temporal resolution with the CRDS G2301, CRDS G2401 and OA-ICOS EP30 are averaged over one minute. Alternating with ambient air measurements, calibration and target gas cylinders are analysed, too. For each cylinder measurement only the last 5 min are used and averaged to avoid that initial stabilization and flushing of the cavity influence the data. Furthermore, the first minute before and after a cylinder measurement is removed in the ambient air time series to account for flushing of the cavity.

At a temporal resolution of one minute the influence of local pollution events is clearly visible in the mole fractions of ambient air measured at Schneefernerhaus, as we will show and discuss later in figure 5.3 and section 5.2. Possible local sources involve snow groomers at the nearby ski resort, gasoline snow blowers, the nearby rack railway tunnel entrance, and human CO_2 respiration at the station. Since the aim is to measure the trace-gas background, data points corresponding to these local events as well as to artefacts and outliers due to changing the cold trap or technical problems are flagged and excluded manually by the station manager from UBA. This is done with the help of additional data from trace gas measurements, meteorological data, as well as station logbooks which document working activities in the research station and corresponding local pollution. In the mountain ridge data only technical artefacts are flagged.

In order to quantify the impact of local pollution at Schneefernerhaus station we compare the mountain ride time series to two data sets from Schneefenerhaus. In the first only artefacts and outliers were excluded, in the second additionally local pollution events.

5.1.4. Calibration strategy

Several gas cylinders are measured regularly to calibrate the ambient air measurements. Every two months four standard reference gases are analysed, to link the measured data to international scale (WMO X2007 scale). These reference gases are provided by the ESRL's Global Monitoring Laboratory (GML) of the National Oceanic and Atmospheric Administration (NOAA) and are spanning a wide range of atmospheric variations from 124 to 269 ppb CO, 379 to 430 ppm CO_2 and 1835 to 2120 ppb CH_4 (table 5.2). Furthermore, a low and a high concentration cylinder (LOW/HIGH) as well as a target cylinder for quality control are measured for 15 minutes every three days and a working standard cylinder every 8 hour. The cylinder of the working standard had to be changed twice between Oct 2018 and Oct 2020.

The usual calibration strategy (strategy 1) applied to the CO_2, CH_4 and CO mole fractions contains several steps. The four WMO standard reference gases are used to determine the reference values for the CO, CO_2 and CH_4 mole fractions of the HIGH

calibration cylinder number	CO_2 [ppm]	CH_4 [ppb]	CO [ppb]	Frequency
WMO1:ND56764	378.6	1834.7	124.18	two month
WMO2:ND56757	399.02	1940.3	154.13	two month
WMO3:ND56763	413.45	1962.1	269.19	two month
WMO4:CB12417	429.52	2119.0	257.20	two month
HIGH	426.80	1985.6	174.75	three days
LOW	386.93	1794.8	75.55	three days
Target	∼404.7	∼1887.1	∼124.6	three days
Working Standard	392-424	1892-19839	127-176	8 hours

Table 5.2.: CO_2, CH_4 and CO_2 mole fractions of the calibration and the target cylinders used at Zugspitze.

and LOW cylinders. The WMO standard reference gas cylinders are measured every two months and are used to calibrate HIGH and LOW cylinder measurements done on the same day.

The reference values of the HIGH and LOW cylinders used to calibrate the working standard cylinder measurements are determined for each year and each analyser independently. Therefore, the calibrated HIGH and LOW measurements of every second month are averaged for each analyser and each year including the last measurement of the previous and the first of the following year. Thus, for each analyser and each year one reference value for CO, CO_2 and CH_4, each, is used for the HIGH and LOW cylinders, which can probably differ slightly from year to year and between the analysers.

These reference values and HIGH and LOW cylinder measurements done every three days in combination with a two-point calibration are used to calibrate the working standard cylinder measurements which were analysed between the HIGH and LOW cylinder measurements. So we get a calibrated working standard measurement every three days. These calibrated working standard measurements are then used as reference values for the working standard measurements done every eight hours with which the minutely averaged ambient air data are calibrated in the end with a single-point calibration. However, if there is no drift or just a reasonable drift in the calibrated working standard measurements, they are averaged to get only one reference value for this cylinder for each year.

This calibration strategy was chosen to take into account short-term fluctuations of the analysers but without consuming the WMO standard reference gases too fast.

Calibrating the data directly with the HIGH and LOW cylinder measurements instead of the working standard measurements has the advantage, that we calibrate the ambient air with a two-point instead of a single-point calibration. With the two-point calibration (section A.1) a possible non-linear response of the analyser can be corrected, which is not possible with the single-point calibration. Thus, by excluding the working standard from the strategy even more accurate results can be obtained as we will show in the next section.

In the usual calibration strategy the working standard is included, since the same

calibration cylinders are used to calibrate N_2O. N_2O is measured with the OA-ICOS LGR EP30 instrument which analyses CO, too. For the N_2O measurements with this analyser the interval between the calibration measurements has to be small to correct instrumental drift. Since we do not analyse N_2O in this study and the instrumental drift in the CO, CO_2 and CH_4 mole fractions is weaker than in N_2O, a calibration strategy with a lower density of calibration measurements is possible.

Therefore, an alternative calibration strategy (strategy 2) is developed in this study to calibrate the time series between Oct 2018 and Oct 2020. Again, the four WMO standard reference gases are used to determine the reference value of CO, CO_2 and CH_4 for the HIGH and LOW cylinders. However, the calibrated HIGH and LOW measurements of every second month are averaged over the whole time interval between September 2018 and November 2020. Instead of using different reference values for the HIGH/LOW cylinder for all instruments, the averaged value of the more precise instrument is used (table 5.2). For CO_2 and CH_4 the G2401 analyser is more precise and for CO the OA-ICOS LGR EP30 analyser. The LOW and HIGH cylinder measurements are then used directly to calibrate the minutely averaged mole fractions of ambient air with a two-point calibration (section A.1).

The results of both calibration strategies are compared for the CO, CO_2 and CH_4 measurements of the target cylinder done every three days in the following section. All ambient air measurements shown in this study are calibrated with strategy 2.

5.1.5. Target measurement for quality control

Every three days a target cylinder for quality control is measured by all three analysers at the same time around 36 hours after the last LOW and HIGH cylinder measurements and 36 h before the next ones. The mole fractions measured for the target cylinder are calibrated with both calibration strategies described in the previous section 5.1.4.

The determined CO, CO_2 and CH_4 mole fractions for both analysers (ZSF: G2301&OA-ICOS EP30 and ZGR: G2401) are shown in figure 5.2. The OA-ICOS EP30 analyser usually measuring ambient air at Schneefernerhaus has a much better precision for CO than the G2401 analyser normally measuring ambient air at the mountain ridge. For CH_4 the precision of the G2401 is better than the one of the G2301 analyser.

The average difference between the target cylinder measurements for ZSF and ZGR analysers calibrated with strategy 1 is 0.8 ± 0.8 ppb in CO, -0.02 ± 0.02 ppm in CO_2 and -0.2 ± 0.2 ppb in CH_4. For all three species, the average difference is below the WMO compatibility goal (WMO, 2020) which is set at 2 ppb for CO, 0.1 ppm for CO_2 and 2 ppb for CH_4.

However, in this study we are interested in small differences between the Schneefernerhaus and mountain ridge time series. In calibration strategy 1 a trend in the difference of the target measurements between ZSF and ZGR analysers can be seen in CO especially and CH_4 of 0.6 ppb CO $year^{-1}$ and -0.13 ppb CH_4 $year^{-1}$.

The CO, CO_2 and CH_4 mole fractions of the calibrated target measurements for ZSF and ZGR analysers have smaller differences in strategy 2 than in strategy 1 and in addition the trend in the differences is reduced in strategy 2 (table 5.3).

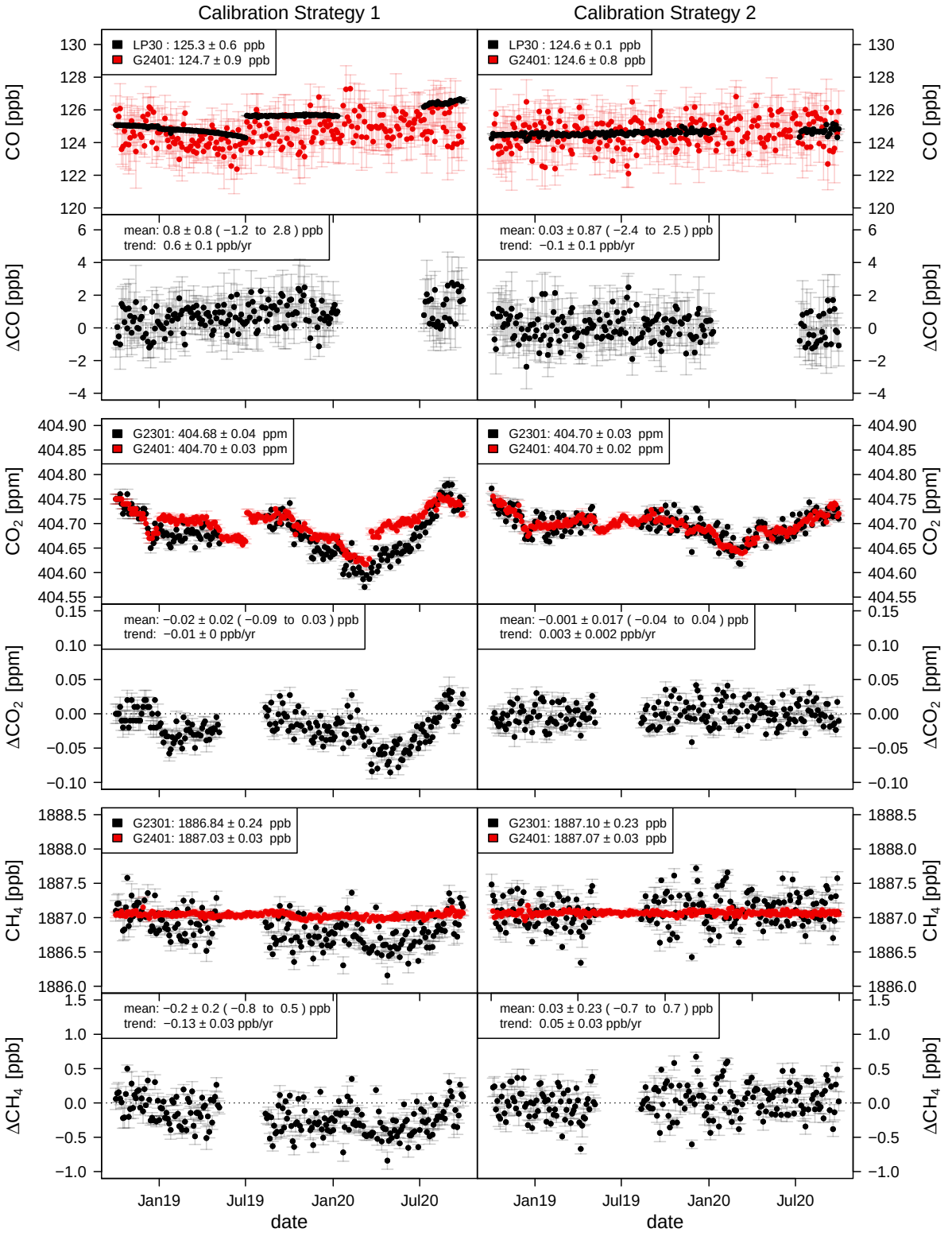

Figure 5.2.: Target cylinder measurements calibrated with two different calibration strategies. The data coloured in black are measured with the OA-ICOS EP30 and CRDS G2301 analyser used to measure ambient air of Schneefernerhaus (ZSF). The red data are measured with the CRDS G2401 usually measuring ambient air of the mountain ridge (ZGM).

analyser	CO_2 [ppm]	CH_4 [ppb]	CO [ppb]
CRDS G2301	404.70 ± 0.03	1887.10 ± 0.23	-
CRDS G2401	404.70 ± 0.02	1887.07 ± 0.03	124.6 ± 0.1
OA-ICOS LGR EP30	-	-	124.6 ± 0.8
difference	-0.001 ± 0.017	0.03 ± 0.23	0.03 ± 0.87
range	-0.04 to 0.04	-0.7 to 0.7	-2.4 to 2.5
drift of difference per year	0.003 ± 0.002	0.05 ± 0.03	-0.1 ± 0.1

Table 5.3.: Target gas measurements performed with the CRDS G2301, G2401 and OA-ICOS LGR EP30 analysers calibrated with strategy 2. The average and standard deviation of each analyser and the differences are shown.

Especially for CO, the mean difference between both analysers decreases to 0.03 ± 0.87 ppb. But also the CH_4 difference of 0.03 ± 0.23 ppb and CO_2 difference of -0.001 ± 0.017 ppm are smaller compared with calibration strategy 1. Furthermore, the differences between ZSF and ZGR analysers are symmetric around the mean value for strategy 2. Moreover, jumps in the CO but also in the CO_2 mole fractions of the target gas measurements which are caused by the change of the working standard in strategy 1, do not occur in strategy 2.

To conclude, calibration strategy 2 achieve more precise results than strategy 1. In addition, the average difference of the target gas measurements calibrated with calibration strategy 2 between the analyser G2301/LGR EP30 and G2401 is negligible for all three species CO_2, CH_4 and CO (table 5.3).

5.1.6. Comparison of analysers

For 15 days in July 2020 all analysers (CRDS G2301, OA-ICOS EP30 and CRDS G2401) measure dried ambient air of Schneefernerhaus. The average difference between CO, CO_2 and CH_4 mole fractions measured with the CRDS G2301&OA-ICOS EP30 and CRDS G2401 are -0.05 ± 1.51 ppb (mean $\pm$ sd) in CO, 0.04 ± 0.07 ppm in CO_2 and 0.3 ± 0.6 ppb in CH_4. The standard deviation decreases to 0.6 ppb in CO, 0.02 ppm in CO_2 and 0.2 ppb in CH_4 when analysing the hourly averages. Therefore, the difference between the ambient air measurements of the analysers are negligible, when the same air is measured.

5.1.7. Data corrections

Ambient air of Schneefernerhaus has a residence time of 35 s before it is measured with the CRDS G2301 and OA-ICOS EP3 analysers. Due to the larger and much longer intake line to the mountain ridge of 290 m the residence time of ambient air measured with the CRDS G2401 is 6 min 40 s. To take into account this time lag between the

analysers, the mountain ridge measurements averaged over one minute are shifted by -6 minutes.

In the experimental set-up two changes were necessary as the measured CO mole fraction was affected by water vapour and by the pumps used. In February 2019 the measurement system was modified to dry ambient air of the mountain ridge as it was already done for the Schneefernerhaus measurement. This decision was motivated by a systematic difference of the ambient CO mole fraction between Schneefernerhaus and mountain ridge of around 5 ppb. To verify whether this difference was caused by an inaccurate water vapour correction by the manufacturer, all three analysers simultaneously measured the same air from the Schneefernerhaus inlet for 50 min. For the CRDS G2301 and OA-ICOS EP30 analysers the air was dried as usual before the measurement. The air for the CRDS G2401 analyser was not dried. The mean difference between Schneefernerhaus and mountain ridge analysers measuring the same ambient air from Schneefernerhaus is 0.04 ± 0.06 ppm (mean $\pm$ sd) in the CO_2 and -0.3 ± 0.6 ppb in the CH_4 mole fraction and thus not significant. The two CO analysers however measure CO mole fractions with a mean difference of 5.2 ± 1.5 ppb. Thus, the strong difference of CO mole fraction in ambient air between Schneefernerhaus and the mountain ridge is caused by an insufficient water correction of the CRDS G2401 analyser. To solve this problem in the water correction, a cold trap was added to dry the ambient air of the mountain ridge before it is measured. Furthermore, another water correction has to be applied to the mountain ridge wet air measurements. An offset of 5.2 ppb is added to the CO mole fractions measured at the mountain ridge until 5 February 2019.

The second modification relocates two pumps out of the direct flow-path to each analyser as they increase the measured CO mole fraction. To test the influence of the pumps on the trace gas measurement, the same gas cylinder is measured with all three analysers simultaneously for 25 min with and without the pump in the flow-path. The CO mole fraction shows a strong difference for the set-up with the pump inside the flow-path (162.5 ppb) and the set-up with the pump outside the flow-path (155 ppb). It seems that the mole fraction of CO increases by 7.5 ppb, if the pump is located inside the direct flow-path to the analysers. As this offset occurs for both analysers, the difference of the CO mole fractions between both instrument measurements is not affected by this change in set-up. For CO_2 and CH_4 no significant change in mole fraction is noticed whether the pump is installed inside the flow-path or not. Therefore, the CO mole fractions of ambient air for both analysers are corrected by an offset of 7.5 ppb until 16 July 2019.

5.2. Comparison between Schneefernerhaus and mountain ridge measurements

Since October 2018 the CO, CO_2 and CH_4 mole fractions have been measured in ambient air of Schneefernerhaus and of the mountain ridge. The time record over two years is shown in figure 5.3. For Schneefernerhaus two time series are presented. In blue the time series which include local pollution events are shown and in black the one in which

these events are excluded manually by the station manager as described in section 5.1.3. 2 % of the CO and CO_2 mole fractions averaged over one minute are strongly influenced by local pollution events, thus ∼12 900 CO and ∼25 900 CO_2 data points had to be flagged manually. Especially in the snow season high CO spikes are caused by snow groomers at the nearby ski resort and by gasoline snow blowers used at the station. In January 2018 high CO_2 and CH_4 spikes were measured corresponding to extremely high CO mole fractions up to 29 328 ppb. During this time gasoline snow blowers had to be used intensively due to heavy snowfall and an avalanche that went over the station.

The CO, CO_2 and CH_4 mole fractions measured at the mountain ridge are displayed in red in figure 5.3 and show no strong spikes caused by local pollution as noticed in the Schneefernerhaus time series. Thus, the new inlet location at the mountain ridge is less influenced by local pollution than Schneefernerhaus. The unpolluted Schneefernerhaus time series and the ones from the mountain ridge have CO, CO_2 and CH_4 mole fractions in the same range: 48 to 342 ppb CO, 390 to 440 ppm CO_2 and 1872 to 2100 ppb CH_4 and follow the same seasonal variations. Larger gaps in the time series occurred when the analysers were sent to ATC in Paris for validation in the course of the ICOS labelling process. In the following sections, the local pollution events are characterised in more

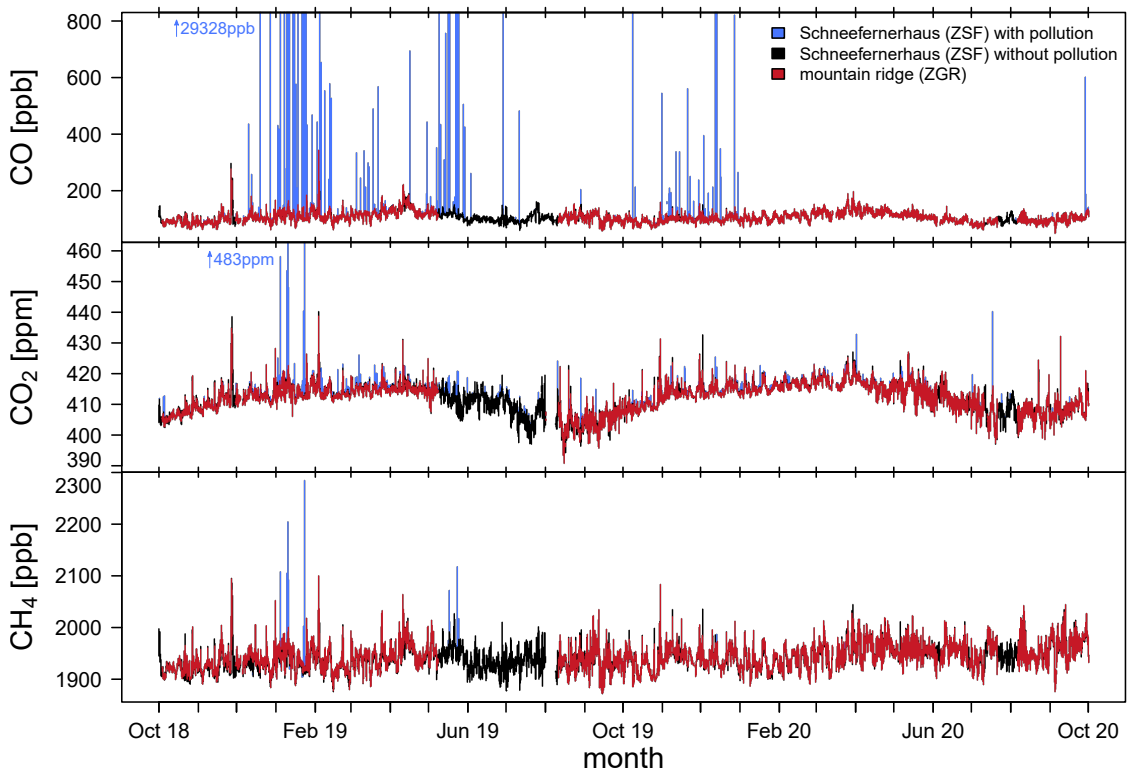

Figure 5.3.: Mole fractions of CO, CO_2 and CH_4 averaged over 1 min and measured at Schneefernerhaus(black) and at the mountain ridge (red). Blue data are flagged out manually from the Schneefernerhaus time series, as they are influenced by local pollution.

detail and the influence of local pollution on the Schneefernerhaus and mountain ridge measurements is analysed.

5.2.1. Local pollution events of CO and CO_2

In the Schneefernerhaus time series 1000 high CO events (∼12 900 minutely values) and 2100 high CO_2 events (∼25 900 minutely values) are monitored which are caused by the influence of local pollution near Schneefernerhaus. The number of manually flagged data points corresponds to 2 % of the available CO and CO_2 data. In figure 5.4 the number of polluted CO and CO_2 data which were manually flagged, are displayed per month (a) and in addition per hour (b). A strong seasonal and diurnal variability can be seen.

Snow groomers and gasoline snow blowers influence the CO measurements at Schneefernerhaus. Snow groomers are used in the nearby ski resort during the ski season (Nov to April) and in the months before and after. The gasoline snow blowers have to be used more often from October to May because more snow tends to fall at Zugspitze during these months. The stronger pollution between October and May can be seen in the occurrence of polluted CO and also CO_2 data points. 94 % and 92 % of the polluted CO and CO_2 data occur in this period of time.

Furthermore, 92 % of polluted CO and 95 % of polluted CO_2 data points can be noticed during the day between 6 and 18 UTC. This confirms again that the high spikes in the time series of CO and CO_2 are caused by anthropogenic pollution since workers as well as tourists are only present at Zugspitze during the day.

To analyse the influence of local CO and CO_2 pollution at Schneefernerhaus on the mountain ridge measurement, we compare the measured pollution events at Schneefernerhaus with the mountain ridge measurement. In figure 5.5 three days with typical CO and CO_2 events are presented as an example. In each column the CO or CO_2 mole frac-

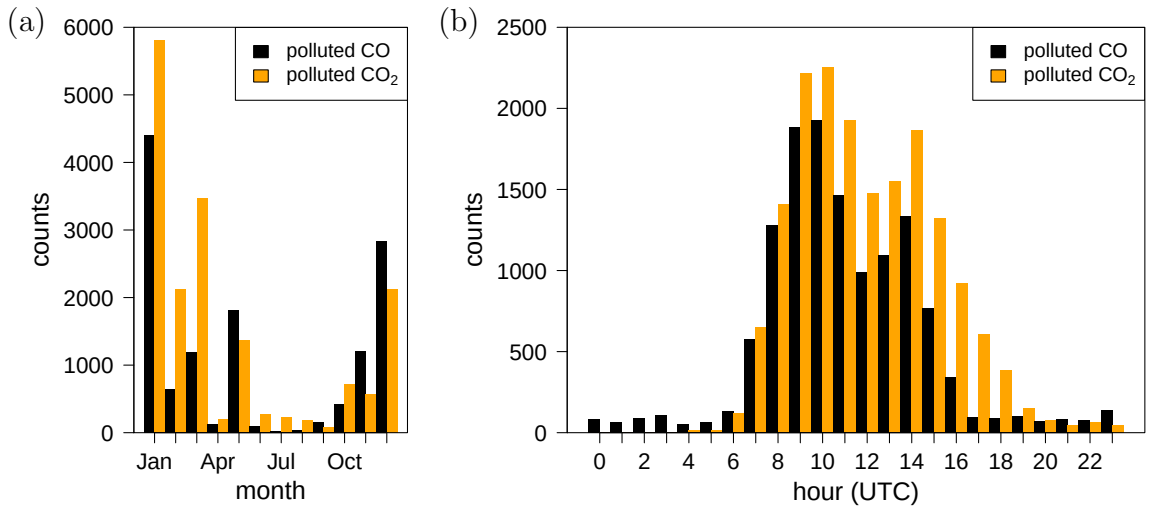

Figure 5.4.: Distribution of measured CO and CO_2 data at Schneefernerhaus influenced by local pollution as function of month and time of day. The minutely averaged data-set is used for this analysis.

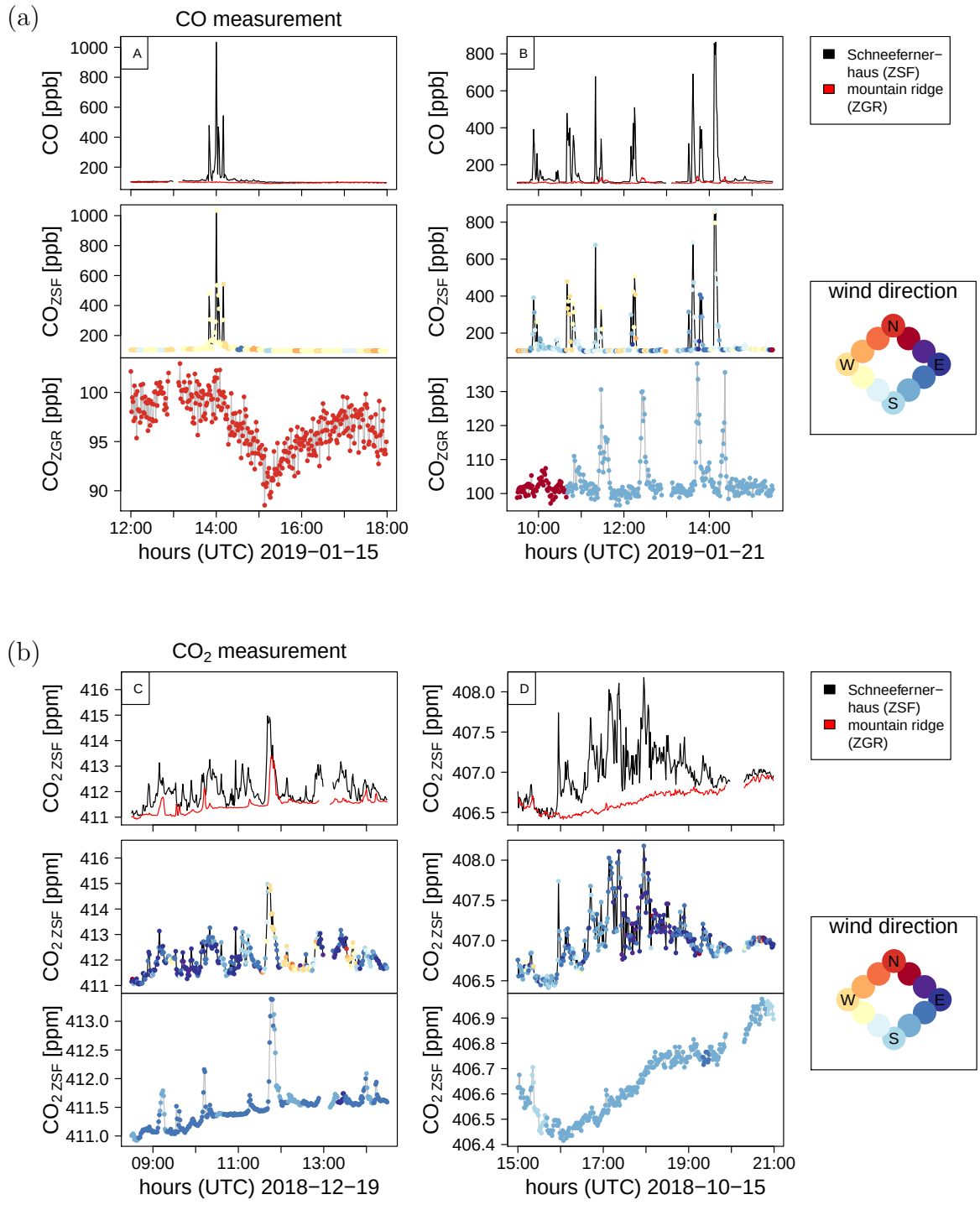

Figure 5.5.: Four typical pollution events to illustrate the impact of local pollution on the CO (a) and CO_2 (b) mole fractions measured at Schneefernerhaus and the mountain ridge.

tions of one pollution event are shown. The top row of each panel shows the CO or CO_2 mole fractions measured at Schneefernerhaus in black and at the mountain ridge in red. The middle rows display the Schneefernerhaus measurement and the bottom rows the mountain ridge measurement. The colours in the middle and bottom rows correspond to the wind direction measured at Schneefernerhaus or mountain ridge respectively.

For all analysed days when pollution events are visible in the Schneefernerhaus time series in 82 % and 84 % of the days no corresponding spikes can be identified at the mountain ridge for CO and CO_2. Example A and C (figure 5.5) show such days. Even when high CO mole fractions of up to 1000 ppb are measured at Schneefernerhaus, no increased CO levels are measured at the mountain ridge.

However, sometimes corresponding spikes can be monitored at the mountain ridge, but mostly with much smaller amplitudes. This is especially the case if the wind blows from south-east that means from Schneefernerhaus to the mountain ridge. As we can see in example B, CO spikes up to 800 ppb are measured at Schneefernerhaus. In the mountain ridge time series these spikes are visible, too, but with much lower amplitudes of less than 40 ppb. Due to the high CO spikes at Schneefernerhaus the hourly averaged values are enhanced between 15 ppb and 65 ppb during six hours. The less prominent CO spikes at the mountain ridge, however, change the hourly values by less than 3 ppb. Even if the wind blows from south-east mostly no influence is noticeable in the mountain ridge time series, as shown in example D.

During the time in which we carried out the comparison measurements at Schneefernerhaus and at the mountain ridge the tourism operations at Zugspitze have been suspended due to Covid-19 pandemic since mid-March to May 2020. In addition, work at Schneefernerhaus and the ski resort was reduced. As the measurements kept running, a reduction of local pollution events during Covid-19 lockdown is clearly noticeable at Schneefernerhaus especially in the NO_2 and CO_2 mole fraction. Unfortunately no CO measurements were carried out at Schneeefernerhaus, since the analyser was at ATC in Paris. However, during a second lockdown starting in November 2020 a reduction of CO spikes measured at Schneefernerhaus can be seen compared to previous years. Even though, local pollution at Zugspitze is reduced due to Covid-19 lockdown, changes observed in the monthly mean mole fractions of CO_2, CO and CH_4 between 2019 and 2020 cannot be distinguished from normal year to year variations. To quantify the effect of less pollution events on the measurements at Schneefernerhaus a more detailed analysis with more data is needed for better statistics.

5.2.2. Local pollution events of CH_4

In the CH_4 time series all high CH_4 mole fractions which are excluded due to local pollution coincide with high CO or CO_2 events, which are marked as local pollution, too.

However, in addition to these high CH_4 spikes, negative CH_4 spikes of several ppb were detected in the CH_4 mole fraction of Schneefernerhaus which were never seen at the mountain ridge. In most cases these events are not isolated in time. Instead, a series of multiple negative spikes extends over a few hours up to a few days and ends as

abruptly as it started (figure 5.6a).

To eliminate the possibility that these negative spikes are caused by the analyser or the set-up two tests were carried out. First, during an event when negative spikes are measured at Schneefernerhaus, the two analysers G2301 and G2401 are switched (figure 5.6b). Thus, the G2301 analyser first measures ambient air of Schneefernerhaus and later of the mountain ridge. The G2401 analyser first measures ambient air of the mountain ridge and later of Schneefernerhaus. In all measurements at Schneefernerhaus (black and blue lines) negative spikes occur for both analysers and no spikes are detected for the mountain ridge measurements (red and orange) for both analysers. Therefore, the analyser G2301 is not responsible for the occurrence of negative CH_4 spikes in the Schneefernerhaus time series.

In a second test, the CRDS analyser G2301 measures ambient air of Schneefernerhaus using the normal set-up described in section 5.1.1. The CRDS G2401 analyser however uses a completely different set-up with a stainless steel intake line starting at the same location as the glass intake line for the normal set-up. CH_4 mole fractions measured with both analysers but different set-ups show strong negative CH_4 spikes. Hence, the experimental set-up is not responsible for negative CH_4 spikes either.

Knowing that the measured negative CH_4 spikes do not occur due to the analyser or

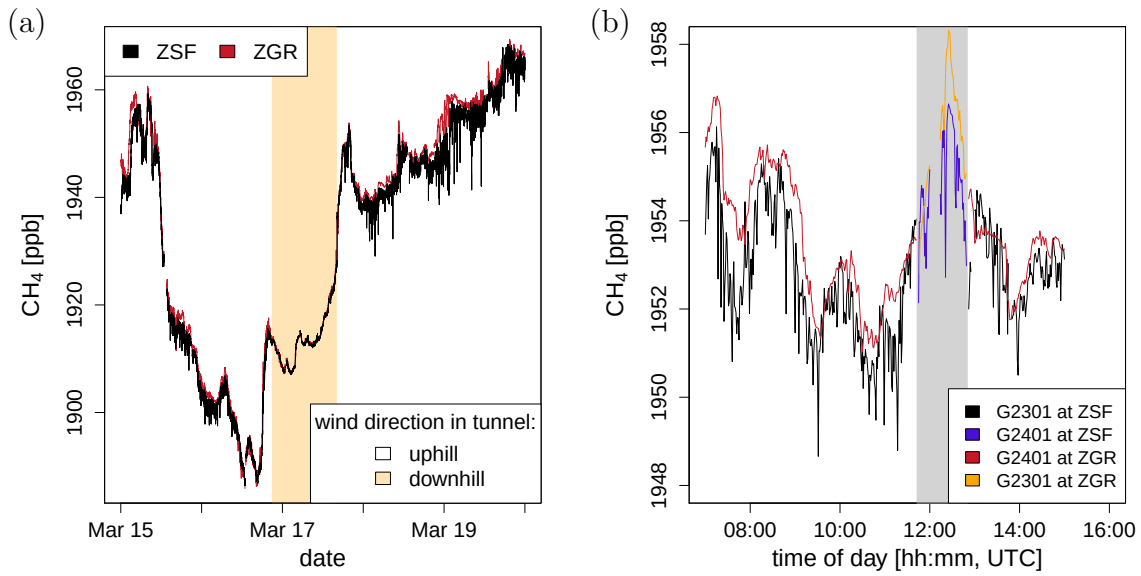

Figure 5.6.: Negative CH_4 spikes measured at Schneefernerhaus.
(a): Example of negative CH_4 spikes measured at Schneefernerhaus (black), but not at the mountain ridge (red). During the time intervals with white background, the wind direction in the rack railway tunnel is uphill and only in the beige coloured time interval it is downhill.
(b): Test to identify if the CRDS G2301 analyser causes the CH_4 spikes. Therefore, the two analysers (G2301 and G2401) are switched (grey area). Both analysers measure negative CH_4 spikes at ZSF (black and blue), but no spikes at ZGR (red and orange).

the set-up, it is most likely that air with lower CH_4 mole fractions than atmospheric conditions occasionally reach the intake line and induce negative spikes. Around 45 m from the intake line on the measurement terrace an opening to the rack railway tunnel is placed. This passage to the tunnel was built to enable Radon enriched air to escape from the tunnel so that the Radon concentration inside the Schneefernerhaus station does not increase too much. At the beginning of the tunnel near the opening the wind direction is measured and shows that the air in the tunnel alternates between flowing downhill and flowing uphill. In addition, a CRDS analyser (3000i) measures the CH_4 mole fraction in the tunnel air for 15 days in November 2020.

In figure 5.7 the measured CH_4 mole fractions of the tunnel air is shown in black and of the ambient air at Schneefernerhaus in blue. The wind direction in the rack railway tunnel is uphill during the time intervals with white background and only downhill in the beige coloured intervals. A strong difference between the measured CH_4 mole fraction can be noticed depending on the direction of the tunnel air flow. When the tunnel air is flowing downhill, atmospheric CH_4 mole fractions are measured which are only slightly below the ones measured at the Schneefernerhaus inlet. The CH_4 mole fractions are nearly the same, because ambient air enters the opening of the tunnel and reaches the CRDS analyser inside the tunnel. However, in case the tunnel air is flowing uphill, extremely low CH_4 mole fractions between 500 and 1000 ppb are measured.

This finding explains the measured negative CH_4 spikes in the Schneefernerhaus time series. During time periods with uphill air transport inside the tunnel, the strongly depleted CH_4 tunnel air is transported through the opening of the tunnel. Local wind patterns can sometimes transport the air further to the inlet at the nearby research

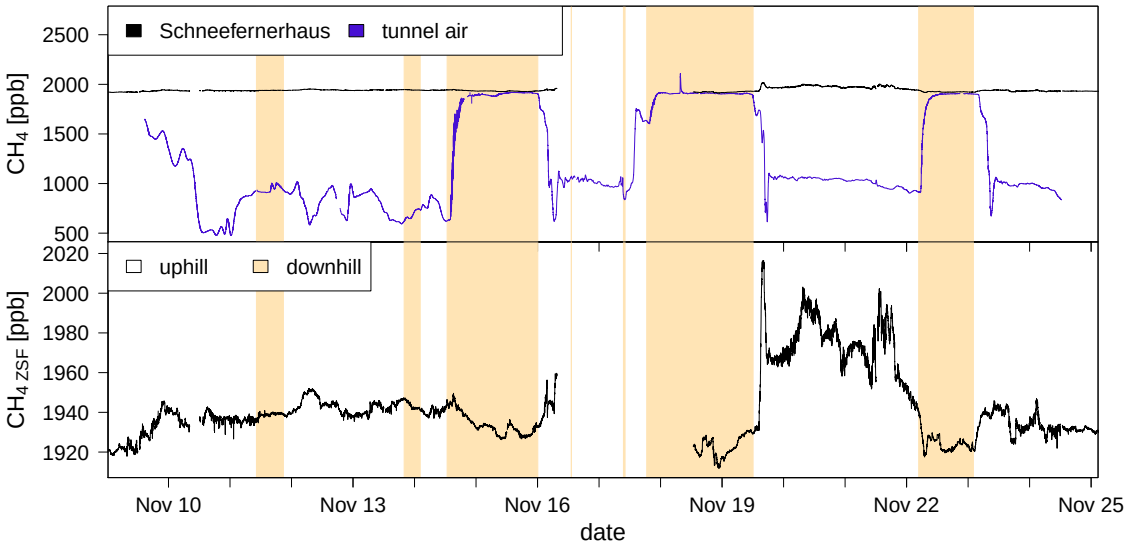

Figure 5.7.: CH_4 mole fraction measured in the tunnel air (blue) and in ambient air at Schneefernerhaus (black). The background colours indicate the wind direction in the rack railway tunnel. White time intervals correspond to an uphill air flow and beige ones to a downhill flow.

terrace. The appearance of negative CH_4 spikes during uphill tunnel wind conditions can be noticed in the Schneefernerhaus CH_4 measurements (figure 5.7) especially on 11 November. On the other hand, during downhill wind condition as observed between the 15 and 16 November the measured CH_4 mole fractions show no such variations.

Moreover, influence of CH_4 depleted tunnel air seems to be larger in winter than in summer, although the higher variability of CH_4 in summer makes the recognition of negative CH_4 spikes more difficult. The analysis of wind data in the tunnel between 2018 and 2021 confirms this finding of a stronger influence of CH_4 depleted air on the measurements in winter compared to summer, since the tunnel air is more often flowing downhill in summer than in winter.

5.2.3. Difference between measurements at Schneefernerhaus and mountain ridge

Ambient air at the mountain ridge is much less influenced. Thus, we investigate the difference between Schneefernerhaus and mountain ridge mole fractions of CO and CO_2 in more detail, to determine the influence of local pollution in the Schneefernerhaus time series. In figure 5.8 the frequency distribution of the differences for CO (panel a) and CO_2 mole fractions (panel b) are shown. The counts are plotted on a logarithmic scale. The data are separated between night-time (18 to 6 UTC) and daytime (6 to 18 UTC) displayed in blue and red respectively.

On the left side of each panel the difference is calculated out of Schneefernerhaus data which include local pollution events. Much stronger deviations to positive values can

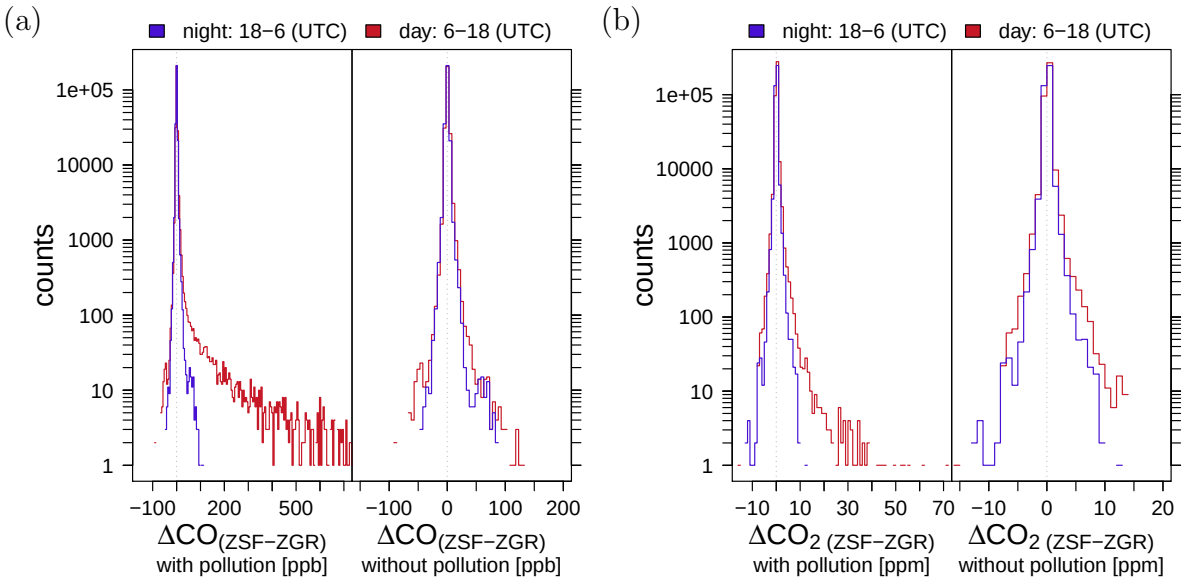

Figure 5.8.: The frequency distribution of the difference between the Schneefernerhaus and the mountain ridge measurement for CO (panel a) and CO_2 (panel b). The counts are plotted on a logarithmic scale. Blue corresponds to night-time (18 to 6 UTC) and red to daytime (6 to 18 UTC) data.

be noticed during the day, which are caused by the stronger polluted Schneefernerhaus data. On the right side of each panel, the Schneefernerhaus data without local pollution events are used to determine the difference between Schneefernerhaus and mountain ridge. The strong positive deviations vanish. Thus, strong local pollution events in the Schneefernerhaus measurements are successfully excluded manually by the station manager. However, it seems that in the CO_2 but also CO time series a few small daytime pollution events are not captured with the manual flagging method.

To analyse the difference between the Schneefernerhaus and mountain ridge measurement in more detail, the hourly mean mole fractions are used. The hourly time series smooth small fluctuations at the locations as well as small differences due to deviations in the air mass transport between Schneefernerhaus and the mountain ridge. Moreover, hourly mean mole fractions are typically submitted to international data bases like WDCGG and are often used for data analysis and comparison with model results (Bergamaschi et al., 2010).

Tests between the Schneefernerhaus and mountain ridge analysers have shown that the difference between them are negligible when measuring the same ambient air (section 5.1.6). Thus, a possible small offset in the trace gases between Schneefernerhaus and mountain ridge data can originate from local pollution at Schneefernerhaus, from the difference in altitude between the two locations or from an influence due to the 290 m long intake line to the mountain ridge. Unfortunately, the difficult location of the inlet at the mountain ridge has prevented a proper line test up to now.

The hourly averaged CO, CO_2 and CH_4 mole fractions for Schneefernerhaus and the mountain ridge as well as the differences between both locations are presented in figure 5.9. We use the Schneefernerhaus time series in which the strong local pollution events are filtered out. The mean differences between the CO, CO_2 and CH_4 time series are smaller or equal to the compatibility goal determined by the WMO (WMO, 2020). For CO the difference is 0.4 ± 2.4 ppb (mean $\pm$ sd), for CO_2 0.1 ± 0.4 ppm and for CH_4 -0.4 ± 3.4 ppb CH_4. To determine the normal fluctuations which occur in the differences between the two analysers even when the same sample is measured, all analysers measures the same ambient air from Schneefernerhaus for 15 days (section5.1.6). The standard deviation of the hourly averages between the Schneefernerhaus analysers and the CRDS normally used to measure ambient air of the mountain ridge is only 0.6 ppb in CO, 0.02 ppm in CO_2 and 0.2 ppb in CH_4. The high standard deviations of the differences between ambient air of Schneefernerhaus and the mountain ridge are not attributed to the analysers but are probably caused by the two different measuring locations where the air masses often occur with a time delay and the local wind conditions are usually different due to the complex topography (figure 3.3b).

To analyse the deviation between CO, CO_2 and CH_4 mole fractions measured at Schneefernerhaus and at the mountain ridge in more detail, the frequency of the differences between both locations is shown on the right panel in figure 5.9. For a better resolution the one minute averaged data are used but again local pollution events are excluded from the Schneefernerhaus time series. The frequency of the whole data set, which is shown in black, is divided into night-time (blue) and daytime (red). If the same mole fraction is measured at both locations, a symmetric distribution should be seen

due to measurement uncertainties. An asymmetric curve indicates the appearance of time intervals or events with higher mole fractions at only one location.

The difference of the CO mole fraction has a symmetric distribution with the same number of data points on the left and right side of the most probable value (mpv=0.3 ppm).

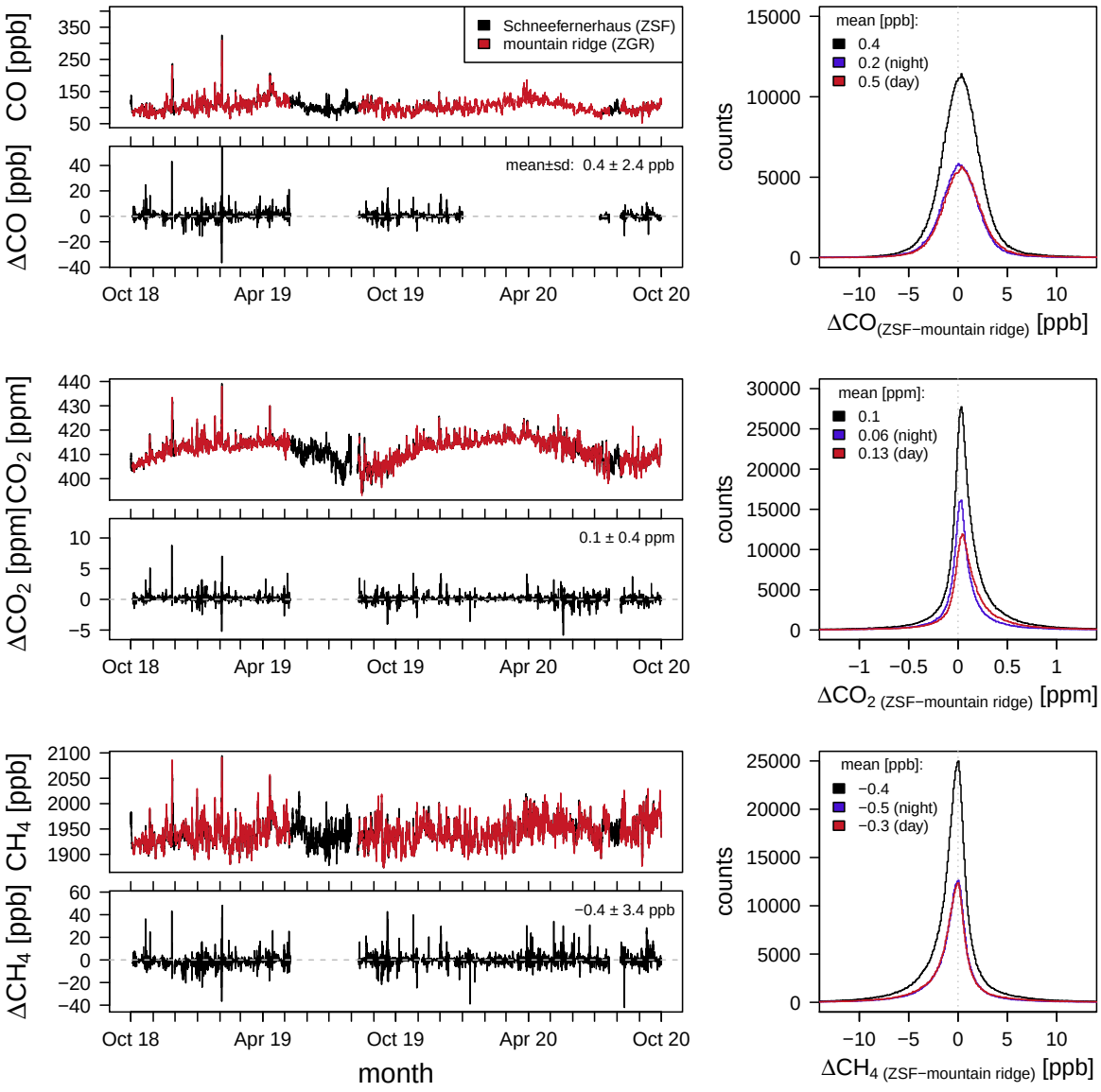

Figure 5.9.: CO, CO_2 and CH_4 measurements at Schneefernerhaus and mountain ridge. Left: hourly averaged Schneefernerhaus (excluding local pollution events) and mountain ridge mole fractions of CO, CO_2 and CH_4 as well as the difference between both locations. Right: The frequency of the differences between Schneefernerhaus and the mountain ridge calculated out of the minutely averaged data. The blue lines correspond to night-time data between 18 and 6 UTC, and the red lines to daytime data.

During the day (6 to 18 UTC), the mean difference shifts 0.3 ppb to larger values compared to the night-time value. As the distribution at night and during the day stays symmetric, the slight CO offset between Schneefernerhaus and mountain ridge could probably be caused by the altitude difference of the two locations so that slightly more CO polluted ambient air reaches the station Schneefernerhaus and not the mountain ridge during the day or it is an influence of the intake line. However, the differences in CO are very low and within the uncertainties of the analysers.

The difference of the CO_2 mole fractions show a strongly asymmetric distribution with more data (59 %) right of the mpv of 0.03 ppm. The higher number of slightly positive CO_2 mole fraction differences indicates higher values at Schneefernerhaus than at the mountain ridge. During the day (6 to 18 UTC) the mean difference increases from 0.06 ppm at night (18-6 UTC) to 0.13 ppm and also the asymmetry distribution intensifies compared to the night. Therefore, it seems that there is still a small but significant influence of local pollution on the daytime CO_2 mole fractions measured at Schneefernerhaus which is not excluded by the manual flagging. However, the influence of local CO_2 pollution at Schneefernerhaus is smaller than the one measured at the mountain station Jungfraujoch with a mean difference of 0.49 ppm between the usual location and a less polluted one during the day and of 0.01 ppm overnight (Affolter et al., 2021).

The CH_4 mole fraction distribution of the differences between Schneefernerhaus and mountain ridge has a higher amount of data (60 %) left of the most probable value (mpv=0 ppb). Thus, at Schneefernerhaus more data points have lower mole fractions than the corresponding mountain ridge measurement. The distribution of the night-time (18 to 6 UTC) and daytime values is similar with only a slightly lower mean value of 0.2 ppb during the night. As the most probable value is zero, the mean difference is probably not caused by the elevation difference or an influence of the intake line. At Schneefernerhaus several time periods with negative CH_4 spikes could be monitored due to CH_4 depleted air from the rack railway tunnel (see section 5.2.2). This lowers the CH_4 mole fraction measured at Schneefernerhaus and probably causes the mean negative difference with respect to mountain ridge data.

5.2.4. Diurnal and annual cycle

The annual and diurnal cycles of the mole fraction of CO, CO_2 and CH_4 measured in ambient air at Schneefernerhaus (black and blue) and the mountain ridge (red) are shown in figure 5.10. The left panels display the monthly mean mole fractions of the two locations and the right panels the diurnal cycles for different seasons.

In the evaluation of the monthly mean values and the diurnal cycles only data are considered where measurements are available for both locations simultaneously. The only exceptions are done in the calculation of the monthly mean mole fractions when measurements of only one location are available for the whole month. The diurnal cycles are determined for each month and are then combined for the high alpine winter (Oct to Mar) and in addition for the summer (Apr to Sep).

The annual and diurnal cycle of CO measured at Schneefernerhaus and the mountain

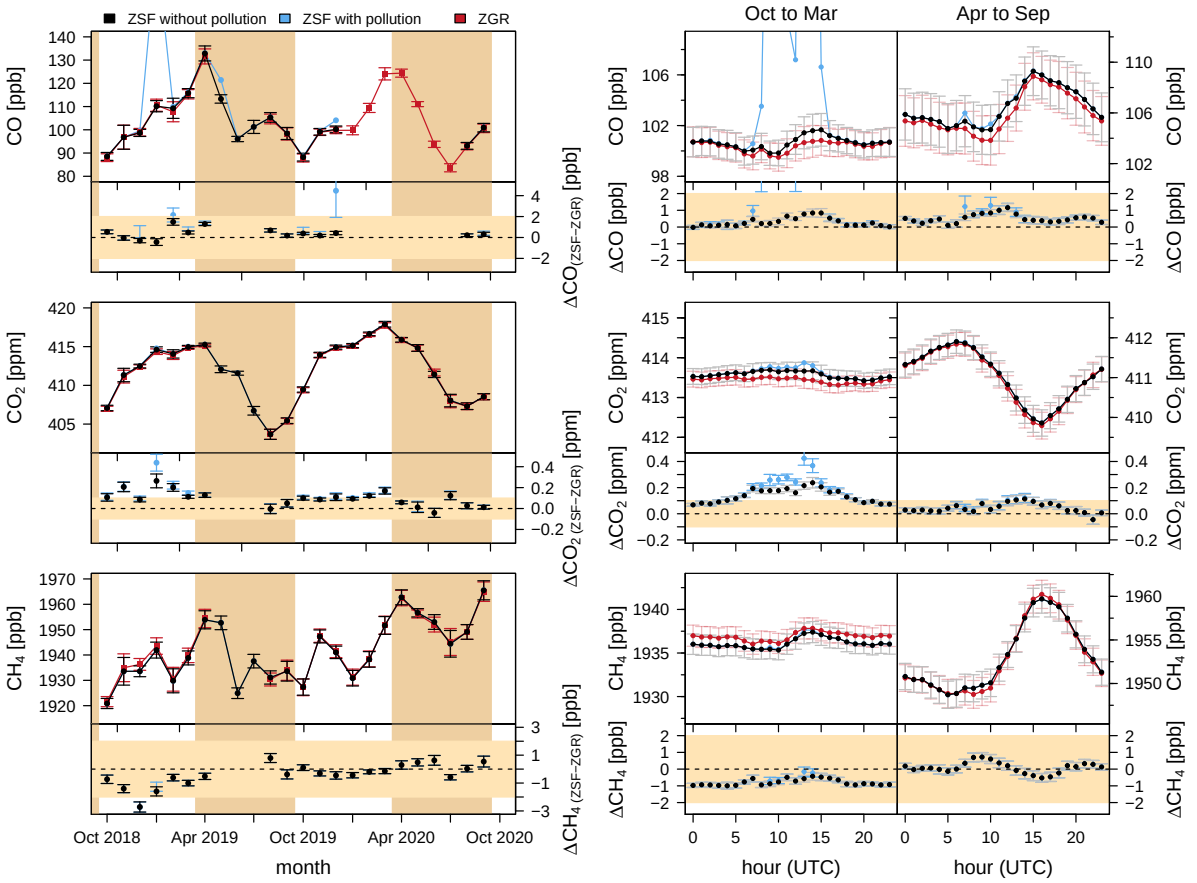

Figure 5.10.: Diurnal and annual cycles in the Schneefernerhaus (black/blue) and mountain ridge (red) measurement. In addition, the difference between the Schneefernerhaus and the mountain ridge is shown.

ridge does not show significant deviations with differences below 2 ppb. Within these 2 ppb, the largest differences occur during the day. This can indicate small influences of local pollution which is not flagged, since the polluted Schneefernerhaus time series also shows larger deviations from the mountain ridge measurements during this time.

This behaviour of stronger positive differences between Schneefernerhaus and the mountain ridge during the day for both Schneefernerhaus data-sets (with and without excluded local pollution events), is more prominent for the CO_2 mole fractions especially in winter. Thus, it seems that for CO_2 local pollution still influences the flagged Schneefernerhaus data-set. While in summer (Apr to Sep), the differences in the monthly CO_2 mole fractions and of the diurnal cycle are usually within 0.1 ppm and thus negligible, the differences are larger in winter (Oct to Mar) showing values up to 0.24 ppm. The diurnal cycle of differences between the measurements at the usual location at Jungfraujoch and a less polluted one show diurnal cycles, too, but with much stronger deviations up to 0.4 ppm in winter and even up to 1.3 ppm in summer (Affolter et al., 2021). Even though the data points marked as local pollution are not excluded, the maximum mean

difference between Schneefernerhaus and mountain ridge is 0.35 ppm in winter (Oct to Mar) during the day. Therefore, at Schneefernerhaus and Jungfraujoch the main local CO_2 pollution seems to originate from different sources. While at Schneefernerhaus the data are influenced more strongly in winter, at Jungfraujoch the strongest impact was found in summer.

At Schneefernerhaus, we can notice two effects. First, the differences between Schneefernerhaus and the mountain ridge are larger during the day than at night and thus the Schneefernerhaus data are probably still influenced by local pollution. This is true for winter and summer values, since the peak-to-peak amplitude of the diurnal cycles of the differences between Schneefernerhaus and the mountain ridge are comparable for winter (0.17 ppm) and summer (0.16 ppm). Secondly, the average night-time (18 to 6 UTC) CO_2 mole fraction in winter (Oct to Mar) with 0.09 ppm is approximately 0.07 ppm larger than in summer (Apr to Sep). The larger differences in CO_2 in winter than in summer can be noticed in the monthly mean CO_2 mole fractions, too. The different offset in the CO_2 mole fraction between Schneefernerhaus and mountain ridge may originate from stronger CO_2 pollution in winter which also has an impact on the night-time values.

The annual and diurnal cycle of CH_4 measured at Schneefernerhaus and the mountain ridge are the same with negligible deviations smaller than 2 ppb, except for one value in December 2018. It seems that the monthly mean CH_4 mole fractions at Schneefernerhaus are slightly lower in the winter 2018/19 but also in the winter 2019/20 than the values at the mountain ridge. We notice that Schneefernerhaus data are particularly low compared to mountain ridge data when strong and multiple negative CH_4 spikes occur due to the influence of the rack railway tunnel. Thus, the influence of the rack railway tunnel probably causes the stronger deviations in winter.

In summary, the differences of the Schneefernerhaus and mountain ridge annual and diurnal cycle are negligible for CO and CH_4 and only small for CO_2. The CO_2 mole fractions during the day in winter is not negligible and may originate from pollution during the day which has not been excluded yet. In addition, especially for CO but also CO_2 it is important to filter out strong local pollution events to assure accurate results in winter.

5.2.5. Weekend dependency

Local pollution of CO and CO_2 at Schneefernerhaus occurs more often during the day. Since more tourists visit mount Zugspitze during the weekend, but work at Schneefernerhaus is usually carried out on weekdays, we analyse the weekend dependency in the CO, CO_2 and CH_4 time series.

For these calculations, data are only used if measurements at Schneefernerhaus and the mountain ridge are available at the same time. These data are first averaged by hour and then by day. Another limitation to preserve the variations within the week is that only complete weeks are used when daily averages are available for each day of the week. In figure 5.11 the CO, CO_2 and CH_4 mole fractions averaged over each weekday are shown for Oct 2018 to Oct 2020. The mountain ridge data are displayed in red and

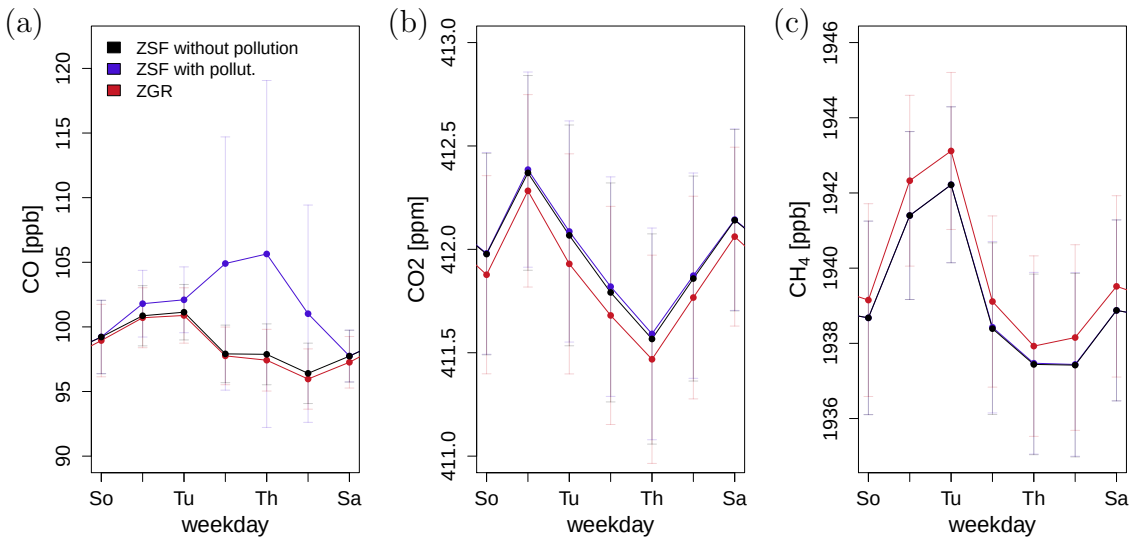

Figure 5.11.: Weekly cycle calculated for the Schneefernerhaus (black and blue) and mountain ridge (red) time series.

the Schneefernerhaus data without and with included local pollution events in black and blue. For CO, CO_2 and CH_4 the unpolluted Schneefernerhaus data (black) and the mountain ridge data have a similar shape with slightly higher values at Schneefernerhaus in CO and CO_2 and slightly lower ones in CH_4. These differences were already noticed in the previous sections when comparing Schneefernerhaus and mountain ridge data and do not vary significantly during the week. While the polluted Schneefernerhaus data (blue) do not vary much from the unpolluted ones (black) in CO_2 and CH_4, a strong increase in the mole fraction during weekdays is noticeable in CO.

For all three trace gases we can notice some variations in the averaged mole fractions for each day of the week. However, the uncertainties of these mole fractions are very large. To determine if these weekly cycles are consistent with natural variability or could be caused by anthropogenic emissions, we analyse if there is a significant difference between weekend and weekday.

To identify if a significant difference between the mean weekday $\overline{X_1}$ and mean weekend mole fraction $\overline{X_2}$ occurs, we examine the t-value of the time series:

$$t = \frac{\overline{X_1} - \overline{X_2} - \omega_0}{\sqrt{\frac{s_1}{n_1} + \frac{s_2}{n_2}}}. \tag{5.1}$$

s are the standard deviations of the weekend or weekday data and n the number of data points. Instead of the normal t-statistic we use a resampling technique (Daniel et al., 2012) in order to determine the distribution to account for temporal autocorrelation in the time series. The idea is to resample new "random" time series out of the original one with a similar temporal autocorrelation and distribution to the original time series. Therefore, a block of data with length l (l following points) is randomly taken out of the original time series and is placed as an entire block in the new time series. This is done

multiple times until the resampled time series has the same length as the original one. As the extracted block is chosen randomly each time, it is possible to resample some data points of the original time series multiple times and others not at all. Following the suggestion of Wilks (1997) we determine the block lengths l out of the number of data points n and the lag-1 autocorrelation coefficient a of the original time series:

$$l = (n - l + 1)^{\left(\frac{2}{3}\right)\left(1-\frac{1-a}{1+a}\right)} \tag{5.2}$$

For 5000 resampled time series we calculate the t-value to determine the distribution function. If the p-value, which is calculated for the original time series using the determined distribution function, is smaller than the significance level of 0.1 or 0.05, it is unlikely that the difference between mean weekday and mean weekend data is caused by natural variabilities.

To apply the resampling technique to our data, we de-trended the daily mean values before averaging over each weekday by subtracting a moving 31 day mean to remove the annual cycle. The general pattern of the averaged values for each weekday for Schneefernerhaus and mountain ridge shown in figure 5.11 does not vary strongly from the pattern of the de-trended one. However, for the resampling method the de-trending of data is necessary. Using the resampling technique, we test if the weekend effect magnitude i.e. the mean weekend value minus the mean weekday value is significant. For CO, CO_2 and CH_4 measured at Schneefernerhaus (including and excluding local pollution events) and at the mountain ridge all time series show no significant ($p > 0.1$) difference between weekend and weekday. The only exception where a significant ($p < 0.1$) weekend effect magnitude is noticed, is the CO time series at Schneefernerhaus, when the local pollution events are not excluded.

In addition to a possible weekly cycle, the diurnal cycles of the measured time series are analysed regarding differences between weekend and weekdays. The hourly averaged mole fractions of CO, CO_2 and CH_4 measured at Schneefernerhaus and the mountain ridge are de-trended by subtracting the night-time (16 to 6 UTC) diurnal average. Instead of the whole day the night-time values are chosen as potential local pollution is more prominent during the working day than during the night. The de-trended diurnal cycles are only used if they contain more than 12 values and only weeks are used if we have at least the Saturday and Sunday diurnal cycles and the diurnal cycles of two weekdays.

The diurnal cycles determined for CO and CH_4 have no significant difference at Schneefernerhaus and the mountain ridge (figure B.1). Also the diurnal cycles for CO_2 have a similar course for weekends and weekdays. The mean weekend (black)and weekday (red) diurnal CO_2 cycles averaged for each season are shown in figure 5.12 for Schneefernerhaus (unpolluted data) and the mountain ridge. Below the mean diurnal cycles the difference between weekday and weekend is displayed. In winter and summer the deviations between the diurnal cycles calculated for weekend and weekday only show small deviation with slightly stronger ones in summer. However, we have to keep in mind that we do not compare measurements done at the same time but on different days of the week, which can cause higher variability. Thus, no significant difference between

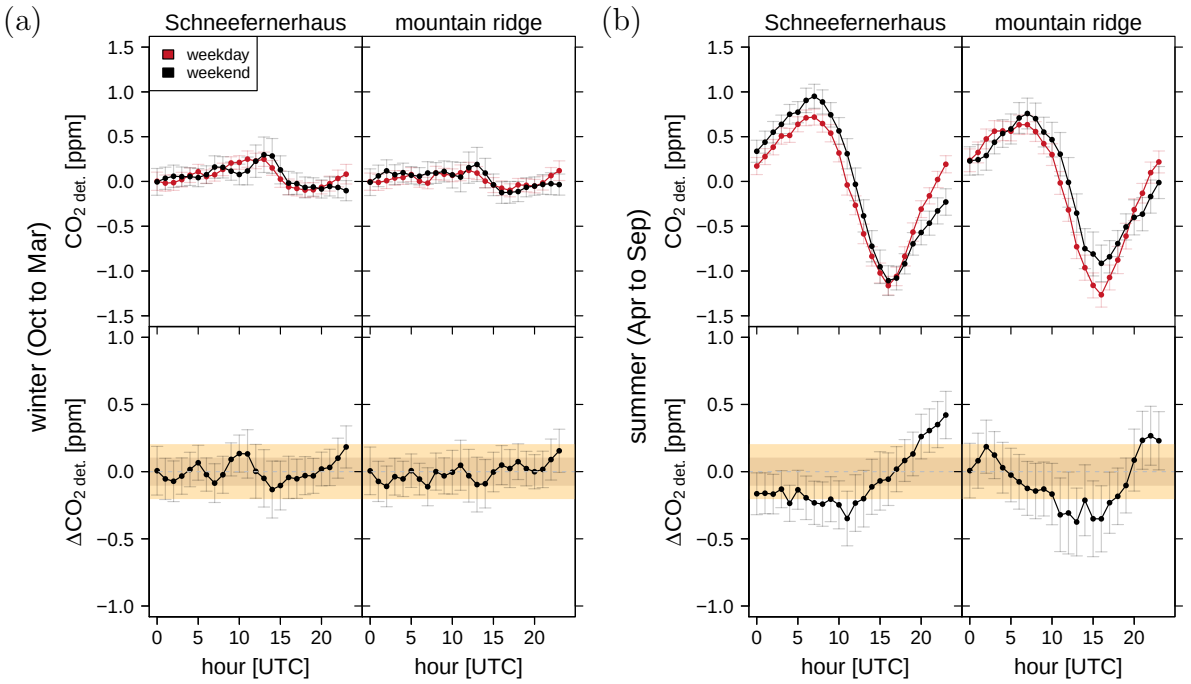

Figure 5.12.: Mean diurnal cycles of CO_2 for Schneefernerhaus and mountain ridge calculated with the weekend (black) and weekday (red) data for two seasons. The data between Oct 2018 and Oct 2020 are divided into winter (panel a) and summer (panel b).

weekend and weekday can be observed in the diurnal cycles, which cannot be explained by natural variability.

In summary, we found no significant difference between the CO, CO_2 and CH_4 mole fraction measured on weekends or on weekdays at Schneefernerhaus (excluding local pollution events) and the mountain ridge. In addition, the diurnal cycles of CO, CO_2 and CH_4 determined for weekend and weekday are similar, too.

5.2.6. Weekend dependency in CO_2 between 2002 and 2019

In this study, no weekly cycle in CO_2 and no difference in the diurnal cycles on weekend and weekday can be found for the time record between October 2018 and October 2020 (section 5.2.5). This is different to the results of an earlier study of Yuan et al. (2019) in which the CO_2 time series for Schneefernerhaus between 2002 and 2016 was analysed. Yuan et al. (2019) describe a weekly cycle with lower CO_2 mole fraction on weekend and higher CO_2 mole fraction on weekdays with a peak-to-peak amplitude of 0.76 ppm. Furthermore, they found stronger diurnal cycles on weekdays with higher values especially in the morning. They explained these findings by local anthropogenic working activities at Schneefernerhaus.

Since we cannot confirm these two findings for the recent time interval in our study, we analyse the CO_2 mole fraction of each year between 2002 and 2019. First, we calcu-

late the weekly CO_2 cycles for each year separately as described in section 5.2.5. The resampling approach is used again to determine if a significant ($p < 0.1$) difference between weekday and weekend mole fraction occurs. Between 2002 and 2006, in 2013, and between 2015 and 2019 no significant ($p < 0.1$) weekend effect magnitude is detected. However, in the years 2007 to 2014 (except for 2013) the weekend average is significantly ($p < 0.1$) lower than the weekday mean. For a further analysis, we separate the CO_2 record in three data sets: 2002 to 2006, 2007 to 2014 and 2015 to 2019.

In figure 5.13 the weekly cycles are shown for the three time intervals. For the three combined data sets only the one from 2007 to 2014 has a significant ($p < 0.05$) weekend effect magnitude. This time interval (2007 to 2014) has a peak-to-peak amplitude of 1.1 ppm which is even higher than the one reported by Yuan et al. (2019), as it is not flattened by averaging over multiple years without significant difference between weekday and weekend mole fraction. The fact that no weekly cycle can be noticed from 2015 to 2019 fits the results of our previous analysis of the CO_2 data between Oct 2018 and Oct 2020.

To analyse possible variations in the diurnal cycle of weekdays and weekends, we determine the diurnal cycles for weekend and weekdays for each year and notice in nearly all the years between 2002 and 2014 higher CO_2 mole fractions during the day on weekends than on weekdays, but no such pattern since 2015. Again, we separate the time series into the three time periods: 2002 to 2006, 2007 to 2014 and 2015 to 2019.

In figure 5.14 the the mean diurnal cycles for weekends and weekdays for summer and winter are shown, calculated in the same way as for the comparison measurement between Schneefernerhaus and mountain ridge as described in the section before. During the time periods from 2002 to 2006 and 2007 to 2014 higher CO_2 mole fraction during

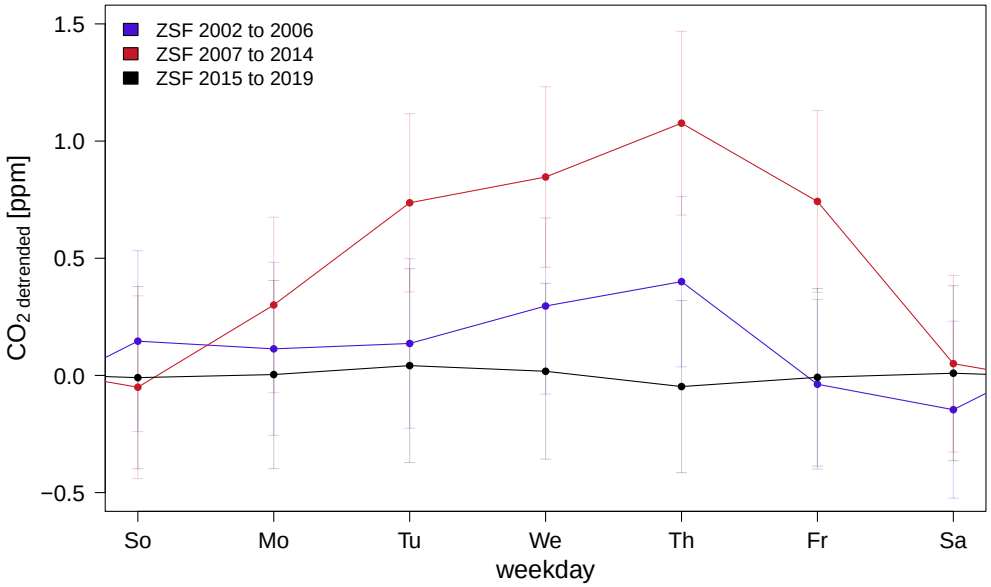

Figure 5.13.: Weekly cycle of CO_2 for three time intervals at Schneefernerhaus between 2002 and 2019 de-trended according to the mean weekend CO_2 mole fraction.

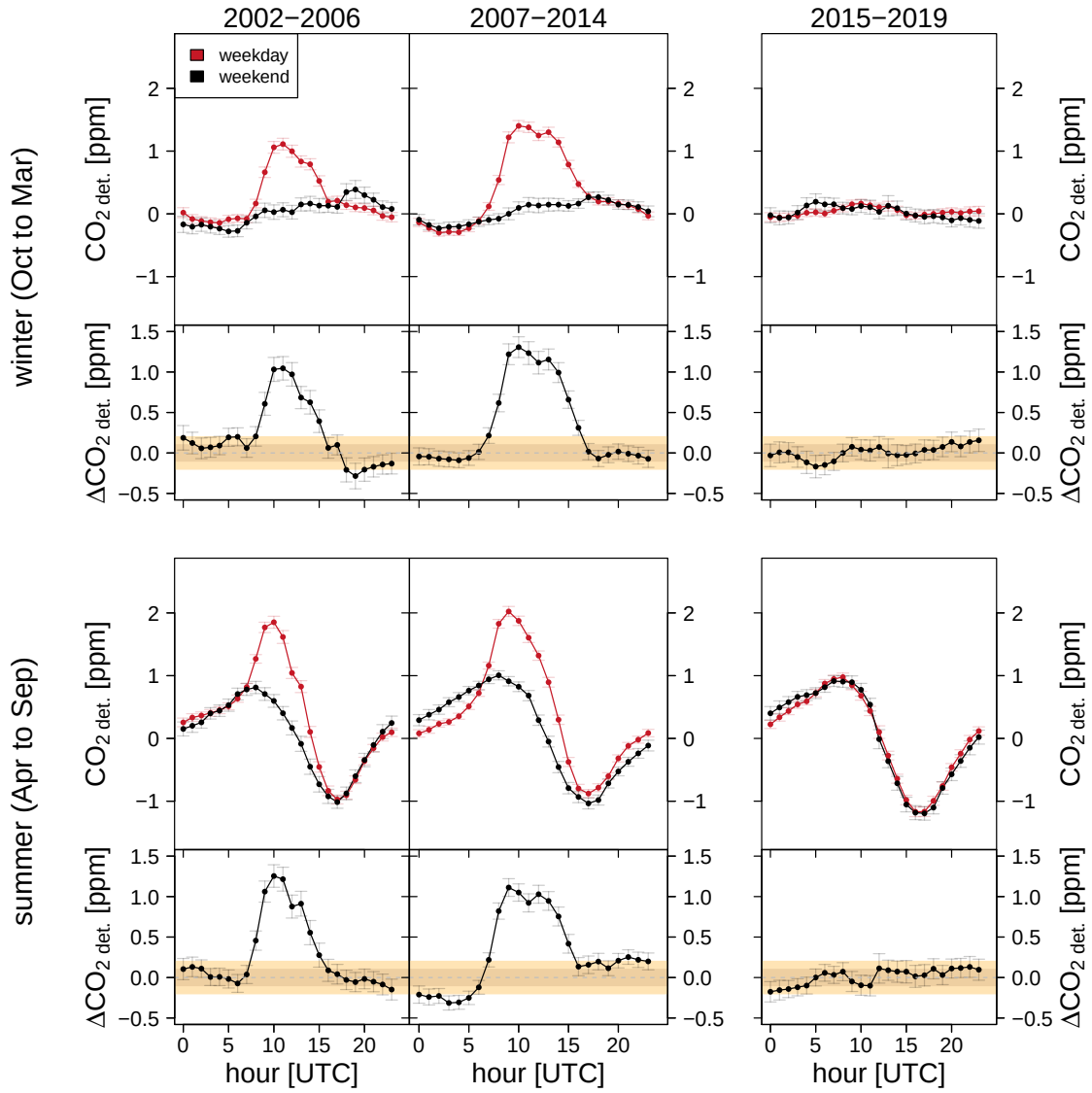

Figure 5.14.: Mean diurnal cycles for Schneefernerhaus calculated out of the weekend and weekday data between 2002 and 2019 for two seasons.

daytime (5 to 15 UTC) on weekdays are noticeable compared to weekend measurements for both seasons. While the difference between weekday and weekend cycle is usually smaller than 0.2 ppm during the night, during the day it reaches values between 1 to 1.5 ppm. Furthermore, no such CO_2 increase during the day on weekdays can be observed for the time period 2015 to 2019. This corresponds well with the observations made between Oct 2018 and Oct 2020 for Schneefernerhaus and mountain ridge. Moreover, the diurnal cycles of the weekends for the three time periods have the same amplitude and shape especially in summer.

In summary, stronger diurnal cycles with higher mole fractions during the day are visible in the CO_2 mole fractions before 2015 similar to the ones Yuan et al. (2019)

found for the combined data-set between 2002 and 20016. Additionally, higher mean weekend values than weekday values occur between 2007 to 2014, which is why Yuan et al. (2019) found a similar weekly cycle in the combined data-set.

Since tourist activities are more prominent during the weekend than on weekdays, the explanation of Yuan et al. (2019) that the two noticed weekend effects are caused by local anthropogenic working activities at Schneefernerhaus seems plausible. However, in this case a change in working activities at Schneefernerhaus must have taken place to explain that no weekend effects have been noticed since 2015. This could be a change in the experimental set-up, the data treatment or a possible impact of human respiration on the measurement. Between 2014 and 2015 no significant change of the analysers or the position of the inlet occurs, which could explain the changed weekend effects. In addition, we examined the unflagged CO_2 mole fractions since Oct 2018 and did not find any significant weekend effects either. Therefore, a change in the flagging routine should not be the reason for the noticed weekend effects until 2015. CO_2 from human respiration can also influence the CO_2 measurements. A change in the behaviour of the people at Schneefernerhaus such as visits of the research terrace is difficult to estimate but it is unlikely that it would cause such a strong impact on the data.

The most likely explanation is a micro leakage in the tubing with slight under-pressure. In this case a small amount of room air from the laboratory could have influenced the CO_2 data before 2015. The CO_2 mole fraction inside the laboratory increases during working hours through human respiration. At the end of 2014 the complete experimental set-up was controlled, which could have closed a possible micro leakage in the system.

5.3. Summary and Outlook

At Schneefernerhaus local pollution events can be noticed in the high resolution time series of CO, CO_2 and CH_4. They originate from human activities like snow groomers in the nearby ski resort, gasoline snow blowers used at the station, the nearby rack railway tunnel and human CO_2 respiration at Schneefernerhaus. These high spikes in CO and CO_2 mainly occur during the winter seasons and during the day. While at Schneefernerhaus approximately 2 % of the minutely CO and CO_2 mole fractions have to be excluded manually from the time series, the comparison measurement of ambient air of the mountain ridge showed a much lower influence by local pollution. On only 18 % and 16 % of the days when local CO and CO_2 pollution events occur at Schneefernerhaus, we can notice corresponding spikes at the mountain ridge but usually with much lower amplitudes.

Moreover, the average difference between the Schneefernerhaus time series, where strong local pollution events are excluded, and the mountain ridge record is not significant. Additionally, no significant difference is noticeable for the annual and diurnal cycles of CO and CH_4. Nevertheless the monthly averaged CH_4 mole fractions from Schneefernerhaus seem to be reduced slightly in winter due to the occurrence of negative CH_4 spikes which are caused by CH_4 depleted air from the nearby rack railway tunnel.

The average difference of the CO_2 mole fraction between Schneefernerhaus and mountain ridge is 0.1 ppm. Larger variations in the CO_2 difference of the two locations can be noticed between summer and winter months during the day but also at night. Furthermore, the diurnal CO_2 cycles indicate a small influence of local pollution during the day, which has not yet been excluded in the Schneefernerhaus time series. Especially in winter the hourly averaged difference between Schneefernerhaus and mountain ridge can reach 0.24 ppm.

By determining the origin of local emission events and their possible influence on the measurement, the measured time series at Zugspitze is now well understood. We showed that the thorough exclusion of local pollution events done manually by the station manager successfully removes the strong influence of local sources. Thus, the impact of local sources on trends and annual cycles determined out of time series from Schneefernerhaus is negligible. Nevertheless, manual flagging of data is time-consuming and more error-prone than measuring at a less polluted location.

This study demonstrates the possibility of reducing local influences of pollution in the time series from Zugspitze by measuring at the mountain ridge. However, the intake line to the mountain ridge is not always accessible, depending on the season as well as the weather, and then only by specially trained climbers. This makes maintenance work at the intake line to the mountain ridge difficult. To ensure a continuous time series but still have the advantage of less pollution and the opportunity to identify rare pollution events at the mountain ridge, the ongoing measurement at both locations Schneefernerhaus and mountain ridge would be important.

Another or complementary approach could be the automatic flagging of local pollution events, to reduce the time consuming manual exclusion of these. El Yazidi et al. (2018) showed that the so-called standard deviation (SD) method can be used for different stations to eliminate local pollution spikes. A first attempt to identify pollution events at Schneefernerhaus with the SD method marked strong local pollution, but it seems to be insufficient and less effective than the manual flagging. A further analysis of this and other peak detection methods is needed to find the one which fits our requirements best.

6. Ten years of high temporal resolution CH_4 measurements at Schauinsland

At the UBA station Schauinsland (see section 3.1.2) the CH_4 mole fraction in ambient air has been measured since 1991. Such time series of several decades are often used in inverse models to study CH_4 emissions on a global or continental scale. Therefore, it is important that the time series show no strong signal from very local sources as these cannot be simulated by models yet.

The CH_4 mole fraction at Schauinsland was measured with gas chromatography with flame ionisation detectors (GC-FID) between 1991 and 2015 (Schmidt et al., 1996).

During the last years new measurement techniques like CRDS enabled us to measure greenhouse gases at high temporal resolution of some seconds. Since 2011, the CH_4 mole fraction at Schauinsland has been measured with a data acquisition rate of approximately three seconds with a CRDS analyser. In those high temporal resolution measurements local pollution events may be detected which were unt noticed in the half-hourly or hourly averages.

At other remote mountain stations such as Pic du Midi (El Yazidi et al., 2018) and Jungfraujoch (Affolter et al., 2021) recent measurements have revealed the occasional influence of local anthropogenic activities. Furthermore, we have shown in chapter 5 that high CO, CO_2 and even CH_4 spikes are noticeable in the high temporal resolution time series from the remote station Schneefernerhaus at Zugspitze.

Therefore, the ten years of high temporal resolution CH_4 measurements at Schauinsland are analysed regarding local pollution. Strong local pollution events are visible in this time series. Thus, the aim of this study is to determine the origin of the pollution events and to quantify their impact on the hourly and monthly averaged CH_4 mole fractions. Furthermore, different peak detection methods are tested to remove the CH_4 spikes from the time series.

6.1. CH_4 spikes in high temporal resolution measurements

6.1.1. Measurement method

Since July 2011 the CRDS G2301 (Picarro, Inc., Santa Clara, CA) analyser has been measured the mole fraction of CH_4, CO_2 and H_2O of ambient air with high temporal resolution every three seconds. The air inlet is 12 m above ground. The CRDS analyser measures the undried ambient air continuously with a gas flow of typically 600 ml min^{-1}. In 2014 a multi-position valve (model: EMT2CSD16UWE, Valco Vici, Switzerland) was installed, which makes the automatic alternation between ambient air and calibration and quality control cylinder measurements possible.

A second CRDS G1301 analyser measures CH_4 and CO_2 in parallel, but without regular calibrations. These results are used for quicklooks and in some cases for gap filling.

To calibrate the CH_4 mole fractions measured at Schauinsland, gas cylinders are measured regularly with the CRDS G2301 analyser. Every few months two or three of 10 WMO standard cylinders are measured. Depending on these measurements the analyser is calibrated internally, approximately four times a year, by the station manager to compensate instrument drift and ensure accurate results. In addition, every day working standards are measured to observe the instrument drift.

In this study, the high temporal resolution CH_4 mole fractions since 2011 are used. Tank and room air measurements or artefacts and outliers, which may occur through technical problems with the analyser, have to be flagged in the time series. Therefore, we use the 1 min averaged data for the first quality check. Until 2014 no multi-position valve (MPV) was installed and cylinder measurements were noted by the station manager in an analogous lab-book. As the ambient air measurements are not dried and the measured cylinders have very low water vapour mole fractions, all data with water vapour mole fractions below a reference value as well as the 10 minutes before and after these values are excluded. Since the MPV has been installed, we take into account the flushing of the cavity by excluding the first five minutes after a change in the MPV position. Furthermore, the first minutes after the occurrence of a data gap, due to instrumental problems, are excluded and single outliers are filtered out from the already flagged data, too. After all invalid data are excluded in the minutely CH_4 time series, we use them to exclude invalid data out of the high temporal resolution time series of 3sec, too. Thus, we exclude all time periods which were recognised as invalid in the minutely CH_4 mole fractions also in the high temporal resolution time series. Additionally outliers are filtered out in the high temporal resolution time series, too.

Since 2014 a quality control target cylinder has been measured approximately every 51.5 hours for 20 minutes. The cylinder was replaced once by a new one in 2018. In figure 6.1 the averaged CH_4 mole fractions for each cylinder measurement are shown.

For short time intervals, the standard deviation of the two target cylinders is 0.2 ppb. However, we can clearly notice instrumental drift which is not removed by the calibration.

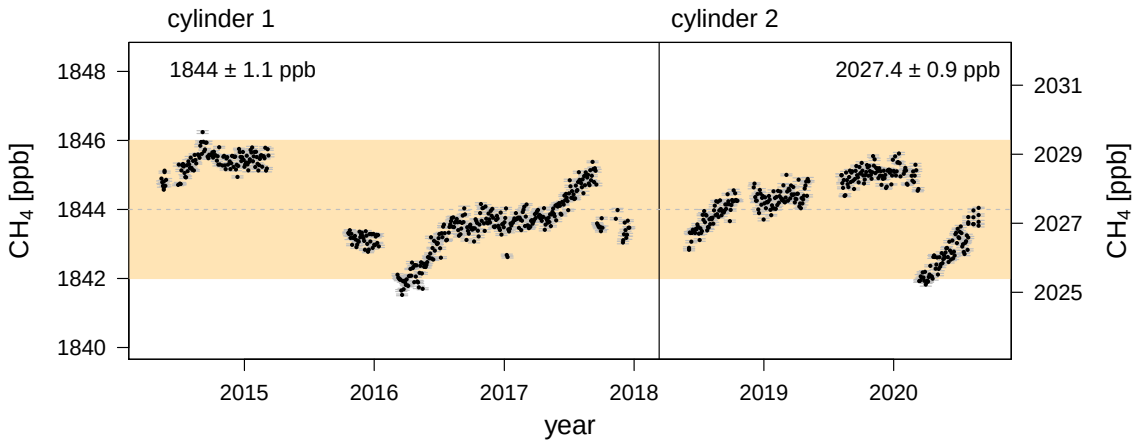

Figure 6.1.: Calibrated and averaged cylinder measurements of CH_4 carried out approximately every 51.5 hours with the CRDS G2301 at Schauinsland. The average and standard deviation of both cylinders are given.

Therefore, the accuracy of the CH_4 measurement would improve if the data are calibrated with a calibration cylinder measured every few days, rather than the internal calibration of the analyser which was performed about four times per year. Since Schauinsland station has recently joined ICOS, the data are now calibrated with the standardised calibration routine recommended by ICOS. Additionally, it must be examined whether a subsequent calibration via cylinder measurements is possible.

Even though there are still drifts in the CH_4 measurement of the two target cylinders, the standard deviation of $\sim$1 ppb is still smaller than the WMO compatibility goal (WMO, 2020) of 2 ppb. Furthermore, most values are within a 2 ppb interval around the cylinder mean. As we analyse the influence of local pollution on the CH_4 time series, the accuracy of the measurement is precise enough.

6.1.2. Measured time series of CH_4

The measured CH_4 mole fractions are normally averaged to hourly values in order to report the data to national and international data bases. In figure 6.2a the hourly CH_4 mole fractions measured between 2011 and 2020 at Schauinsland are shown in red revealing no strong pollution events. However, when having a closer look at the high resolution ($\sim$ 3 second) CH_4 values (black), strong and brief CH_4 peaks (spikes) with mole fractions of more than 2 500 ppb are noticeable especially during summer (beige areas).

In figure 6.2b the year 2017 is shown in more detail as an example. From June until the end of October strong CH_4 mole fractions occur. The fact that each individual spike only lasts a few seconds up to minutes (figure 6.2c) indicates a nearby source. Mobile measurements around the station have revealed two main sources of CH_4 close to the station. CH_4 is emitted by around 10 cows grazing in the surrounding meadows during summer and by the sewage pit of the station.

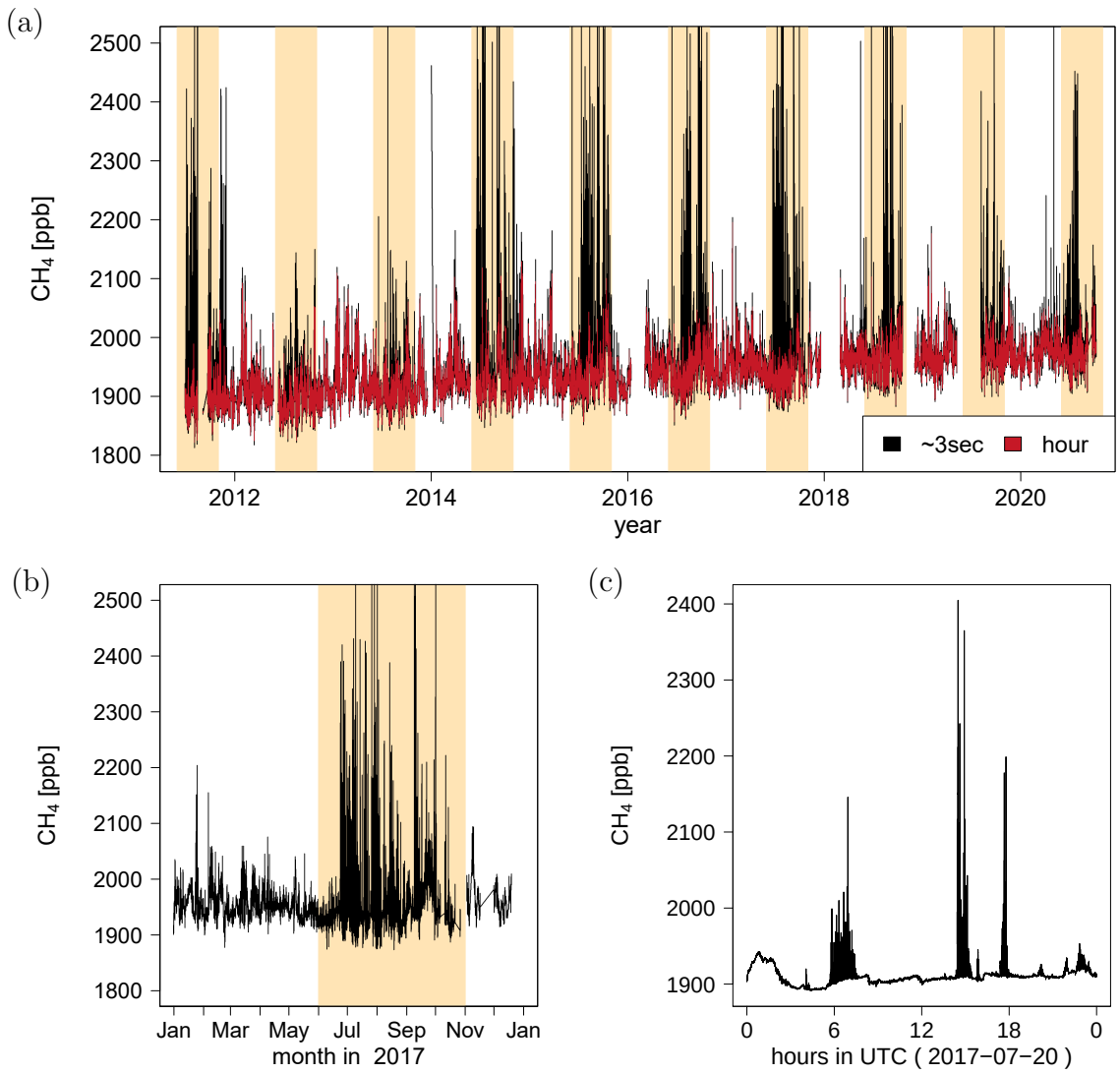

Figure 6.2.: High temporal resolution (∼3 seconds) CH_4 mole fractions measured at Schauinsland from 2011 to 2020 (a). The beige coloured areas indicate the time period from June to start of November for each year. In addition, the representative year 2017 (b) and a single day (c) are shown.

6.2. Identification of the origin of CH_4 spikes

We can assume that CH_4 emissions from cows and sewage pit have a seasonal variability. According to the local farmer (Meinrad Lorenz, personal communication) cows graze on the pastures near the station Schauinsland between mid June and October, which is exactly the time interval most of the high CH_4 mole fractions occur.

In sewage treatment facilities biogenic processes can produce CH_4. At the mountain station Pic du Midi, El Yazidi et al. (2018) noticed several high CH_4 spikes in the time series and could identify a small sewage treatment facility to be responsible. At

Schauinsland waste water is collected in a sewage pit right next to the station. As the biogenic processes producing CH_4 are temperature dependent, higher temperatures in summer and early autumn can lead to stronger CH_4 emissions from the sewage pit. During winter months the soil around Schauinsland is mostly covered with snow and microbial processes are less active.

6.2.1. Characterisation of emissions from the sewage pit and cows

In order to identify the source of the high CH_4 mole fractions both potential sources (sewage pit and cows) are characterised. Therefore, the isotopic source signatures of CH_4 and CO_2 as well as the CH_4 to CO_2 ratio are calculated using measurements of sewage pit and cow emissions. These measurements were carried out with a mobile set-up and the CRDS G2201-i analyser. The analyser measures the CH_4 and CO_2 mole fraction as well as the ^{13}C isotopic ratio.

Experimental set-up

Ambient air which enters the intake line of the set-up is filtered for coarse particles and is then dried with a Nafion dryer before it is measured by the analyser (figure 6.3). In addition, a second split-off flow leads ambient air through a so-called AirCore (Karion et al., 2010). The AirCore is a 25 m long Dekarbon tube and it enables us to store air from the last 2 min for later analysis. The experimental set-up can be installed inside a vehicle and ambient air which enters the air intake line 20 cm above the vehicle roof is measured with the CRDS G2201-i analyser while driving. The emissions from a source, for example cows, are then measured by driving downwind through the emission plume. Especially for the measurement of the ^{13}C isotopic ratio a higher accuracy can be achieved by remeasuring the emission plume with a smaller flow using the AirCore to increase the time resolution. The above described mobile set-up including the AirCore is explained in more detail in Hoheisel et al. (2019).

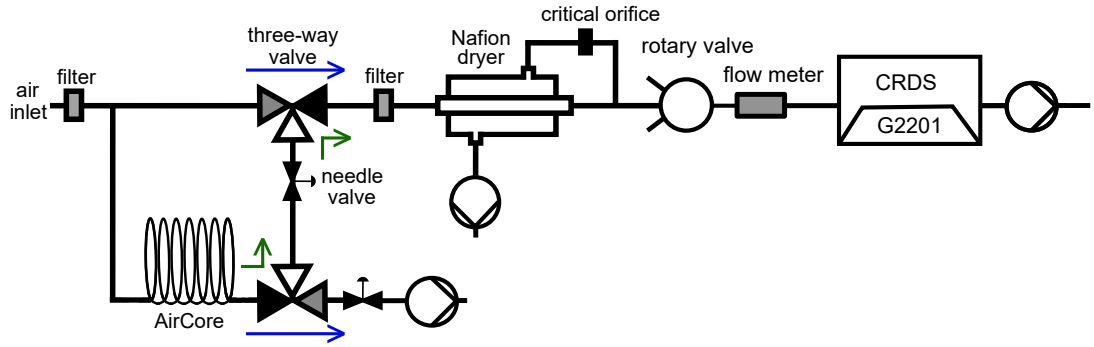

Figure 6.3.: Mobile ambient air measurement set-up to characterise the emission from sewage pit and cows. The blue arrows show the air flow in "monitoring mode" when ambient air is measured directly. The green arrows correspond to "replay mode", when the air stored in the AirCore is remeasured.

Measurements

Measurements at the sewage pit are carried out by installing the air inlet of the set-up near the venting tube of the pit. Four data sets are used to characterise the emissions. The measurements directly at the sewage pit show high and short CH_4 peaks of several seconds up to minutes which ranging from 2 500 up to 350 000 ppb. Thus CH_4 emissions from the pit are not continuous, but high CH_4 spikes can frequently be measured. In figure 6.4 two exemplary time intervals of 30 minutes are shown. All used data-sets are presented in figure C.2. A fifteen-hour night-time measurement was done at the sewage pit in March 2018 using an intake line which was placed seven centimetres within the vent of the pit (sewage pit 1). Short spikes of several minutes occurred with mole fractions up to 14 000 ppb. For four days in August 2019 air at different heights above the venting tube of the sewage pit was analysed. For the characterisation we distinguish between one continuous night-time measurement (sewage pit 2) from 19 to 3 UTC ($\sim$ 8 h) and all daytime measurements (sewage pit 3) with a total measurement time of $\sim$ 10 h done with the intake line seven centimetres within the venting tube of the sewage pit. In addition, all measurements done within zero to ten centimetres above the vent (sewage pit 4) are used ($\sim$2 h). Since the CH_4 and $\delta^{13}CH_4$ measurements are most accurate for mole fractions below 13 000 ppb, data with CH_4 mole fractions above this value are excluded.

Measuring several hours directly next to the cows, as it was done for the sewage pit measurement, was not possible as the cows move freely on a large meadow and the wind direction changed strongly. Therefore, we carried out measurements of the emission

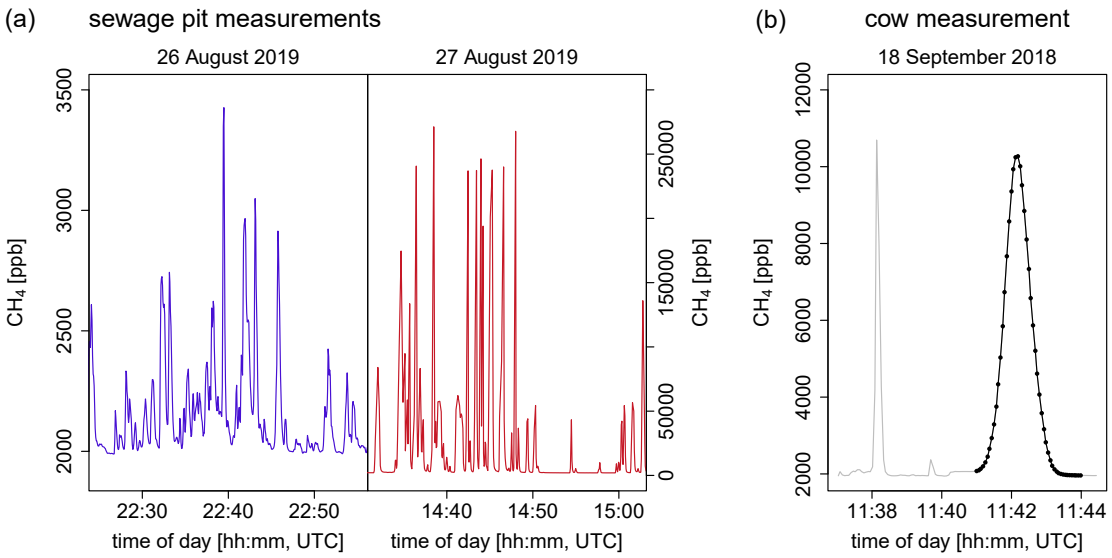

Figure 6.4.: Measured CH_4 emissions from the sewage pit (a) and from cows (b). The different colours in panel (a) correspond to different measurement intervals. In panel (b) the plume transect measured while driving are shown in grey and the corresponding AirCore measurement in black.

plume downwind of the cows in September 2018. The measured CH_4 mole fractions were mostly below 15 000 ppb within the plume. Three times the transect through the emission plume of the cows was remeasured with the so-called AirCore. While passing the emission plume of the cows, the AirCore is filled with ambient air. The air which is stored in the AirCore can be remeasured afterwards with a lower flow and thus with a higher temporal resolution. One of these measurements is shown in figure 6.4. The CH_4 mole fractions measured while driving through the emission plume are displayed in grey and the following AirCore measurement in black. These AirCore measurements are used to characterise the emission of the cows.

Analysis

The isotopic source signatures of CH_4 are determined for the four measurements at the sewage pit and the three AirCore measurements near the cows. As described in section 4.4.1 the Miller-Tans method and the York fit are used (figure 6.5a). The sewage pit has an isotopic CH_4 source signature of -51 ± 2 ‰ (mean ± standard error of the mean) and CH_4 emitted by cows of -71 ± 1 ‰. The extremely depleted CH_4 emitted by the cows can be attributed to a diet of 100 % grass (see also Levin et al., 1993). The isotopic source signature of the sewage pit is similar to the value of -50.7 ± 1.1 ‰ determined by Zazzeri (2016) for the anaerobic digester on a sewage treatment plant.

The isotopic source signature of CO_2 (figure 6.5b) is determined analogously to CH_4. The calculated source signature of one sewage pit measurement (#4) differs from the other ones. The same can be noticed for one cow measurement (#1). An explanation can be that for these two measurements the peak height is below 150 ppm CO_2. If the peak height relative to the background concentration is small compared to the precision of thr $\delta^{13}CO_2$ measurement the linear behaviour is less prominent and in addition the fit error often underestimates the inaccuracy of the determination. To calculate the mean isotopic source signature of CO_2, these two measurements with peak heights lower 150 ppm CO_2 are excluded. The sewage pit has an isotopic CO_2 source signature of -29 ± 1 ‰ (mean ± standard error of the mean) and the cows of -27 ± 1 ‰. Compared to the isotopic source signature of CH_4 the difference between sewage pit and cows is less prominent for CO_2. Former studies of Metges et al. (1990) or Passey et al. (2005) have shown, that the isotopic composition of CO_2 emitted by cows strongly depends on the diet and hence can vary from -28 to -11 ‰. More depleted values are noticed when the diet has a higher content of C_3-plants. This is the case at Schauinsland, where the cows are fed with grass. Thus, our result of -27 ± 1‰ agrees with these studies.

Furthermore, we calculate the CH_4 to CO_2 ratio. The ratios calculated for each of the four sewage pit measurements deviate strongly. Also no consistent ratio can be determined for the emissions of cows out of the three AirCore measurements.

In summary, the emissions of sewage pit and cows differ significantly in the isotopic source signature of CH_4, but no clear difference can be determined for the CO_2 source signature or the CH_4 to CO_2 ratio.

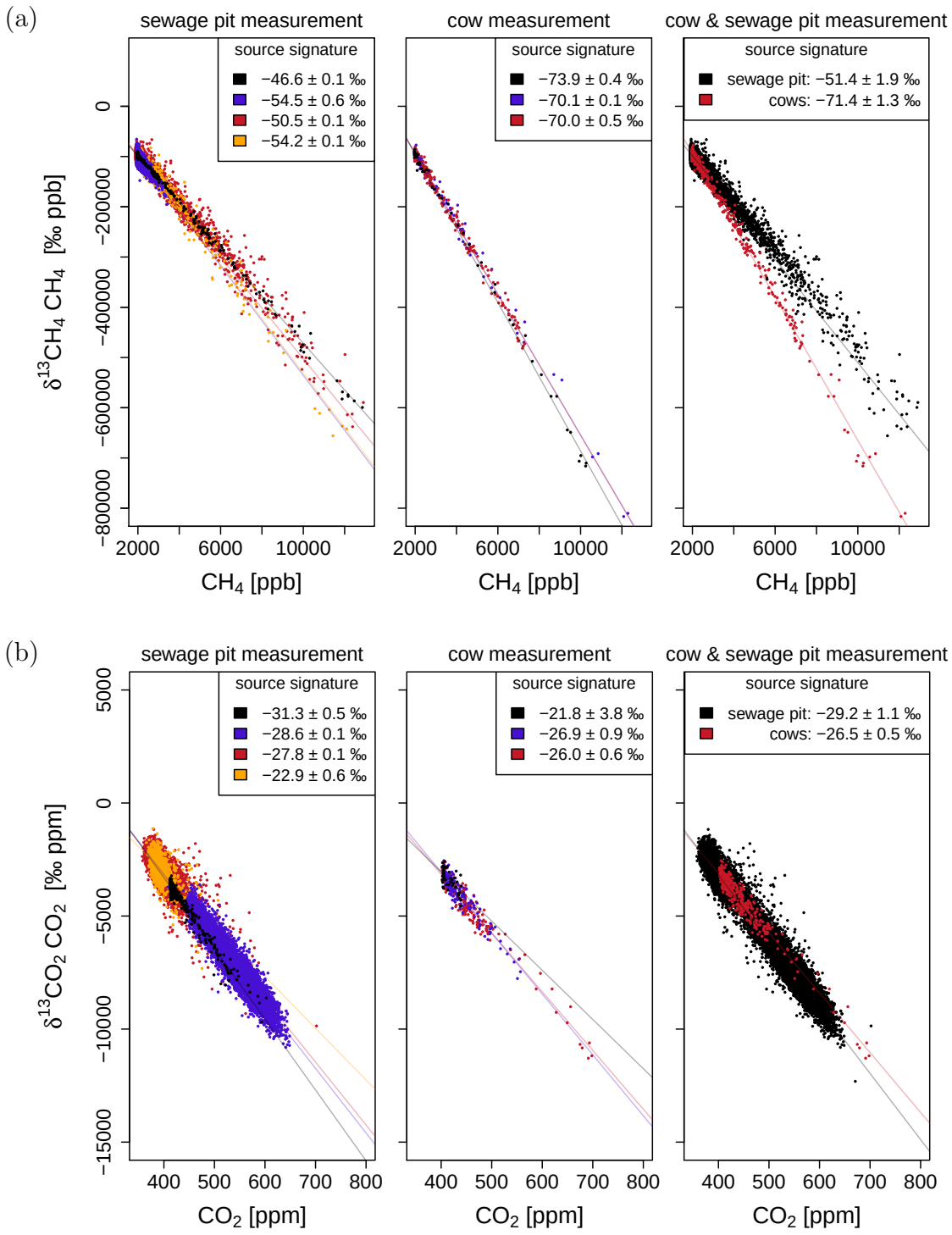

Figure 6.5.: Miller-Tans approach to determine the isotopic source signature of CH_4 (a) and CO_2 (b) for the measurements done at the sewage pit and near the cows.

6.2.2. Ambient $\delta^{13}CH_4$ measurements

The finding that the two local CH_4 sources strongly deviate in the CH_4 source signature by 20 ‰ can be used to determine which one probably causes the high and short CH_4 spikes noticed in the CH_4 record (described in section 6.1.2). When measuring these high CH_4 spikes in ambient air at Schauinsland, a parallel high temporal resolution measurement of $\delta^{13}CH_4$ was used to calculate the source signature of the emitted CH_4 spikes following the Miller-Tans approach. Since $\delta^{13}CH_4$ is not measured continuously at Schauinsland, the CRDS G2201-i analyser was installed there for three measurement campaigns. For one month in Sep/Oct 2018 and Feb/Mar 2019 as well as within four days in August 2019 the CRDS G2201-i analyser measured $\delta^{13}CH_4$ and $\delta^{13}CO_2$ in addition to CH_4 and CO_2. For these campaigns the CRDS G2201-i analyser used the same intake line as the continuous measurements done at Schauinsland by UBA, but the air was dried before the measurement. The experimental set-up used for these campaigns is described in more detail in appendix C.3.

In the three ambient air measurement campaigns with the G2201-i analyser we only captured high and short CH_4 spikes during the third campaign. In the first one, ambient air was dried with a cold trap. Due to the volume of the cold trap the signal was flattened so that the narrow spikes could not be measured. The second campaign was in February and during winter these high and short spikes did not occur. However, in the third campaign two events of strong CH_4 spikes could be monitored. Unfortunately, in both cases calibration measurements were performed during these events thereby shortening our ambient air data-set.

In figure 6.6 the two pollution events with high CH_4 mole fractions compared to background values are shown. In the bottom panels the corresponding Miller-Tans plots are displayed. Due to the low precision of the $\delta^{13}CH_4$ measurement with the CRDS G2201-i analyser in combination with relatively small peak heights no clear straight line is visible. Thus, although the measured CH_4 spikes are high for the CH_4 time series at Schauinsland, they are not high enough to get accurate isotopic source signatures using measurements done with the CRDS G2201-i analyser.

The determined isotopic source signatures of CH_4 are -84 ± 9 ‰ and -85 ± 11 ‰ respectively and thus indicate more biogenic sources such as cows. However, the values are about 10 ‰ more depleted than the isotopic source signature calculated for the cows at Schauinsland and have large uncertainties.

The CO_2 mole fraction measured when high CH_4 spikes appear do not show CO_2 spikes at all. The determination of the isotopic source signature of CO_2 is thus not possible.

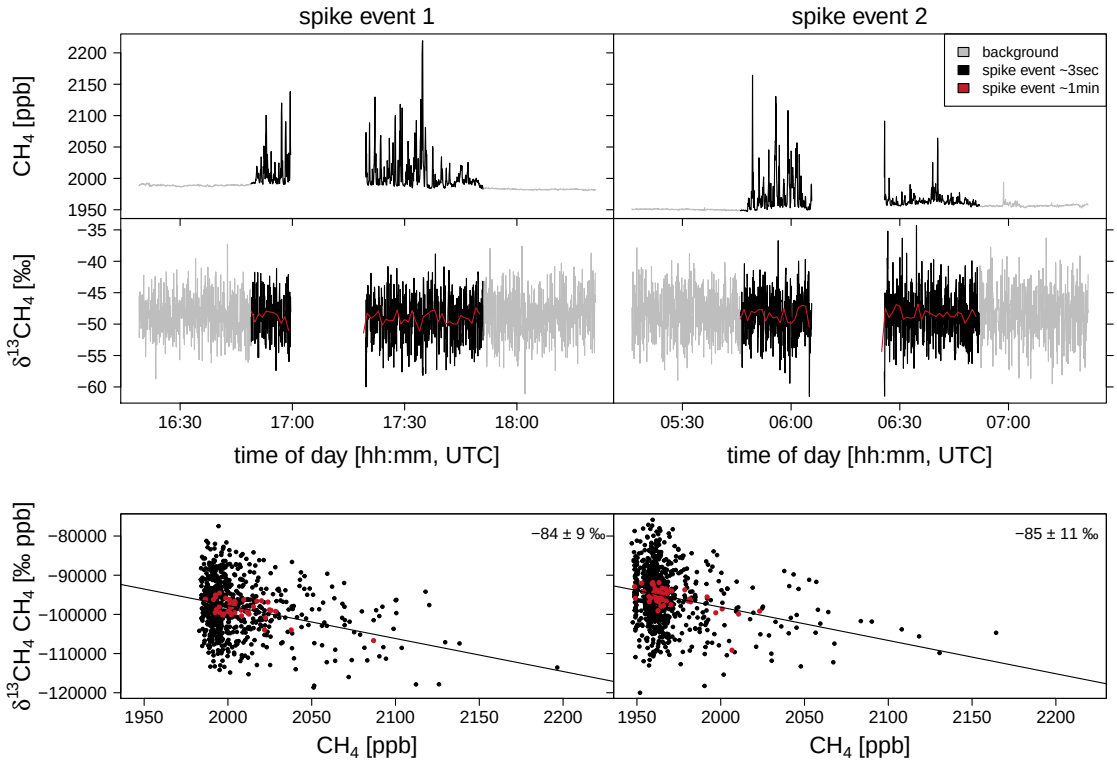

Figure 6.6.: Two time periods with high CH_4 spikes measured in ambient air at Schauinsland with the CRDS G2201 analyser. In the bottom panel the corresponding Miller-Tans plots to determine the isotopic source signature are shown. The resulting source signatures are displayed in the upper right corners.

6.2.3. Emissions from cows as origin of CH_4 spikes

Ambient air measurements of CH_4 and $\delta^{13}CH_4$ seem to indicate that the high CH_4 spikes originate from a sources like cows which emits strongly depleted CH_4. However, the determined source signature calculated from ambient air measurements is very imprecise.

Another indication that cows are responsible for the monitored CH_4 spikes is the observation of a typical event with high CH_4 mole fractions in August 2019 (figure 6.7a). At around 6:00 UTC we noticed that cows grazed right next to the station at the water trough (figure 6.7b). When looking at the CH_4 mole fractions measured at Schauinsland, we found that high CH_4 spikes started shortly before we noticed the cows nearby. The high CH_4 spikes are no longer visible after the cows were gone around 13 UTC. Thus, the sharp spikes occurred exactly when the cows were near the station.

Each year between June and September cows graze on a large pasture, one corner of which is adjacent to the station (Meinrad Lorenz, personal communication). The area which is part of this pasture is framed in yellow in figure 6.7b. Due to the size and hillside location, the cows are most of the time further away from the station and not visible until they move right next to the station to a water trough. Moreover, between 2018 and 2020 the wind blew in around 41 % of the time from south-west, which is

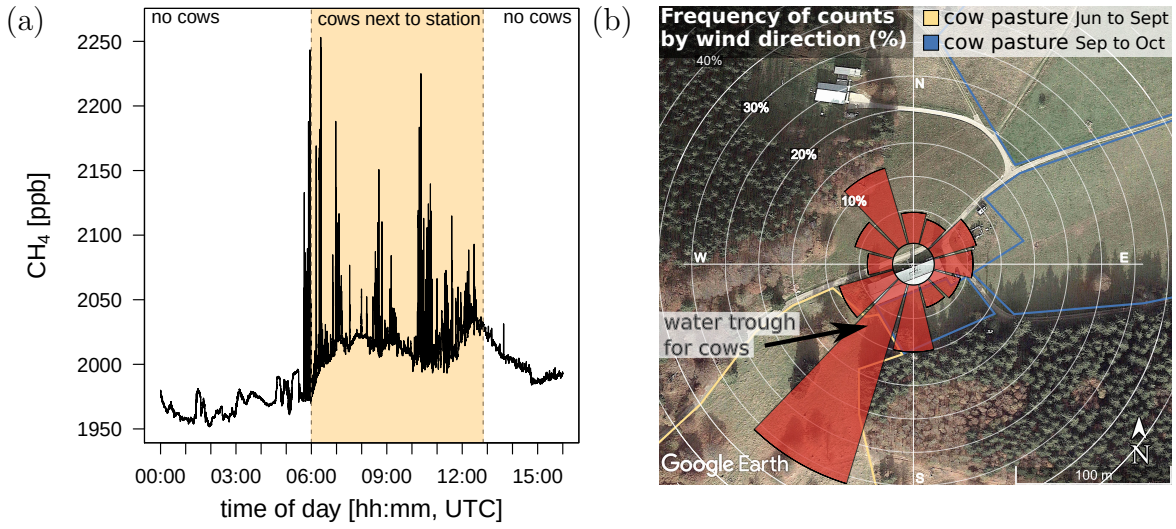

Figure 6.7.: Emissions from cows are the origin of CH_4 spikes.
(a): Observed event with high CH_4 spikes. The beige coloured area indicates when the presence of cows was noticed.
(b): At Schauinsland cows graze between Jun to Sep in the yellow bordered area south-west of the station. The cow pastures framed blue are used between Sep and Oct. In addition, the frequency of data points by wind direction between 2018 and 2020 are shown.

exactly the direction of the pasture. Between September and October the cows graze more east of the station (Meinrad Lorenz, personal communication) where the wind is less frequently blowing from.

Between 22 July 2020 and 21 August 2020 a camera was installed at the station to validate the assumption that the observed CH_4 spikes originate from cows. The camera is oriented to the south-west and takes a picture of the water trough every 10 minutes.

The CH_4 mole fractions measured during this time interval are shown in figure 6.8a. Whenever multiple high CH_4 spikes are measured, cows are visible in the pictures taken with the camera. As we can monitor only the part of the meadow right next to the station, smaller CH_4 spikes may originate from cows further away which are not visible for the camera. In figure 6.8b two days with CH_4 spike events are shown in more detail, to verify that cows are the main source of multiple high CH_4 spike events.

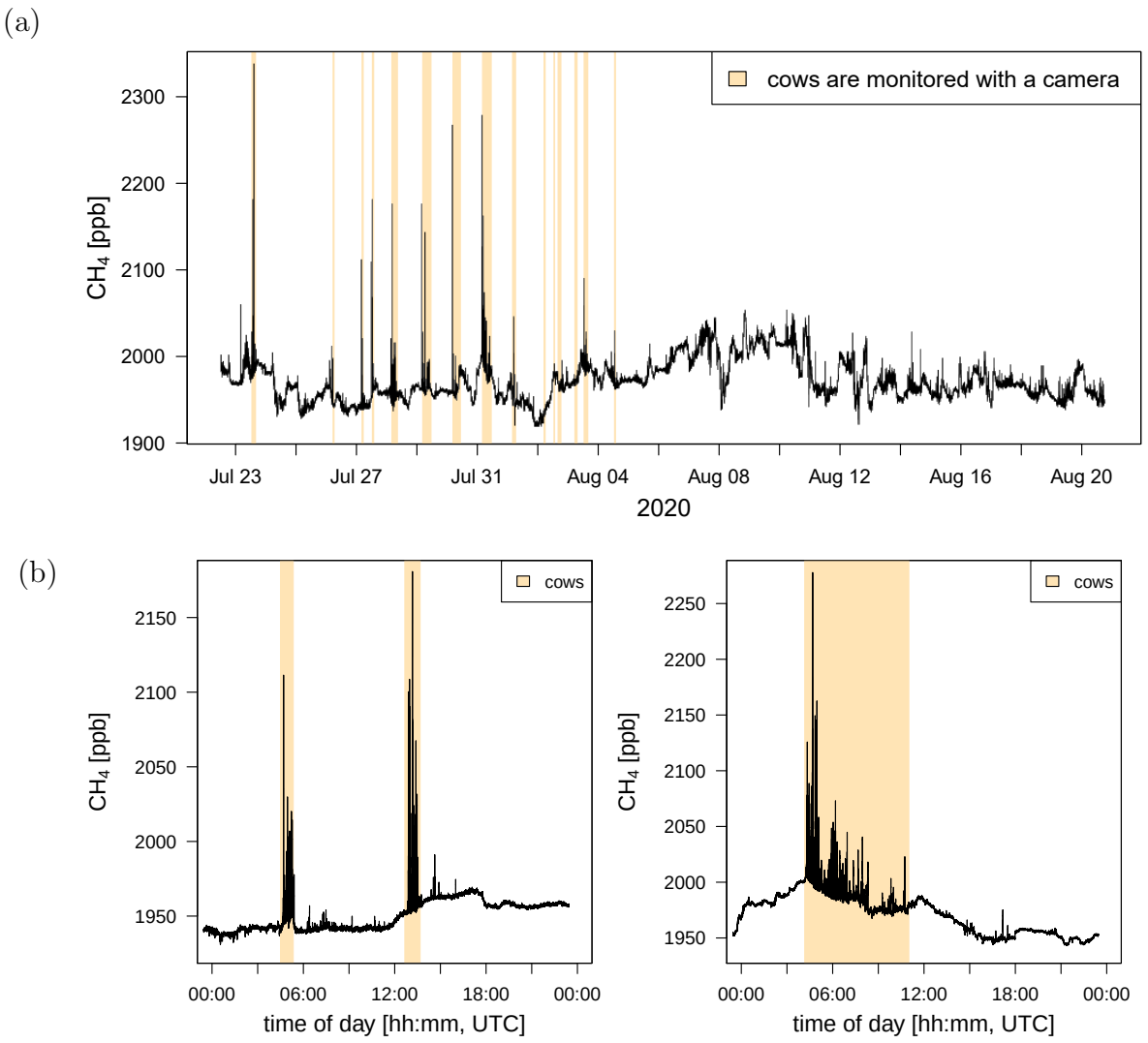

Figure 6.8.: CH_4 mole fraction measured at Schauinsland between July and August when a camera monitored the presence of cows (a). The beige time intervals indicate when cows were observed near the station. In addition, two days are shown in more detail in (b).

6.2.4. CH_4 emission flux from the sewage pit

To make sure that the CH_4 emissions from the sewage pit are no further source of CH_4 spikes, flow chambers were installed at the sewage pit during three campaigns to determine the CH_4 flux out of it. The idea is to measure the increasing CH_4 mole fraction in a known volume/chamber which is placed above the vent of the sewage pit. The emission flux j [kg s^{-1}] is then calculated out of the change of mole fraction with time $\frac{\Delta C}{\Delta t}$ [ppb s^{-1}] assuming pressure P [kPa] and temperature T [K] to be constant:

$$j = \frac{\Delta C}{\Delta t} \cdot \frac{V}{R} \frac{P}{T} \cdot M \tag{6.1}$$

V is the volume [m^3] combining flux chamber, tubing and cavity. M is the molar mass [$g\,mol^{-1}$] and R the universal gas constant $R = 8.3145\,J\,(Kmol)^{-1}$.

At the first two measurement campaigns in October 2019 and July 2020 a chamber with a volume of around $50\,l$ was installed above the vent of the sewage pit. As expected, the CH_4 concentration inside the chamber increased most of the time. However, the growth rates of CH_4 inside the chamber varied strongly with time and sometimes even decreasing mole fractions were measured. These variations may occur since the CH_4 emissions from the sewage pit are not constant, which was shown by measurements directly at the vent of the sewage pit. Instead of a continuous emission, the sewage pit emits high CH_4 mole fractions irregularly. This and the large volume of the chamber lead to an inhomogeneous CH_4 mole fraction inside the chamber. Therefore, only a rough estimation of the CH_4 (14 to 185 $mg\,day^{-1}$) and CO_2 (6 to 15 $g\,day^{-1}$) flux out of the sewage pit was possible.

To improve the flux measurement a different set-up was used in October 2020: a LiCor analyser (LI-7810,LI-COR, Inc., USA) in combination with a flux chamber (LI-8100A, LI-COR, Inc., USA). The flux chamber set-up has a much smaller volume of approximately $8\,l$. Therefore, the measured increase in CH_4 and CO_2 mole fraction is much more stable than in the experiments done before. In addition, the measurement time can be reduced to three minutes.

In figure 6.9 the increase in CH_4 and CO_2 inside the flux chamber is shown. The CH_4

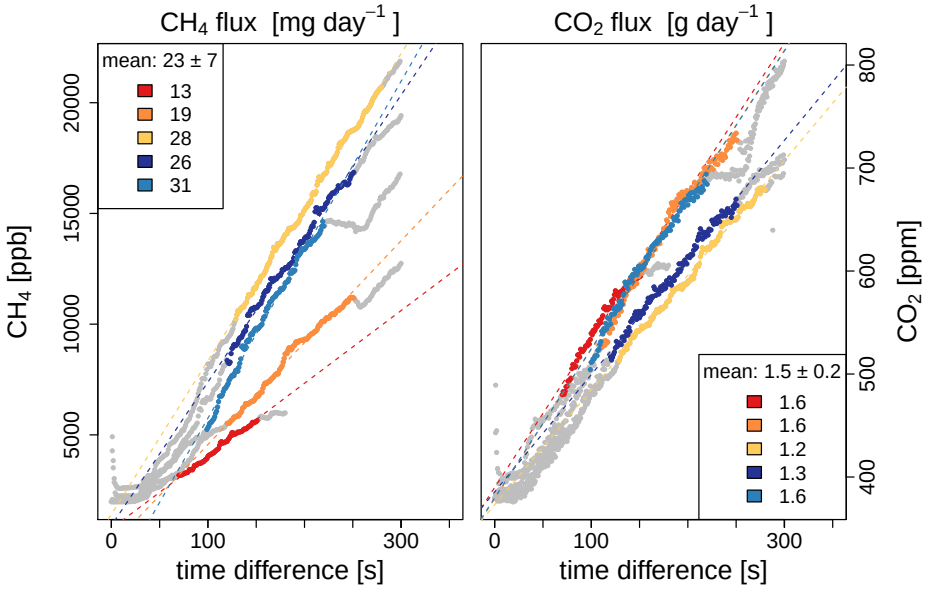

Figure 6.9.: Flux chamber measurements done at the sewage pit vent at Schauinsland. The flux chamber is installed directly above the vent of the sewage pit. The CH_4 and CO_2 mole fractions inside the chamber are measured with the LiCor analyser. The measured air is directed back inside the flux chamber to form an air flow cycle. The flux out of the sewage pit can be calculated with the increase in mole fraction inside the chamber.

flux is 23 ± 7 (13-31) mg day^{-1} and for CO_2 1.5 ± 0.2 (1.2-1.6) g day^{-1}. In comparison, one cow emits between 39.8 to 135.0 kg CH_4 yr^{-1} depending on the age and the use for milk production, breeding or slaughter (Jentsch et al., 2009). The cows around Schauinsland are young cattle that have not yet calved. Therefore, their CH_4 release is approximately 60.6 kg yr^{-1} per animal (Jentsch et al., 2009) or 166 g day^{-1}. Thus, the emission from the sewage pit (0.013 to 0.185 g day^{-1}) is several orders of magnitude smaller than the CH_4 emission of around 10 cows (1660 g day^{-1}).

Moreover, in addition to chamber measurements at the sewage pit soil flux measurements were done near the station in July 2020 and October 2020. The CH_4 soil uptake was calculated to be around -0.6 mg day^{-1} m^{-2} in July 2020 and only -0.08 mg day^{-1} m^{-2} in October 2020. The CO_2 soil flux was around 7 g day^{-1} m^{-2} in July 2020 and approximately 4 g day^{-1} m^{-2} in October 2020. A more detailed analysis of the soil flux measurements can be found in appendix C.4.

6.2.5. CH_4 measurements at different heights above the sewage pit

Although high CH_4 spikes can be frequently measured at the vent of the sewage pit, flux measurements indicate that the sewage pit is not responsible for high and short CH_4 spikes noticeable in the CH_4 record of Schauinsland. To estimate the reduction of CH_4 mole fraction further away from the sewage pit vent, measurements of CH_4 were carried out at different heights (-7 to 45 cm) above the sewage pit vent in August 2019 (figure 6.10).

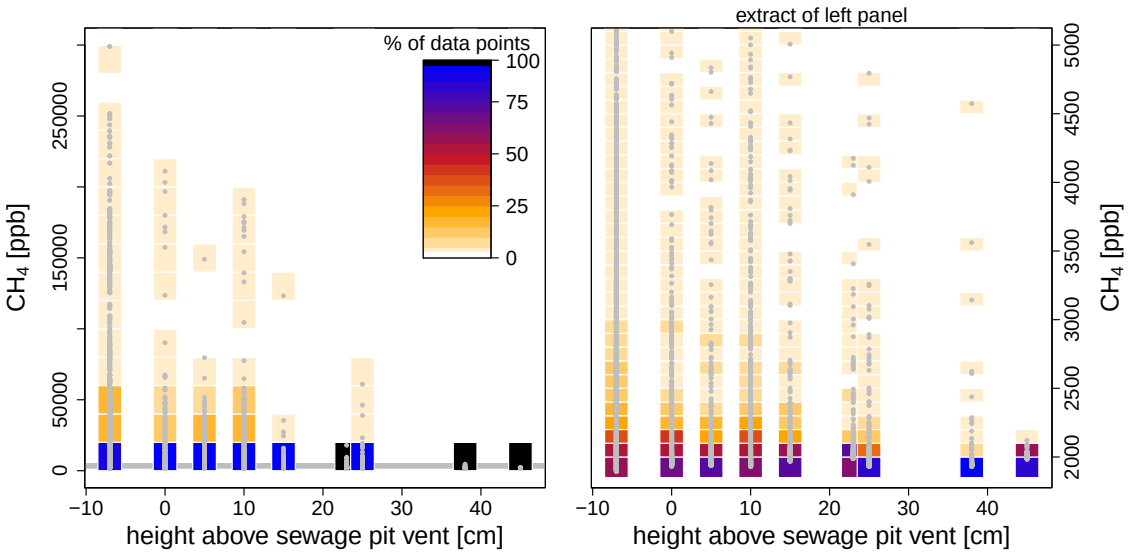

Figure 6.10.: The CH_4 mole fractions measured at different heights above the sewage pit vent are shown as grey data points. In addition, the percentage of data points for each measurement height within a CH_4 mole fraction range are given as coloured boxes with high values in blue and low ones in yellow. The right panel shows an extraction of the left one (grey area) with CH_4 mole fractions lower 5 000 ppb.

At every distance, short lasting CH_4 spikes are measured. However, the peak height and number of high CH_4 mole fractions decreases strongly with distance. When measuring above the sewage pit vent at heights below 10 cm between 5 and 10 % of data points are above 20 000 ppb. At higher distances, however, the percentage is below 1 %. On the right panel in figure 6.10 an extract of the measurement is shown for CH_4 mole fractions below 5 000 ppb. On the left panel this extract is marked as grey area. While at heights below 10 cm only 48 to 72 % of data points are below 2 200 ppb, at heights above 30 cm more than 98 % are below this threshold. Thus, even when CH_4 mole fractions up to 300 000 ppb are measured directly in the vent of the sewage pit, the CH_4 mole fractions measured 38 cm above the vent are less than 4 600 ppb. At 45 cm height, the measured CH_4 spikes have even mole fractions below 2 120 ppb. Therefore, it is unlikely to measure CH_4 spikes with CH_4 mole fractions larger than 2 100 ppb at the air inlet which is 12 m higher than the sewage pit vent and horizontally 20 m away.

6.3. Influence of CH_4 spikes on the CH_4 measurements

The high CH_4 spikes noticeable in the high temporal resolution time series for the last decade are not filtered out before averaging the CH_4 mole fractions to minutely or hourly data. Therefore, these local pollution events originating from nearby cows may have an influence on the hourly measurements. To quantify the impact of CH_4 emissions from cows on the hourly and monthly data, we exclude the CH_4 spikes first manually in two examples and later with an automatic peak detection method in the whole time series. Since cows have also grazed around Schauinsland since 2011 prior to the high temporal resolution measurements, knowing the strength of the influence today is important to estimate the influence on GC measurements since 1991.

6.3.1. First estimation of the influence of CH_4 spikes

The impact of high CH_4 spikes originating from cows at Schauinsland is estimated by using two exemplary time intervals which were manually filtered for the high CH_4 mole fraction events (figure 6.11).

In the upper panels the CH_4 mole fractions measured every ∼3 s are shown in black. All CH_4 spikes which are influenced by emissions from cows are excluded manually in the red time series. In the middle panel the hourly averaged CH_4 mole fractions calculated out of the measured data and the data manually filtered for CH_4 spikes are shown. An averaging interval of one hour was chosen as this is the typical time interval CH_4 mole fractions are reported to international data bases. The bottom panel shows the difference between the unfiltered and filtered hourly averaged CH_4 mole fractions.

In the first time period (figure 6.11a) we analyse CH_4 measurements from July to August 2020 in more detail. During this time camera measurements were available to indicate when high spikes are caused by emissions from cows. These CH_4 spikes were manually excluded from the time period. The hourly average CH_4 mole fractions calculated out of the measured data and the data which were manually filtered for CH_4

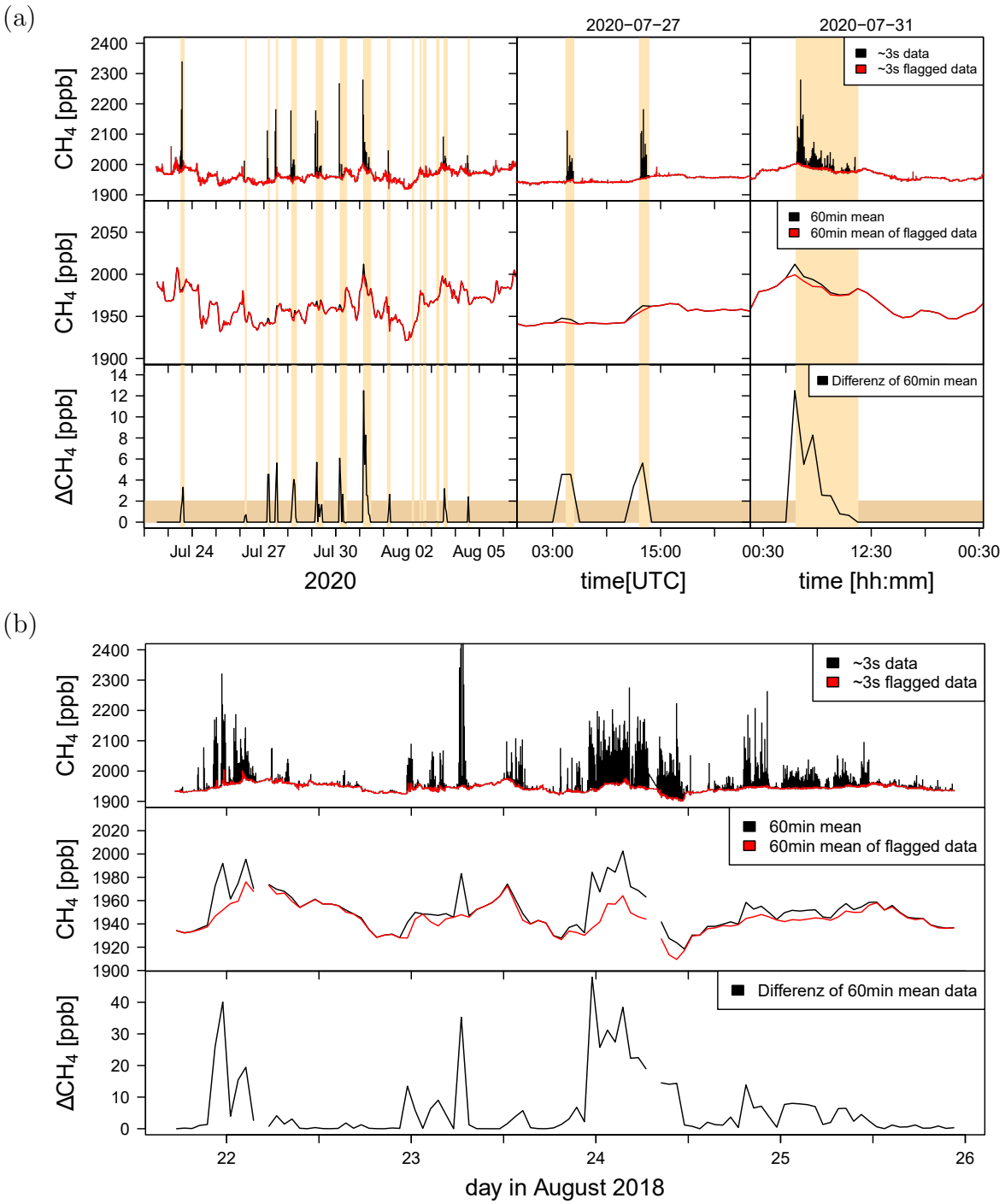

Figure 6.11.: Influence of CH_4 spikes on hourly CH_4 mole fractions for two different time periods (a,b). The top panels show the measured high temporal resolution CH_4 mole fractions (black) and the data manually filtered for CH_4 spikes due to cows (red). The panels in the middle display the hourly averaged CH_4 mole fraction from the measured and manually filtered data. The difference between both hourly values is given in the bottom panel. During the beige time intervals cows were present near Schauinsland station. For the second time period (b) no information about the presence of cows was available.

spikes can differ up to 12 ppb. Thus the hourly mean CH_4 values can be increased up to 12 ppb due to the influence of cows.

The second time interval of six days in August 2018 (figure 6.11b) was chosen, as it represents a time where CH_4 spikes occur more often than in our first example. During periods with multiple strong CH_4 spikes in the high temporal resolution data, the CH_4 mole fractions averaged over one hour can be increased even up to 40 ppb.

Such very local signals from the nearby cows cannot be simulated by regional models yet. With inverse modelling (Bergamaschi et al., 2010, 2018) these spikes could be seen as a large-scale peak of the whole region, and thus wrongly be attributed to a higher regional CH_4 source. In addition, a seasonal bias could be caused by the occurrence in summer.

This result is only a short example. To get better statistics, a comparison between measured data and data which are filtered for CH_4 spikes is needed for a longer time interval. However, this filtering of large data-sets cannot be done manually, as it is to labour intensive to be applied on a regular basis. Therefore, different automatic peak detection methods are tested to filter the CH_4 spikes.

6.3.2. Performance of automatic peak detection methods

All CH_4 data which are strongly biased by local pollution should be excluded from the time series to achieve accurate results, which are representative of regional and large-scale CH_4 mole fractions. El Yazidi et al. (2018) tested three automatic peak detection methods, which detect positive short-duration spikes in minutely averaged time series of CO_2, CH_4 and CO at four different stations. The marine background station Amsterdam Island (AMS), the regional marine background station Finokalia (FKL), the continental rural tower station Observatoire Pérenne de l'Environnement (OPE) and the high mountain site Pic du Midi (PDM). The applied algorithms are the coefficient of variation (COV) method (Hagler et al., 2010, Brantley et al., 2014), the standard deviation of the background (SD) method (Drewnick et al., 2012) and the robust extraction of baseline signal (REBS) method (Ruckstuhl et al., 2012). They have in common that the detection of spikes is based on the calculation of the standard deviation. In each method a background and a threshold are determined. If the difference between the measured value and the determined background is larger than the defined threshold, this value is identified as a spike. El Yazidi et al. (2018) found that all three algorithms were capable of detecting short-duration spikes in the time series, but recommend the use of the SD method.

Since all three algorithms worked for quite different stations, we test all of them, to achieve the best solution for the Schauinsland CH_4 data-set. Different to El Yazidi et al. (2018) who used the minutely averaged time series, we use the high temporal resolution CH_4 mole fractions of approximately every three seconds in this study, because the spikes are most prominent there. In the following, I give a short overview of the COV, SD and REBS methods before discussing their efficiency on the basis of representative examples.

Coefficient of variation method

In the coefficient of variation (COV) method (Hagler et al., 2010, Brantley et al., 2014 and El Yazidi et al., 2018) the COV coefficient for each data point x_i is calculated by dividing the standard deviation of five data points by the mean mole fraction of the time series $\bar{x}_{\text{all}}$.

$$COV_i = \frac{\sum_{j=i-2}^{i+2}(x_j - \bar{x})^2}{\bar{x}_{\text{all}}} \tag{6.2}$$

$\bar{x}$ is the average of the five CH_4 mole fractions including the two points before and after x_i. All data points x_i whose corresponding COV_i is larger than a threshold are filtered out as well as the two data points before and after. In this study, we test the 99^{th} and 95^{th} percentile of the COV as threshold. Since high temporal resolution data of every three seconds are used, the COV method is not applied to the complete time series of 10 years but to the yearly data sets. Smaller time intervals e.g. of months or weeks are not chosen for the COV method as the CH_4 spikes do not occur evenly distributed over the year, but more often in summer.

Standard deviation of the background method

The standard deviation of the background (SD) method (Drewnick et al., 2012, El Yazidi et al., 2018) takes the first data point of a data set as unpolluted reference value x_{unf}. Compared to that point the following data points x_i are filtered out if they are larger than a threshold which depends on the parameter α, the standard deviation σ and the number of data points n since the last uncontaminated point x_{unf}:

$$x_i \geq x_{\text{unf}} + \alpha \cdot \sigma + \sqrt{n} \cdot \sigma \tag{6.3}$$

If one of the following data points x_i is smaller than this expression, it is used as new starting point x_{unf}. In our study, we tested the SD method with different values for α and for the standard deviation σ. In six scenarios α is chosen to be 0.5, 1 or 3 and the standard deviation is calculated one time out of all data points below the median σ_{50} and another time out of the data which fall between the first and third quartile of the data-set σ_{25-75}. To identify short term spikes, it is important to reduce the impact of long-term variations to the calculated σ like the seasonal cycle. Thus, the SD method is applied to weekly data-sets.

Robust extraction of baseline signal method

The Robust extraction of baseline signal (REBS) method (Ruckstuhl et al., 2012, El Yazidi et al., 2018) filters all data when the measured CH_4 mole fraction is larger than the sum of the baseline $\hat{\mathrm{g}}(\mathrm{t}_i)$ and the parameter β times the standard deviation σ.

$$Y(t_i) \geq \hat{g}(t_i) + \beta \cdot \sigma \tag{6.4}$$

The baseline $\hat{\mathrm{g}}(\mathrm{t}_i)$ can be determined using the rfbaseline function of the IDPmisc package (Locher and Ruckstuhl, 2020) in R, which is a modified version of the robust baseline estimation method developed by Ruckstuhl et al. (2001). To determine the baseline at t_i for each data point $x(t_i)$ a weighted linear regression of the nearest data points is used whereas the influence of these data points decreases with their distance from t_i.

To get a baseline which describes the data correctly, the number of data points used in the regression is important. In our study the baseline which is calculated out of all data points within 10 min describes our time series best. The standard deviation σ is calculated out of the negative residuals, The parameter β adjusts the filtering strength. El Yazidi et al. (2018) used $\beta = 8$ after testing different values in a sensitivity test. Ruckstuhl et al. (2012) applied the REBS method with $\beta = 3$ to identify background CO measurements at the high-alpine site Jungfraujoch. Therefore, we tested different values for β ranging from one to eight to find the best solution for our purpose. Like the SD method, the REBS method is applied to the high temporal resolution weekly data-sets.

Implementation of COV, SD and REBS methods on three exemplary time periods

To determine which peak detection methods exclude the measured CH_4 spikes most efficiently, we analyse three different test data-sets. For the first two data-sets described already in the previous section we have manually excluded the CH_4 spikes (see section 6.3.1). The third data-set was chosen to be a week in January, since no cows graze near the station during this time period.

The three different peak detection methods are applied to the three data-sets. In addition, we vary the parametrisation for each method. For the COV method we test the 99^{th} and 95^{th} percentile as threshold. In the SD method six scenarios are tested. The parameter α was varied to assume the values 0.5, 1 and 3 and σ was calculated out of all data points below the median σ_{50} and another time with the data which fall between the first and third quartile of the data-set σ_{25-75}. In the REBS method we tested different values for β ranging from one to eight.

In figure 6.12 the measured high temporal resolution CH_4 mole fractions (grey) and the results of the peak detection methods (colours) are displayed in the top panels for a time period with strong and multiple CH_4 spikes. Especially for the COV and REBS method a strong reduction of high CH_4 mole fractions can be noticed.

Visually, the SD method seems to be the least effective method to exclude CH_4 spikes since high CH_4 values are still present in the time series (figure 6.12). Depending on the σ scenario only 31 % (σ_{50}) or 39 % (σ_{25-75}) of the 30887 manually excluded data points are filtered out with the SD methods with the parameter $\alpha = 0.5$. Higher values of alpha decrease this percentage and the method filters out even fewer CH_4 spikes.

For the COV method the scenario with the 95^{th} percentile as threshold achieves the best results. While the 99^{th} percentile scenario only excludes 60 % of the manually flagged data-points, the 95^{th} percentile scenario even marks 93 % as polluted.

The percentage of data points marked as pollution by the REBS method strongly depends on the parameter β and ranges from 91 % ($\beta = 1$) to 46 % ($\beta = 8$). However, in all of the REBS methods the highest CH_4 spikes are excluded successfully, even for $\beta = 8$ (figure 6.12).

The CH_4 mole fractions with high temporal resolution are averaged over each hour. In the lower panels of figure 6.12 the difference ΔCH_4 between $CH_{4\,\text{unflag}}$ or $CH_{4\,\text{auto}}$ and $CH_{4\,\text{manual}}$ is shown. The time series $CH_{4\,\text{unflag}}$ represents the hourly CH_4 mole fractions at

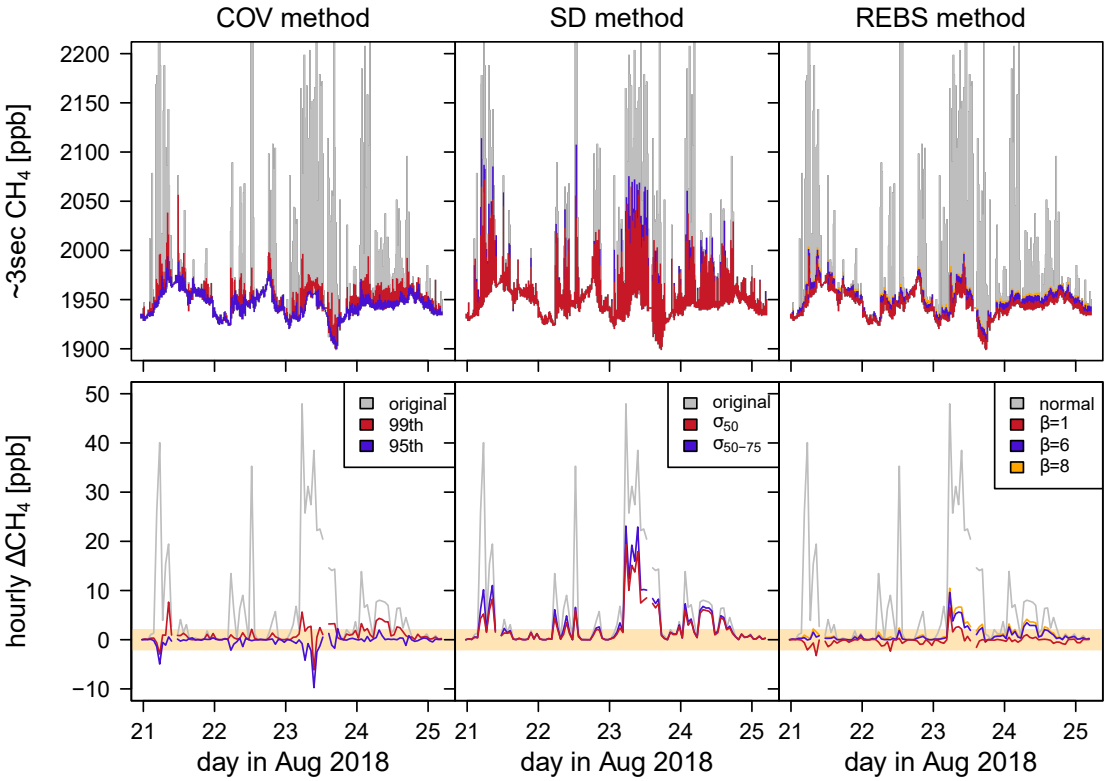

Figure 6.12.: Comparison between different peak detection methods for a time period with strong and multiple CH_4 spikes. The high resolution CH_4 mole fractions (top) and the hourly differences ΔCH_4 (bottom) are shown. ΔCH_4 is the difference between the data-sets in which spikes are excluded manually or with a peak detection method. The beige area corresponds to deviations less than 2 ppb.

which the high temporal resolution data are not flagged. In the time series $CH_{4\,\mathrm{manual}}$ the spikes are excluded manually before averaging over each hour and in $CH_{4\,\mathrm{auto}}$ the spikes are excluded automatically with the different peak detection methods. This difference ΔCH_4 indicates the influence of the CH_4 spikes on the hourly values and thus can be used as additional observable to quantify the performance of the different peak detection methods. A strong influence of CH_4 spikes occurs, if this difference is larger than 2 ppb.

In figure 6.13 the frequency of ΔCH_4 is displayed in the first column for the first data-set. The difference $\Delta CH_{4\ \mathrm{auto}}$ between $CH_{4\,\mathrm{auto}}$ and $CH_{4\,\mathrm{manual}}$ of the hourly values is shown in red and in addition the difference $\Delta CH_{4\ \mathrm{unflag}}$ between $CH_{4\,\mathrm{unflag}}$ and $CH_{4\,\mathrm{manual}}$ in grey. As expected, the SD method again shows the weakest performance. At least 76 % of $\Delta CH_{4\ \mathrm{unflag}}$ which are influenced more than 2 ppb have still $\Delta CH_{4\,\mathrm{auto}}$ values higher than 2 ppb after the SD method was applied. This reduces strongly for the other two methods. Especially high $\Delta CH_{4\,\mathrm{unflag}}$ are successfully removed by the REBS and COV (95^{th} percentile) method. Therefore, the COV (95^{th} percentile) and REBS ($\beta = 1$) methods are most capable of excluding nearly all the CH_4 spikes and thus their impact on the hourly values.

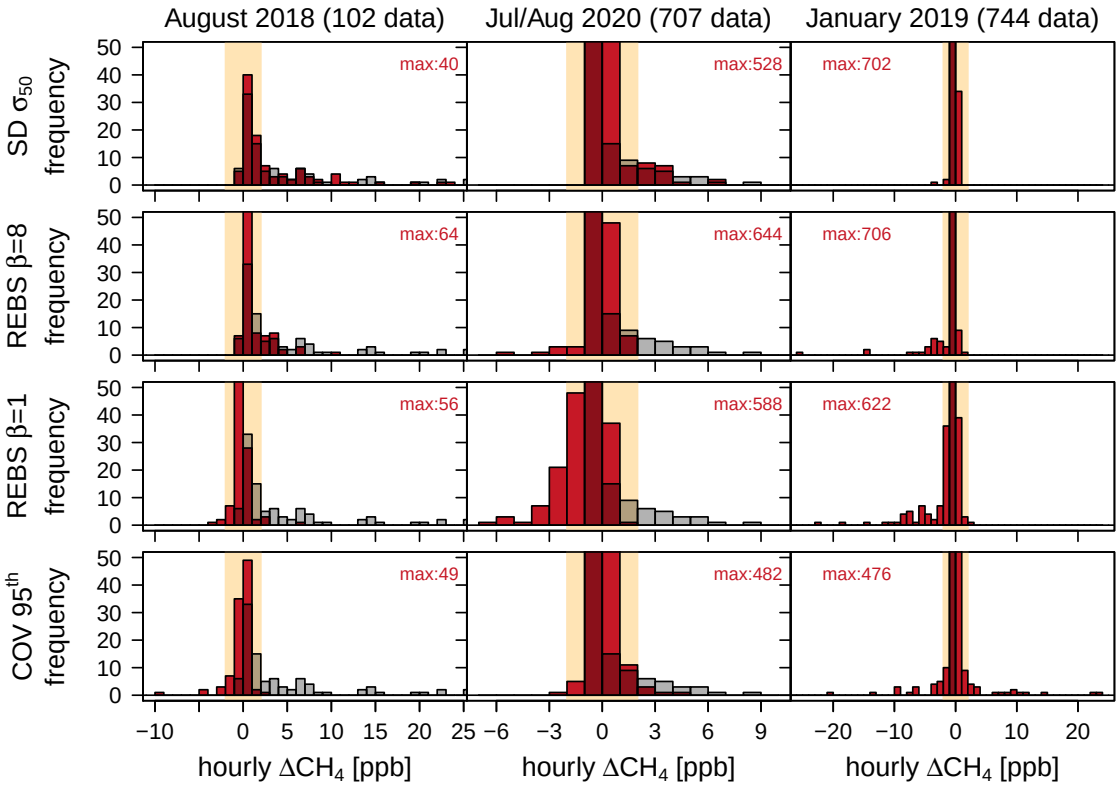

Figure 6.13.: Frequency distribution of $\Delta CH_{4\ \mathrm{auto}}$ (red) and $\Delta CH_{4\,\mathrm{unflag}}$ (grey) for different peak detection methods and time periods.

However, when we apply the automatic peak detection methods to less polluted data from July and August 2020, we can notice that especially the REBS ($\beta = 1$) methods seem to remove too many data points. This is shown in the hourly $\Delta CH_{4\,\mathrm{auto}}$ values displayed in the second column of figure 6.13. While several high CH_4 spikes which leads to $\Delta CH_{4\,\mathrm{unflag}}$ larger than 2 ppb are not filtered by the SD method, the REBS methods excludes all and the COV (95^{th} percentile) method nearly all of them. However, more than 79 % of the data points automatically detected by the REBS $\beta = 1$ method are not marked as pollution manually. Due to the exclusion of data which are not influenced by emissions from cows, the hourly CH_4 mole fractions can be shifted by more than -2 ppb.

For the time period in January 2019 where no CH_4 spike events occur, as no cows graze near the station, we can again notice several hours which are probably influenced by the false exclusion of spikes (see third column in figure 6.13). This effect is more prominent for the REBS method especially when β is small. The COV (95^{th} percentile) method shows fewer hourly differences below -2 ppb, but on the other hand, almost the same number of differences occurs at values above 2 ppb. The latter is probably another effect caused by false exclusion of data points, since no strong CH_4 spikes occurred during this period.

For our three exemplary data-sets, the REBS and COV (95^{th} percentile) methods seem to be suitable for the reduction of CH_4 spikes in our time series. However, in the COV

method the number of data points filtered out is assessed a priori by choosing a percentile as threshold. Thus, the CH_4 spikes are probably filtered out more or less successfully in different years, since the number and density of CH_4 spikes varied from year to year. Adjusting the threshold for each year is not possible because the information about the number and density of spikes is not available a priori. The REBS $\beta = 1$ scenario excludes nearly all CH_4 spikes. However, since this scenario filters out CH_4 mole fractions which are probably not influenced by local pollution, the REBS $\beta = 8$ scenario was chosen, too, as this method seems to mark nearly no data falsely. But on the other hand the REBS $\beta = 8$ scenario detects fewer CH_4 spikes.

Therefore, we chose to apply the COV (95^{th} percentile) and the REBS ($\beta = 1$ and 8) methods to the CH_4 time series between 2011 and 2020.

Moreover, we applied all peak detection methods to the minutely values, too, as was successfully done by El Yazidi et al. (2018) for different remote stations. However, for Schauinsland the influence of local pollution cannot be removed, when using minutely averaged mole fractions. The local polluted CH_4 spikes at Schauinsland usually occur in series of multiple high CH_4 mole fractions extended over a few hours whereas each spike only occurs between some seconds and some minutes. Averaging the three second CH_4 values before excluding the CH_4 spikes influences the minutely values. Unfortunately, the influenced minutely CH_4 mole fractions are usually not filtered out when applying the peak detection methods to the minutely data-set. Therefore, the peak detection methods are applied to data with the high temporal resolution and not to the minutely averages to exclude the impact of CH_4 spikes.

6.3.3. Peak detection methods applied to long-term measurements

The comparison of different peak detection methods with manually flagged data have shown that CH_4 spikes which are caused by emissions from cows can be successfully removed by the COV and the REBS method. However, all methods showed some weaknesses like the insufficient exclusion of CH_4 spikes, the elimination of unpolluted data points, or a necessary a priori knowledge about the CH_4 spike number. Therefore, to estimate the influence of CH_4 pollution on the measured CH_4 time series, we use the COV (95th percentile) and the REBS ($\beta = 1$ and 8) methods to remove CH_4 spikes from the high temporal resolution ambient air CH_4 mole fractions and assume that these time series are unpolluted afterwards. With this assumption, the difference between the results of the automatic detection methods $CH_{4\,\text{auto}}$ and the original CH_4 mole fraction $CH_{4\,\text{unflag}}$ describes the impact of local pollution on the measurements.

The REBS ($\beta = 1$) method excludes 15 % of all data points as polluted, the REBS ($\beta = 8$) method only 2 % and the COV (95^{th} percentile) method 8 %.

For our further analysis we study the differences between the results of the automatic peak detection methods $CH_{4\,\text{auto}}$ and the original CH_4 mole fraction $CH_{4\,\text{unflag}}$ which are averaged over each hour. These differences are used as an estimate of the potential influence of local pollution. For the REBS ($\beta = 1$ & $\beta = 8$) method 0.4 % (295 or 255) of all hourly data points have a difference larger than 10 ppb between $CH_{4\,\text{unflag}}$ and $CH_{4\,\text{auto}}$ with nine values even higher than 60 ppb. In fact, 3 to 4 % (2980 or 1857)

of all data points show differences higher than 2 ppb. Although, the REBS $\beta = 8$ method excludes nearly eight times fewer data points than the REBS $\beta = 1$ method the percentage of strongly influenced hourly CH_4 mole fractions is similar for both scenarios. The determined differences between $CH_{4\,\mathrm{unflag}}$ and $CH_{4\,\mathrm{auto}}$ for the COV (95^{th} percentile) method which excludes a number of data points between the other two scenarios, show a maximum difference of 65 ppb with only 1.2 % or 0.05 % of all hourly differences larger than 2 ppb and 10 ppb respectively.

In figure 6.14a the frequency of the differences between CH_{unflag} and CH_{auto} which are larger than 2 ppb are displayed. We can notice a strong seasonal variability in the number of strongly influenced hourly CH_4 mole fractions. For all three peak detection methods, the hourly CH_4 mole fractions $CH_{4\,\mathrm{unflag}}$ are more often influenced from June to November. That agrees with our observation of more CH_4 spikes during this time period when cows craze near the station. Since the REBS $\beta = 1$ method excludes most data points, it is not surprising that a higher number of hourly differences with values larger than 2 ppb are detected than for the other methods. However, even though the number of data points excluded by the REBS $\beta = 8$ method is only one quarter of the number of data points excluded by the COV method, more hourly values with high differences can be found.

To estimate the influence of CH_4 spikes caused by cows on the monthly averaged mole fractions, the difference between $CH_{4\,\mathrm{unflag}}$ and $CH_{4\,\mathrm{auto}}$ for each month is displayed in figure 6.14b. Again, we see a stronger impact of pollution during summer and autumn for all three peak detection methods. Compared to the other years, the difference between $CH_{4\,\mathrm{unflag}}$ and $CH_{4\,\mathrm{auto}}$ in 2012 and 2013 is lower. This agrees well with the

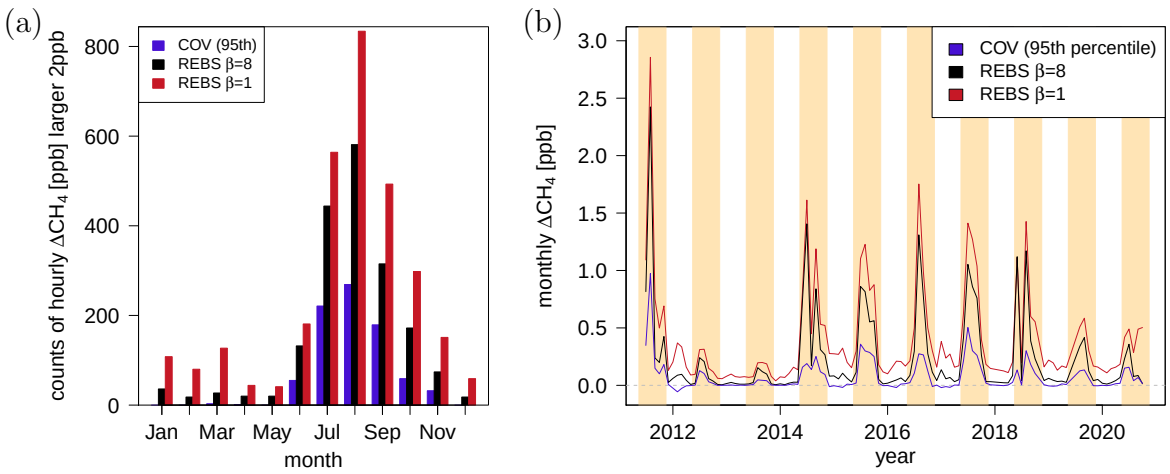

Figure 6.14.: Influence of CH_4 spikes on hourly and monthly averages.
(a): The number of hourly data points at which differences between $CH_{4\,\mathrm{unflag}}$ and $CH_{4\,\mathrm{auto}}$ are lager than 2 ppb are shown for each month.
(b): Monthly averaged differences between $CH_{4\,\mathrm{unflag}}$ and $CH_{4\,\mathrm{auto}}$. The beige coloured areas correspond to the months June to November when cows graze near the station.

observation, that during these years less pollution events occured in the CH_4 time series (see figure 6.2a). The COV method shows no difference between $CH_{4\,\mathrm{unflag}}$ and $CH_{4\,\mathrm{auto}}$ between December and May with an average difference of 0.00 ± 0.01 ppb (mean $\pm$sd). From June to November the differences increase up to 1 ppb. On average the monthly mean mole fractions from June to November are influenced by 0.1 ± 0.2 ppb from CH_4 emitted by cows. The REBS methods estimate an influence of CH_4 emissions from cows in summer and autumn which is four to five times stronger than the influence calculated with the COV method. On average the monthly mean difference between $CH_{4\,\mathrm{unflag}}$ and $CH_{4\,\mathrm{auto}}$ is 0.2 ppb larger for the scenario with $\beta = 1$ than for $\beta = 8$. This mean deviation of 0.2 ppb in summer (Jun to Nov) and even in winter (Dec to May) is caused by the more rigorous and probably too strong filtering for the $\beta = 1$ scenario.

In the REBS $\beta = 8$ method the mean deviation between $CH_{4\,\mathrm{unflag}}$ and $CH_{4\,\mathrm{auto}}$ of 0.04 ± 0.03 ppb is small from Dec to May. Thus, no strong impact of the REBS $\beta = 8$ method on the monthly data due to the exclusion of uncontaminated data is noticeable as it was the case for the REBS $\beta = 1$ method. During summer and autumn the mean difference and thus the impact of CH_4 spikes on the monthly values is 0.4 ± 0.5 ppb with values up to 2.4 ppb. Although, the REBS $\beta = 8$ method excludes nearly eight times fewer data points than the REBS $\beta = 1$ method, the determined impact of CH_4 spikes on the monthly values is similar for both scenarios except for an offset. It is even more interesting that the COV method excludes four times more data points than the REBS $\beta = 8$ method, but a four times lower influence during summer and autumn is noticeable for this method. It seems that the COV method does not filter the impact of CH_4 spikes on the time series as effectively as the REBS $\beta = 8$ method.

However, even with peak detection methods which probably mark too many data points as pollution, the monthly averaged values are influenced by less than 2 ppb except for August 2011. Thus the impact of CH_4 emissions by cows on the monthly averaged CH_4 mole fractions is not significant.

Furthermore, no strong diurnal dependency of the impact of CH_4 emissions from cows on the hourly data can be detected. In winter (Dec to May) the hourly CH_4 mole fractions $CH_{4\,\mathrm{unflag}}$ show a slightly higher number of strong differences to $CH_{4\,\mathrm{auto}}$ data during the day between 9 to 15 UTC than over night. Since in summer (June to November) the number of high differences shows less deviations between day and night than in winter (Dec to May), we can assume that the weak diurnal variability in ΔCH_4 noticed during the time cows graze at the station (June to November) is more likely caused by stronger CH_4 variability during the day than by CH_4 emission from cows itself. The determined mean diurnal cycles for winter (Dec to May) and summer (June to November) show no significant difference between $CH_{4\,\mathrm{unflag}}$ and $CH_{4\,\mathrm{auto}}$.

To determine if the former CH_4 measurements done with a GC are also affected by local CH_4 emissions, we compare the hourly CH_4 mole fractions measured with the GC with hourly CH_4 mole fractions calculated from filtered and unfiltered CRDS measurements. The REBS $\beta = 8$ method is used for spike detection as it is the most conservative method which filters out the least data points but is still very effective. From 2011 up to the end of 2014 parallel measurements between CRDS and GC were done and both instruments agree well. In figure 6.15 an exemplary day with measured CH_4 spikes is shown. The

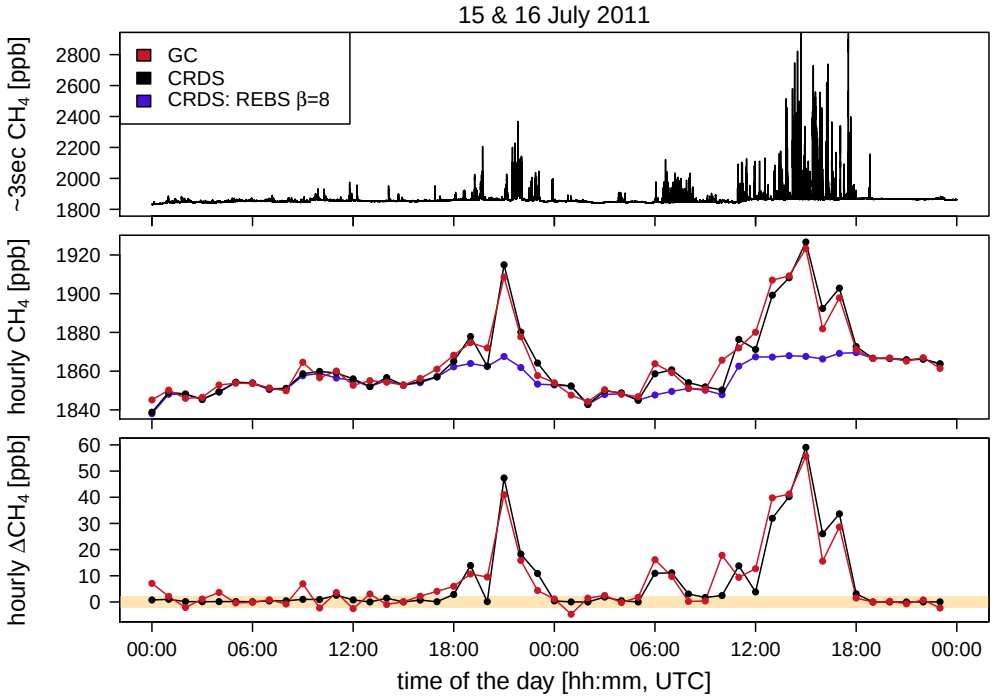

Figure 6.15.: Impact of grazing cows on the GC measurements. The top panel shows the high temporal resolution CRDS measurement (black) and the filtered time series (blue) calculated with the REBS ($\beta = 8$) method. The middle row presents the hourly averages of the unfiltered and filtered CRDS measurements and in addition the hourly values of the GC measurement (red). The last panel shows the difference between the hourly filtered CRDS measurement with the unfiltered (black) or the GC (red) measurements.

hourly averaged CH_4 mole fractions calculated from CRDS or GC measurements, show a significant difference of up to 60 ppb to the CH_4 data in which the CH_4 spikes were excluded automatically. Therefore we can assume that the former GC measurements are also influenced by CH_4 emitted by cows grazing next to the station.

To summarise, the CH_4 emissions of cows induce strong CH_4 spikes in the high temporal resolution time series. The influence of these emissions on the hourly averaged CH_4 mole fractions is often not negligible and can reach values up to 60 ppb. However, the monthly mean CH_4 mole fractions and thus the annual cycle as well as the mean diurnal cycle at Schauinsland show no significant influences of the local pollution.

6.4. Summary and Outlook

In the high temporal resolution time series of CH_4 measured at Schauinsland, large CH_4 spikes with mole fractions up to 3 000 ppb occurred each year between June and November. These spikes are not isolated in time, but instead a series of multiple high CH_4 mole fractions extends over a few hours.

Mobile measurements at the station reveal two local sources: cows in the nearby pasture and a sewage pit. The characterisation of the isotopic source signatures (sewage pit: -51 ± 2 ‰, cows: -71 ± 1 ‰), flux chamber measurements at the sewage pit and the installation of a camera to monitor the presence of cows have shown that the high CH_4 spikes are caused by the approximately 10 cows grazing near the station from June to November.

The COV and REBS peak detection methods can be used to successfully exclude these CH_4 spikes and to reduce the influence of cow emissions on the hourly average mole fractions. However, we have noted that no perfect detection method could be chosen. On the one hand, the methods do not filter out all contaminated data, on the other hand more restrictive methods exclude also uncontaminated data.

Nevertheless, by testing three peak detection methods we can estimate that the influence of cows on the hourly averaged CH_4 mole fractions is often higher than 2 ppb and can reach even values above 40 to 60 ppb. This effect is averaged out in the mean diurnal variations. Furthermore, the emissions from cows shift the monthly average CH_4 mole fraction about 1 ppb in the summer and autumn months.

Therefore we can assume that the long-term trends and the annual variations, which are usually determined from the monthly mean values, do not show an influence. However, hourly values from the summer and autumn months can include a strong signal from emission of the nearby cows, which has to be considered by the interpretation.

Therefore, it is important to exclude the influence of CH_4 emissions from cows on the hourly values. This could be done by installing a camera during the months cows graze at the station. Then the data are filtered according to the presence of cows as it was done for one exemplary month in this thesis. This method reliably filters out high CH_4 spikes, but it is relatively labour intensive.

From the automatic peak detection methods tested in this thesis the REBS ($\beta = 8$) method is the most conservative one which still filters out the most prominent spikes. This method is best suited to detect spikes in the CH_4 time series measured at Schauinsland and thus to remove the influence of CH_4 emitted by the nearby cows on the hourly CH_4 mole fractions.

Another possibility would be to change the location of the intake line to a less influenced position. In summer 2021 an intake line is planned to be installed leading to the top of a 30 m high radio tower near the station Schauinsland. Parallel measurements of CH_4 at the current location and at the radio tower will give us the opportunity to analyse whether the new location of the intake line is less affected by CH_4 emissions from nearby cows due to its larger altitude.

7. Conclusion and Outlook

High temporal resolution time series of greenhouse gases were successfully analysed regarding local and regional emission sources at the urban station Heidelberg and the remote stations Zugspitze and Schauinsland.

We have shown that the mean source signature in the catchment area of Heidelberg can be determined with different approaches which are based on the Miller-Tans method. The high temporal resolution CH_4 and $\delta^{13}CH_4$ measurements done with a CRDS analyser make it even possible to calculate the mean source signatures for short time intervals from one to several hours using the moving Miller-Tans approach.

All approaches result in similar mean source signatures of -52.5 ± 0.3 ‰ and show an annual cycle with more depleted values in summer. This annual cycle cannot be explained completely by seasonal variations in the emissions from domestic heating as the comparison with emission inventories has shown. Therefore, further research on seasonal variations of CH_4 emissions especially from biogenic sources is important.

As all three approaches which are based on the Miller-Tans method show comparable results, we can assume that even the monthly approach determines reasonable and accurate mean source signatures. Therefore, this method can be used at remote stations where the diurnal variability is insufficient for application of night-time or moving Miller-Tans approach. For two measurement campaigns done at Schauinsland we tested the monthly method and got more depleted mean source signatures than in Heidelberg. This agrees with local emission inventories provided by LUBW and ERGAR 5.0 which estimated a stronger contribution of more biogenic CH_4 emissions around Schauinsland.

Furthermore, the determined mean source signatures and the CH_4 flux of the catchment area of Heidelberg calculated out of atmospheric measurements were used to verify these two emission inventories. The LUBW inventory represents the composition of CH_4 emission well, but seems to underestimate the total amount of emission. However, in EDGAR v5.0 emissions from enriched CH_4 sources such as waste incineration and the sector energy for buildings are overestimated. Especially for Mannheim EDGAR v5.0 reports high CH_4 emissions from the natural gas sector which strongly increased between 2010 and 2011. A possibility of verifying these emissions would be to carry out mobile measurement campaigns in and around Mannheim. In addition, further studies should also target CH_4 emissions rates and their isotopic composition from waste incineration, heating (wood and coal) and traffic.

A further analysis of regional and local CH_4 sources can be done by simulating the atmospheric CH_4 and $\delta^{13}CH_4$ measurements carried out in Heidelberg during the last six years using atmospheric transport models like STILT or CHIMERE. Such evaluations could confirm our assumptions and complement our results.

Moreover, our studies at Zugspitze and Schauinsland have demonstrated how the impact of local pollution events visible in high temporal resolution time series can be quantified and several possibilities of removing the influence of local sources have been discussed.

We have shown that local pollution events visible in the time series at Schneefernerhaus can be excluded successfully by the station manager using – among others – station logbooks which document working activities in the research station. Since CH_4 spikes in the measurements done at Schauinsland originate from cows grazing in the near pastures, the documentation of the presence of cows with a logbook or with a camera could be a reliable method to filter out influenced data. The evaluation of camera pictures was successfully used in this study to exclude CH_4 spikes for a period of one month.

However, the manual flagging of data is very labour intensive. Tests of different automatic peak detection methods applied to Schauinsland data have demonstrated that the REBS method excludes the influence of emissions from cows on the CH_4 measurement quite well. Furthermore, the automatic methods are a valuable tool to estimate the influence of pollution events on averaged data. While the monthly mean CH_4 mole fractions at Schauinsland are shifted only by around 1 ppb between June and November, the hourly averaged CH_4 mole fractions can be effected up to 40 to 60 ppb. Thus, we can assume that the emissions from cows have no significant influence on the trend analysis or the evaluation of annual cycles. However, the analysis of CH_4 on short time scales using hourly values has to be done and interpreted carefully when the CH_4 spikes are not excluded first.

As the choice of method and parameters has a strong influence on how efficiently the method excludes invalid data, but also on how many unpolluted data are misidentified as peaks, the methods have to be carefully tested before they are used as default for excluding pollution events. Such a careful analysis of the different methods has to be done in future to find the suitable peak detection method for the CO, CO_2 and CH_4 time series at Schneefernerhaus.

However, the best solution would be to avoid the contamination of data. At Zugspitze this can be done by measuring ambient air of the mountain ridge instead of Schneefernerhaus. In this study we showed that the influence of local pollution on the measurement at the mountain ridge is less frequent and much weaker than at Schneefernerhaus.

At Schauinsland the measurement of ambient air at higher altitudes may also reduce the impact of emissions from cows. This summer, an intake line will be installed on a radio tower. The measurements will show whether the change of the measurement location reduces the influence of local pollution at Schauinsland, as it is the case at Zugspitze.

A. Supplementary material on measurements in Heidelberg

A.1. Single-point and two-point calibration

In this thesis, two calibration strategies – the single-point calibration and the two-point calibration – are used. In both cases, all sample measurements $X_{meas}(t_n)$ are calibrated using the nearest calibration measurement in time before and after the sample time t_n. Therefore, each calibration measurement is averaged. For each sample measurement $X_{meas}(t_n)$ a calibration value $X_{intStd}(t_n)$ is calculated for the sample time (t_n) by linear interpolation between the averaged calibration measurements (figure A.1). Then, each sample measurement data-point $X_{meas}(t_n)$ is calibrated with an individual calibration line.

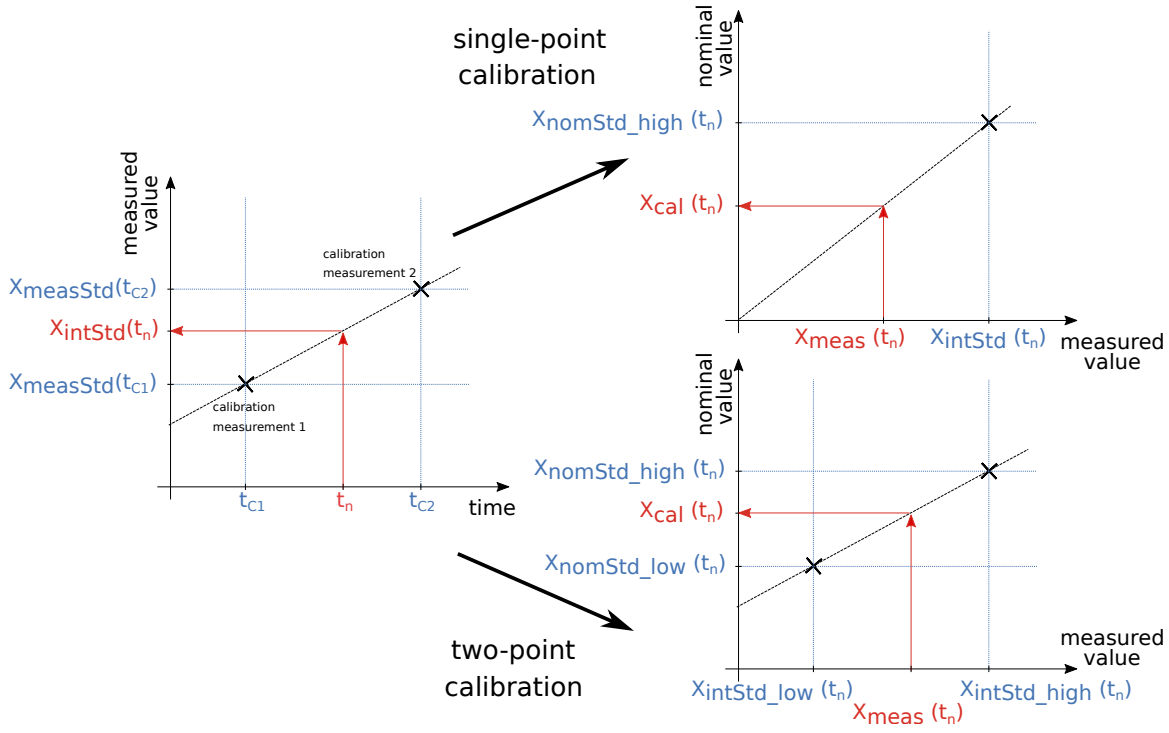

Figure A.1.: Schematic representation of single and two-point calibration.

In the **single-point calibration** this calibration line is a straight line determined through the nominal calibration gas value X_{nomStd}, the interpolated calibration gas value X_{intStd} and the origin (figure A.1). The nominal calibration gas value X_{nomStd} is the known "true" value of the calibration gas. The sample measurement X_{meas} is calibrated by multiplication with the ratio of the nominal calibration gas value X_{nomStd} and the interpolated calibration gas value X_{intStd}

$$X_{cal}(t_n) = \frac{X_{nomStd}}{X_{intStd}(t_n)} \cdot X_{meas}(t_n). \tag{A.1}$$

In the **two-point calibration** two calibration gases are used which ideally span the measured range. Instead of one, two interpolated calibration values $X_{intStd\_high}(t_n)$ and $X_{intStd\_low}(t_n)$ are calculated as described above. Each sample measurement X_{meas} is then calibrated by a straight calibration line determined through the two interpolated calibration values on the x-axis and the nominal calibration values on the y-axis (figure A.1).

$$X_{cal}(t_n) = m(t_n) \cdot (X_{meas}(t_n) - X_{intStd\_high}(t_n)) + X_{nomStd\_high} \tag{A.2}$$

with

$$m(t) = \frac{X_{nomStd\_high} - X_{nomStd\_low}}{X_{intStd\_high}(t_n) - X_{intStd\_low}(t_n)} \tag{A.3}$$

A.2. Mobile measurement campaigns in the catchment area of Heidelberg

To identify and characterise possible CH_4 sources in Heidelberg and in the surroundings mobile measurement campaigns between 2016 and 2020 with a CRDS G2201-i analyser were done. A detailed description of the mobile set-up, the measurement and analysis methods can be found in Hoheisel et al. (2019). Due to its location, CH_4 emissions measured in Heidelberg can originate from biogenic (e.g. dairy cows, waste water treatment plants), thermogenic (e.g. natural gas), and even pyrogenic (e.g. traffic) sources. In figure A.2 the isotopic source signatures for different CH_4 categories measured around Heidelberg are shown.

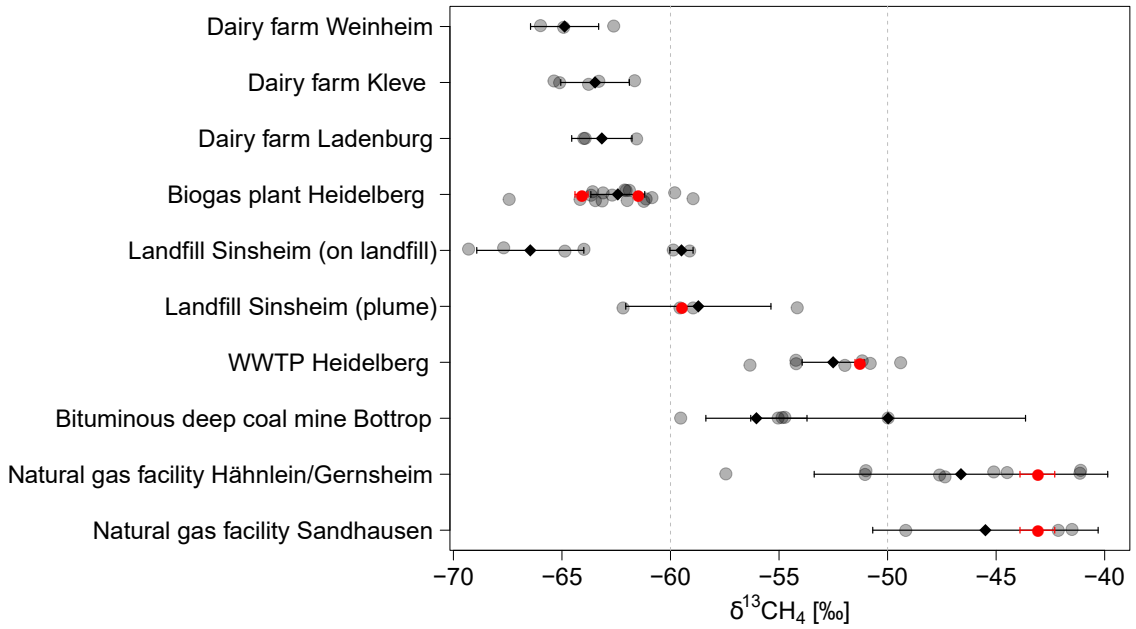

Figure A.2.: Isotopic signature of CH_4 sources measured using mobile measurements (Source: Hoheisel et al., 2019).

A.3. Allan standard deviation of CH_4, CO_2 and their ^{13}C isotopes

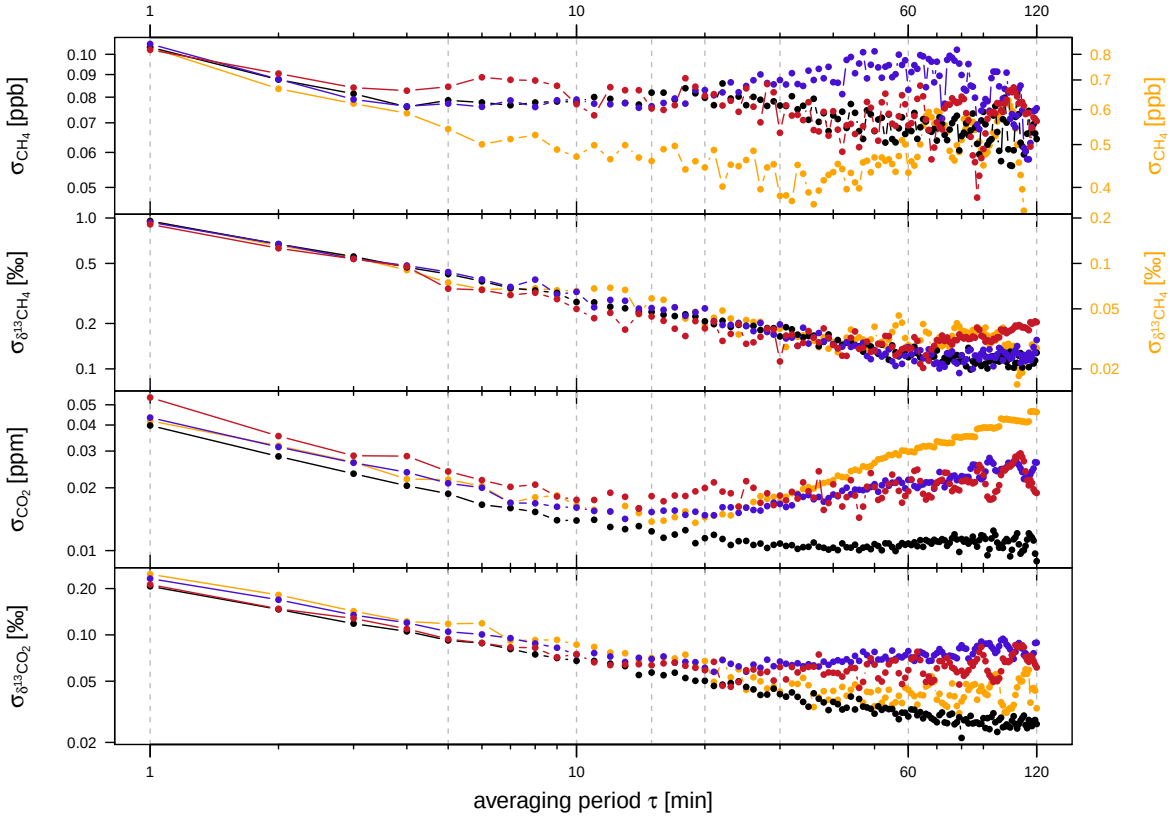

Figure A.3.: Allan standard deviation of CRDS G2201 determined for CH_4, CO_2 and their ^{13}C isotopes. One cylinder was measured in 2013 (black) and the other three in 2019 (blue, red and orange). One cylinder contains 10 000 ppb CH_4 instead of atmospheric mole fractions and its measurements are shown in orange and correspond to the right axis.

A.4. Measurements of six intercomparison cylinders of air sampled at Neumayer station

Sample ID	Analysis Date	$\delta^{13}CH_4$ [‰] mean ± std error	CH_4 [ppb] mean ± std error
GvN 88/20	May 2018	-47.73 ±0.12	1635.65 ± 0.01
	May 2018	-47.63 ±0.11	1635.77 ± 0.01
	May 2019	-47.45 ±0.07	1635.49 ± 0.01
GvN 92/12	May 2018	-47.49 ±0.11	1682.17 ± 0.01
	May 2018	-47.60 ±0.12	1682.18 ± 0.01
	May 2019	-47.67 ±0.12	1682.15 ± 0.03
	May 2019	-47.69 ±0.11	1681.94 ± 0.01
GVN96/03	May 2018	-46-97 ± 0.11	1685.30 ± 0.01
	May 2018	-47.04 ± 0.10	1685.30 ± 0.01
	April 2019	-47.19 ± 0.10	1685.29 ± 0.01
GVN99/14	Jun 2018	-47.12 ± 0.12	1723.29 ± 0.02
	April 2019	-47.13 ± 0.11	1723.00 ± 0.01
GvN 06/14	May 2019	-47.12 ± 0.08	1746.72 ± 0.01
	Feb 2020	-47.35 ± 0.09	1747.30 ± 0.02
	Feb 2020	-47.31 ± 0.11	1747.39 ± 0.01
GvN 08/034	Feb 2020	-47.43 ± 0.11	1720.12 ± 0.02
	Feb 2020	-47.06 ± 0.12	1720.08 ± 0.01

Table A.1.: Measurements of six intercomparison cylinders of air sampled at Neumayer station, Antarctica, done with CRDS G2201-i.

A.5. Night-time and daytime STILT footprints for Heidelberg

Footprints calculated with STILT (Lin et al., 2003 and Kountouris et al., 2018) for the station Heidelberg are used to estimate the catchment area of Heidelberg. In figure A.4 50 % of the footprint for 2018, that means the highest cell values that add up to 50 % of the total sensitivity, are shown. In panel (a) only daytime (time: 18, 21, 0, 3) data are used in the calculations and in panel (b) only night-time data (time: 6, 9, 12 and 15). We can clearly notice a stronger influence of local sources during the night compared to the day.

For these calculations the STILT footprint tools[1] and the STILT jupyter notebook service[2] were used.

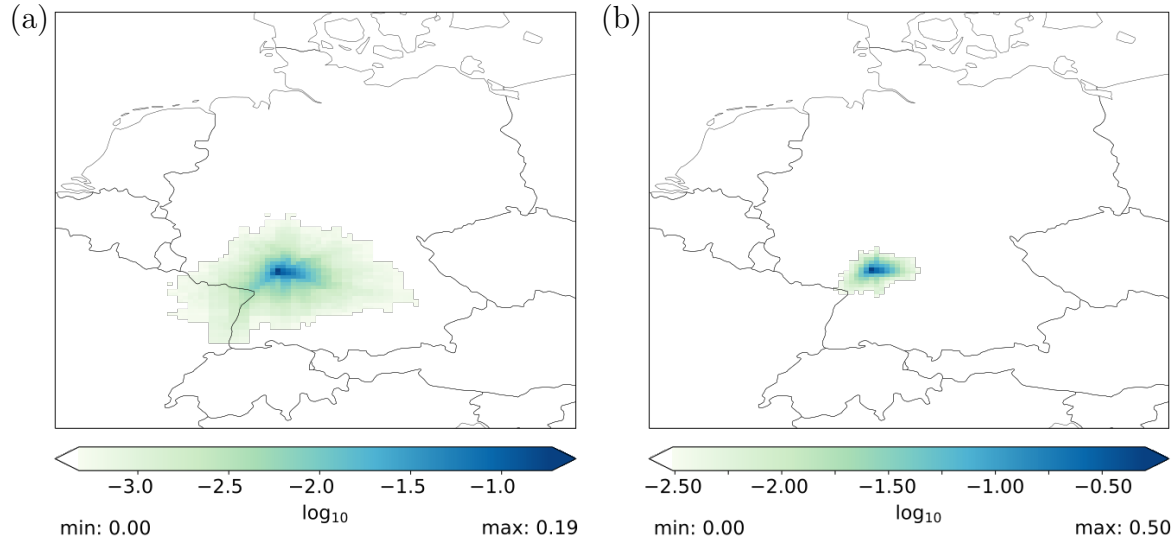

Figure A.4.: 50 % of the surface sensitivity calculated with STILT for the year 2018 for the station Heidelberg (30 m). In (a) the footprint is determined using day-time data (time: 6, 9, 12 and 15) and in (b) with night-time data (time: 18, 21, 0, 3)

[1]STILT footprint tools: `https://www.icos-cp.eu/data-services/tools/stilt-footprint`
[2]STILT jupyter notebook service: `https://www.icos-cp.eu/data-services/tools/jupyter-notebook`

B. Supplementary material on measurements at Zugspitze

B.1. Diurnal cycles on weekend and weekday for CO and CH_4

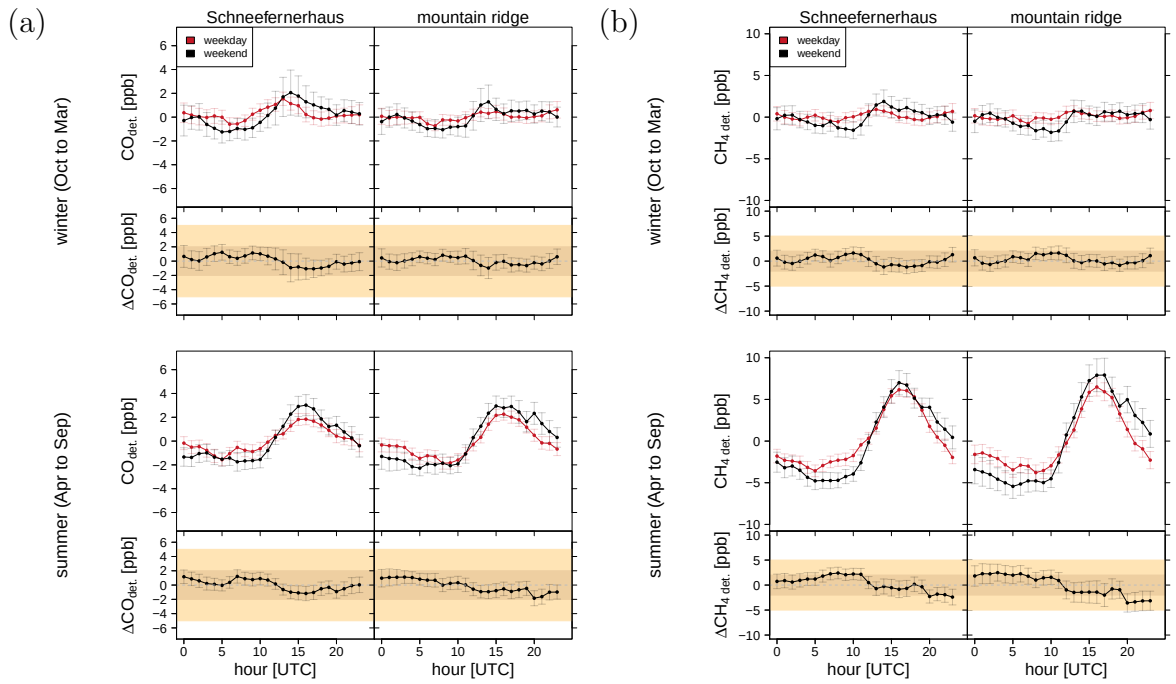

Figure B.1.: Mean diurnal cycles of CO (a) and CH_4 (b) for Schneefernerhaus and mountain ridge calculated out of the weekend (black) and weekday (red) data for two seasons.

C. Supplementary material on measurements at Schauinsland

C.1. Mobile measurement campaigns at Schauinsland

On three days, twice in September and once in March, mobile measurements in the surroundings of Schauinsland and Freiburg am Breisgau were performed using the same set-up and methods as described in Hoheisel et al. (2019). During the measurements, the focus was on the rural area in the direct surroundings of Schauinsland station, the industrial estate in the city of Freiburg, and some CH_4 sources like a landfill, a spherical gas container and a biogas plant.

In the surroundings of Schauinsland station, no strong CH_4 sources were found. However, in September some CH_4 peaks were seen which originate from cows (up to 2400 ppb). In addition, we noted that right next to the station cows were grazing in summer and fall and that the sewage pit of the station also emits CH_4. A more detailed analysis of the potential influence of these nearby cows and the sewage pit is done in section 6.2. In general higher CH_4 mole fractions were measured in the city of Freiburg. Especially in the September measurement campaign low wind speeds lead to an accumulation and therefore higher CH_4 mole fractions in the industrial area of Freiburg. Furthermore, strong emission plumes were measured downwind of the landfill (up to 2400 ppb and 2100 ppb) and the biogas plant (up to 4200 ppb). Around the spherical gas container an increase in the CH_4 mole fractions to 2600 ppb was measured only once.

The measured CO_2 mole fraction seems to depend strongly on traffic. On the more rural roads around Schauinsland and around the biogas plant the CO_2 mole fraction is lower than at the high traffic roads in Freiburg. Especially high CO_2 mole fractions were measured at highways and by driving through tunnels.

In addition to the mole fraction of CH_4 also the isotopic composition was measured. The CH_4 source signatures were determined by the Miller-Tans method as explained in Hoheisel et al. (2019). The isotopic source signature calculated for the cows is -71 ± 1 ‰. More enriched CH_4 is emitted by the landfill -50 ± 2 ‰ and the biogas plant -50 ± 1 ‰. CH_4 from the spherical gas container is, as we would expect from natural gas, even more enriched with -42 ± 1 ‰. The isotopic source signature for CH_4 sources in the industrial area of Freiburg were difficult to determine, since we could not catch a single plume peak. We estimated an isotopic signature between -40 to -46 ‰. The only strong CH_4 peak measured in the industrial area results in an isotopic signature of -31 ± 10 ‰. CH_4 emitted in the industrial area is therefore isotopically enriched.

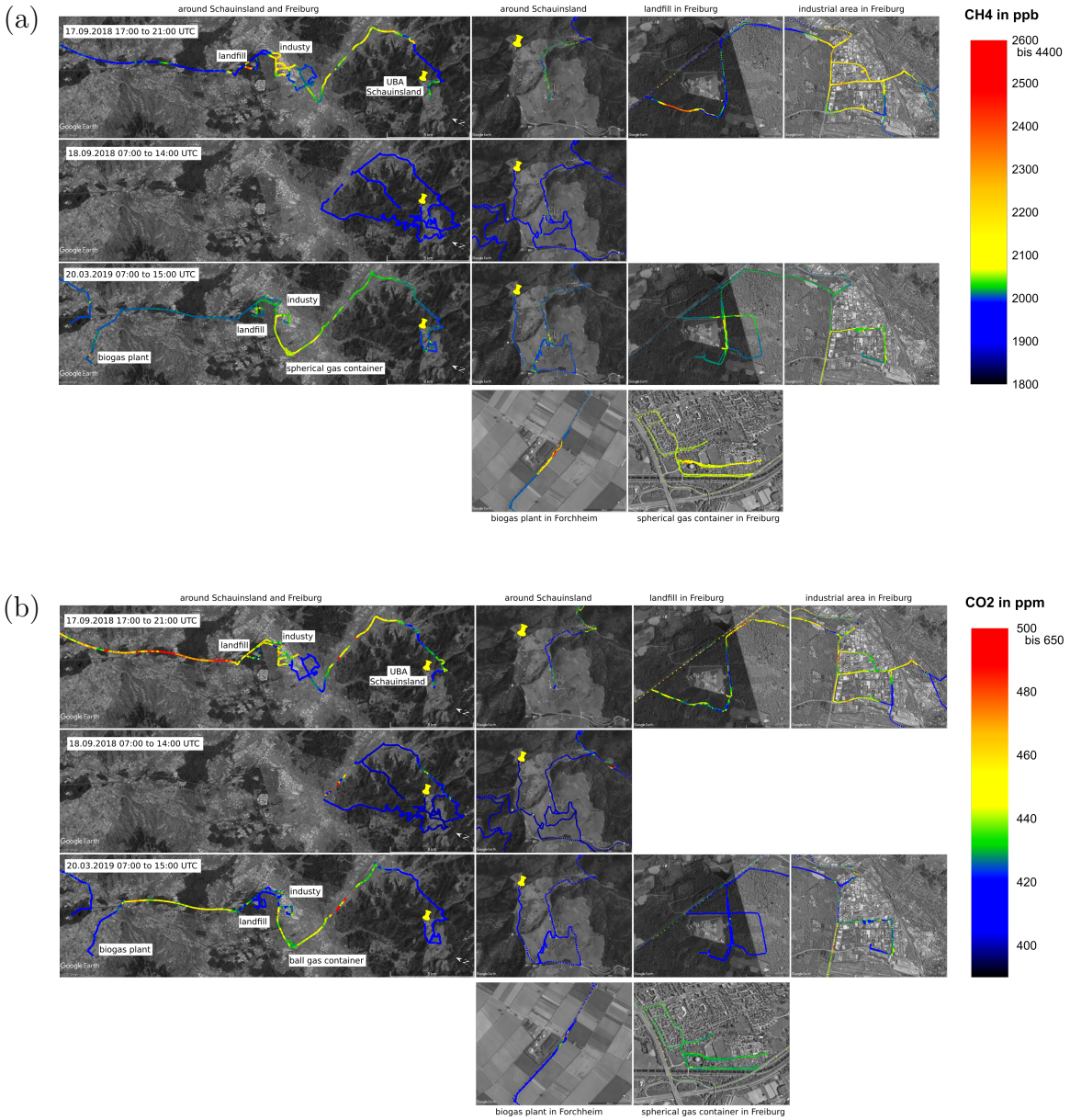

Figure C.1.: Mobile CH_4 (a) and CO_2 (b) measurements around Schauinsland and Freiburg.

C.2. Measurements at the sewage pit and near cows at Schauinsland

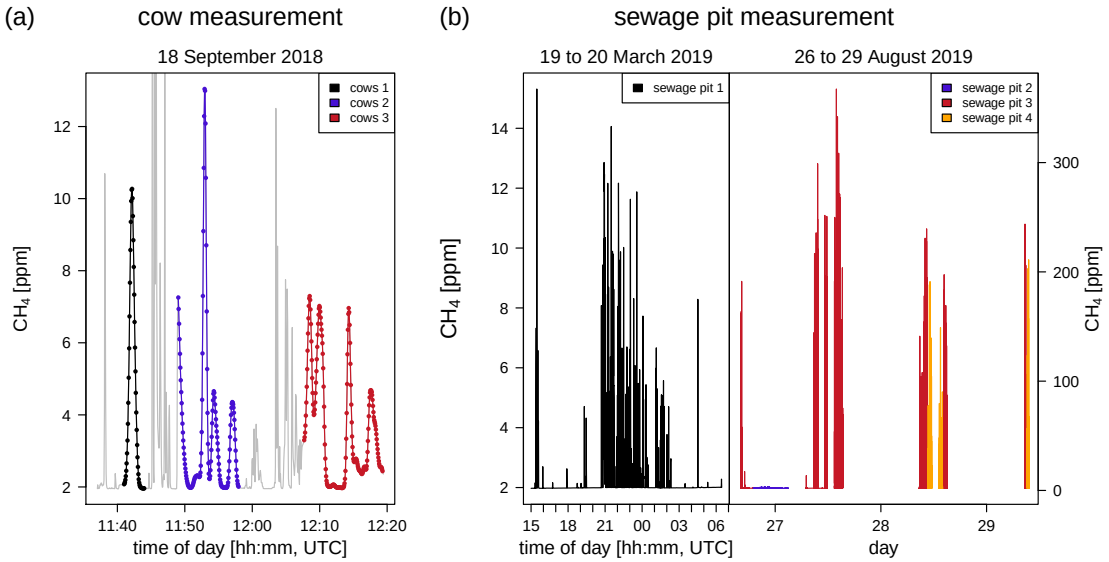

Figure C.2.: All CH_4 mole fraction measurements done directly near the cows (a) and sewage pit (b). The different colours correspond to different measurement intervals. In (a) all plume transects measured directly while driving are shown in grey and the three AirCore measurements in colour.

C.3. Ambient air measurement of $\delta^{13}CH_4$ and $\delta^{13}CO_2$ at Schauinsland

During three measurement campaigns the CRDS G2201-i analyser from the Institute of Environmental Physics in Heidelberg was installed at Schauinsland. In addition to the mole fraction of $^{12}CH_4$, $^{12}CO_2$ and H_2O the analyser also measured the mole fraction of $^{13}CH_4$ and $^{13}CO_2$. So the isotopic composition $\delta^{13}CH_4$ and $\delta^{13}CO_2$ was analysed continuously during these measurement campaigns. The first campaign was carried out in autumn 2018 from 19 September to 18 October and the second one in spring 2019 between 15 February and 19 March. In addition, to these two campaigns of one month the analyser was installed at Schauinsland for four days in August 2019.

Experimental set-up
Before entering the CRDS G2201-i analyser through a 16-port rotary-valve (model: EMT2CSD16UWE, Valco Vici, Switzerland), the ambient air was dried. During the first campaign a cold trap cooled by a cryogenic cooler was used to dry the air .However, since some leakages showed up in the first campaign and the volume of the cold trap acted as buffer, we used a Nafion dryer in the following measurement campaigns. Every five hours regular calibration and quality control gas measurements were done for 20 min each with a flow between 25 to 35 ml min^{-1}.

For the measurement campaigns compressed air with atmospheric mole fractions were used as calibration and target gas. The reported CH_4, CO_2, $\delta^{13}CH_4$ and $\delta^{13}CO_2$ values were calibrated with a single-point calibration.

Measurements and mean isotopic source signatures
In figure C.3 the measured CH_4 and CO_2 mole fractions as well as their isotopic δ^{13} compositions are shown.

During the first measurement campaign two time intervals have to be flagged since the data were contaminated with room air. The measured mean CH_4 mole fraction during both campaigns (summer and winter) are the same with 1945 $\pm$ 24 ppb (mean $\pm$ sd). However, $\delta^{13}CH_4$ averaged over the summer campaign measurements is -48.4 ± 1.1 ‰ (mean $\pm$ sd). Thus it is around 0.4 ‰ more depleted than in winter (-47.9 ± 1.1 ‰).

Furthermore, the mean isotopic source signature is determined by the Miller-Tans approach and the York fit. Again, a difference between summer and winter is noticeable. In summer the mean isotopic source signature is -60.3 ± 0.7‰ and in winter around

time period	CH_4 [ppb]	$\delta^{13}CH_4$ [‰]	CO_2 [ppm]	$\delta^{13}CO_2$ [‰]
autum 2018 and spring 2019	1993.34	-48.25	435.28	-9.83
summer 2019	2002.41	-48.36	407.71	-8.89

Table C.1.: Calibration cylinder used during measurement campaigns at Schauinsland.

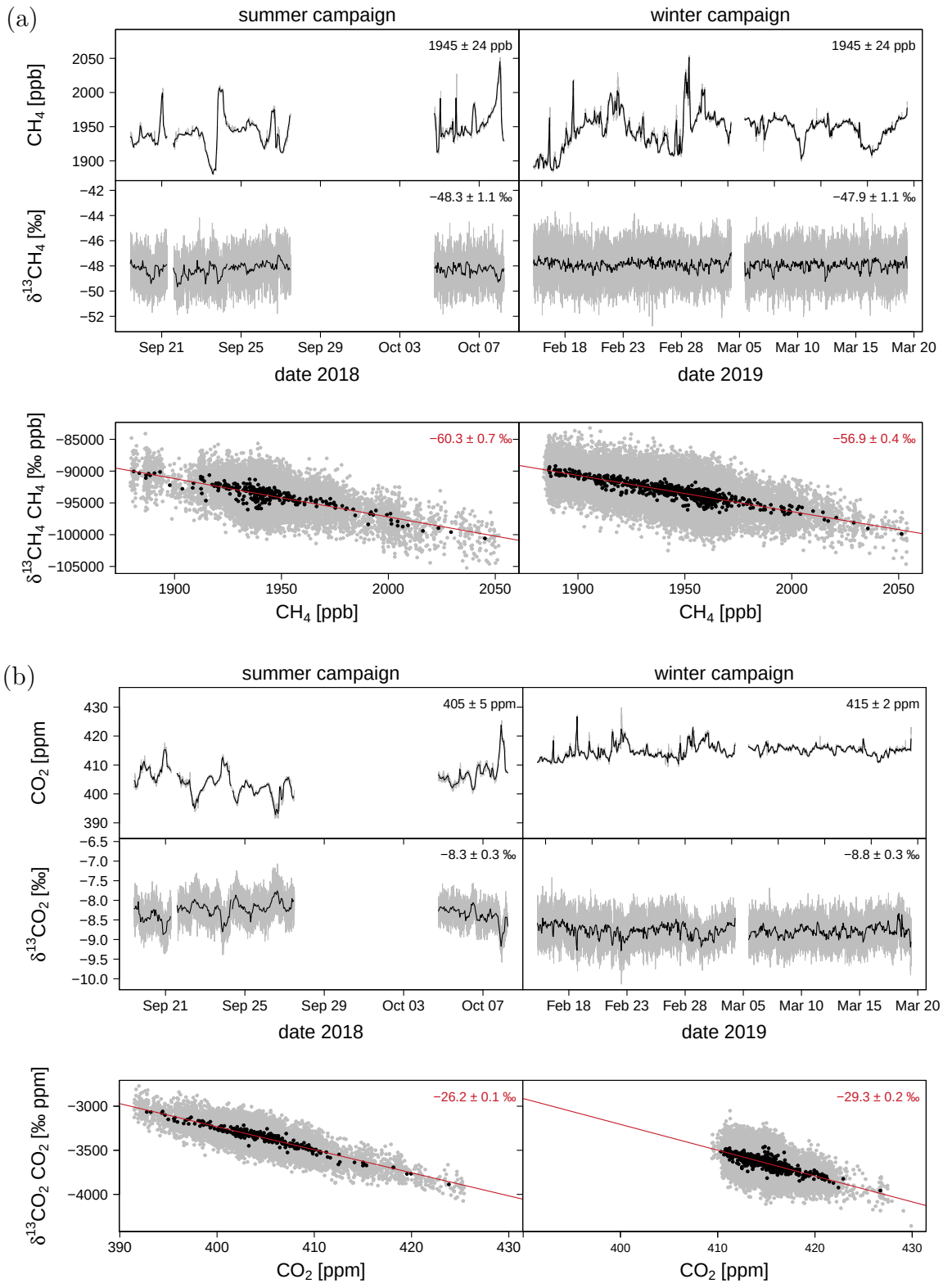

Figure C.3.: Isotopic ^{13}C measurements during two campaigns at Schauinsland. One in summer and one in winter. In addition to the CH_4 and CO_2 mole fractions, the isotopic ^{13}C composition is measured. At the bottom of each panel (a) and (b) the Miller-Tans plot to determine the mean isotopic source signature is shown. In the upper right corners the averages and standard deviations are displayed in black and the determined mean source signatures in red.

3.4 ‰ more enriched. Thus, more biogenic CH_4 sources contribute to the measured CH_4 in summer.

In addition, the G2201-i analyser measures the CO_2 mole fraction and $\delta^{13}CO_2$. While the CO_2 mole fractions differ around 10 ppm between summer (405 ± 6 ppm) and winter (415 ± 2 ppm), the isotopic composition shows a difference of 0.5 ‰ with more enriched values in summer.

More enriched values are also noticeable in the mean isotopic source signature of CO_2. In summer the source signature is -26.2 ± 0.1 ‰ and in winter -29.3 ± 0.2 ‰. The larger relative contribution of CO_2 from fossil fuels (Levin, 1987), which are more depleted than CO_2 emitted by the biosphere, can explain the more depleted mean source signature in winter. Levin (1987) determined a mean isotopic source signature of -25.7 ± 1.4 ‰ at Schauinsland between 1977 and 1985. For Heidelberg Vardag et al. (2016) calculated similar mean source signatures for summer (-25 ± 1 ‰) and winter (-32.5 ± 2.5 ‰) in 2012.

Comparison with emission inventories

The first estimate of CH_4 emissions and mean isotopic source signature measured at Schauinsland was calculated out of the local CH_4 emission inventory provided by LUBW for Freiburg (FR) and Breisgau-Hochschwarzwald (BH). This calculation followed the one done for Heidelberg as described in section 4.6

While the city of Freiburg (FR) has a source composition similar to Heidelberg (HD) and Mannheim (MA), the one for Breisgau-Hochschwarzwald (BH) is more representative of Baden-Württemberg with a higher amount (69 %) of agricultural emissions (figure C.4a). The emission estimates of counties provided by LUBW show that around Schauinsland (FR and BH) 60 % of the CH_4 emissions are emitted by livestock farming and around Heidelberg (HD, MA and RNK) only 28 %. Therefore, the mean source signature of CH_4 emissions around Schauinsland (FR and BH) is -56 ± 2‰.

Although, the EDGAR v5.0 inventory estimated a much lower contribution of livestock farming at Breisgau-Hochschwarzwald, the larger fraction of CH_4 emissions from waste treatment (landfills and waste water treatment plants) especially for Freiburg results in a similar mean source signature for Schauinsland of -55 ± 2‰.

For both emission inventories the determined mean source signature seems to be more enriched than the result from atmospheric measurements (winter: -56.9 ± 0.4‰ and summer: -60.3 ± 0.7‰). This is especially the case for the mean source signatures calculated for late summer/autumn. A possible explanation could be the cows which graze near the station. The impact of strongly depleted CH_4, which is emitted by cows directly next to the station, on the atmospheric measurement of $\delta^{13}CH_4$ can shift the determined mean isotopic source signature to more depleted values. These very local CH_4 emissions cannot be represented by regional emission inventories.

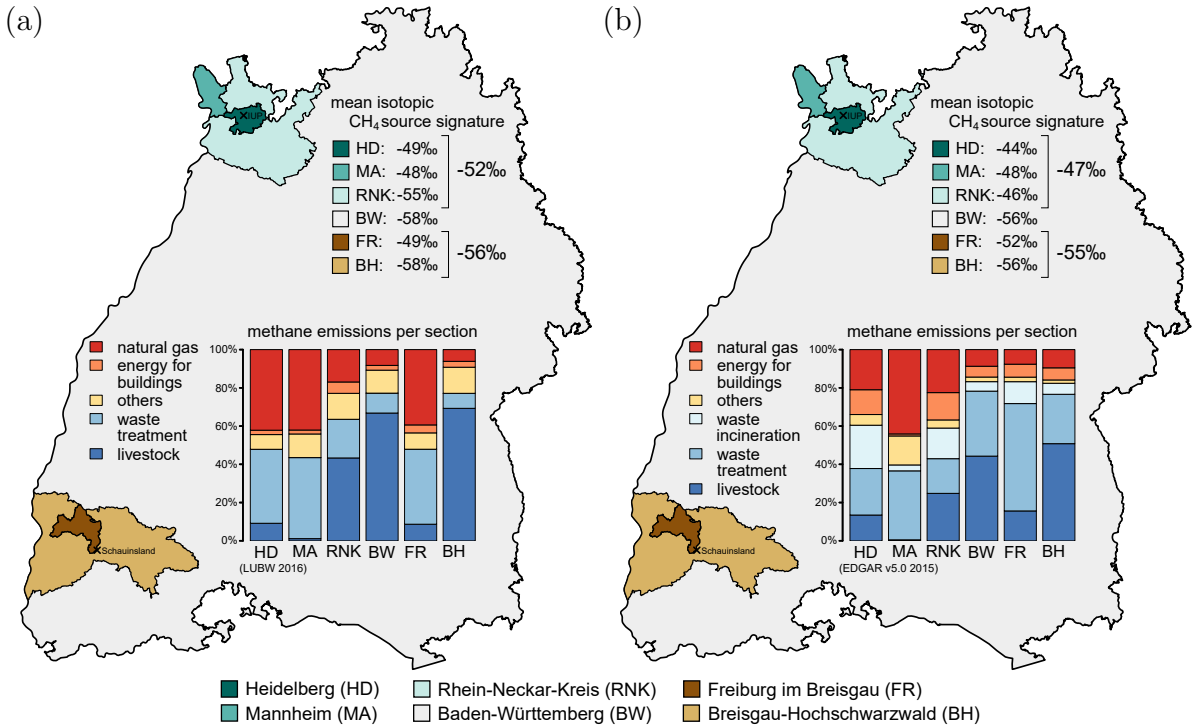

Figure C.4.: Mean isotopic source signature for different counties around Schauinsland and the fraction of CH_4 emissions for different sections for these counties. Panel (a) shows the emissions provided by LUBW for 2016 and panel (b) depicts the emissions reported by the EDGAR v5.0 inventory for 2015.

C.4. CH_4 and CO_2 soil flux

In July 2020 and October 2020 soil flux measurements were done in addition to chamber measurements at the sewage pit (figure C.5). The measurements clearly show the sink character of soil for CH_4 and that soil is a CO_2 source. However, the flux determined for both measurement campaigns is quite different. In July 2020 the CH_4 soil uptake was calculated to be around $-0.63 \pm 0.05\text{mg} \cdot (\text{day m}^2)^{-1}$ and in October 2020 only $-0.08 \pm 0.01\text{mg} \cdot (\text{day m}^2)^{-1}$. The CO_2 soil flux is around $6.8 \pm 0.4\text{g} \cdot (\text{day m}^2)^{-1}$ in July 2020 and approximately $3.9 \pm 0.4\text{g} \cdot (\text{day m}^2)^{-1}$ in October 2020.

The CH_4 flux into the soil was determined at a meadow next to the forest at Schauinsland. A higher CH_4 flux into the soil was measured in July than in October. With values of 0.22 and $0.02\,\text{g m}^{-2}\text{yr}-1$ the CH_4 flux into the soil is in the same range as the one for temperate grassland (0.002 to $0.2\,\text{g m}^{-2}\text{yr}-1$) found by Born et al. (1989). They studied the CH_4 flux into the soil at five forest sites near Heidelberg and from other cultivated soils in western Germany. For the five temperate forest sites average CH_4 fluxes between 0.09 to $1.3\,\text{g m}^{-2}\text{yr}-1$ into the soil were determined. At these sites, higher CH_4 uptake in summer was noticed than in winter, too. However, the variability between the averaged CH_4 fluxes for the different sites is much stronger than the temporal variability at each site, which is lower than a factor of two (Born et al., 1989). At Schauinsland, the CH_4 fluxes into the soil in summer and autumn deviate by a factor of 10. The much higher factor could be caused by the lower fluxes determined for Schauinsland. The deviation between the two fluxes at Schauinsland is smaller than most temporal variabilities measured by Born et al. (1989) in forests. In addition, the determined soil fluxes at two days only might not be representative for the season.

The CO_2 flux out of soil depends more strongly on soil temperature than the CH_4 flux into the soil (Born et al., 1989). Thus, a prominent annual cycle of soil respiration can be seen for the Rhine Valley area near Heidelberg (Dörr and Münnich, 1989). Dörr and Münnich (1989) found a minimum CO_2 flux in February which strongly increases to a maximum in June and July of around $9\,\text{mmol m}^{-2}\text{h}^{-1}$. Then, the flux slowly decreases from summer to winter. The monthly averaged CO_2 fluxes range between 0.5 to $10\,\text{mmol m}^{-2}\text{h}^{-1}$. The CO_2 fluxes determined for Schauinsland also indicate an annual cycle with $7\,\text{mmol m}^{-2}\text{h}^{-1}$ in July and $4\,\text{mmol m}^{-2}\text{h}^{-1}$ in October. These fluxes are comparable with the ones determined by Dörr and Münnich (1989).

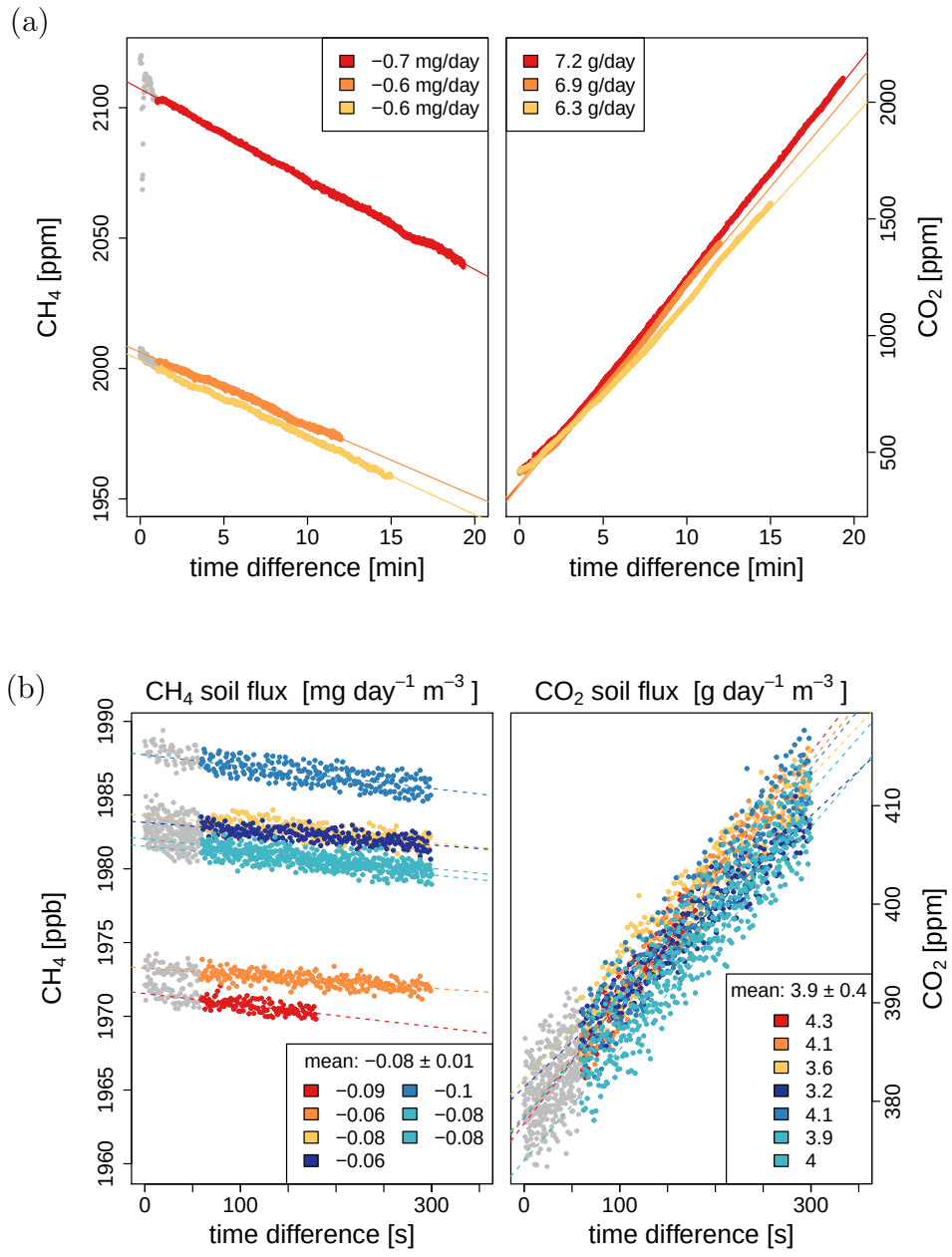

Figure C.5.: Soil flux chamber measurements done in July 2020 (a) and October 2020 (b) at Schauinsland. The measured CH_4 (left panel) and CO_2 (right panel) mole fractions are shown and the corresponding fluxes are displayed. Different flux chamber measurements carried out in July or October are coloured differently. Thus, corresponding CH_4 and CO_2 mole fractions have the same colour.

Bibliography

Affolter, S., Schibig, S., Berhanu, T., Bukowiecki, N., Steinbacher, M., Nyfeler, P., Hervo, M., Lauper, J. and Leuenberger, M.: Assessing local CO_2 contamination revealed by two near-by high altitude records at Jungfraujoch, Switzerland, Environ. Res. Lett. in press https://doi.org/10.1088/1748-9326/abe74a.

Allan, D. W.: Statistics of atomic frequency standards. P. IEEE, 54, 221-230, 1966.

Assan, S., Vogel, F. R., Gros, V., Baudic, A., Staufer, J., and Ciais, P.: Can we separate industrial CH4 emission sources from atmospheric observations? - A test case for carbon isotopes, PMF and enhanced APCA, Atmos. Environ., 187, 317-327, 10.1016/j.atmosenv.2018.05.004, 2018.

Baer, D. S., Paul, J. B., Gupta, J. B., and O'Keefe, A.: Sensitive absorption measurements in the near-infrared region using off-axis integrated-cavity-output spectroscopy, Appl. Phys. B-Lasers Opt., 75, 261-265, 10.1007/s00340-002-0971-z, 2002.

Bayerische Zugspitzbahn Bergbahn Aktiengesellschaft Garmisch-Partenkirchen: Jahresabschluss zum Geschäftsjahr vom 01.11.2018 bis zum 31.10.2019, `www.bundesanzeiger.de`, 2020, last access: 22 April 2021.

Bergamaschi, P., Krol, M., Meirink, J. F., Dentener, F., Segers, A.,Van Aardenne, J., Monni, S., Vermeulen, A. T., Schmidt, M., Ra-monet, M., Yver, C., Meinhardt, F., Nisbet, E. G., Fisher, R. E.,O'Doherty, S., and Dlugokencky, E. J.: Inverse modeling of Eu-ropean CH_4 emissions 2001–2006, J. Geophys. Res.-Atmos.,115, D22309, https://doi.org/10.1029/2010JD014180, 2010.

Bergamaschi, P., Karstens, U., Manning, A. J., Saunois, M., Tsuruta, A., Berchet, A., Vermeulen, A. T., Arnold, T., Janssens-Maenhout, G., Hammer, S., Levin, I., Schmidt, M., Ramonet, M., Lopez, M., Lavric, J., Aalto, T., Chen, H. L., Feist, D. G., Gerbig, C., Haszpra, L., Hermansen, O., Manca, G., Moncrieff, J., Meinhardt, F., Necki, J., Galkowski, M., O'Doherty, S., Paramonova, N., Scheeren, H. A., Steinbacher, M., and Dlugokencky, E.: Inverse modelling of European CH4 emissions during 2006-2012 using different inverse models and reassessed atmospheric observations, Atmos. Chem. Phys., 18, 901-920, 10.5194/acp-18-901-2018, 2018.

Birmili, W., Ries, L., Sohmer, R., Anastou, A., Sonntag, A., Konig, K., and Levin, I.: Fine and ultrafine aerosol particles at the GAW station Schneefernerhaus/Zugspitze, Gefahrst. Reinhalt. Luft, 69, 31-35, 2009.

Born, M., DÖrr, H. and Levin, I.:Methane consumption in aerated soils of the temperate zone, Tellus B: Chemical and Physical Meteorology, 42:1, 2-8, DOI: 10.3402/tellusb.v42i1.15186, 1990.

Bousquet, P., Gaudry, A., Ciais, P., Kazan, V., Monfray, P., Simmonds, P.G.,Jennings, S.G., O'Connor, T.C.: Atmospheric CO_2 concentration variations recorded at Mace Head, Ireland, from 1992 to 1994. Phys. Chem. Earth 21, pp. 477-481, 1996.

Brantley, H. L., Hagler, G. S. W., Kimbrough, E. S., Williams, R. W., Mukerjee, S., and Neas, L. M.: Mobile air monitoring dataprocessing strategies and effects on spatial air pollution trends, Atmos. Meas. Tech., 7, 2169–2183, https://doi.org/10.5194/amt-7-2169-2014, 2014.

Chanton, J. P., Rutkowski, C. M., Schwartz, C. C., Ward, D. E., and Boring, L.: Factors influencing the stable carbon isotopic signature of methane from combustion and biomass burning, J. Geophys. Res.-Atmos., 105, 1867-1877, 10.1029/1999jd900909, 2000.

Crippa, M., Oreggioni, G., Guizzardi, D., Muntean, M., Schaaf, E., Lo Vullo, E., Solazzo, E., Monforti-Ferrario, F., Olivier, J.G.J., Vignati, E.: Fossil CO2 and GHG emissions of all world countries - 2019 Report, EUR 29849 EN, Publications Office of the European Union, Luxembourg, 2019, ISBN 978-92-76-11100-9, doi:10.2760/687800, JRC117610.

Crosson, E. R.: A cavity ring-down analyzer for measuring atmospheric levels of methane, carbon dioxide, and water vapor, Appl. Phys. B-Lasers Opt., 92, 403-408, 10.1007/s00340-008-3135-y, 2008.

Daniel, J. S., Portmann, R. W., Solomon, S., and Murphy, D. M.: Identifying weekly cycles in meteorological variables: The importance of an appropriate statistical analysis, J. Geophys. Res.-Atmos., 117, 14, 10.1029/2012jd017574, 2012.

Dinger, F.: Characterisation of a Cavity Ring-Down Spectrometer for measuring CO_2, CH_4, $\delta^{13}CO_2$ and $\delta^{13}CH_4$ in ambient air. MA thesis. University of Heidelberg, 2014.

Dlugokencky, E. J., Masarie, K. A., Lang, P. M., and Tans, P. P.: Continuing decline in the growth rate of the atmospheric methane burden, Nature, 393, 447-450, 10.1038/30934, 1998.

Dlugokencky, E. J., Myers, R. C., Lang, P. M., Masarie, K. A., Crotwell, A. M., Thoning, K. W., Hall, B. D., Elkins, J. W., and Steele, L. P.: Conversion of NOAA atmospheric dry air CH_4 mole fractions to a gravimetrically prepared standard scale, J. Geophys. Res.-Atmos., 110, 8, 10.1029/2005jd006035, 2005.

Dlugokencky, E. J., Thoning, K. W., Lang, P. M., and Tans P.P.: NOAA Greenhouse Gas Reference from Atmospheric Carbon Dioxide Dry Air Mole Fractions from the NOAA ESRL Carbon Cycle Cooperative Global Air Sampling Network. Data Path: `ftp://aftp.cmdl.noaa.gov/data/trace_gases/co2/flask/surface/`, 2019A.

Dlugokencky, E.J., Lang, P. M., Crotwell, A. M., Thoning, K. W. and Crotwell, M.J.: Atmospheric Methane Dry Air Mole Fractions from the NOAA ESRL Carbon Cycle Cooperative Global Air Sampling Network. Data Path: `ftp://aftp.cmdl.noaa.gov/data/trace_gases/ch4/flask/surface/`, 2019B.

Dlugokencky, E. J., Crotwell, A. M., Mund, J. W., Crotwell, M. J. and Thoning, K. W., Atmospheric Methane Dry Air Mole Fractions from the NOAA GML Carbon Cycle Cooperative Global Air Sampling Network, 1983-2019, Version: 2020-07, https://doi.org/10.15138/VNCZ-M766, 2020.

Dlugokencky, E. J., Mund, J. W., Crotwell, A. M., Crotwell, M. J. and Thoning, K. W.: Atmospheric Carbon Dioxide Dry Air Mole Fractions from the NOAA GML Carbon Cycle Cooperative Global Air Sampling Network, 1968-2019, Version: 2021-02, https://doi.org/10.15138/wkgj-f215, 2021.

Dlugokencky, E., NOAA/ESRL (`www.esrl.noaa.gov/gmd/ccgg/trends_ch4/`), 2021, last access: 26 April 2021.

Dörr, H. and Münnich, K. O.: Annual variation in soil respiration in selected areas of the temperate zone, Tellus 39B, 114-121, 1989.

Drewnick, F., Böttger, T., von der Weiden-Reinmüller, S.-L., Zorn, S. R., Klimach, T., Schneider, J., and Borrmann, S.: Design of a mobile aerosol research laboratory and data processing tools for effective stationary and mobile field measurements, Atmos. Meas. Tech., 5, 1443–1457, https://doi.org/10.5194/amt-5-1443-2012, 2012.

El Yazidi, A., Ramonet, M., Ciais, P., Broquet, G., Pison, I., Abbaris, A., Brunner, D., Conil, S., Delmotte, M., Gheusi, F., Guerin, F., Hazan, L., Kachroudi, N., Kouvarakis, G., Mihalopoulos, N., Rivier, L., and Serça, D.: Identification of spikes associated with local sources in continuous time series of atmospheric CO, CO2 and CH4, Atmos. Meas. Tech., 11, 1599–1614, `https://doi.org/10.5194/amt-11-1599-2018`, 2018.

Environmental Research Station Schneefernerhaus, `https://www.schneefernerhaus.de`, last access: 24 Sept 2020, 2020.

Etheridge, D. M., Steele, L. P., Langenfelds, R. L., Francey, R. J., Barnola, J. M., and Morgan, V. I.: Natural and anthropogenic changes in atmospheric CO2 over the last 1000 years from air in Antarctic ice and firn, J. Geophys. Res.-Atmos., 101, 4115-4128, 10.1029/95jd03410, 1996.

Etheridge, D. M., Steele, L. P., Francey, R. J., and Langenfelds, R. L.: Atmospheric methane between 1000 AD and present: Evidence of anthropogenic emissions and climatic variability, J. Geophys. Res.-Atmos., 103, 15979-15993, 10.1029/98jd00923, 1998.

European Commission: Commission welcomes provisional agreement on the European Climate Law [Press release]. 21 April 2021. Available at: `https://ec.europa.eu/commission/presscorner/detail/en/ip_21_1828`, last access: 23 April 2021.

Frank, G., Salvamoser, J., Steinkopff, T. and Ries, L.: Radon-222 und Beryllium-7 als natürlicher tracer, UFS-Wissenschaftliche Resultate 2015/2016, 2017.

Friedlingstein, P., O'Sullivan, M., Jones, M. W., Andrew, R. M., Hauck, J., Olsen, A., Peters, G. P., Peters, W., Pongratz, J., Sitch, S., Le Quere, C., Canadell, J. G., Ciais, P., Jackson, R. B., Alin, S., Aragao, L., Arneth, A., Arora, V., Bates, N. R., Becker, M., Benoit-Cattin, A., Bittig, H. C., Bopp, L., Bultan, S., Chandra, N., Chevallier, F., Chini, L. P., Evans, W., Florentie, L., Forster, P. M., Gasser, T., Gehlen, M., Gilfillan, D., Gkritzalis, T., Gregor, L., Gruber, N., Harris, I., Hartung, K., Haverd, V., Houghton, R. A., Ilyina, T., Jain, A. K., Joetzjer, E., Kadono, K., Kato, E., Kitidis, V., Korsbakken, J. I., Landschutzer, P., Lefevre, N., Lenton, A., Lienert, S., Liu, Z., Lombardozzi, D., Marland, G., Metzl, N., Munro, D. R., Nabel, J., Nakaoka, S. I., Niwa, Y., O'Brien, K., Ono, T., Palmer, P. I., Pierrot, D., Poulter, B., Resplandy, L., Robertson, E., Rodenbeck, C., Schwinger, J., Seferian, R., Skjelvan, I., Smith, A. J. P., Sutton, A. J., Tanhua, T., Tans, P. P., Tian, H., Tilbrook, B., Van der Werf, G., Vuichard, N., Walker, A. P., Wanninkhof, R., Watson, A. J., Willis, D., Wiltshire, A. J., Yuan, W. P., Yue, X., and Zaehle, S.: Global Carbon Budget 2020, Earth Syst. Sci. Data, 12, 3269-3340, 10.5194/essd-12-3269-2020, 2020.

Fujita, R., Morimoto, S., Umezawa, T., Ishijima, K., Patra, P. K., Worthy, D. E. J., Goto, D., Aoki, S., and Nakazawa, T.: Temporal Variations of the Mole Fraction, Carbon, and Hydrogen Isotope Ratios of Atmospheric Methane in the Hudson Bay Lowlands, Canada, J. Geophys. Res.-Atmos., 123, 4695-4711, 10.1002/2017jd027972, 2018.

Ghasemifard, H., Yuan, Y., Luepke, M., Schunk, C., Chen, J., Ries, L., Leuchner, M., and Menzel, A.: Atmospheric CO2 and delta C-13 Measurements from 2012 to 2014 at the Environmental Research Station Schneefernerhaus, Germany: Technical Corrections, Temporal Variations and Trajectory Clustering, Aerosol Air Qual. Res., 19, 657-670, 10.4209/aaqr.2018.01.0010, 2019.

Giemsa, E., Jacobeit, J., Ries, L., and Hachinger, S.: Investigating regional source and sink patterns of Alpine CO2 and CH4 concentrations based on a back trajectory receptor model, Environ. Sci Eur., 31, 24, 10.1186/s12302-019-0233-x, 2019.

Glatzel-Mattheier, H.: Bilanzierung von CH_4-Emissionen in Deutschland anhand atmosphärischer Messungen in Heidelberg. PhD thesis. University of Heidelberg, 1997.

Griffith, P. and de Haseth, J.: Fourier Transform Infrared Spectrometry, volume 171. John Wiley & Sons, 2007.

Hagler, G. S. W., Thoma, E. D., and Baldauf, R. W.: High-Resolution Mobile Monitoring of Carbon Monoxide and Ultrafine Particle Concentrations in a Near-Road Environment, J.Air Waste Manage., 60, 328–336, https://doi.org/10.3155/1047-3289.60.3.328, 2010.

Heimann, I., Griffiths, P. T., Warwick, N. J., Abraham, N. L., Archibald, A. T., and Pyle, J. A.: Methane Emissions in a Chemistry-Climate Model: Feedbacks and Climate Response, J. Adv. Model. Earth Syst., 12, 19, 10.1029/2019ms002019, 2020.

Hoheisel, A., Yeman, C., Dinger, F., Eckhardt, H., and Schmidt, M.: An improved method for mobile characterisation of $\delta^{13}CH_4$ source signatures and its application in Germany, Atmos. Meas. Tech., 12, 1123-1139, 10.5194/amt-12-1123-2019, 2019.

Integrated non-CO_2 Greenhouse gas Observing System (InGOS): Ambient atmospheric methane observations from the ICOS/InGOS network 2000-2015. ICOS ERIC - Carbon Portal. https://doi.org/10.18160/P7E9-EKEA, 2018.

IPCC (2006): IPCC Guidelines for National Greenhouse Gas Inventories, Prepared by the National Greenhouse Gas Inventories Programme, edited by: Eggleston, H. S., Buendia, L., Miwa, K., Ngara, T., and Tanabe, K., Institute for Global Environmental Strategies, Japan, 2006.

IPCC (2013): Climate Change 2013: The Physical Science Basis. Contribution of Working Group I to the Fifth Assessment Report of the Intergovernmental Panel on Climate Change, edited by: Stocker, T.F., D. Qin, G.-K. Plattner, M. Tignor, S.K. Allen, J. Boschung, A. Nauels, Y. Xia, V. Bex and P.M. Midgley, Cambridge University Press, Cambridge, United Kingdom and New York, NY, USA, 1535 pp, 2013.

IPCC (2018): Global Warming of 1.5°C. An IPCC Special Report on the impacts of global warming of 1.5°C above pre-industrial levels and related global greenhouse gas emission pathways, in the context of strengthening the global response to the threat of climate change, sustainable development, and efforts to eradicate poverty, edited by: Masson-Delmotte, V., P. Zhai, H.-O. Pörtner, D. Roberts, J. Skea, P.R. Shukla, A. Pirani, W. Moufouma-Okia, C. Péan, R. Pidcock, S. Connors, J.B.R. Matthews, Y. Chen, X. Zhou, M.I. Gomis, E. Lonnoy, T. Maycock, M. Tignor, and T. Waterfield. In Press, 2018.

Jentsch, W., Piatkowski, B., Röntgen, M. and Derno, M.: Quantitative results for methane production of cattle in Germany. Archiv fur Tierzucht. 52.10.5194/aab-52-587-2009, 2009.

Karion, A., Sweeney, C., Tans, P., and Newberger, T.: AirCore: An Innovative Atmospheric Sampling System, J. Atmos. Ocean. Technol., 27, 1839-1853, 10.1175/2010jtecha1448.1, 2010.

Keeling, C. D.: The concentration and isotopic abundances of atmospheric carbon dioxide in rural areas, Geochim. Cosmochim. Acta, 13, 322-334, 10.1016/0016-7037(58)90033-4, 1958.

Keeling, C. D.: The concentration and isotopic abundances of carbon dioxide in rural and marine air. Geochim. Cosmochim. Acta. 24, 277–298. doi:10.1016/0016-7037(61)90023-0, 1961.

Keeling, C. D., Bacastow, R. B., Bainbridge, A. E., Ekdahl, C. A., Guenther, P. R., Waterman, L. S., and Chin, J. F. S.: ATMOSPHERIC CARBON-DIOXIDE VARIATIONS AT MAUNA-LOA OBSERVATORY, HAWAII, Tellus, 28, 538-551, 1976.

Kossmann, M., U. Corsmeier, S. De Wekker, F. Fiedler, R. Vögtlin, N. Kalthoff, H. Güsten, and B. Neininger: Observations of handover processes between the atmospheric boundary layer and the free troposphere over mountainous terrain, Contrib. Atmos. Phys., 72(4), 329– 350, 1999.

Kountouris, P., Gerbig, C., Rödenbeck, C., Karstens, U., Frank Koch, T. and Heimann, M.: Technical Note: Atmospheric CO2 inversions on the mesoscale using data-driven prior uncertainties: Methodology and system evaluation, Atmos. Chem. Phys., 18(4), 3027–3045, doi:10.5194/acp-18-3027-2018, 2018.

Landesanstalt für Umwelt Baden-Württemberg (LUBW): `https://www.lubw.baden-wuerttemberg.de/luft/kataster` and personal communication with M. Vogel and T. Leiber from LUBW in April and December 2019.

Lelieveld, J., Gromov, S., Pozzer, A., and Taraborrelli, D.: Global tropospheric hydroxyl distribution, budget and reactivity, Atmos. Chem. Phys., 16, 12477-12493, 10.5194/acp-16-12477-2016, 2016.

Levin, I., Atmosphärisches CO2, Quellen und Senken auf dem Europäischen Kontinent, PhD thesis, University of Heidelberg, Germany, 1984.

Levin, I.: Atmospheric CO_2 in continental Europe, an alternative approach to clean air CO_2 data. Tellus 39B, 21–28, 1987.

Levin, I., Bergamaschi, P., Dörr, H., and Trapp, D.: Stable isotopic signature of methane from major sources in Germany, Chemosphere, 26, 161-177, 10.1016/0045-6535(93)90419-6, 1993.

Levin, I., Glatzel-Mattheier, H., Marik, T., Cuntz, M., Schmidt, M., and Worthy, D. E.: Verification of German methane emission inventories and their recent changes based on atmospheric observations, J. Geophys. Res.-Atmos., 104, 3447-3456, 10.1029/1998jd100064, 1999.

Levin, I., Hammer, S., Eichelmann, E. and Vogel F. R.: Verification of greenhouse gas emission reductions: the prospect of atmospheric monitoring in polluted areas Phil. Trans. R. Soc. A.3691906–1924 http://doi.org/10.1098/rsta.2010.0249, 2011.

Lin, J. C., Gerbig, C., Wofsy, S. C., Andrews, A. E., Daube, B. C., Davis, K. J. and Grainger, C. A.: A near-field tool for simulating the upstream influence of atmospheric observations: The Stochastic Time-Inverted Lagrangian Transport (STILT) model, J. Geophys. Res. D Atmos., 108(16), doi:10.1029/2002JD003161, 2003.

Locher, R. and Ruckstuhl, A: IDPmisc: IDPmisc: 'Utilities of Institute of Data Analyses and Process Design (www.zhaw.ch/idp)', available at: https://CRAN.R-project.org/package=IDPmisc, (last access: 20 April 2021), 2020.

Lowry, D., Holmes, C. W., Rata, N. D., O'Brien, P., and Nisbet, E. G.: London methane emissions: Use of diurnal changes in concentration and δ^{13}C to identify urban sources and verify inventories, Journal of Geophysical Research: Atmospheres, 106(D7), 7427–7448, doi:10.1029/2000JD900601, 2001.

Menoud, M., van der Veen, C., Scheeren, B., Chen, H., Szénási, B., Morales, R. P., Pison, I., Bousquet, P., Brunner, D., and Röckmann, T.: Characterisation of methane sources in Lutjewad, The Netherlands, using quasi-continuous isotopic composition measurements, Tellus B: Chemical and Physical Meteorology, 72, 1-20, 10.1080/16000889.2020.1823733, 2020.

Metges, C., Kempe, K., and Schmidt, H. L.: Dependence of the carbon-isotope contents of breath carbon-dioxide, milk, serum and rumen fermentation products on the delta-C-13 value of food in dairy-cows, Br. J. Nutr., 63, 187-196, 10.1079/bjn19900106, 1990.

Miller, J. B., and Tans, P. P.: Calculating isotopic fractionation from atmospheric measurements at various scales, Tellus Ser. B-Chem. Phys. Meteorol., 55, 207-214, 10.1034/j.1600-0889.2003.00020.x, 2003.

Mook, W.G.: Environmental Isotopes in the Hydrological Cycle - Principles and Applications. UNESCO, IAEA, 2000.

Nisbet, E. G., Dlugokencky, E. J., and Bousquet, P.: Methane on the Rise-Again, Science, 343, 493-495, 10.1126/science.1247828, 2014.

Nisbet, E. G., Dlugokencky, E. J., Manning, M. R., Lowry, D., Fisher, R. E., France, J. L., Michel, S. E., Miller, J. B., White, J. W. C., Vaughn, B., Bousquet, P., Pyle, J. A., Warwick, N. J., Cain, M., Brownlow, R., Zazzeri, G., Lanoiselle, M., Manning, A. C., Gloor, E., Worthy, D. E. J., Brunke, E. G., Labuschagne, C., Wolff, E. W., and Ganesan, A. L.: Rising atmospheric methane: 2007-2014 growth and isotopic shift, Glob. Biogeochem. Cycle, 30, 1356-1370, 10.1002/2016gb005406, 2016.

Nisbet, E. G., Manning, M. R., Dlugokencky, E. J., Fisher, R. E., Lowry, D., Michel, S. E., Myhre, C. L., Platt, M., Allen, G., Bousquet, P., Brownlow, R., Cain, M., France, J. L., Hermansen, O., Hossaini, R., Jones, A. E., Levin, I., Manning, A. C., Myhre, G., Pyle, J. A., Vaughn, B. H., Warwick, N. J., and White, J. W. C.: Very Strong. Atmospheric Methane Growth in the 4 Years 2014-2017: Implications for the paris Agreement, Glob. Biogeochem. Cycle, 33, 318-342, 10.1029/2018gb006009, 2019.

Passey, B. H., Robinson, T. F., Ayliffe, L. K., Cerling, T. E., Sponheimer, M., Dearing, M. D., Roeder, B. L., and Ehleringer, J. R.: Carbon isotope fractionation between

diet, breath CO2, and bioapatite in different mammals, J. Archaeol. Sci., 32, 1459-1470, 10.1016/j.jas.2005.03.015, 2005.

Platt, U. and Stutz, J.: Differential Optical Absorption Spectroscopy: Principles and Applications. Series: Physics of Earth and Space Environments, Springer-Verlag Berlin Heidelberg, 2008.

Prather, M. J.: Time scales in atmospheric chemistry: Theory, GWPs for CH4 and CO, and runaway growth, Geophys. Res. Lett., 23, 2597-2600, 10.1029/96gl02371, 1996.

Rella, C. W., Hoffnagle, J., He, Y., and Tajima, S.: Local- and regional-scale measurements of CH_4, $\delta^{13}CH_4$, and C_2H_6 in the Uintah Basin using a mobile stable isotope analyzer, Atmos. Meas. Tech., 8, 4539-4559, 10.5194/amt-8-4539-2015, 2015.

Röckmann, T., Eyer, S., van der Veen, C., Popa, M. E., Tuzson, B., Monteil, G., Houweling, S., Harris, E., Brunner, D., Fischer, H., Zazzeri, G., Lowry, D., Nisbet, E. G., Brand, W. A., Necki, J. M., Emmenegger, L., and Mohn, J.: In situ observations of the isotopic composition of methane at the Cabauw tall tower site, Atmos. Chem. Phys., 16, 10469-10487, 10.5194/acp-16-10469-2016, 2016.

Ruckstuhl, A. F., Jacobson, M. P., Field, R. W., and Dodd, J. A.: Baseline Subtraction Using Robust Local Regression Estimation, J. Quant. Spectrosc. Ra., 68, 179–193, 2001.

Ruckstuhl, A. F., Henne, S., Reimann, S., Steinbacher, M., Vollmer, M. K., O'Doherty, S., Buchmann, B., and Hueglin, C.: Robust extraction of baseline signal of atmospheric trace species using local regression, Atmos. Meas. Tech., 5, 2613–2624, https://doi.org/10.5194/amt-5-2613-2012, 2012.

Saunois, M., Stavert, A. R., Poulter, B., Bousquet, P., Canadell, J. G., Jackson, R. B., Raymond, P. A., Dlugokencky, E. J., Houweling, S., Patra, P. K., Ciais, P., Arora, V. K., Bastviken, D., Bergamaschi, P., Blake, D. R., Brailsford, G., Bruhwiler, L., Carlson, K. M., Carrol, M., Castaldi, S., Chandra, N., Crevoisier, C., Crill, P. M., Covey, K., Curry, C. L., Etiope, G., Frankenberg, C., Gedney, N., Hegglin, M. I., Hoglund-Isaksson, L., Hugelius, G., Ishizawa, M., Ito, A., Janssens-Maenhout, G., Jensen, K. M., Joos, F., Kleinen, T., Krummel, P. B., Langenfelds, R. L., Laruelle, G. G., Liu, L. C., Machida, T., Maksyutov, S., McDonald, K. C., McNorton, J., Miller, P. A., Melton, J. R., Morino, I., Muller, J., Murguia-Flores, F., Naik, V., Niwa, Y., Noce, S., Doherty, S. O., Parker, R. J., Peng, C. H., Peng, S. S., Peters, G. P., Prigent, C., Prinn, R., Ramonet, M., Regnier, P., Riley, W. J., Rosentreter, J. A., Segers, A., Simpson, I. J., Shi, H., Smith, S. J., Steele, L. P., Thornton, B. F., Tian, H. Q., Tohjima, Y., Tubiello, F. N., Tsuruta, A., Viovy, N., Voulgarakis, A., Weber, T. S., van Weele, M., van der Werf, G. R., Weiss, R. F., Worthy, D., Wunch, D., Yin, Y., Yoshida, Y., Zhang, W. X., Zhang, Z., Zhao, Y. H., Zheng, B., Zhu, Q., Zhu, Q. A., and Zhuang, Q. L.: The Global Methane Budget 2000-2017, Earth Syst. Sci. Data, 12, 1561-1623, 10.5194/essd-12-1561-2020, 2020.

Schaefer, H., Fletcher, S. E. M., Veidt, C., Lassey, K. R., Brailsford, G. W., Bromley, T. M., Dlugokencky, E. J., Michel, S. E., Miller, J. B., Levin, I., Lowe, D. C., Martin, R. J., Vaughn, B. H., and White, J. W. C.: A 21st-century shift from fossil-fuel to biogenic methane emissions indicated by (CH4)-C-13, Science, 352, 80-84, 10.1126/science.aad2705, 2016.

Schaefer, H.: On the Causes and Consequences of Recent Trends in Atmospheric Methane, Curr. Clim. Chang. Rep., 5, 259-274, 10.1007/s40641-019-00140-z, 2019.

Schmidt, M., Graul, R., Sartorius, H., and Levin, I.: Carbon dioxide and methane in continental Europe: A climatology, and (222)Radon-based emission estimates, Tellus Ser. B-Chem. Phys. Meteorol., 48, 457-473, 10.3402/tellusb.v48i4.15926, 1996.

Schmidt, M.: Messung und Bilanzierung anthropogener Treibhausgase in Deutschland, PhD thesis, University of Heidelberg, Germany, 1999.

Schmidt, M., Glatzel-Mattheier, H., Sartorius, H., Worthy, D. E. and Levin, I.: Western European N_2O emissions—a top down approach based on atmospheric observations. J. Geophys. Res. 106, 5507–5516. (doi:10.1029/2000JD900701),2001.

Schmidt, M., Graul, R., Sartorius, H., and Levin, I.: Carbon dioxide and methane in continental Europe: A climatology, and (222)Radon-based emission estimates, Tellus Ser. B-Chem. Phys. Meteorol., 48, 457-473, 10.3402/tellusb.v48i4.15926, 1996.

Schüßler, W.: Effektive Parameter zur Bestimmung des Gasaustauschs zwischen Boden und Atmosphäre. PhD thesis, University of Heidelberg, Germany, 1986.

Sherwood, O. A., Schwietzke, S., Arling, V. A., and Etiope, G.: Global Inventory of Gas Geochemistry Data from Fossil Fuel, Microbial and Burning Sources, version 2017, Earth Syst. Sci. Data, 9, 639-656, 10.5194/essd-9-639-2017, 2017.

Solazzo, E., Crippa, M., Guizzardi, D., Muntean, M., Choulga, M., and Janssens-Maenhout, G.: Uncertainties in the Emissions Database for Global Atmospheric Research (EDGAR) emission inventory of greenhouse gases, Atmos. Chem. Phys., 21, 5655–5683, https://doi.org/10.5194/acp-21-5655-2021, 2021.

Sperlich, P., Uitslag, N. A. M., Richter, J. M., Rothe, M., Geilmann, H., van der Veen, C., Röckmann, T., Blunier, T., and Brand, W. A.: Development and evaluation of a suite of isotope reference gases for methane in air, Atmos. Meas. Tech., 9, 3717-3737, 10.5194/amt-9-3717-2016, 2016.

Spokas, K., Bogner, J., and Chanton, J.: A process-based inventory model for landfill CH4 emissions inclusive of seasonal soil microclimate and CH4 oxidation, J. Geophys. Res.-Biogeosci., 116, 19, 10.1029/2011jg001741, 2011.

Szénási, B.: Atmospheric monitoring of methane emissions at the European scale, PhD thesis, University Paris-Saclay, 2020.

Dr. Pieter Tans, NOAA/GML (www.esrl.noaa.gov/gmd/ccgg/trends/) and Dr. Ralph Keeling, Scripps Institution of Oceanography (scrippsco2.ucsd.edu/), 2021, last access: 26 April 2021.

Ulyatt, M. J., Lassey, K. R., Shelton, I. D., and Walker, C. F.: Seasonal variation in methane emission from dairy cows and breeding ewes grazing ryegrass/white clover pasture in New Zealand, New Zeal. J. Agr. Res., 45, 217–226, https://doi.org/10.1080/00288233.2002.9513512, 2010.

Umezawa, T., Brenninkmeijer, C. A. M., Röckmann, T., van der Veen, C., Tyler, S. C., Fujita, R., Morimoto, S., Aoki, S., Sowers, T., Schmitt, J., Bock, M., Beck, J., Fischer, H., Michel, S. E., Vaughn, B. H., Miller, J. B., White, J. W. C., Brailsford, G., Schaefer, H., Sperlich, P., Brand, W. A., Rothe, M., Blunier, T., Lowry, D., Fisher, R. E., Nisbet, E. G., Rice, A. L., Bergamaschi, P., Veidt, C., and Levin, I.: Interlaboratory comparison of δ^{13}C and δD measurements of atmospheric CH4 for combined use of data sets from different laboratories, Atmos. Meas. Tech., 11, 1207–1231, 10.5194/amt-11-1207-2018, 2018.

Umweltbundesamt (UBA): Emissionen ausgewählter Treibhausgase nach Kategorien, available at: `https://www.umweltbundesamt.de/sites/default/files/medien/384/bilder/dateien/4_tab_emi-ausgew-thg-kat_2020.pdf`, last access: 09 March 2021, 2020.

UNFCCC (2015): The Paris Agreement. United Nations Framework Convention on Climate Change. Retrieved from `http://unfccc.int/paris_agreement/items/9485.php`, 2015.

UNFCCC-Submission UBA (2020): Submission under the United Nations Framework Convention on Climate Change and the Kyoto Protocol 2020: National Inventory Report for the German Greenhouse Gas Inventory 1990 - 2018, edited by: Strogies, M. and Gniffke, P.Federal Environment Agency (Umweltbundesamt), Dessau-Roßlau Germany, http://www.umweltbundesamt.de/publikationen, 2020.

VanderZaag, A. C., Flesch, T. K., Desjardins, R. L., Balde, H., and Wright, T.: Measuring methane emissions from two dairy farms: Seasonal and manure-management effects, Agric. For. Meteorol., 194, 259-267, 10.1016/j.agrformet.2014.02.003, 2014.

Vardag, S. N., Hammer, S., and Levin, I.: Evaluation of 4 years of continuous delta C-13(CO2) data using a moving Keeling plot method, Biogeosciences, 13, 4237-4251, 10.5194/bg-13-4237-2016, 2016.

Werle, P., Mücke, R., and Slemr, F.: The limits of signal averaging in atmospheric trace-gas monitoring by tunable diode-laser absorption spectroscopy (TDLAS), Applied Physics B-Photophysics and Laser Chemistry, 57, 131-139, 10.1007/bf00425997, 1993.

Werner, R. A., and Brand, W. A.: Referencing strategies and techniques in stable isotope ratio analysis, Rapid Commun. Mass Spectrom., 15, 501-519, 10.1002/rcm.258, 2001.

White, J. W. C., Vaughn, B. H. and Michel, S. E.: Stable Isotopic Composition of Atmospheric Methane (13C) from the NOAA ESRL Carbon Cycle Cooperative Global Air Sampling Network, 1998-2017, University of Colorado, Institute of Arctic and Alpine Research (INSTAAR), Version: 2018-09-24, Path: `ftp://aftp.cmdl.noaa.gov/data/trace_gases/ch4c13/flask/`, 2018.

Widory, D.: Combustibles, fuels and their combustion products: A view through carbon isotopes, Combust. Theory Model., 10, 831-841, 10.1080/13647830600720264, 2006.

Wilks, D. S.: Resampling hypothesis tests for autocorrelated fields, J. Clim., 10(1), 65–82, doi:10.1175/1520-0442(1997)010¡0065:RHTFAF¿2.0.CO;2, 1997.

20th WMO/IAEA Meeting on Carbon Dioxide, Other Greenhouse Gases and Related Measurement Techniques (GGMT-2019), Jeju Island, South Korea 2–5 September 2019. GAW Report No. 255.

World Data Center for Greenhouse Gases (WDCGG): `https://gaw.kishou.go.jp/`, 2021.

York, D., Evensen, N. M., Martinez, M. L., and Delgado, J. D.: Unified equations for the slope, intercept, and standard errors of the best straight line, Am. J. Phys., 72, 367-375, 10.1119/1.1632486, 2004.

Yuan, Y., Ries, L., Petermeier, H., Trickl, T., Leuchner, M., Couret, C., Sohmer, R., Meinhardt, F., and Menzel, A.: On the diurnal, weekly, and seasonal cycles and annual trends in atmospheric CO2 at Mount Zugspitze, Germany, during 1981–2016, Atmos. Chem. Phys., 19, 999–1012, https://doi.org/10.5194/acp-19-999-2019, 2019.

Zazzeri, G.: Methane emissions in the UK: deciphering regional sources with mobile measurements and isotopic characterisation, PhD thesis, Royal Holloway, University of London, 2016.

Zazzeri, G., Lowry, D., Fisher, R. E., France, J. L., Lanoisellé, M., Grimmond, C. S. B. and Nisbet, E. G.: Evaluating methane inventories by isotopic analysis in the London region, Sci. Rep. 7, 4854. doi: 10.1038/s41598-017-04802-6, 2017.

Zheng, B., Chevallier, F., Yin, Y., Ciais, P., Fortems-Cheiney, A., Deeter, M. N., Parker, R. J., Wang, Y. L., Worden, H. M., and Zhao, Y. H.: Global atmospheric carbon monoxide budget 2000-2017 inferred from multi-species atmospheric inversions, Earth Syst. Sci. Data, 11, 1411-1436, 10.5194/essd-11-1411-2019, 2019.

Zobitz, J., Keener, J., Schnyder, H. and Bowling, D.: Sensitivity analysis and quantification of uncertainty for isotopic mixing relationships in carbon cycle research, Agricultural and Forest Meteorology, 136 (1) (2006) 56-75, ISSN 0168-1923, http://dx.doi.org/10.1016/j.agrformet.2006.01.003, 2006.

List of Figures

2.1. Atmospheric CO_2 and CH_4 mole fractions determined from ice cores and from direct atmospheric measurements. 5
2.2. Global carbon budget and global CH_4 budget. 7

3.1. Location of the three measurement sites Heidelberg, Schauinsland and Zugspitze. 11
3.2. Characterisation of the three measurement stations Heidelberg, Schauinsland and Zugspitze. 13
3.3. Wind roses for ZGR, ZSF and ZUG. 15
3.4. Long-term record of CO_2 and CH_4 mole fractions measured at Heidelberg, Schauinsland, Zugspitze and Mace Head and the corresponding annual cycles. 17
3.5. Diurnal cycle of CH_4 in Heidelberg, Schauinsland and Zugspitze. 21

4.1. Experimental set-up for ambient air measurements in Heidelberg. 26
4.2. Allan standard deviation of CRDS G2201 determined from four cylinders. 28
4.3. CH_4 and $\delta^{13}CH_4$ of the calibration cylinder measurements and the calibrated target cylinder measurements in Heidelberg. 29
4.4. Atmospheric CH_4 mole fraction and $\delta^{13}CH_4$ measured in Heidelberg and corresponding annual cycles. 33
4.5. Diurnal cycle of CH_4 and $\delta^{13}CH_4$ in Heidelberg. 34
4.6. Comparison of CH_4 mole fraction and $\delta^{13}CH_4$ measurements done in Heidelberg between 2014 and 2021 with former measurements in the 1990s and with measurements done at the marine background station Mace Head. 36
4.7. Three typical dependencies of CH_4 and $\delta^{13}CH_4$ in the Heidelberg time series. 39
4.8. Miller-Tans plot to determine the isotopic source signature out of all Heidelberg measurements. 41
4.9. The monthly averages and the annual cycle of the mean isotopic source signatures of emissions in Heidelberg. 42
4.10. Frequency distribution of the determined mean isotopic source signatures. 46
4.11. Atmospheric CH_4 and mean isotopic source signatures depending on wind speed and wind direction 48
4.12. Radon-based CH_4 fluxes calculated for individual nights in 2016. 49
4.13. CH_4 emissions and relative proportion of different source categories reported by LUBW and EDGAR v5.0. 51

4.14. Mean isotopic source signatures for different counties around Heidelberg and the fraction of CH_4 emissions for different sections for these counties. 55
4.15. Annual variability in the monthly mean isotopic source signatures calculated with emission inventories. 58

5.1. Experimental set-up to measure the CO, CO_2 and CH_4 mole fractions in ambient air of Schneefernerhaus and of the mountain ridge in parallel. . . 64
5.2. Target cylinder measurements calibrated with two different calibration strategies at Schneefernerhaus. 69
5.3. Mole fractions of CO, CO_2 and CH_4 averaged over 1 min and measured at Schneefernerhaus and at the mountain ridge. 72
5.4. Distribution of measured CO and CO_2 data at Schneefernerhaus influenced by local pollution as function of month and time of day. 73
5.5. Four typical pollution events at Schneefernerhaus and the mountain ridge. 74
5.6. Negative CH_4 spikes measured at Schneefernerhaus. 76
5.7. CH_4 mole fraction measured in the tunnel air and in ambient air at Schneefernerhaus. 77
5.8. The frequency distribution of the difference between the Schneefernerhaus and the mountain ridge measurement for CO and CO_2. 78
5.9. CO, CO_2 and CH_4 measurements at Schneefernerhaus and mountain ridge. 80
5.10. Diurnal and annual cycles in the Schneefernerhaus and mountain ridge measurement. 82
5.11. Weekly cycle calculated for the Schneefernerhaus and mountain ridge time series. 84
5.12. Mean diurnal cycles of CO_2 for Schneefernerhaus and mountain ridge calculated with the weekend and weekday data for two seasons. 86
5.13. Weekly cycle of CO_2 for three time intervals at Schneefernerhaus between 2002 and 2019. 87
5.14. Mean diurnal cycles for Schneefernerhaus calculated out of the weekend and weekday data between 2002 and 2019 for two seasons. 88

6.1. Calibrated and averaged cylinder measurements of CH_4 at Schauinsland. 93
6.2. High temporal resolution CH_4 mole fractions measured at Schauinsland from 2011 to 2020. 94
6.3. Mobile ambient air measurement set-up to characterise the emission from sewage pit and cows. 95
6.4. Measured CH_4 emissions from the sewage pit and from cows. 96
6.5. Miller-Tans approach to determine the isotopic source signature of CH_4 and CO_2 for the measurements done at the sewage pit and near the cows. 98
6.6. Two time periods with high CH_4 spikes measured in ambient air at Schauinsland with the CRDS G2201 analyser. 100
6.7. Emissions from cows are the origin of CH_4 spikes. 101
6.8. CH_4 mole fraction measured at Schauinsland between July and August when a camera monitored the presence of cows. 102

6.9. Flux chamber measurements done at the sewage pit vent at Schauinsland. 103
6.10. The CH_4 mole fractions measured at different heights above the sewage pit vent. 104
6.11. Influence of CH_4 spikes on hourly CH_4 mole fractions for two different time periods. 106
6.12. Comparison between different peak detection methods for a time period with strong and multiple CH_4 spikes. 110
6.13. Frequency distribution of $\Delta CH_{4\ \mathrm{auto}}$ and $\Delta CH_{4\,\mathrm{unflag}}$ for different peak detection methods and time periods. 111
6.14. Influence of CH_4 spikes on hourly and monthly averages. 113
6.15. Impact of grazing cows on the GC measurements. 115

A.1. Schematic representation of single and two-point calibration. 119
A.2. Isotopic signature of CH_4 sources measured using mobile measurements. . 121
A.3. Allan standard deviation of CRDS G2201 determined for CH_4, CO_2 and their ^{13}C isotopes. 122
A.4. 50 % of the surface sensitivity calculated with STILT for the year 2018 for the station Heidelberg. 124

B.1. Mean diurnal cycles of CO and CH_4 for Schneefernerhaus and mountain ridge calculated out of the weekend and weekday data for two seasons. . 125

C.1. Mobile CH_4 and CO_2 measurements around Schauinsland and Freiburg. . 128
C.2. All CH_4 mole fraction measurements done directly near the cows and sewage pit. 129
C.3. Isotopic ^{13}C measurements during two campaigns at Schauinsland. 131
C.4. Mean isotopic source signature for different counties around Schauinsland and the fraction of CH_4 emissions for different sections for these counties. 133
C.5. Soil flux chamber measurements done in July 2020 and October 2020 at Schauinsland. 135

List of Tables

4.1. CH_4 mole fraction and isotopic ratio of the two calibration gases used in Heidelberg. 29
4.2. $\delta^{13}CH_4$ measurements of six intercomparison cylinders 32
4.3. CH_4 fluxes reported by LUBW and EDGAR inventory for different areas around Heidelberg. 53
4.4. Isotopic signatures of different CH_4 sources. 54
4.5. Mean isotopic source signatures determined from LUBW and EDGAR v5.0 inventory for different areas. 56

5.1. Modifications of the experimental set-up to measure CO, CO_2 and CH_4 at Schneefernerhaus and the mountain ridge. 65
5.2. CO_2, CH_4 and CO_2 mole fractions of the calibration and the target cylinders used at Zugspitze. 67
5.3. Target gas measurements performed with the CRDS G2301, G2401 and OA-ICOS LGR EP30 analysers calibrated with strategy 2 at Schneefernerhaus. 70

A.1. Measurements of six intercomparison cylinders of air sampled at Neumayer station, Antarctica, done with CRDS G2201-i. 123

C.1. Calibration cylinder used during measurement campaigns at Schauinsland. 130

Danksagung

An dieser Stelle möchte ich all jenen Menschen danken, die mich während meiner Promotion unterstützt und motiviert haben.

Vielen Dank an Dr. Martina Schmidt für die Betreuung meiner Dissertation, für die Unterstützung mit hilfreichen Anregungen, zahlreiche interessante Diskussionen und dass sie immer ein offenes Ohr für meine Fragen hatte.

Weiterhin möchte ich mich bei Prof. Norbert Frank bedanken, dass er mich als Doktorandin angenommen und das Erstgutachten übernommen hat, sodass meine Dissertation möglich wurde.

Prof. André Butz möchte ich dafür danken, dass er sich bereit erklärt hat Zweitgutachter meiner Dissertation zu sein.

Mein besonderer Dank gilt auch Frank Meinhardt und Cédric Couret von den UBA-Messstellen Schauinsland und Zugspitze-Schneefernerhaus, auf deren Messungen große Teile meiner Arbeit aufbauen. Ohne die Zusammenarbeit mit ihnen und ihre vielfältige Unterstützung wäre diese Arbeit so nicht möglich gewesen.

Vielen Dank auch an Henrik Eckhardt und Julia Wietzel dafür, dass sie mich auf die Messkampagnen zum Schauinsland und zur Zugspitze begleitet und mich bei meinen Messungen dort unterstützt haben.

Bei Tobias Schmitt und Heinrike Braß möchte ich mich für das Korrekturlesen meiner Arbeit und die vielen Anregungen bedanken.

Ein besonderer Dank auch an Martin Braß für die moralische Unterstützung, das Korrekturlesen meiner Arbeit und die vielen wertvollen Tipps und Anregungen. Ich kann mich glücklich schätzen im letzten Jahr meiner Dissertation einen so großartigen Homeoffice-Partner gehabt zu haben.